T Cell Dominance in Malaria and COVID-19

Daniel Joseph Browne, BMgt/BSc (Hons)

July 2024

A thesis submitted for the degree of Doctor of Philosophy at James Cook University

Student Number:13727792

Australian Institute of Tropical Health and Medicine

College of Public Health, Medical and Veterinary Science

Acknowledgements

Statement of Contribution of Others

Nature of assistance	Contribution	Names, titles (if relevant) and affiliations of co-contributors
General (all chapters)		
Financial Support	Stipend and tuition-fee waiver.	Prestige Research Training Program Stipend from James Cook University (JCU)
Intellectual Support	Design, review and revisions to all chapters.	Prof. Doolan (AITHM)
Artificial Intelligence	I acknowledge the use of AI to review my writing. I reviewed the feedback generated critically and based on this, revised the writing using my own words and expressions.	The following AI tools were used: https://chatgpt.com/ https://www.grammarly.com/ https://scholarai.io/
Editorial Support	Formatting.	Donna Armstrong (professional editor)
Chapter 1		
Section 1.1		
Intellectual Support	Drafting the paragraph describing systems biology. Provided review and revisions.	Ms Kelly (AITHM)
Section 1.2		
Intellectual Support	Aiding in drafting the introduction and conclusion sections. Kelly for drafting the Innate Adaptive Interface section and producing Fig 1.6. Sarathkumara for drafting the Humoral Immunity section. Both provided review and revisions.	Ms Kelly, Dr. Sarathkumara (AITHM)

Chapter 2		
Sample and Data Collection	Designing the flow cytometry panel and assisting with experiments. Providing review and revisions.	Dr. Loiseau, Ms Brady (AITHM)
Intellectual Support	Assessing statistical testing.	Dr. Waardenberg (AITHM)
Chapter 3		
Sample and Data Collection	Aiding in the collection of RT-qPCR data.	Ms Kelly (AITHM)
Intellectual Support	Aiding in the design of RT-qPCR experiments. Provided review and revisions.	Ms Kelly, Ms Brady (AITHM)
Chapter 4		
Animal Care & Husbandry	Animal ethics protocol. Performed injections.	Dr. Pattinson (AITHM)
Sample Collection	Assisted in the collection and processing of animal tissue.	Dr. Pattinson, Ms Kelly, Dr. Sarathkumara, Ms Brady (AITHM)
Data Collection	Collected liver-stage parasite burden data by FACS.	Dr. Pattinson (AITHM)
Data Collection	Aided in the collection of RT-qPCR data.	Ms Kelly (AITHM)
Intellectual Support	Aided in the design of RT-qPCR experiments.	Dr. Pattinson and Ms Brady (AITHM)
Intellectual Support	Aided in statistical testing.	Dr. Proietti (AITHM)
Intellectual Support	Provided review and revisions.	Dr. Pattinson, Ms Kelly, Dr. Sarathkumara, Ms Brady (AITHM)
Chapter 5		
Sample Collection	Collection and processing of human tissue.	Prof. Doolan and previous Doolan team members (QIMRB)

Chapter 6		
Sample Collection	Collection and processing of human tissue.	Prof. Smith, Ms Crooks (QIMRB)
Intellectual Support	Design, review and revisions.	A/Prof. Miller
Chapter 7 (Discussion)		
Intellectual Support	Design, review and revisions.	A/Prof. Miller

Research Outputs Included in this Thesis

Publications

1. **Browne, D. J.**, Kelly, A. M., & Doolan, D. L. (2024). Malaria in the COVID-19 era: A historical review of malaria and malaria vaccine development with insights from COVID-19. (Submitted, in revision for: *Clinical Microbiology Reviews*) **Chapter 1**

Chapter No.	Nature and extent of intellectual input by each author
1.1	Browne and Kelly wrote the first draft. Browne revised the manuscript after editing by Kelly and Doolan.

2. **Browne, D. J.**, Kelly, A. M., Sarathkumara, Y. D., & Doolan, D. L. (2024). *Plasmodium* immunology: Insights to inform pre-erythrocytic-stage malaria vaccine design. (Pending submission) **Chapter 1**

Chapter No.	Nature and extent of intellectual input by each author
1.1	Browne, Kelly and Sarathkumara wrote the introduction and conclusion sections equally. Browne wrote the section on T-cell biology. Kelly wrote the section on the Innate Adaptive Interface. Sarathkumara wrote the section on B-cell biology. The manuscript was revised after editing by Browne, Kelly, Sarathkumara and Doolan.

3. **Browne, D. J.**, Brady, J. L., Waardenberg, A. J., Loiseau, C., & Doolan, D. L. (2020). An analytically and diagnostically sensitive RNA extraction and RT-qPCR protocol for peripheral blood mononuclear cells. *Front Immunol*, *11*, 402. https://doi.org/10.3389/fimmu.2020.00402 **Chapter 2**

Chapter No.	Nature and extent of intellectual input by each author
2	Browne and Doolan developed the research question. Browne, Loiseau and Brady designed the experiments. Browne and Waardenberg performed analyses. Browne gathered data and wrote the first draft and revised the manuscript following revision by all authors.

4.   **Browne, D. J.**, Kelly, A. M., Brady, J. L., & Doolan, D. L. (2022). A high-throughput screening RT-qPCR assay for quantifying surrogate markers of immunity from PBMCs. *Front Immunol*, *13*, 962220. https://doi.org/10.3389/fimmu.2022.962220 **Chapter 3**

Chapter No.	Nature and extent of intellectual input by each author
3	Browne and Doolan developed the research question. Browne, Brady, and Doolan designed the experiments. Browne and Kelly gathered data. Browne performed analyses, wrote the first draft and revised the manuscript after revision by all authors.

5.   **Browne, D. J.**, Kelly, A. M., Brady, J., Proietti, C., Sarathkumara, Y. D., Pattinson, D. J., & Doolan, D. L. (2023). Evaluating the stability of host-reference gene expression and simultaneously quantifying parasite burden and host immune responses in murine malaria. *Sci Rep*, *13*(1), 21071. https://doi.org/10.1038/s41598-023-48066-9 **Chapter 4**

Chapter No.	Nature and extent of intellectual input by each author
4	Browne, Pattinson and Doolan developed the research question. Browne, Brady, Pattinson and Doolan designed the experiments. Browne, Kelly, Sarathkumara and Pattinson gathered data. Browne and Proietti performed analyses. Browne wrote the first draft and revised the manuscript after revision by all authors.

6.   **Browne, D. J.**, Crooks, P. Miller, C. M., Smith, C., & Doolan, D. L. (2024). Differential reactivity of SARS-CoV2 S-protein T-cell epitopes in vaccinated versus naturally infected individuals. (Pending submission) **Chapter 6**

Chapter No.	Nature and extent of intellectual input by each author
6	Browne, Smith, and Doolan developed the research question. Browne and Doolan designed the experiments. Browne and Crooks gathered data. Browne and Miller performed analyses. Browne wrote the first draft and revised the manuscript after revision by all authors.

7.   **Browne, D. J.**, Miller, C. M., & Doolan, D. L. (2024). Technical pitfalls when collecting, cryopreserving, thawing, and stimulating human T-cells. *Front Immunol*, *15*, 1382192. https://doi.org/10.3389/fimmu.2024.1382192 **Chapter 7 (Discussion)**

Chapter No.	Nature and extent of intellectual input by each author
7	Browne wrote the first draft and revised the manuscript after revision by Miller and Doolan.

Abstract

The diseases malaria and COVID-19 present significant global health challenges and cellular immunity plays a critical role in the adaptive immune response to both diseases. However, human T cell immunity to malaria and COVID-19 is incompletely understood. It remains uncertain which antigens or T cell epitopes are recognised as dominant by the human immune system following pathogen infection or in patients with different immune statuses. Such information regarding antigen and epitope immunodominance could provide important insights to facilitate effective vaccine design. Human T cell dominance studies are often challenged by limited sample availability combined with the large number of antigens and epitopes to screen. This thesis directly addressed this challenge by testing and optimising a strategy to identify immunodominant T cell epitopes from very small numbers of human peripheral blood mononuclear cells (PBMCs). Initially focused on malaria, the project optimised a sensitive reverse-transcription quantitative PCR (RT-qPCR) protocol to detect *interferon-gamma* (*IFN-γ*) mRNA expression changes following peptide epitope stimulation from low numbers of PBMCs, providing an alternative to small-scale and expensive protein-based assays. This protocol was further refined into a high-throughput screening (HTS) tool, maintaining high sensitivity and accuracy. This RT-qPCR expertise was applied to a murine model of malaria to identify stable reference genes for accurate quantification of liver-stage *Plasmodium yoelii* parasite burden which is critical for testing the protective capacity of *Plasmodium* antigens. The optimised HTS-RT-qPCR technique was applied to human malaria, to investigate the immunoreactivity of liver-stage *Plasmodium falciparum* antigens in malaria-experienced donors. Following the outbreak of COVID-19, the focus of this thesis pivoted to apply the technical and intellectual foundation developed for malaria to the study of COVID-19. The aim was to identify immunoreactive SARS-CoV2 Spike-protein epitopes in vaccinated versus naturally infected individuals using a high-throughput screen. Overall, this thesis presents a disease-agnostic molecular diagnostic method to identify immunoreactive T cell epitopes with proof-of-concept established for both malaria and COVID-19. The findings reported herein advance our understanding of T cell dominance in these diseases and provide insights to inform the development of effective and enduring vaccines.

Contents

List of Tables

List of Supplementary Tables

List of Figures

List of Supplementary Figures

Chapter 1: Introduction

1.1 Malaria in the COVID-19 era: A historical review of malaria and malaria vaccine development with insights from COVID-19

The work presented in this section comprises a publication to be resubmitted to *Clinical Reviews Microbiology* following feedback from the Editor-in-Chief.

Malaria in the COVID-19 era: A historical review of malaria and malaria vaccine development with insights from COVID-19

Daniel J. Browne[1], Ashton M. Kelly[1,2], and Denise L. Doolan[1,2#]

[1] Centre for Molecular Therapeutics, Australian Institute of Tropical Health and Medicine, James Cook University, Cairns, QLD 4878, Australia

[2] Institute for Molecular Bioscience, University of Queensland, St Lucia, Brisbane, QLD 4067, Australia

1.1.1 Key messages

- Malaria has profoundly influenced human history for over 5,000 years, impacting social structures, genetics, and scientific advancements.

- Progress in reducing malaria stalled in 2015 and was further disrupted by the COVID-19 pandemic, resulting in a resurgence in malaria-related morbidity and mortality.

- The development of an effective malaria vaccine that can significantly reduce malaria incidence is challenged by the parasite's complex evolutionary history, lifecycle, and immune evasion capabilities.

- Applying lessons from the rapid development of COVID-19 vaccines, including understanding immune heterogeneity and leveraging systems biology may improve malaria vaccine efficacy.

- Applying COVID-19 vaccine distribution lessons, including addressing vaccine hesitancy and distribution inequality, would benefit malaria vaccine deployment.

1.1.2 Abstract

Malaria has been recorded for almost 5000 years as a persistent threat to global public health responsible for the deaths of billions of people. Phylogenetic analysis of the causative agent of the disease, *Plasmodium* spp. protists, has revealed that at least several species of *Plasmodium* parasites have coevolved with human ancestors for millions of years. Large-scale public health initiatives involving vector control and chemoprophylactic drugs launched throughout the 19th, 20th and 21st centuries have significantly reduced the global burden of malaria. However, the reduction in malaria incidence stalled in 2015 and worsened from 2020 with the onset of the SARS-CoV2 (COVID-19) pandemic. There is an urgent need for a sustained solution to eradicate the disease, and the development of an effective prophylactic malaria vaccine is considered a global health priority. Despite extensive research spanning more than half a century, a vaccine that induces robust long-term protection has proved challenging. Herein, we position the development of malaria vaccines within a historical perspective. We outline the epidemiological history of malaria, the evolutionary history of *Plasmodium*, and a brief history of malaria vaccine development efforts. We contrast this long history of malaria vaccine development with the rapid development and distribution of COVID-19 vaccines and explore potential lessons and insights from the SARS-CoV2 pandemic that may help accelerate malaria vaccine development.

1.1.3 Epidemiological history of malaria

Malaria is one of the most culturally, economically, and genetically significant infectious diseases in human history [1]. First documented by Chinese scribes almost 5,000 years ago, malaria has infected and killed billions of people, including many important historical figures including Pharaoh Tutankhamun (1327 BC), Alexander the Great (323 BC), Genghis Khan (1227 AD), and Oliver Cromwell (1658 AD), among others [2]. Hippocrates (460 BC), and other early medical practitioners, were aware that people who lived in marshy environments experienced a disease characterised by cyclical fevers and splenomegaly [1]. Thus, the disease was called *mal-aria*, meaning 'bad air', and the concept that miasmas rising from swaps was the cause of malaria persisted for almost 2500 years. It was not until the advent of the *Germ-Theory of Disease* by Robert Koch (1843–1910) and Louis Pasteur (1822–1895) during the late 19th century that it was recognised that pathogenic microorganisms cause communicable diseases such as malaria.

It is now known that malaria is caused by parasitic *Plasmodium* spp. protists [3], with the primary vector for transmission being female *Anopheles* spp. mosquitoes [4]. Elucidating the complex multi-stage lifecycle of *Plasmodium* spp. took nearly a century (**Fig. 1.1**). The French military surgeon Charles-Louis Alphonse Laveran (1845–1922) won a Nobel Prize in Physiology or Medicine for his discovery in 1880 of *Plasmodium* parasites in the peripheral blood of malaria patients [5]. The British medical doctor Ronald Ross (1857–1932) won the same Nobel Prize by establishing in 1897 that mosquitoes were the vector responsible for transmitting *Plasmodium* parasites [6]. The sexual-stage of the *Plasmodium* lifecycle was discovered in 1897 by the Canadian-American physician and pathologist William MacCallum (1874–1944), who observed sexual dimorphic fusing of male and female *Plasmodium* gametes in the mosquito midgut [7]. It was not until the 1940's that the British parasitologists Henry Shortt (1887–1987) and Cyril Garnham (1901–1994) discovered the pre-erythrocytic stage of a *Plasmodium* infection [8].
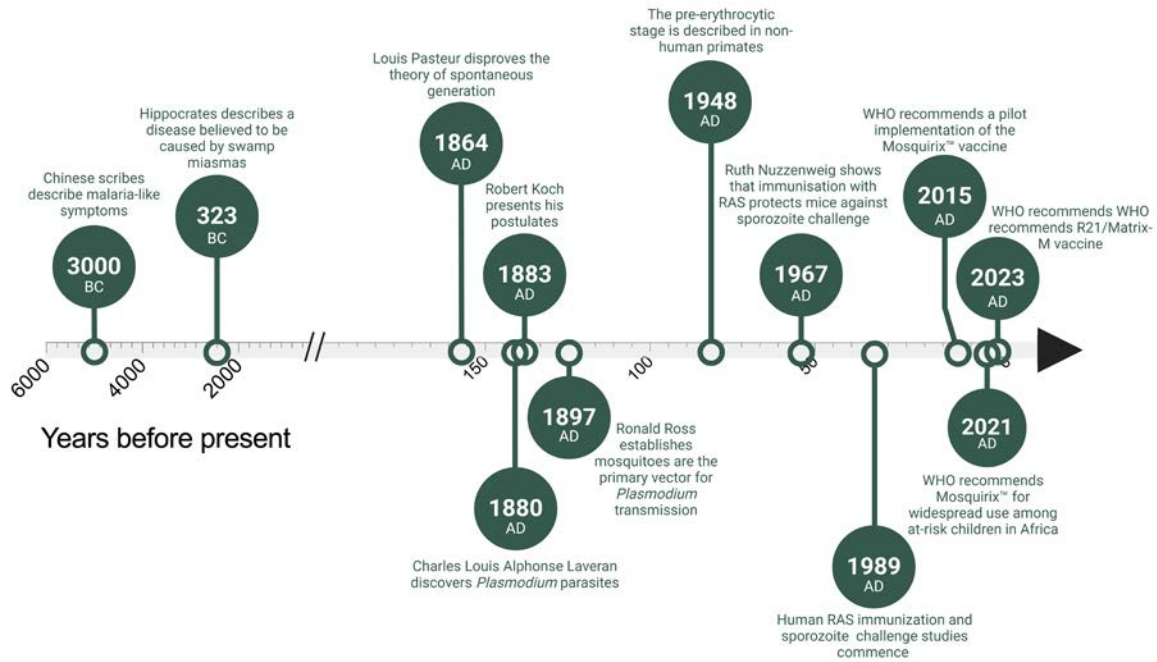
Figure 1.1. Major milestones in malaria research. Relative timeframe of key advances in medical research against the disease malaria. Radiation Attenuated Sporozoite (RAS).

It was during the 1940s with the advent of molecular epidemiology that Linus Pauling (1901-1994) identified a homozygotic glutamic-acid to valine substitution in the human β-globin gene as responsible for the autosomal-recessive disease sickle cell anaemia [9]. During this period, James Neel (1915-2000) proposed the *Heterozygote Advantage Hypothesis*, suggesting malaria drove the persistence of the sickle cell trait [10]. In the 1950's the Duffy blood group system was discovered [11], which is now known to contain five polymorphic forms of the Duffy (CD234) protein [12]. Allelic and loss-of-function (Duffy negative) variants of the Duffy protein are associated with the selective pressure caused by certain species of *Plasmodium* [13]. More recently, the dawning of the "Genomics Era" [14] has allowed unprecedented insight into the complex human-*Plasmodium* host-parasite relationship. Thousands of genetic polymorphisms have been linked with *Plasmodium* selective pressure [15], such as mutations in the α- or β-like globin chain genes which significantly reduce haemoglobin production and cause the disease Thalassemia [16]. Genomic research will likely continue to identify genetic alterations, such as epigenetic modifications [17], that have been influenced by the intense selective pressure exerted on humans by malaria.

In the 19th century, the global burden of malaria was decreased by a range of public health initiatives, including the drainage of swamps, improved building and construction techniques,

the introduction of widespread use of the antimalarial drugs quinine and chloroquine, which both disrupt the malaria parasite's ability to replicate [18]. At the beginning of the 20th century, malaria remained an endemic or seasonal pandemic disease across more than 50% of the Earth's surface, extending into temperate regions as far north as Inverness, Scotland [19]. Over the last 20 years, the implementation of effective physical and chemical preventative measures such as insecticide-treated bed nets, indoor residual spraying [20], and chemoprophylactic drugs [21] has reduced the global impact of malaria. Nevertheless, an estimated 40-50% of the global population remains at risk of malaria [22] spanning almost a third of the Earth's surface [18]. Malaria-endemic regions are highly concentrated in the tropics and sub-tropics where climatic factors such as temperature, humidity and rainfall support the lifecycle of *Anopheles* spp. [22], but climate change modelling has predicted an expansion in the range of *Anopheles* spp. in response to increasing global temperatures [23].

Figures compiled by the World Health Organization (WHO) in 2022 reveal that between 2000 and 2015 the global burden of malaria, as measured by global malaria case incidences, steadily reduced from 245 to 230 million cases (**Fig. 1.2**) [24]. However, from 2015 to 2019, case incidence stalled with 232 million cases recorded in 2019. During the SARS-CoV2 (COVID-19) pandemic between 2019 and 2022, on average, an annual increase of 13.4 million malaria infections and 10% more malaria deaths were recorded [24]. This was despite considerable efforts to maintain malaria-related healthcare services and case-reduction efforts during the pandemic. Historically, the most successful approach to curtailing the spread of any communicable diseases has been the strategic implementation of public health initiatives, guided by epidemiological data [25]. Vaccination has been an extremely effective adjunct medical intervention to further reduce the global burden of many diseases, and, for some diseases exemplified by smallpox, achieved complete eradication [26]. However, unlike the robust and sustained protection provided by many vaccines listed on global adolescent immunisation schedules [27, 28], such as hepatitis A (HepA) and B (HepB), the measles, mumps and rubella (MMR), and inactivated-poliovirus vaccines, there is currently no licensed malaria vaccine which provides similar long-term protection [29-32]. The continued population growth in malaria-endemic regions, the increasing development of insecticide resistance in the *Anopheles* spp. vector and drug resistance in the *Plasmodium* spp. parasite [33], combined with the challenges associated with delivering critical healthcare during the aftermath of COVID-19 [34], highlights the need for an effective prophylactic malaria vaccine.
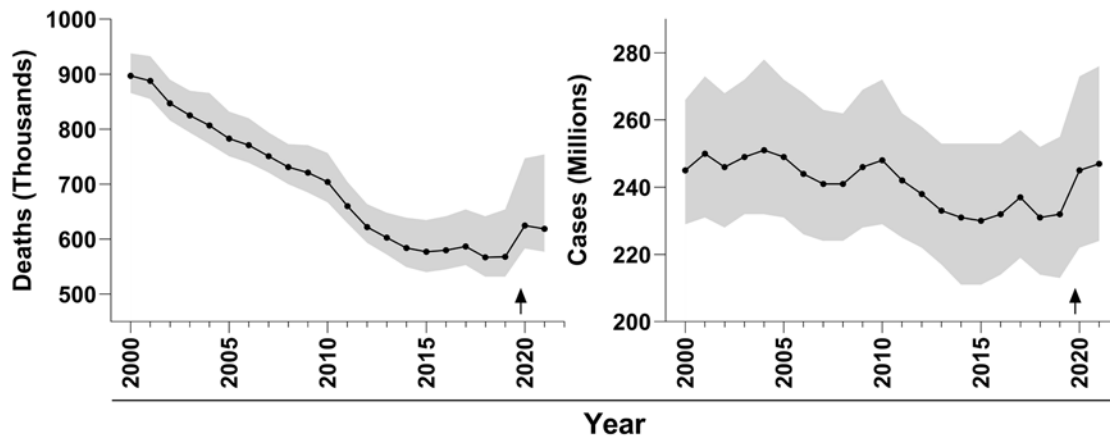
Figure 1.2. Estimated global malaria deaths and cases from 2000 to 2021. Upper and lower estimates (greyscale) and point (final estimate; black points) deaths in hundreds of thousands and cases in hundreds of millions. **Black arrow**: Beginning of the COVID-19 pandemic in late 2019. Adapted from [24].

1.1.4 Evolutionary history of *Plasmodium*

Plasmodium is a genus of *Apicomplexans*, a phylum within the highly diverse eukaryotic unicellular protist infrakingdom *Alveolata* [35]. Molecular sequencing and fossil records suggest alveolates evolved around 850 million years ago from a common ancestor which contained a plastid of red algal origin [36]. This plastid (termed the apicoplast) has been maintained in *Apicomplexa*, and all known *apicomplexans* are obligate intracellular parasites [37]. Morphologically, *apicomplexans* adapted to their obligate intracellular lifestyle by losing flagella and developing a complex substrate-dependent locomotion known as gliding motility [38]. However, the most notable innovation of *Apicomplexan* evolution was the development of a complex life cycle. Phylogenetically, the *Plasmodium* genus sits within the order *Haemosporida* (*i.e.,* an apicomplexan order which infects erythrocytes), and family *Plasmodiidae* (*i.e.,* a haemosporidian family separated by hemozoin pigment production and asexual reproduction technique) [39]. Although historical molecular phylogenies remain unclear, oocysts and sporozoites of a malaria parasite (*Haemospororida: Plasmodiidae)* were identified in a 100 million-year-old fossil of an extinct species of biting midge which likely fed on large cold-blooded vertebrates [40].

Today, the *Plasmodium* genus comprises more than 200 known species infecting various birds, mammals, and reptiles. Of these, five species of *Plasmodium* parasites cause the majority of

malaria in humans; four are obligate human parasites (*P. falciparum, P. vivax, P. malariae*, and *P. ovale*) [41], and one is a zoonotic pathogen (*P. knowlesi*) [42]. Although much rarer [43], other species of zoonotic *Plasmodium* have been reported to cause malaria in humans (*e.g., P. simium [44], P. brasilianum [45], P. cynomolgi,* and others [46]). The true extent to which these zoonotic species infect humans remains unclear. Their numbers are likely significantly under-reported, and debate continues regarding the phylogenetic differences between many species [43]. Nevertheless, these species may represent zoonotic reservoirs, potentially having a significant impact on human health.

Of the obligate human parasites, *P. falciparum* is the most common species across Africa and is also considered the most virulent, associated with the most fatalities globally [47]. *P. falciparum* is likely to have evolutionarily diverged from a common *Plasmodium* ancestor, which infected Western Lowland Gorilla (*i.e., Gorilla gorilla*) hosts as early as 10,000 years before present (YBP) [48]. *P. vivax* is widespread globally but is rare in Africa due to the high prevalence of the 'Duffy Negative' mutation in African human populations. Duffy Negative mutations have evolved independently at least twice and are protective against *P. vivax* infection [13]. Mitochondrial sequencing of global *P. vivax* strains suggests that the time to the most recent common ancestor is between 217,000 and 304,000 YBP [49]. These data imply that *P. vivax* has remained a clinically relevant parasite since anatomically modern humans first arose at the end of the Lower Palaeolithic [50]. *P. malariae* and *P. ovale* infections make up an estimated 1% and 2% of the global burden of malaria, respectively, although these figures may be an under-representation due to potential co-infection and low parasitemia rates [51]. Recent genomic sequencing data suggests *P. malariae* diverged from *P. brasilianum* between 3.5-4 million YBP [52] and *P. ovale* appears to have speciated some 20 million YBP [52]. It is clear a complex co-evolutionary history between the human host and *Plasmodium* parasite has occurred (**Fig. 1.3**).
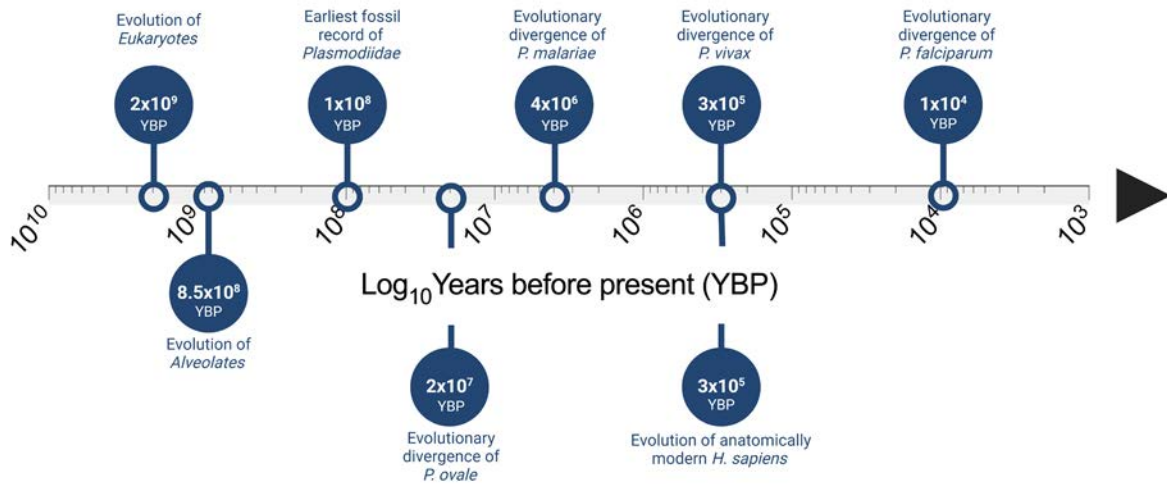
Figure 1.3. Major milestones of *Plasmodium* spp. evolution. The relative timeframe of key landmarks in obligate human *Plasmodium* parasites (*P. falciparum, P. vivax, P. malariae, and P. ovale*) and human (*Homo sapiens*) evolution presented on a Log$_{10}$ scale of years before present (YBP).

All clinically relevant *Plasmodium* parasites have a similar multi-stage life cycle with distinct stages in the vertebrate host and the *Anopheles* mosquito vector [4, 39]. The life cycle involves successive pre-erythrocytic (*i.e.,* sporozoite and liver), erythrocytic (*i.e.,* blood) and sexual or mosquito stages [53] (**Fig. 1.4**). The pre-erythrocytic sporozoite-stage of a *Plasmodium* spp. infection is initiated when *Plasmodium* sporozoites are inoculated into the host dermis via the saliva of an infected female *Anopheline* mosquito. Post-inoculation, sporozoites rapidly travel to the liver to initiate the liver-stage of infection. The pre-erythrocytic liver-stage of infection begins when sporozoites typically cross through several structures and ultimately establish within a single final hepatocyte [54]. Within the hepatocyte, the parasite surrounds itself with a protective phospholipid membrane, known as a parasitophorous vacuole, wherein it begins multiplication into thousands of daughter cells [55].
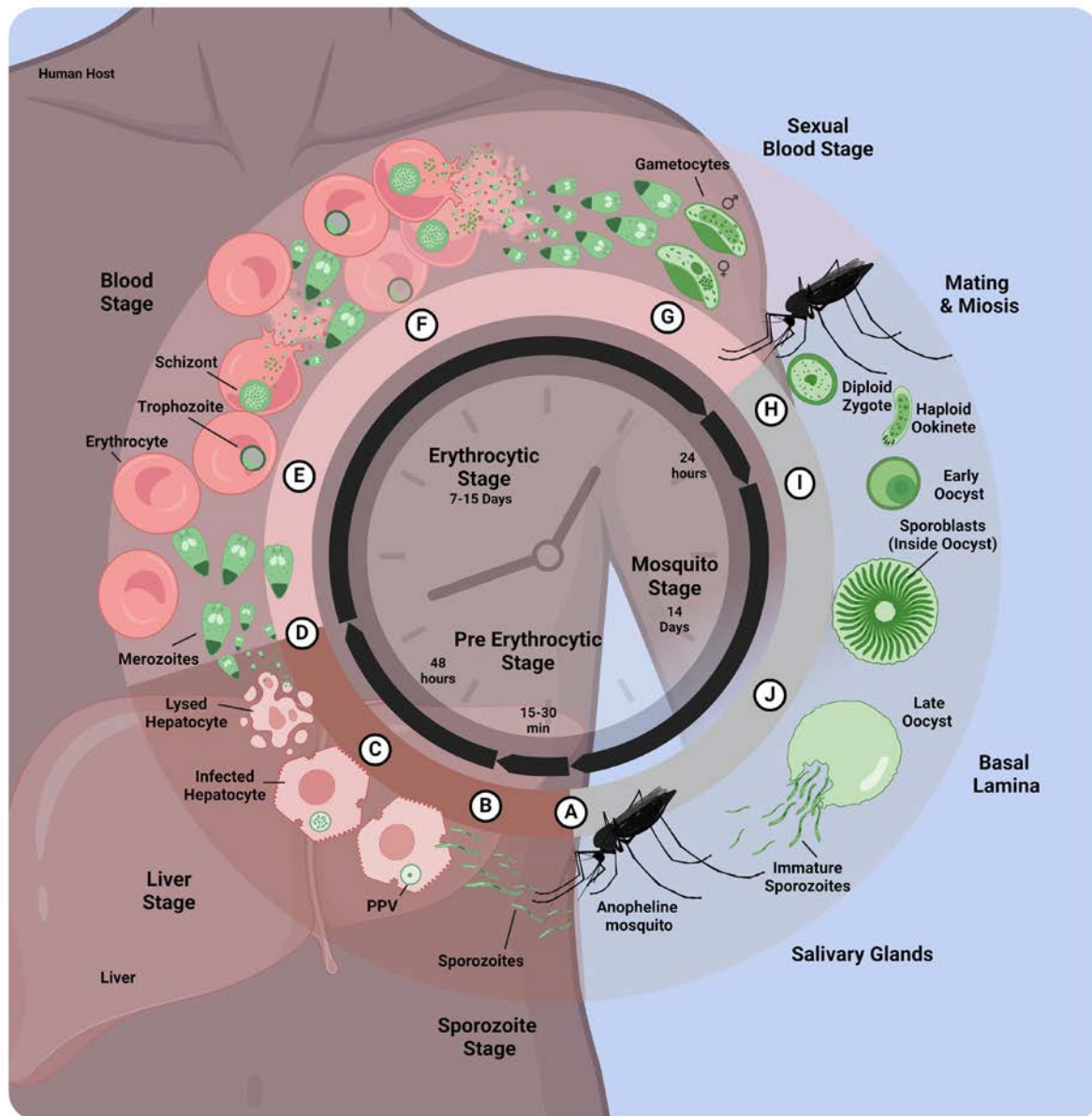
Figure 1.4. The *Plasmodium* spp. life cycle (Historical Review) . **(A)** *Plasmodium* spp. sporozoites are transmitted into a vertebrate host through the bite of an infected female *Anopheline* mosquito. **(B)** The liver stage starts when sporozoites infect liver hepatocytes. **(C)** Inside the hepatocytes, the parasite forms a parasitophorous vacuole (PPV) and multiplies into thousands of daughter cells. **(D)** Roughly 48 hours later, numerous merozoites burst from the infected hepatocyte into the bloodstream. **(E)** Merozoites invade erythrocytes, differentiate into trophozoites, and commence haemoglobin digestion. These trophozoites mature into erythrocytic schizonts, which divide into more merozoites and then rupture, infecting additional erythrocytes. **(F)** This cycle of rupture, multiplication, and reinfection repeats several times. **(G)** Between 7 and 10 days later, a fraction of the parasites differentiate into sexual male and female gametocytes. **(H)** When an *Anopheline* mosquito feeds on an infected host, it ingests these gametocytes. Inside the mosquito, they mate to form a diploid zygote, which rapidly undergoes meiosis to become a haploid ookinete. **(I)** Within 24 hours, the ookinete penetrates the mosquito's basal lamina and forms an oocyst. **(J)** Over the next 14 days, sporoblasts develop within the

oocyst. These sporoblasts eventually leave the oocyst, invade the mosquito's salivary glands, and become ready for transmission to another host. Adapted from [56].

Approximately 48 hours post-sporozoite inoculation, the erythrocytic (*i.e.,* blood) stage of infection begins. Spherical or elongated-teardrop-shaped *Plasmodium* spp. merozoites [57] rupture from an infected hepatocyte into the bloodstream in a highly synchronised manner, rapidly enter erythrocytes, differentiate into ring-shaped trophozoites, and begin digesting host haemoglobin. Merozoites have recently been found to infiltrate erythrocytes with their 'wider apical end' first, turning the topology of the parasite upside down from classical models [38, 57]. Trophozoites mature into multi-nucleated erythrocytic schizonts and then divide into merozoites, which rupture once again into the peripheral blood circulation [58]. There are multiple rounds of this synchronous rupture, multiplication, and reinfection [59, 60] which associate with the onset of the clinical symptoms of malaria, typically presenting as cycles of fever and chills [61]. The sexual blood-stage begins when a small proportion of cells differentiate into sexual male and female gametocytes over 7-15 days [62]. A female *Anopheline* mosquito must take up these gametocytes in a blood meal to complete the parasite life cycle. Within the mosquito midgut, the gametes mate to produce a diploid zygote. The zygote performs miosis into an invasive haploid ookinete that can traverse and imbed within the mosquito basal lamina and transform into an oocyst within approximately 24 hours [63]. Within each oocyst, thousands of sporoblasts replicate asexually over two weeks. The sporoblasts ultimately break through the oocyst, invade the mosquito salivary glands, and undergo further development before inoculation back into the vertebrate host to continue the parasitic life cycle (**Fig. 1.4**) [64, 65].

In response to a *Plasmodium spp.* infection, human hosts mount complex and coordinated innate and adaptive immune responses. Due to the complex co-evolutionary relationship that has developed between *Plasmodium* spp. and humans, the parasites rapidly progress through the innate immunity phase, so adaptive immunity is predominantly responsible for clearing a *Plasmodium* spp. infection. Following pathogen exposure, adaptive immunity allows the development of memory cells, which provide immunity to future challenges [66]. Therefore, induction of *Plasmodium*-specific adaptive immune memory is a key goal of malaria vaccine development. The two main arms of the adaptive immune response - cellular and humoral immunity - synergistically cooperate to clear *Plasmodium* spp. infections. Cellular immunity has been identified as the critical effector of liver stage adaptive immunity [67, 68];

specifically, the action of CD8^{+} T cells destroying infected hepatocytes [69]. Humoral immunity is the critical effector of sporozoite and erythrocytic-stage adaptive immunity; specifically, the production of high-affinity antibodies that target multiple merozoite, trophozoite, schizont or gametocyte surface antigens [70]. *Plasmodium* spp. have evolved intricate methods to thwart or avoid host adaptive immunity. These strategies include changing expression of variant surface proteins throughout the life cycle [71], maintaining multiple redundant invasion mechanisms [72], modulating the expression of proteins (*i.e.,* antigenic variation or antigen polymorphism) [73], secreting immunomodulatory molecules [74], or maintaining a high degree of intra-species genetic variation [75]. The complexity of these host-immune evasion strategies has significantly impeded the creation of an effective malaria vaccine.

The effectiveness of immune evasion strategies used by *Plasmodium* spp. is evident when considering the development of naturally acquired immunity (NAI) in individuals following long-term exposure to the parasite [76]. *Plasmodium* spp. blood-stage parasites are typically found in the peripheral circulation of adults with NAI residing in malaria-endemic regions in concentrations that would otherwise be almost universally lethal to those without NAI [53]. NAI protects millions of people globally and, amongst exposed adults, has virtually 100% efficacy against severe disease [76]. However, the number of infections required to develop robust NAI to a *Plasmodium* spp. infection is remarkable, often requiring repeated infections over several years. This is in contrast to simpler viral pathogens such as smallpox where a single infection can induce robust and sustained life-long protection [76]. Additionally, NAI does not confer solid anti-parasite immunity, and typically only provides clinical immunity (*i.e.,* minimises disease symptoms).

1.1.5   A brief history of malaria vaccine development

Until the 1940's, there were no well-established *in vivo* animal models to study malaria or malaria vaccines [77]. Throughout the 1940's several avian models, including chickens and ducks infected with *P. lophurae,* were used as anti-malaria drug screening models. The American immunologist Jules Freund (1890-1960) and his associates attempted the earliest reported malaria vaccination studies by immunising ducklings with Freund's adjuvant and inactivated (killed) *P. lophurae [78].* However, avian models proved poor substitutes for studying mammalian malaria. In 1948, the Belgian physician Ignace Vinke (1906-1971) and his associates discovered a rodent malaria parasite, *P. berghei* which infected African

woodland thicket rats (*Grammomys surdaster*) [79]. Following inoculation with infected erythrocytes, this parasite could cause infections in laboratory mice. Once the parasite life cycle was replicated in rodent *in vivo* models, an explosion of malaria research occurred [80].

In 1967, a seminal study by the Brazilian immunologist Ruth Sonntag Nussenzweig (1928-2018) and colleagues showed that sterile immunity against sporozoite challenge could be induced in mice by immunisation with *P. berghei* radiation attenuated sporozoites (RAS) [81], a finding that was later confirmed in human volunteers immunised with *P. falciparum* RAS [82-84]. Efforts to immunise against malaria using other *Plasmodium* stages, including merozoites [85] and gametocytes [86], were trialled. However, only attenuated sporozoite immunisation provided consistent successful immunity, although protection was not absolute and decreased over time [87]. These studies established for the first time two critical milestones in malaria vaccine development: i) the feasibility of developing an effective malaria vaccine; and ii) that sterile protective immunity was possible with pre-erythrocytic stage host adaptive immunity [88]. However, live-attenuated sporozoite vaccines faced significant cost and logistical deployment challenges (*i.e.,* large quantities of aseptic, well-characterised, and stable sporozoites must be dissected from salivary glands of thousands of infected mosquitoes, couriered cryopreserved to remote locations, and inoculated intravenously). Therefore, the next major focus of malaria research was to develop subunit vaccines that conferred the sterile immunity observed following RAS vaccination by identifying parasitic antigens expressed during the pre-erythrocytic stage.

Originally, the sporozoite stage of malaria was considered non-immunogenic because anti-sporozoite antibodies were not detected in people bitten by infected mosquitoes [87]. However, following RAS vaccination, species-specific, often strain-transcending, anti-sporozoite antibodies were detected. The highly expressed Circumsporozoite protein (CSP) which coats the complete *Plasmodium* sporozoite was identified [89] and recognised as immunodominant [90], and antibody titers against it were associated with protection [91]. In 1984, the *Plasmodium* CSP was cloned for the first time. This breakthrough was achieved when a clone of complementary DNA encoding the *Plasmodium falciparum* CSP was isolated from *E. coli* [92]. Subsequently, almost all pre-erythrocytic stage subunit vaccine efforts have focused on CSP [93-96]. While CSP has long been considered an ideal vaccine antigen, there are however, compelling reasons to suggest CSP is not an ideal antigen for a malaria subunit vaccine: i) CSP-specific subunit vaccines provide only modest protection when compared to RAS vaccines [97]; ii) CSP expression ceases midway through development within the

parasitophorous vacuole [98]; iii) CSP-specific immunity is not required for protective immunity following RAS immunisation [84]; and iv) CSP may have evolved as a mechanism of immune evasion [99]. Indeed, it has been hypothesised that other antigenic targets may provide more protective than CSP [97, 100], and even suggested that CSP has evolved as an immunodominant 'red-herring' to distract our immune system from these antigens [101].

Historically, research directed towards developing subunit vaccines has been dominated by investigations into a very small number of antigens such as CSP [102], which are typically presented on the parasite surface during the pre-erythrocytic stage [94, 103, 104]. Since the late 1980's several erythrocytic stage antigens were trialled including Merozoite Surface protein 1 (MSP1) and Apical Membrane Antigen 1 (AMA1) [105]. All these leading blood-stage candidates failed in field testing. More recently, efforts have focused on RH5 and the Rh5 complex proteins [106]. In 2015, the European Medicines Agency approved the first licenced *P. falciparum* subunit vaccine RTS,S/AS01 (Mosquirix™) which targets the CSP antigen [107, 108]. Mosquirix™, comprises a hepatitis B virus surface antigen virus-like particle genetically fused to a truncated *P. falciparum* CSP antigen. In 2021 Mosquirix™ was recommended by the WHO for widespread use in children living in regions with moderate to high transmission of malaria [109], although protection is relatively low and short-lived. In 2023 the WHO recommended the second-generation pre-erythrocytic subunit vaccine R21/MM for the prevention of malaria in children [109]. R21/MM is a CSP-based VLP formulated in Matrix-M adjuvant vaccine with a reported 77% efficacy in children ages 5-17 months, even one year after vaccination [29, 110]. Despite being the goal of CSP-based research for decades, hope remains that a better understanding of the immune response to CSP [97], or improved vaccine design (*i.e.,* such as advanced adjuvants) [111] can generate further generations of increasingly efficacious CSP-based subunit vaccines.

The limited effectiveness of subunit vaccines has prompted exploring various strategies to improve malaria vaccine design. One approach has been to identify other more immunogenic antigens from the complete *Plasmodium* genome by using large 'omic' (*e.g.,* genomic, proteomic, transcriptomic, metabolomic) datasets and systems immunology. By considering the holistic view of the interaction of the host immune system and pathogen target, systems immunology can facilitate the identification of novel antigens from *Plasmodium* genomes, transcriptomes, or proteomes that are the key targets of host-parasite protective immunity. This offers a rational, systematic approach to vaccine and target selection which has previously been approached in an *ad hoc* manner [94, 100, 102, 112]. Another approach involved revisiting

attenuated sporozoite vaccines. In 2003, the company Sanaria™ Inc, led by the American clinician scientist Dr. Stephen Hoffman, was founded with the intent to build on the seminal studies conducted by the Nussenzweig team to develop, commercialise, and deploy RAS vaccines [113]. The current leading whole parasite vaccine is *P. falciparum* RAS vaccination (*Pf*SPZ) developed by Sanaria™ using metabolically active *P. falciparum* sporozoites (sometimes combined with pyrimethamine or chloroquine chemoprophylaxis) [114, 115]. The Sanaria™ *Pf*SPZ vaccine has progressed to phase 2 field studies (*e.g.,* testing for efficacy) in malaria-exposed individuals in Kenya [116], Equatorial Guinea [117], Tanzania [118] and other countries. Despite concerns raised [119] regarding the feasibility of widespread deployment of whole-parasite vaccines, Sanaria™ is demonstrating that overcoming these logistical challenges is achievable [88, 113, 118].

1.1.6 Lessons learnt and insight gained from the COVID-19 pandemic

In late 2019, clinicians in Wuhan, China, reported a cluster of severe acute respiratory syndrome (SARS)-like cases to the WHO. Within weeks, the causative agent was identified as a novel coronavirus and named SARS-Coronavirus 2 (SARS-CoV2) [120]. The resulting disease was named coronavirus disease 2019 (COVID-19), and rapidly spread throughout the globe, killing millions of people. The response of the international community was to impose strict government quarantines and shutdowns, which resulted in a severe disruption to malaria services. For instance, between 2020 and 2022, more than a quarter of the requested insecticide-treated mosquito nets were not distributed, with certain regions receiving none at all [24]. This disruption to malaria control efforts was reflected in substantial increases in malaria incidence, with the WHO reporting an estimated additional 13 million cases and 69,000 deaths due to COVID-19 disruptions [24]. Malaria vaccine development was also severely disrupted, and it is anticipated that laboratory closures, research supply disruption, and diversion of funding will be widely felt long after the pandemic is over [121]. In contrast, COVID-19 vaccine development occurred at an astonishing rate, with the majority being subunit vaccines specifically targeting the SARS-CoV2 Spike-Protein (S-protein) [122]. By the beginning of 2022, over 150 COVID-19 vaccine candidates had entered clinical trials, and dozens were licensed and administered globally [123]. Despite these achievements, today it is clear that challenges remain for COVID-19 vaccines, including emergent variants of concern, sporadic global vaccine distribution, and rapidly declining post-vaccination immunogenicity and efficacy [124]. Understanding the development and distribution of COVID-19 vaccines may inform future strategies to develop a more efficacious malaria vaccine.

Although COVID-19 and malaria are epidemiologically distinct, their vaccine development and distribution share common features and challenges (**Fig. 1.5**). Like *Plasmodium*, a single SARS-CoV2 protein, the S-protein, was selected as the leading vaccine antigen, but other SARS-CoV2 antigens may provide more effective and longer-term protection. Indeed, immune responses have been detected against the whole SARS-CoV2 proteome, and other proteins, including the membrane (M) and nucleocapsid (N) proteins, have been identified as immunodominant antigens [125]. Robust humoral and cellular immunity consistent with long-term protective immunity targeting multiple SARS-CoV2 proteins has been reported in many convalescent SARS-CoV2 patients [126]. As with malaria [127, 128], it is likely that multivalent vaccines comprising multiple rationally selected antigens may be more effective than a monomeric vaccine (**Fig. 1.5A**). COVID-19 vaccines that present multiple S-protein variants are already available [129] and available data suggest these may induce more robust and durable immunity than monomeric antigens [130].

The speed of COVID-19 subunit vaccine development was greatly improved by the availability of multiple vectors capable of accommodating the S-protein antigen [131]. A prominent example is the Chimpanzee Adenovirus (ChAd) vaccine platform, which was originally designed as a vector for malaria vaccines [132]. The cost-efficient scalable production technology developed for ChAd for malaria was rapidly applied to COVID-19 [133]. In 2020, very rare (1:100,000) side effects of thrombosis and thrombocytopenia syndrome were associated with ChAdOx1 [134]. This halted distribution of the AstraZeneca vaccine in many countries and led to the widespread uptake of mRNA vaccinations (*i.e*., Pfizer–BioNTech (BNT162b2) and Moderna (mRNA-1273) vaccines) [134, 135]. This development highlighted the advantages of heterologous boosting. Those who had received an mRNA boost following an adenovirus primary immunisation (heterologous prime-boost) displayed enhanced humoral and cellular immunity [136, 137]. Since the early 1990's, heterologous boosting has been investigated as a method to synergistically improve vaccine immunogenicity [138], including in the malaria field [139-142]. However, that vaccination concept had not seen widespread adoption until the COVID pandemic (**Fig. 1.5A**). The prevalent use of heterologous vaccination regiments for COVID in millions of people established that vaccine regimens incorporating heterologous boosting is tolerised, safe, and effective on a global scale [143, 144].
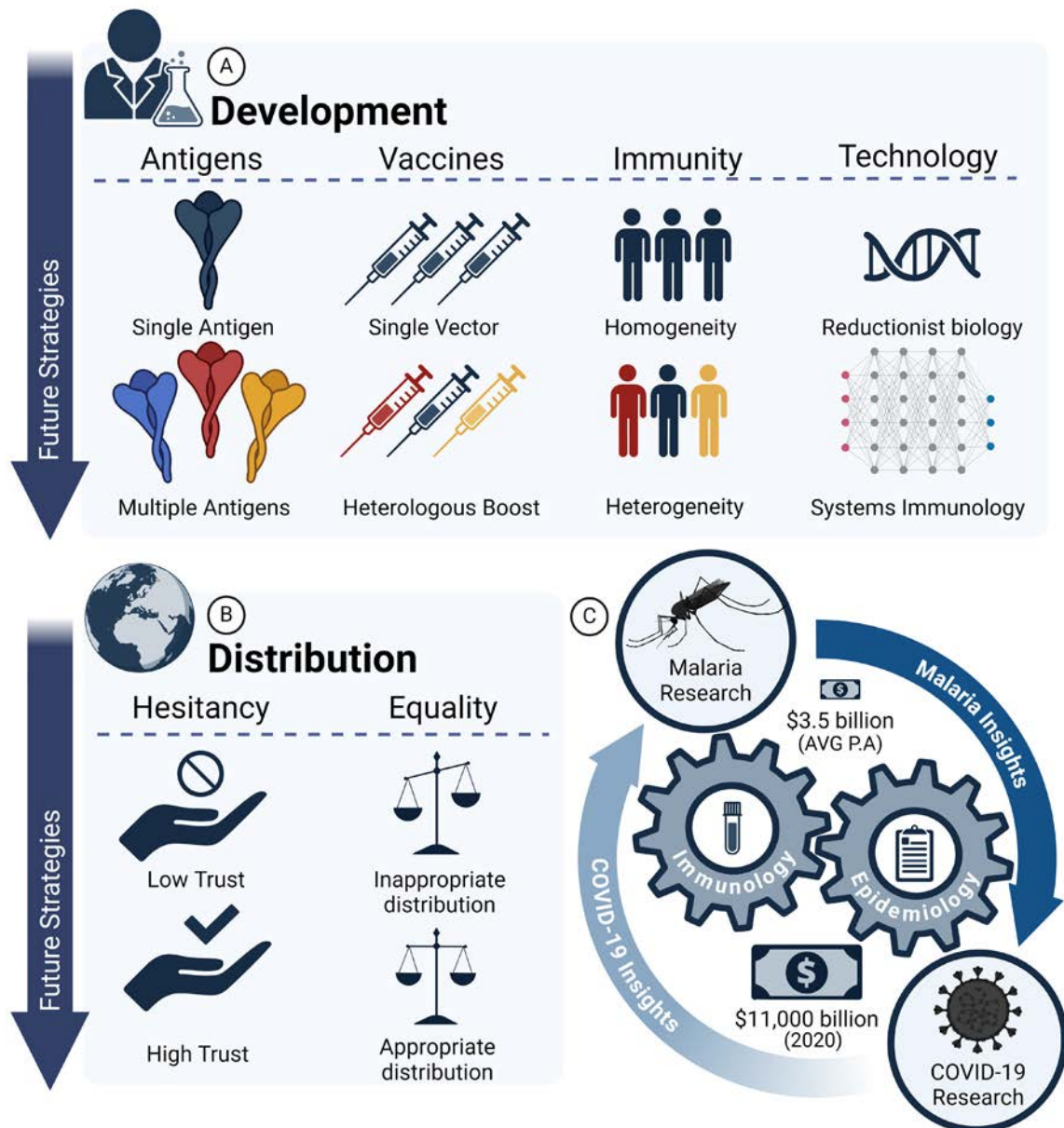
Figure 1.5. Commonalities between COVID-19 and malaria vaccine development and distribution. **(A)** Currently licensed vaccines for both diseases use a single antigen delivered via a single vector to a population assumed to be immunologically homogenous. Future vaccines may need multiple antigens and heterologous boosts for immunologically heterogenous populations. **(B)** Vaccine deployment has faced challenges like hesitancy and inequitable distribution, with wealthier nations acquiring more doses. Future efforts should involve trusted figures to combat misinformation and equitable strategies to decrease disease rates. **(C)** Integration of immunological and epidemiological data from ongoing research is essential for optimizing strategies against both diseases.

Vaccines such as the HepA, HepB, MMR, and inactivated-poliovirus vaccines provide long-lasting immunity, often exceeding 90% efficacy for decades [145]. In contrast, vaccine-induced immunity from COVID-19 vaccines such as BNT162b2 and mRNA-1273 wanes within months [146]. Similarly, the efficacy of the RTS,S malaria vaccine decreases to 36% after four years [147], and the R21/MM vaccine is also likely to require booster shots to maintain protective immunity [148]. The immunology behind the relatively rapid decrease of COVID-19 and malaria vaccines' efficacy is incompletely understood. While both SARS-CoV2 and pathogenic *Plasmodium* spp. are genetically diverse with many circulating variants, this variability does not fully explain the significant heterogeneity in human immune responses, clinical outcomes, and the endurance of protection efficacy [149] (**Fig. 1.5A**). Furthermore, the protective efficacy of subunit-based COVID-19 vaccines wanes faster than the protective immunity induced following infection with the SARS-CoV2 virus [150]. This may be due to a broader immune response launched against a more diverse range of antigens. Alternatively, existing immune memory, which has expanded against conserved epitopes within the S-protein, may interfere with the development of responses against other potentially more protective antigens and epitopes. This process, known as immune imprinting, has been speculated to influence the efficacy of malaria vaccines [151], specifically where the efficacy of vaccines in malaria-endemic regions is substantially lower than that reported in malaria-naïve volunteers [152]. The implication is that understanding immune heterogeneity and the interaction between long-term immune efficacy, immune imprinting, and vaccination may help improve malaria vaccine efficacy, especially against inter-species strains and variants.

A significant shift in the fields of vaccinology and immunology spurred by the COVID-19 pandemic was the integration of computational sciences and systems biology [153-155]. The transition from the traditional reductionist immunological approach to a systems immunology framework has the potential to revolutionise vaccine development. From understanding immune heterogeneity and predicting vaccine candidates to predicting disease epidemiology and transmission, technologies including Machine Learning and Artificial Intelligence (AI) are now in widespread use, including multiple disease settings [156, 157]. Harnessed and further developed as a consequence of the COVID-19 pandemic, these tools have been used for many years in other disease settings [158-160]. This includes the malaria field, where machine-learning technologies have been used to predict responses to malaria vaccines [161], and genomic data has been used to identify potential immune-dominant antigens for future vaccine studies [100, 102, 162-164]. During the COVID-19 pandemic, large multi-omics datasets were

used to inform and better understand the human immune system, individual responses to infection, and epidemiological trends [165-167] (**Fig. 1.5A**). While the field of systems immunology is still developing, the use of high-throughput multi-omic technologies to understand immune heterogeneity is likely to enhance the efficacy of future vaccines. Furthermore, this highlights the significance of earlier malarial immunological studies, which utilised and developed the precursors to the omics technologies used during the COVID-19 pandemic [163, 168, 169].

An important consideration for all vaccine researchers, which the COVID-19 pandemic has highlighted, is vaccine hesitancy; wherein people elect to refuse vaccination even during a global pandemic emergency. Anxiety about the use of vaccines, which leads to vaccine hesitancy, has occurred since the introduction of vaccines in the late 19th century, and a significant amount of research has been conducted into this phenomenon. It has been found that vaccine hesitancy generally results from a complex mix of cultural, social, religious, and political beliefs and influences [170]. These culminate into an individual's ability to receive and interpret health and scientific information. The spread of inaccurate and misleading information has been massively increased by improved information-sharing technologies [171]. Malaria vaccination trials have been hindered by a range of myths and misinformation that were spread in malaria-endemic regions [172]. During the COVID-19 pandemic, inaccurate and misleading information intensified public confusion and anxiety [170]. The WHO has declared that vaccine hesitancy is becoming a serious threat to vaccination programs [170], and all future vaccination programs will likely need to consider this problem (**Fig. 1.5B**). Ultimately, misinformation must be countered with appropriately trusted and knowledgeable individuals who can communicate vaccine safety and population health benefits [173]. Identifying appropriate individuals to counter misinformation in malaria-endemic regions will remain a significant challenge for malaria vaccine distribution.

Another aspect of vaccinology that has come to light as a result of the COVID-19 pandemic, and that has direct application to malaria, is vaccine inequality. Inequality has greatly influenced both COVID-19 and malaria vaccine development and distribution. Prior to the emergence of COVID-19, the market for developing vaccination technologies, including malaria vaccines, was often perceived as commercially unattractive [174]. Government, non-profit, and philanthropic organisations (*e.g.,* The Bill and Malinda Gates Foundation, The Welcome Trust) provided the majority of funding for malaria vaccine development efforts [175]. In contrast, the majority of COVID-19 vaccines were developed by industry and, once

created, were overwhelmingly secured for use in developed countries [131] (**Fig. 1.5B**). Furthermore, many vaccine platforms require complicated manufacturing, or ultra-low temperature cold chains, making them unsuitable for deployment in many malaria-endemic regions. Incentivising and prioritising the development of novel vaccine platforms suited for local manufacturers and tropical deployment will be optimal for the next generation of COVID-19 and malaria vaccines [131].

Ultimately, integrating immunological and epidemiological data from ongoing COVID-19 and malaria research will be essential for optimizing future deployment and distribution strategies against both diseases (**Fig. 1.5C**). The WHO reports that, on average, $3.5 billion is spent on malaria annually [24]. In contrast, the global economic impact of COVID-19 in 2020 was approximately $11 trillion [176], of which tens of billions were committed to developing single vaccines [177]. Insights gained from malaria research have contributed to the development and distribution of COVID-19 vaccines, and herein, we have discussed several insights from COVID-19 that may improve malaria vaccine development and distribution. However, the contrast in funding levels suggests that many more insights from COVID-19 research could be ascertained to benefit malaria research (**Fig. 1.5C**). Furthermore, if resources on the scale allocated to COVID-19 were similarly directed towards malaria, the prospects for malaria control and eradication could be substantially improved.

1.1.7 Conclusion

On 5th May 2023, the Director-General of the WHO, Tedros Adhanom Ghebreyesus, declared the COVID-19 pandemic over as a global health emergency, 1,221 days after the causative virus was first reported to the WHO [178]. In contrast, malaria continues to persist, much as it has over the last 5,000 years. To end the COVID-19 pandemic, trillions of dollars were spent, and more than 13.3 billion vaccine doses were administered [178]. Applying the immense amount of research collected during the COVID-19 pandemic to develop an effective prophylactic malaria vaccine offers a pathway to significantly curtail the rising global incidence of malaria [94, 179]. While progress towards the development of a highly effective malaria vaccine has been slow, despite extensive efforts spanning more than half a century, recent successes leveraging modern science to develop an effective vaccine against SARS-CoV2 suggests developing an effective vaccine for malaria is achievable.

Acknowledgments

1.2 *Plasmodium* immunology: Insights to inform pre-erythrocytic-stage malaria vaccine design

The work presented in this section comprises a publication pending submission.

Plasmodium immunology: Insights to inform pre-erythrocytic-stage malaria vaccine design

Daniel J. Browne [a,*], Ashton M. Kelly [a,b*], Yomani D. Sarathkumara [a,b*] and Denise L. Doolan [a,b#]

[a] Centre for Molecular Therapeutics, Australian Institute of Tropical Health and Medicine, James Cook University, Cairns, QLD 4878, Australia

[b] Institute for Molecular Biosciences, The University of Queensland, St Lucia, QLD 4072, Australia

1.2.1 Abstract

There is an urgent need for a sustained solution to eradicate the disease malaria, such as the development of a safe and effective prophylactic vaccine. A vaccine directed at the pre-erythrocytic (sporozoite/liver) stage of the *Plasmodium* life cycle would be highly desirable, as such a vaccine would prevent clinical symptoms in the host and halt transmission of the disease. Both the innate and adaptive immune systems contribute to host protection during the pre-erythrocytic-stage of infection, however, many of the critical host-parasite immunological interactions remain unresolved. Herein, we provide an overview of the current understanding of the host immunological response to the pre-erythrocytic stage of a *Plasmodium* infection.

1.2.2 Malaria and the *Plasmodium* life cycle

With almost half of the world's population living within a malaria endemic region, the disease malaria continues to pose a substantial global public health challenge [180, 181]. In 2022, the World Health Organization (WHO) estimated there were 249 million cases and 608,000 deaths attributable to severe malaria. Approximately 75% of these deaths occurred in children under the age of five [181]. In addition to this enormous mortality and morbidity toll, malaria also causes significant economic loss, particularly within developing nations [182]. Malaria is caused by parasitic apicomplexan protists within the genus of *Plasmodium*, which are transmitted by *Anopheline* mosquito vectors. There are four obligate human *Plasmodium* species (*P. falciparum*, *P. vivax*, *P. malariae*, and *P. ovale*) [41, 183], and one zoonotic pathogen (*P. knowlesi*) [42]. However, other under-reported zoonotic species likely also infect humans [43]. Genetic and molecular analyses of *Plasmodium* spp. parasites suggest that these pathogens have been co-evolving with humans and human ancestors for millions of years (**Chapter 1.1: Historical Review**). As part of this complex host-pathogen relationship, the parasite has developed a complex life cycle that transitions between the mammalian host and mosquito vector.

All clinically relevant *Plasmodium* spp. have three main life cycle stages: the (i) pre-erythrocytic (sporozoite and liver-stage), (ii) erythrocytic (blood-stage), and (iii) sexual (or mosquito) stages [41, 183, 184]. The pre-erythrocytic stage begins when an infected female *Anopheline* mosquito draws a blood meal from a mammalian host (**Fig. 1.6A**). *Plasmodium* spp. sporozoites within the mosquito salivary glands are inoculated intradermally and migrate randomly within the skin [185], with most sporozoites having left the injection site within 1-3 hours post inoculation [186]. When the sporozoites encounter a blood vessel, they rapidly

egress through the bloodstream to the liver, typically spending less than 30 minutes in the blood [187] (**Fig. 1.6B**). Within the liver, sporozoites breach through several structures before each infects a single hepatocyte [186]. During the liver-stage, the parasites replicate asexually within a parasitophorous vacuole which matures into a schizont. Each liver-stage schizont may contain between 2,000 to 40,000 developing *Plasmodium* merozoites [188]. During the final stages of the pre-erythrocytic stage, some species of *Plasmodium* schizonts develop as a merosome, an immune-evasion vesicle-like structure [189] (**Fig. 1.6B**).

During a human malaria infection, the erythrocytic stage begins synchronously, typically five to ten days following infection [190]. Although, parasites of some *Plasmodium* species can persist inside hepatocytes for weeks to years [191]. Merozoites may be released following the rupture of an infected hepatocyte, or following merogony (budding) of merosomes secreted into the hepatic portal vein [189]. The individual merozoites rapidly, and synchronously, invade a host erythrocyte, mature into trophozoites, and undergo another round of asexual multiplication developing into an erythrocytic stage schizont [60] (**Fig. 1.6C**). Each erythrocytic schizont contains between 8 to 36 merozoites [192]. These erythrocytic schizonts then burst in a synchronous pattern, releasing the next round of merozoites into the bloodstream, most of which continue replicating asexually, creating more erythrocytic schizonts. The growing parasitemia, following waves of reinfection and rupture, causes the paroxysms of fever alternated with periods of fatigued wellness, which are the characteristic clinical symptoms of malaria [193]. Severe malaria can develop during the erythrocytic stage, typically as parasitised erythrocytes sequester within the host microvasculature [194].

During the erythrocytic stage, a small proportion of merozoites will mature into gametocytes, commencing the sexual stage of the parasite's life cycle (**Fig. 1.6D**). To complete the life cycle, a female *Anopheline* mosquito must take up mature male (microgametocytes) and female (macrogametocytes) gametocytes during a blood meal. Within the mosquito's midgut, the microgametocytes penetrate the macrogametocytes, creating a diploid zygote. The zygote rapidly performs meiosis to produce haploid daughter cells [195], which attach to the midgut wall, form an oocyst, and reproduce by mitosis into thousands of daughter cells. These cells mature into sporoblasts, which ultimately lyse the oocyst, enter the mosquito's salivary glands, mature into sporozoites, and prepare to continue the cycle during the next blood meal. [183, 196] (**Fig. 1.6E**).
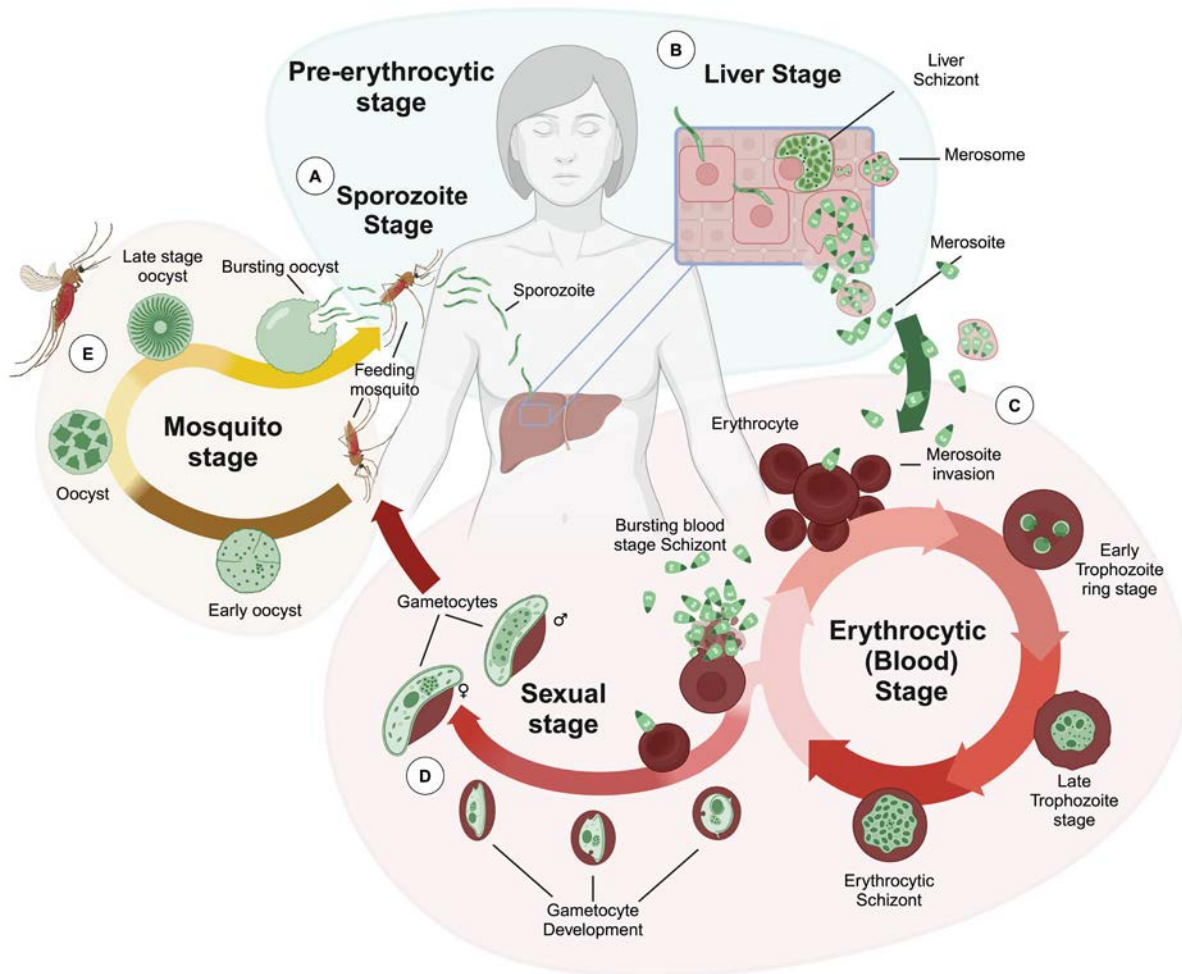
Figure 1.6. The *Plasmodium* spp. life cycle (Immunological Review). **(A)** The life cycle begins in the obligate human host when an individual is bitten by an *Anopheline* mosquito infected with *Plasmodium* spp. sporozoites. Then sporozoites quickly traverse through the bloodstream to **(B)** the liver, where a single sporozoite traverses through multiple hepatocytes to settle in one. **(C)** The sporozoite will then rapidly begin to asexually reproduce, creating schizonts of merozoites, which will burst, leading to merozoite invasion of red blood cells, beginning the erythrocytic stage of infection. Blood-stage schizonts, upon bursting, can either continue in asexual reproduction or enter the **(D)** sexual stage of the *Plasmodium* life cycle, where merozoite-infected red blood cells will begin to produce male and female gametocytes. **(E)** Eventually, during an Anopheline mosquito blood meal, these male and female gametocytes may be taken up, leading to the mosquito stage of the *Plasmodium* spp. life cycle, where gametocytes will infect the mosquito midgut and begin sexual reproduction, producing oocysts of immature sporozoites, which then travel to the mosquito salivary glands, ready to infect another human. Image created by Ms Ashton Kelly.

1.2.3 Naturally acquired immunity to malaria

The human immune response to a *Plasmodium* spp infection is complex and not completely understood. Naturally acquired immunity (NAI) to *Plasmodium* spp infection typically only provides protection against severe malaria and does not confer sterile protective immunity [76]. Furthermore, NAI is only observed in individuals chronically exposed to *Plasmodium*, as a remarkably high number of repeated and sustained infections are required to attain and maintain NAI [76]. Nevertheless, NAI protects millions of people globally and, amongst chronically exposed individuals, has virtually 100% efficacy against severe disease [76]. The immune response of NAI primarily promotes tolerance to blood-stage parasites and has been extensively reviewed elsewhere [70, 197-200]. In general, blood-stage human immunity is characterised by a B cell-driven humoral (antibody) response [201], both T cell-independent and T cell dependent (supported by $CD4^+$ T helper cells) [202]. Ideally, a prophylactic malaria vaccine would be able to confer sterile protective immunity, thus an erythrocytic-stage vaccine would be required to exceed the protection afforded by NAI. Several promising erythrocytic stage vaccines in development are demonstrating that improving blood-stage immunity is possible [200, 203]. Alternatively, an effective pre-erythrocytic stage prophylactic malaria vaccine would prevent the host from experiencing clinical symptoms (*i.e.,* symptomatic blood-stage parasitemia) and prevent further transmission of the disease (*i.e.,* sexual stage reservoir vector transmission) [3], and therefore, would be ideal for controlling malaria [69, 200, 204].

1.2.4 Induction of pre-erythrocytic stage immunity

During the late 1960s and early 1970s, a series of seminal studies demonstrated that sterile immunity against *Plasmodium* sporozoite challenge could be induced in mice and humans following radiation attenuated sporozoite (RAS) immunization [81]. Critically, these studies demonstrated the optimal dosage of radiation to produce an effective RAS vaccine required the attenuated sporozoites to remain metabolically active enough to infect the liver, but not progress to the blood stage of infection [82-84]. These studies established that pre-erythrocytic stage adaptive immunity could provide sterile infection-blocking protective immunity against subsequent sporozoite challenge. This promise was further bolstered by the cloning of the coat protein of the *Plasmodium* sporozoite, the Circumsporozoite protein (CSP), in 1984 [92], which subsequently become the leading vaccine antigen. The two currently licenced malaria vaccines specifically promote pre-erythrocytic stage immunity against CSP [107, 110]. However, despite these and other successes driven by efforts spanning more than half a century, a highly

effective malaria vaccine has not yet been developed. In part, this can be attributed to a relatively poor understanding of the innate and adaptive immune response to the pre-erythrocytic stage of malaria. Herein, we will review the current understanding of immunity to the pre-erythrocytic stage of a *Plasmodium* infection and consider how these insights may inform pre-erythrocytic stage vaccine development.

1.2.5 Sporozoite-stage immunity

The sporozoite stage of the pre-erythrocytic stage of a *Plasmodium* infection occurs over a relatively short period (*i.e.,* several hours), representing a comparatively small window of opportunity for host immunity to respond to infection. *Plasmodium* sporozoites are inoculated through the epidermal barrier and avoid innate and adaptive immunity with gliding motility and rhoptry-mediated cytosis [205-207]. Furthermore, adaptive immunity appears suppressed while sporozoites remain in the skin (**Fig. 1.7A**). This is potentially due to CD4$^+$ regulatory T (T$_{reg}$) cells, which control the immune response by providing immunologically suppressive signals [208, 209]. T$_{reg}$ cells appear to be indirectly activated following a mosquito bite, specifically by factors present in mosquito saliva [209]. As sporozoites migrate intra-dermally, those that enter the lymphatic system are typically phagocytosed by dendritic cells (**Fig. 1.7B**) [210]. This process appears to be an important route for adaptive immune activation [3, 211].

It has been hypothesised that sporozoites are most vulnerable to humoral immunity when they are in the skin (**Fig. 1.7A**) [212]. Antibody-mediated immunity, therefore, plays a major role in controlling the pre-erythrocytic stage of a *Plasmodium* infection. Antibodies can opsonize sporozoites, initiate phagocytosis, inhibit sporozoite gliding-motility, initiate antibody-mediated complement lysis, and block rhoptry-mediated endocytosis, ultimately preventing sporozoite invasion or traversal in the skin or into host hepatocytes (**Fig. 1.7C**) [205-207]. As sporozoites 'trickle out' of the inoculation site and enter the blood, they rapidly egress to the liver. Therefore, antibodies can only act against sporozoites in the blood for a relatively short window of time, and it is likely that high titers of antibodies will be required to provide effective sterile protection (14). It was first demonstrated in 1972 in a *P. berghei* mouse infection model that anti-sporozoite peripheral-blood antibodies increased clearance rates after receiving passively transferred serum from RAS-immunized mice [213]. Similar results were reported in a liver-humanized mouse model, where liver-stage parasite burden was decreased in mice following *P. falciparum* challenge after sera infusion from RAS immunized human volunteers [212, 214, 215]. During the initial skin-stage of a *Plasmodium* infection, antibody-mediated

immunity was observed by intravital microscopic studies. These studies demonstrated antibody-driven inhibition of sporozoite motility and sporozoite invasion of dermal blood vessels in RAS immunized mouse models [216-218]. Several studies have demonstrated that opsonised sporozoites can be phagocytosed *in vitro* by Kupffer cells (KCs) [219-221], or monocytes [222, 223], or targeted by complement-mediated lysis. Additionally, titers of anti-CSP antibody isotypes and subclasses (IgG1, IgG3, and IgM) have a reported association with protection [224-226].
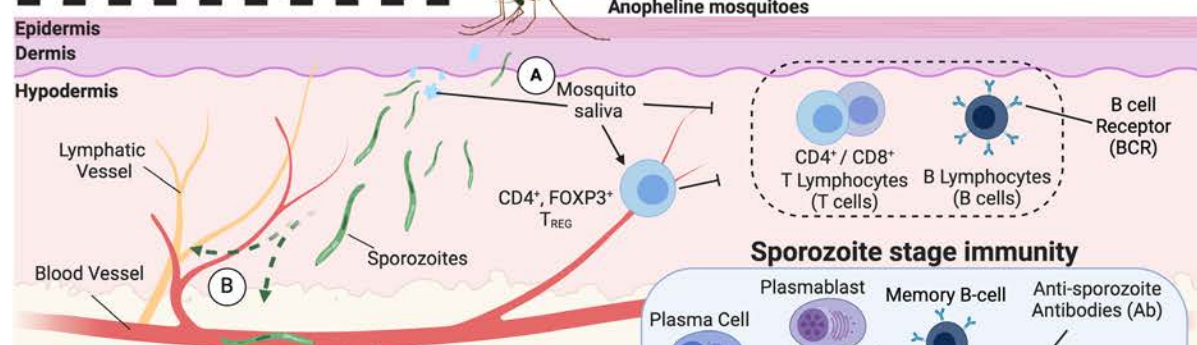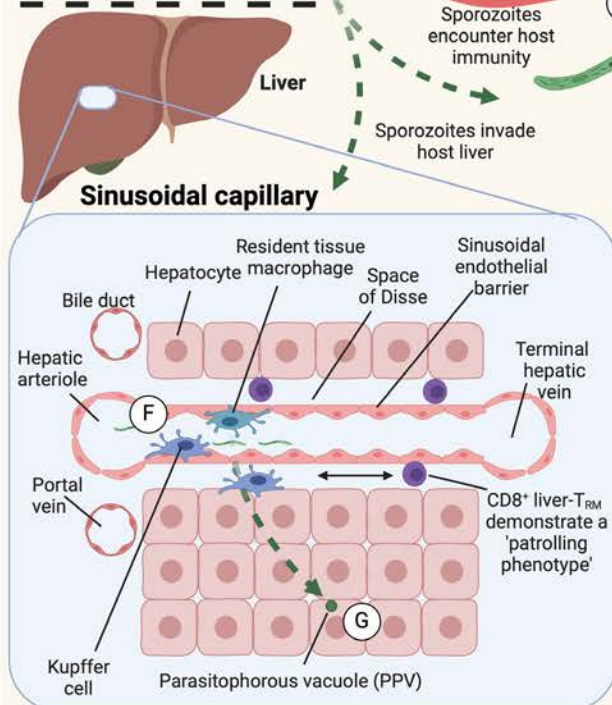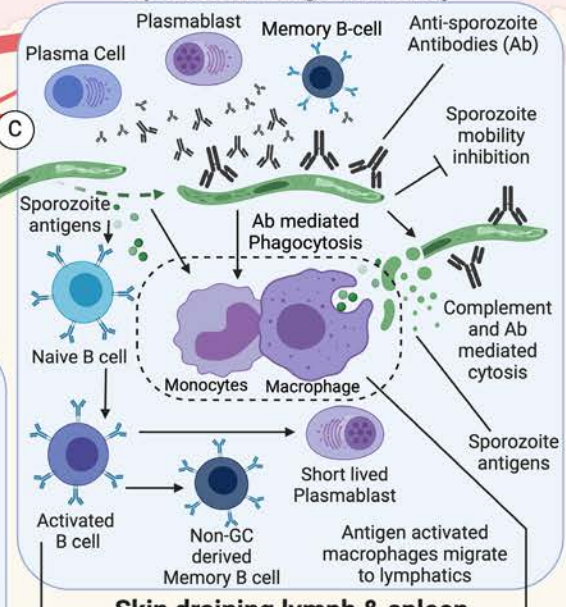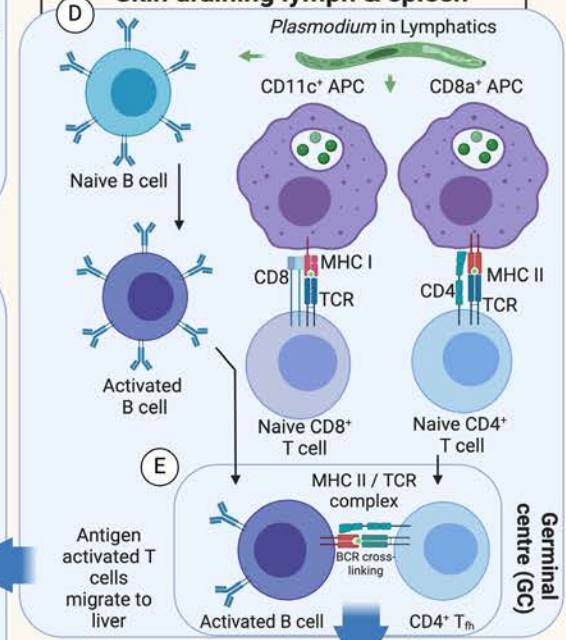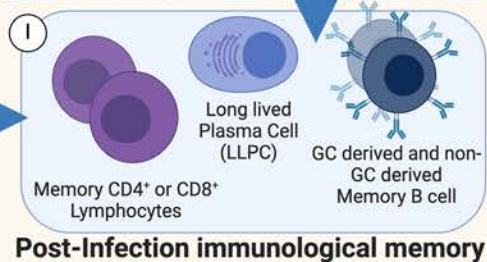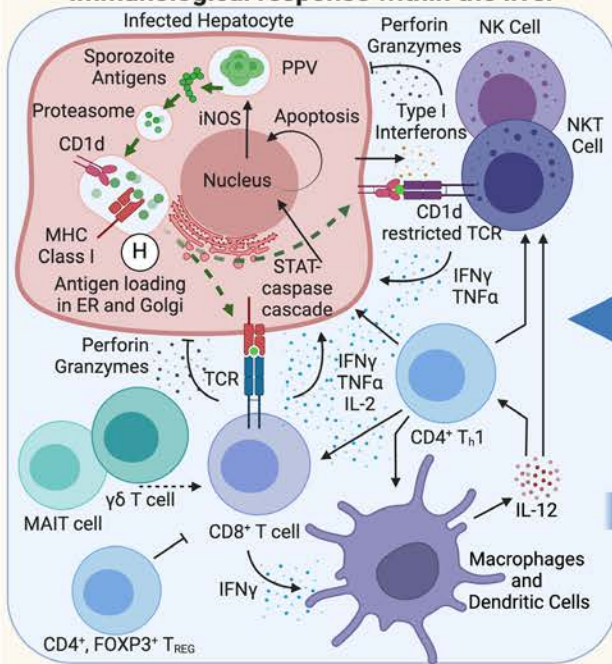
Figure 1.7. Host immunological response to the pre-erythrocytic stage of a *Plasmodium* infection.
The immunological response of the pre-erythrocytic stage is divided between the 'sporozoite stage' and
the 'liver-stage'. **(A)** Inoculated sporozoites migrate intradermally with rhoptry and microneme-
mediated cytosis. **(B)** Sporozoites egress into peripheral blood or lymphatic vessels. **(C)** While in the
skin and the blood, sporozoites can be opsonised by sporozoite-specific antibodies (Abs), leading to i)
initiate phagocytosis, ii) inhibition of sporozoite motility and traversal or iii) complement-meditated
lysis. Naïve B cells are activated and differentiate upon encountering sporozoite antigen in the
periphery. Some of these activated B cells proliferate and differentiate into plasmablasts, secreting
short-lived Abs as an immediate response to infection, and others develop into Germinal centre (GC)
independent early memory B cells (MBCs). **(D)** Naïve B cells can also become activated at the spleen
and the skin draining lymph. **(E)** Activated B cells migrate to the GC, and within the GC, B cells interact
with CD4$^+$ T follicle (T$_{fh}$) cells activated by antigen presenting cells (APCs). **(I)** These GC activated B
cells differentiate into long-lived plasma cells (LLPCs) secreting high affinity isotype-switched
antibodies or into mature memory B cells (MBCs). **(F)** Sporozoites which avoid sporozoite stage
immunity migrate to the liver where they enter host hepatocytes by crossing the sinusoidal endothelial
barrier, often traversing through liver resident macrophage Kupffer cells and several layers of host
hepatocytes. **(G)** The sporozoite surrounds itself with a parasitophorous vacuole (PVV) and begins
multiplication into thousands of daughter cells. **(H)** Intracellular sporozoite antigens are processed and
displayed extracellularly on major histocompatibility complex (MHC) proteins such as MHC class I
(for recognition by CD8$^+$ T cells) and CD1d (for recognition by Natural Killer T (NKT) cells).
Innate/adaptive interface cells such as gamma-delta T cells ($\gamma\delta$ T cells) and mucosal invariant T (MAIT)
cells have been associated with protection and may provide support to CD8$^+$ T cells. T cells activated
in the spleen or skin draining lymphatics migrate to the liver. CD4$^+$ T cells, Natural Killer (NK) cells
and NKT cells are stimulated further by IL-12 secreted by IFN-γ activated liver macrophages. CD8$^+$ T
cells, NK cells and NKT cells secrete IFN-γ, and TNFα which induce infected host-hepatocytes to clear
PVVs by producing iNOS, or can secrete perforin and granzymes to induce host-hepatocyte apoptosis.
Pathology from over-stimulated immunity is controlled by CD4$^+$ FOXP3$^+$ T regulatory (T$_{reg}$) cells. **(I)**
Post-infection a small population of long-lived CD4$^+$ and CD8$^+$ T cells, Tissue-resident (T$_{RM}$) T cells,
and LLPCs or Memory B cells remain as memory cells to provide an immediately reactive adaptive
immune response. Generating an effective memory population is a major goal of pre-erythrocytic stage
vaccines.

Adaptive humoral immunity is driven by activated B lymphocytes (B cells). Initial binding and
recognition of a parasite antigen by B cell receptors (BCR) activate naïve B cells, which can
differentiate into short-lived memory cells (*i.e.,* non-germinal centre derived memory B cells)
or effector short-lived plasmablasts (**Fig. 1.7C**). Short-lived plasmablasts are proliferating cells

rapidly formed in secondary lymphoid organs which may only live for few days [227]. Plasmablasts express unswitched or isotype-switched immunoglobulin (Ig), which provides a rapid antigen clearance response by secreting antibodies (*i.e.*, IgM, IgD); however, these antibodies have a relatively lower affinity [228]. To develop long-term humoral immunity, some activated B cells can migrate to the lymphatic germinal centre (GC) to undergo somatic hypermutation, affinity maturation, and class-switch in the Ig genes [228]. B cells are antigen-presenting cells that can present sporozoite antigens as peptide epitopes on major-histocompatibility complex class II (MHC II). Additionally, in the GC, $CD4^+$ T follicular helper ($CD4^+$ T_{fh}) cells provide specialized help to GC B cells through cognate T-B cell interactions [229] (**Fig. 1.7E**). These interactions in the GC between activated $CD4^+$ T cells and antigen-presenting B cells facilitates hypermutations in Ig genes and Ig isotype switch [228, 230]. These GC activated B cells differentiate into mature memory B cells (MBCs) or long-lived plasma cells (LLPCs) (**Fig. 1.7I**), which persistently produce class-switched (i.e., IgG) and high-affinity antibodies and form the basis of long-lived protective humoral immunity [231].

The process underlying sporozoite-specific formation of MBCs is poorly characterized [232]. Nevertheless, long-term high-affinity MBCs are reliably detected in individuals who live in malaria seasonally pandemic areas [233], emigrants from endemic areas [234], those who have been infected while traveling through endemic areas [235], or RAS immunized individuals [236]. Counterintuitively, epidemiological studies in naturally exposed human populations in malaria-endemic areas have revealed unusually slow development of malaria-specific B cells, which are associated with a relatively short-lived antibody response [237, 238]. It has been hypothesised that the inefficient development of humoral immunity in populations continuously challenged by *Plasmodium* is the result of Memory B cell exhaustion [232, 239-241]. The mechanism which causes memory B cells to develop an exhausted phenotype is currently unknown [232].

While continually infected individuals in endemic areas have a lower prevalence of MBCs and LLPCs than those not chronically infected, they tend to have an increased number of atypical memory B Cells (aMBCs) [240, 242]. These atypical memory B cells are a population of memory B cells which are defined by their lack of CD27 expression. The mechanism for generating these aMBCs is unknown [242]. Although MBCs and aMBCs share a common developmental history, the functional characteristics of aMBCs are challenging to study *in vitro*

due their minimal response to classic BCR cross-linking [242, 243]. Interestingly, the expansion of aMBCs has also been observed in malaria-naïve individuals vaccinated with RTS/S [244], and these cells have been associated with autoimmunity, and increased disease severity, including during a *P. vivax* infection [245-247].

1.2.6 Liver-stage immunity

The liver-stage of a *Plasmodium* spp. infection is initiated when sporozoites in the peripheral circulation enter a liver hepatocyte. This process involves the sporozoites crossing the sinusoidal endothelial barrier, often transiting through KCs (**Fig. 1.7F**) [248, 249] and multiple hepatocytes before infecting a final host hepatocyte (**Fig. 1.7G**) [54]. The most important innate immune response to an initial *Plasmodium* spp. infection is the secretion of type 1 Interferon (IFN) cytokines by infected hepatocytes to recruit innate lymphoid cells such as Natural Killer (NK) cells, Natural Killer T (NKT) cells, and T cells with semi-invariant T cell receptors (TCRs) such as gamma-delta T (γδT) cells [248, 250] (**Fig. 1.7H**). KCs are also thought to play an important role in liver innate immunity by releasing innate lymphoid cell chemoattractant cytokines. Mouse models have demonstrated that KCs can be inactivated or destroyed following sporozoite infection [251-253], while others have shown KCs may persist [254]. It is currently unknown if human KCs are killed or can present peptide epitopes to T cells and secrete cytokines following sporozoite traversal [248]. The physical structure and function of the liver make the organ vulnerable to parasitic infection, while simultaneously facilitating host immunity (**Table 1.1**).

Table 1.1. Physical features of the liver that influence immunity

	Physical feature	**Mechanism of action**	**Reference**
Facilitate parasite invasion	Large blood volume (1.5$_{L/min}$) passes through the liver	Draws parasite rapidly to organ	[248]
	Tight junctions are not present between sinusoidal endothelial cells	Parasites quickly cross the initial barrier	[255]
	Endothelial cells and hepatocytes are not separated by a basement membrane	The parasite can move rapidly through the space of Disse	[255]
	Vascularity and surface area of the liver reduces blood flow (relative to other organs)	Increased parasite contact time with the organ	[256]
	The hepatic portal venous system	Constant exposure to non-self-antigens creates an immune-privileged window of opportunity for parasitic infection	[257]
Facilitate host immunity	High blood volume and open architecture allows constant exposure of hepatocytes to CD8$^+$ T cells	Cytotoxic lymphocytes are constantly patrolling hepatocytes and testing potential presented antigens	[258]

It is now appreciated that several cell types conventionally thought of as innate also share characteristics with the adaptive immune system. For example, NK cells blur the commonly recognised boundaries that were presumed to exist between innate and adaptive immunity [259, 260]. NK cell subsets can exhibit memory phenotypes, such as responding rapidly to previously presented viral antigens with enhanced immune effector function [261-264]. Two key pathways associated with memory in NK cells are specificity to viral antigens and recalled responses to specific cytokine signalling cascades [262, 265-270]. Memory-like NK cells can react more quickly than naïve NK cells and can persist in secondary lymphoid organs following infection [265, 266, 269]. Indeed, NK cells have been associated with RAS and DNA vaccine-induced protection in mouse models of *P. yoelii* challenge [271]. A proposed mechanism involves NK cell activation from Interleukin 12 (IL-12) secreted by Interferon-gamma (IFN-γ) activated liver macrophages (**Fig. 1.7H**) [69]. However, NK cell activation and production of IFN-γ and TNF-α can also be regulated by CD4$^+$ and CD8$^+$ T cells [272]. The specific role NK cells in immunity to malaria remains largely unresolved [273].

Other cell populations at the interface of the innate and adaptive immune systems, such as Natural Killer T (NKT) cells, γδ T cells, Mucosal Associated Invariant T (MAIT) cells, have also been implicated in pre-erythrocytic stage *Plasmodium* immunity (**Fig. 1.7H**). NKT cells share some similar effector functions to NK cells [274], and are divided into two larger subgroups: Type I NKT (invariant/iNKT) and Type II NKT (variant/vNKT) [275]. Mouse models have suggested that iNKTs are required for Type I IFN-mediated immune responses following *P. yoelii* challenge [276]. However, excessive NKT cells have also been associated with splenomegaly in a mouse model following *P. berghei* challenge, suggesting a potential pathogenic role for this cell population [277]. The exact role of NKT cells in immunity to *Plasmodium* remains unresolved as NKT cell-deficient mice (CD1d$^{-/-}$) can still control the sporozoite challenge [278].

γδ T cell expansion has been identified following natural *Plasmodium* spp. infection of children and adults, typically observed in acute infections [279, 280]. The proportions of γδ T cells (specifically the Vγ9Vδ2 chains subsets [281, 282]) before and after vaccination with RAS correlated with higher rates of sterile protection in both pre-clinical mouse and human trials [215]; however, this effect appears to be age-dependent, with Vδ2$^+$ T cells representing only a minor subset of the γδ T cell repertoire in infants [116]. Interestingly, recent reports have identified Vδ2$^+$ γδ T cells as being inversely associated with prolonged exposure to malaria, whereby individuals repeatedly infected have fewer, or even dysfunctional, Vδ2$^+$ γδ T cells [283, 284]. Varying roles of γδ T cells have been reported, with different populations having either beneficial or harmful effects depending on the type of infection or vaccination and the duration of exposure [285, 286]. MAIT cells, which comprise an estimated 20-50% of the T cell population of the human liver [287], appear likely to have effector roles in the context of *Plasmodium* spp. immunity [288, 289]. However, their specific roles remain unresolved with several proposed effector functions [67, 290].

Once a sporozoite has infected a host hepatocyte, conventional T lymphocytes become the key effector immune cells. Conventional T cells can be further classified into CD4$^+$ T cells and CD8$^+$ T cells. CD4$^+$ T cells typically promote the effector function of other immune cells (*e.g.,* B cells and CD8$^+$ T cells); while CD8$^+$ T cells (*i.e.,* cytotoxic T lymphocytes) can secrete proteins which induce host-cell apoptosis [291-293]. CD8$^+$ T cells are considered the critical effector cell mediating protective immunity directed at the liver-stage of *Plasmodium* spp. infection [67, 69, 272, 294]. The cytokine IFN-γ produced by CD8$^+$ T cells is considered the primary immune effector mechanism of liver-stage immunity [69, 295]. CD8$^+$ T cells are

typically activated by hepatocytes displaying parasite antigen; however, they may also be activated by macrophages and dendritic cells that have phagocytosed sporozoites in the skin, blood, spleen or peripheral lymph nodes [3].

CD8^{+} T cells primarily act indirectly on infected hepatocytes by secreting pro-inflammatory cytokines such as IFN-γ and Tumour Necrosis Factor (TNF) (**Fig. 1.7H**). Signalling by IFN-γ can activate inducible nitric oxide synthase (iNOS) through the L-arginine-dependent pathway, eliminating intrahepatic schizonts through the production of nitric oxide, and enhance antigen presentation by upregulating genes associated with peptide processing and presentation through the MHC I pathway [69, 296]. The crucial role of IFN- γ has been shown in mice where wild-type mice were protected against *P. berghei* sporozoite challenge by intravenous administration of IFN-γ [297, 298]. Similarly, wild-type mice depleted of IFN-γ by administration of anti-IFN-γ mAb or IFN-γ receptor knockout mice following immunisation with *P. yoelii* RAS were not protected against *P. yoelii* sporozoite challenge [272, 299]. In addition to this indirect effector role of CD8^{+} T cells, there is also evidence that during a *Plasmodium* spp. infection, CD8^{+} T cells can act directly in a cytotoxic fashion by secreting perforin or granzymes to induce infected hepatocyte apoptosis through STAT-caspase cascade [69, 300].

The importance of CD8^{+} T cells in protection against *Plasmodium* spp. infection was originally contentious since the number of sporozoites inoculated is relatively low, and the liver-stage of the *Plasmodium* spp. life cycle was considered too short to offer adaptive immunity time to mount an optimal response [301]. This was based upon the assumption that CD8^{+} T cell activation required interactions with infected hepatocytes which would be relatively rare [301, 302]. However, it is now apparent that skin draining peripheral lymph nodes is a major site of CD8^{+} T cell activation with smaller contributions by spleen and hepatocytes [303]. Indeed, once activated in the periphery, CD8^{+} T cells circulate and quickly migrate to the liver to seek out infection, though the molecular mechanism of this biological seeking is currently unknown [248]. Nevertheless, it has been estimated that 100-1000 times more CD8^{+} T cells are required for sterile protection following *Plasmodium* infection than for sterile protection against viral and bacterial pathogens [304, 305]. It is unclear why such large numbers of CD8^{+} T cells are required [248].

CD4^{+} T cells (*i.e.,* T helper cells) play an important role across all stages of *Plasmodium* spp. pre-erythrocytic immunity [67, 306]. CD4^{+} T cells can be sub-classified into five major groups

dependent upon the cytokines, surface markers and transcription factors they express: (i) T-helper 1 CD4$^+$ T (T$_h$1) cells primarily support cell-mediated immunity by producing IFN-γ, Interleukin-2 (IL-2) and TNF cytokines; (ii) T-Helper 2 CD4$^+$ T (T$_h$2) cells primarily support humoral immunity by producing IL-4, IL-5, IL-10 and IL-13 [307]; (iii) Follicular B helper T (CD4$^+$ T$_{fh}$) cells facilitate B cell maturation into higher affinity and longer-lived cells in germinal centres; (iv) T-helper regulatory (T$_{reg}$) cells express the FOX/P3 transcription factor and control the immune response by providing immunologically suppressive signals, such as producing IL-10 [308]; and (v) T$_h$17 CD4$^+$ T cells produce IL-17 which suppresses T$_{reg}$ function [309].

T$_h$1 CD4$^+$ T cells appear to be a key CD4$^+$ T cell immune effector in liver-stage immunity to *Plasmodium* spp. infection. T$_h$1 CD4$^+$ T cells act by secreting IFN-γ and Interleukin 2 (IL-2) [310-312]. IFN-γ and IL-2 secreted by T$_h$1 CD4$^+$ T cells can act directly upon infected hepatocytes or influence other immune effector cells, such as stimulating CD8$^+$ T cells, macrophages, NK, NKT cells and others (**Fig. 1.7H**) [313]. Sporozoite antigen-experienced CD4$^+$ T$_{fh}$ cells migrate to germinal centres and mediate the selection and survival of *Plasmodium* antigen-specific B cells (**Fig. 1.7E**) [67, 306]; *P. berghei* and *P. yoelii* mouse models have shown that CD4$^+$ T cell-dependant (T$_h$2) B cell responses can neutralise the ability of sporozoites to invade hepatocytes [216-218]. Despite conflicting results following T$_{reg}$ depletion assays in malaria mouse models, a growing body of evidence suggests that T$_{reg}$ cells maintain homeostasis during a *Plasmodium* spp. infection by curtailing over-vigorous effector responses (**Fig. 1.7H**) [314]. As with other CD4$^+$ T cell types, the exact induction and mode of action of T$_{reg}$ cells during pre-erythrocytic immunity to a *Plasmodium* spp. infection remains unclear [67]. It is likely that harnessing CD4$^+$ T cell subsets to improve pre-erythrocytic stage vaccine efficacy will be required to provide sterile protective immunity to malaria. However, it remains an outstanding question in immunological research: what CD4$^+$ T cell subsets can be harnessed to improve vaccines, or what kind of contribution they can make to the outcomes of malaria [288, 314].

Once a *Plasmodium* spp. infection is cleared, a small population of long-lived CD4$^+$ and CD8$^+$ T cells remain as memory T cells (**Fig. 1.7I**). Memory T cells have traditionally been classified into two broad categories: effector memory T cells (T$_{EM}$) found in peripheral tissue (defined by the markers: CD45RO$^+$, CCR7$^-$ and CD62L$^-$), and central memory T cells (T$_{CM}$) found in lymphatic tissue (defined by the markers: CD45RO$^+$, CCR7$^+$ and CD62L$^+$) [315]. Following further exposure to antigen, memory T cells can become terminally differentiated (*i.e.,*

CD45RA$^+$ TEMRA cells) [316], potentially resulting in T cell exhaustion [317] and eventual senescence and apoptosis [318, 319]. More recently, tissue-resident memory T cells (T$_{RM}$) have been identified as an important memory subset [320], with significant diversity specifically within CD4$^+$ T lymphocyte tissue-resident memory cells (T$_H$T$_{RM}$). Each CD4$^+$ T cell subset has individual memory T cell lineages, with potentially further T$_H$T$_{RM}$ embedded subsets [66]. Tissue-resident CD8$^+$ memory T cells have been found in all tissue types thus far studied, and the distribution and subtyping of these cells continue to be an area of active research within immunology [321].

Although both CD4$^+$ and CD8$^+$ memory T cells appear essential in providing long-lived sterile immunity following the sporozoite challenge, it is not known if they act alone or only provide a 'sensing and alarm' function [322]. Mouse models have demonstrated populations of CD8$^+$ liver-T$_{RM}$ which have correlated with protection against intravenous sporozoite challenge [104, 302, 323, 324]. *Plasmodium* specific liver-T$_{RM}$ reside within sinusoids and space of Disse [302, 325], and when in the sinusoid, demonstrate a patrolling phenotype [326]. When equivalent numbers of antigen-specific CD8$^+$ T cells or activated CD8$^+$ liver-T$_{RM}$ cells were transferred into mice which were later intravenously challenged with *P. yoelii* sporozoites, only those who had received liver-T$_{RM}$ cells displayed a reduction in parasite burden [323]. This supports that the induction of robust CD8$^+$ (and CD4$^+$) liver resident liver-T$_{RM}$ against *Plasmodium* spp. antigens by vaccination would be important for protection against *Plasmodium* sporozoites. Theoretically, such vaccine-induced memory cells would provide an immediately responsive cell population rather than waiting for recruitment from circulating memory cells upon future *Plasmodium* infections.

1.2.7   Conclusion and future directions

Developing an effective prophylactic pre-erythrocytic stage malaria vaccine offers a pathway to significantly curtail the disease malaria [94, 179]. However, no currently licenced malaria vaccine provides optimal efficacy or duration of protection [107, 110]. Herein we have reviewed the current literature regarding the cellular and humoral immune response to the pre-erythrocytic stage of *Plasmodium* infection to provide insights to improve pre-erythrocytic vaccine development. Overall, sporozoites inoculated into the skin and traversing the peripheral circulation are primarily vulnerable to antibody-based humoral immunity. In contrast, sporozoites that reach the liver and invade host hepatocytes are predominantly cleared by CD4$^+$ and CD8$^+$ T-cell-based cellular immunity. Humoral immunity will likely require

extremely high titres of antibodies, and cellular immunity will require high numbers of antigen-specific T cells to provide effective sterile immunity.

There are numerous immune mechanisms and host-parasite interactions during the pre-erythrocytic stage that remain unresolved. Highly clinically significant insights could be gained by elucidating the mechanisms underlying the relatively slow development, short duration, and limited memory formation of sporozoite-specific B cells. During the liver stage, the definitive roles of innate and innate-adaptive interface cells, such as Kupffer cells, NK cells, NKT cells, $\gamma\delta$ T cells, and MAIT cells, are unclear. Understanding the precise induction, mode of action, and pathways of memory cell formation of $CD8^+$, Th1 $CD4^+$, and T_{reg} T cells during liver-stage pre-erythrocytic immunity to *Plasmodium* spp. infection is expected to clarify why such large numbers of cells are required for protective immunity and, therefore, provide further insights for the next generation of pre-erythrocytic stage vaccines.

Acknowledgments

1.3 Thesis objective and aims

1.3.1 Background

Vaccination remains the most successful medical intervention in history. Highly effective vaccines that induce long-term immunity have been instrumental in eradicating smallpox and dramatically reducing the incidence of dozens of infectious diseases including polio, measles, mumps, rubella, anthrax, chickenpox, meningococcal and pneumococcal [26]. However, for many diseases, effective vaccines still do not exist. An example of a pathogen that has been extremely resistant to vaccine development efforts is the *Plasmodium spp* parasite [31]. These complex parasites have co-evolved with human and human ancestors for millions of years and developed extremely sophisticated immune evasion strategies [76]. Another example is the more recently evolved and far less complex pathogen, Severe Acute Respiratory Syndrome coronavirus 2 (SARS-CoV2). The proteome of SARS-CoV2 is highly immunogenic, and vaccines that include the highly expressed SARS-CoV2 Spike-protein antigen offer robust protection, yet, vaccine-induced humoral and cellular immunity against SARS-CoV2 is not long-lived [124]. Developing a thorough understanding of the T cell immune responses to these pathogens following vaccination and natural infection may provide insight for the development of vaccines that can provide enduring protection.

Long-term protective immunity is dependent on the development of long-lived memory B and T cells [322]. When considering *Plasmodium* infection, T cell-based cellular immunity is critical for protective immunity during the pre-erythrocytic infection, the only stage where sterile protective immunity against *Plasmodium* challenge has been observed [76, 272]. When considering SARS-CoV2 infection, mild COVID-19 has been associated with rapid development of T cell immunity [327], and individuals with rare hypogammaglobulinemia disorders (*i.e.,* are unable to generate endogenous antibodies) have similar rates of mortality [328]. It is clear, and increasingly well documented in the growing literature, that cellular immunity plays a critical role in both *Plasmodium* and SARS-CoV2 infections. Understanding the development of T cell immunity, specifically which T cell epitopes are immunoreactive and immunodominant following infection or vaccination, is crucial to understand the complexities of host-pathogen immunity to inform the development of effective and enduring vaccines for both malaria and COVID-19.

1.3.2 Immunodominance

T cell epitope immunodominance is the phenomena whereby the bulk of responding T cells recognise only a tiny fraction of potential pathogen peptide epitopes [329]. The formation of an immunodominance hierarchy of T cell peptide epitopes is a complex and incompletely understood process which can be broadly categorised as: i) factors intrinsic to the antigen (*e.g.*, protein abundance, protease cleavage) or, ii) factors intrinsic to the epitope (*e.g.*, antigen processing, major histocompatibility complex (MHC) binding affinity, and T cell precursor frequency) [330-332]. For the initiation of a strong adaptive immune response, native antigen must be efficiently protolyzed into antigenic peptides, loaded onto a MHC class I or II complex and subsequently recognised by an appropriate TCR repertoire [333]. Indeed, the tripartite interaction of the TCR-MHC-peptide is the dominant paradigm of the major determinants of immunodominance [334-338]. Of this tripartite, MHC-peptide binding appears to be the major determinant of immunodominance, as only around 1% of potential peptide epitopes bind with sufficient affinity to any given MHC allele to elicit a T cell response [329]. Peptides must bind with high affinity to the MHC binding cleft in order to be displayed for recognition by the T cell, and as such, antigenic peptide epitopes are restricted to recognition in the context of certain MHC alleles (*i.e.*, MHC restriction) [339]. Although MHC restriction significantly reduces the number of potential epitopes, the interaction between the TCR and the MHC-peptide complex further narrows this pool, often to just a few dozen or even less epitopes. Each individual T cell expresses a unique TCR, generated by V(D)J genetic recombination [340]. If a TCR binds with high affinity to an MHC-peptide complex, a series of cellular signalling cascades occur which culminate in an adaptive cellular immune response. Immunodominant peptide epitopes are recognised by more abundant T cell populations, while subdominant epitopes are recognised by less abundant T cell populations [329, 341].

1.3.3 Foundational studies

To enhance our understanding of T cell immunodominance following *Plasmodium* infection (**Objective 1**), this thesis builds upon foundational data generated by the Doolan Laboratory [342]. The genome of clinically relevant *Plasmodium* range between 21 and 36 Mb in size and encode more than 5,000 putative proteins [343, 344], with each protein potentially containing tens of thousands of peptide epitopes. Therefore, there are potentially millions of *Plasmodium* peptide epitopes available for an adaptive cellular immune response. The Doolan laboratory has previously identified, from the complete *P. falciparum* proteome, the subset of antigens

preferentially expressed targeted by T cell responses [Unpublished Data]. For those studies, a set of ~1500 proteins representing all proteins thought to be expressed in the sporozoite and liver stage were determined from all *Plasmodium* genomic, transcriptomic, and proteomic information available via the *Plasmodium* bioinformatics repository (www.PlasmoDB.org). Putative CD4+ and CD8+ T cell epitopes which bound with high affinity to MHC Class I (HLA-A2, -A3/11, -A24) and MHC class II (HLA-DR) HLA 'super-types' [345] were predicted for each antigen and allele combination using the epitope prediction tool of the Immune Epitope DataBase (www.iedb.org). The T-cell epitope prediction algorithm was designed to identify peptides that can be recognized by a global population. Specifically, 5 epitopes from each antigen were designed to be presented by each HLA-A2, -A3/11, -A24, and -DR supertypes [346, 347]. This strategy ensures that, theoretically, at least one or more the peptide epitopes would be recognized by all individuals globally regardless of ethnicity or geographical location, due to the prevalence of at least one of these HLA alleles in almost all populations and known cross-reactivity between HLA alleles within a given HLA supertype family [348].

For each of the 5 target HLA supertypes, peptides predicted to bind with the highest affinity were commercially synthesised (Mimotopes, Australia), and peptide pools (n=20; 5 peptides per each HLA-A2, -A3/A11, -A24, and -DR) tested for recognition by T cells from individuals with clinical immunity to malaria. To screen for T-cell immunoreactivity, PBMCs from life-long malaria-exposed individuals from Papua New Guinea (PNG) were stimulated with peptide antigen pools containing the 20 predicted T-cell peptide epitopes and assayed by IFN-γ ELIspot. Antigens were then ranked based on frequency and magnitude of T cell response to produce a rank priority list of the 1500 liver-stage antigens (immunodominance hierarchy of antigens); the immunoreactive epitope(s) within the antigenic peptide pool were not defined. Unexpectedly, the Doolan group found some of the 1500 antigens were also immunoreactive to malaria-naïve local donor controls. This suggested the presence of an immune evasion strategy, which may occur through the initiation of decoy immune responses triggered by cross-reactivity [342]. The identification of these potential immune evasion antigens may have implications for the development of effective malaria vaccines. Approximately 30% of the tested proteome was reproducibly recognized (unpublished data, D. Doolan, with permission; **Fig. 1.8**). It is possible there are highly immunogenic peptide epitopes (even in the context of being restricted to HLA-supertypes) that were not identified bioinformatically. Nevertheless, the *in silico* epitope prediction approach taken is widely considered to identify a high proportion of T cell epitopes presented by a pathogen for recognition by the host immune

system [349]. Accordingly, *Plasmodium falciparum* antigens were ranked based on the frequency and magnitude of IFN-γ ELIspot T cell reactivity to generate a prioritized list of proteins recognized by T cells from subjects with clinical immunity to malaria. This dataset of prioritized T cell *Plasmodium* antigens provided the foundation for my doctoral studies aimed at developing a more detailed understanding of T cell immunity and T cell dominance following *Plasmodium* infection.
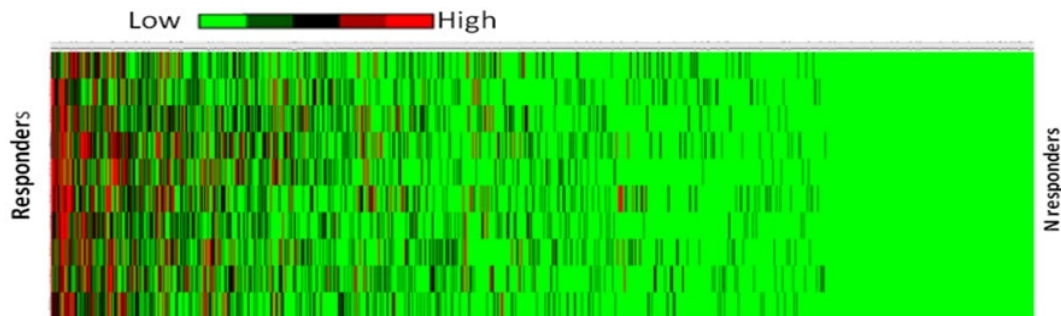
Figure 1.8. *Plasmodium falciparum* **antigen-specific T cell responses from individuals with lifelong exposure to malaria (with permission)**. Pools of peptides representative of putative epitopes predicted to bind to HLA-A2, -A3/A11, -A24 or -DR were assayed by IFN-g ELIspot for recognition by PBMCs from 10 clinically immune adults with life-long exposure to malaria in Papua New Guinea. LHS: magnitude (Spot Forming Cells); RHS: Frequency. Adapted from [342] with permission.

To enhance our understanding of T cell immunity following SARS-CoV2 infection or vaccination (**Objective 2**), we investigated the cellular immune response to the SARS-CoV2 Spike-protein (S-Protein). The SARS-CoV2 S-protein is the major antigen of most COVID-19 vaccines and is well-established to be a highly protective immune target [143]. the S-protein is a highly immunodominant antigen following infection, and dozens of immunodominant epitopes within the S-protein have been identified [125]. We sought to expand upon this understanding of T cell immunity against the S-protein by investigating the kinetics of T cell epitope immunodominance across naïve, vaccinated, and infected individuals (**Fig. 1.9**). Specifically investigating a large pool of immunodominant peptide epitopes (170 peptides: classified as HLA-A2 (23 peptides), -A3/A11 (23 peptides), -A24 (23 peptides), -B7 (47 peptides), -B8 (23 peptides), -DR (25 peptides) or other (6 peptides)) were identified *in silico* using the same epitope prediction strategy used for malaria.
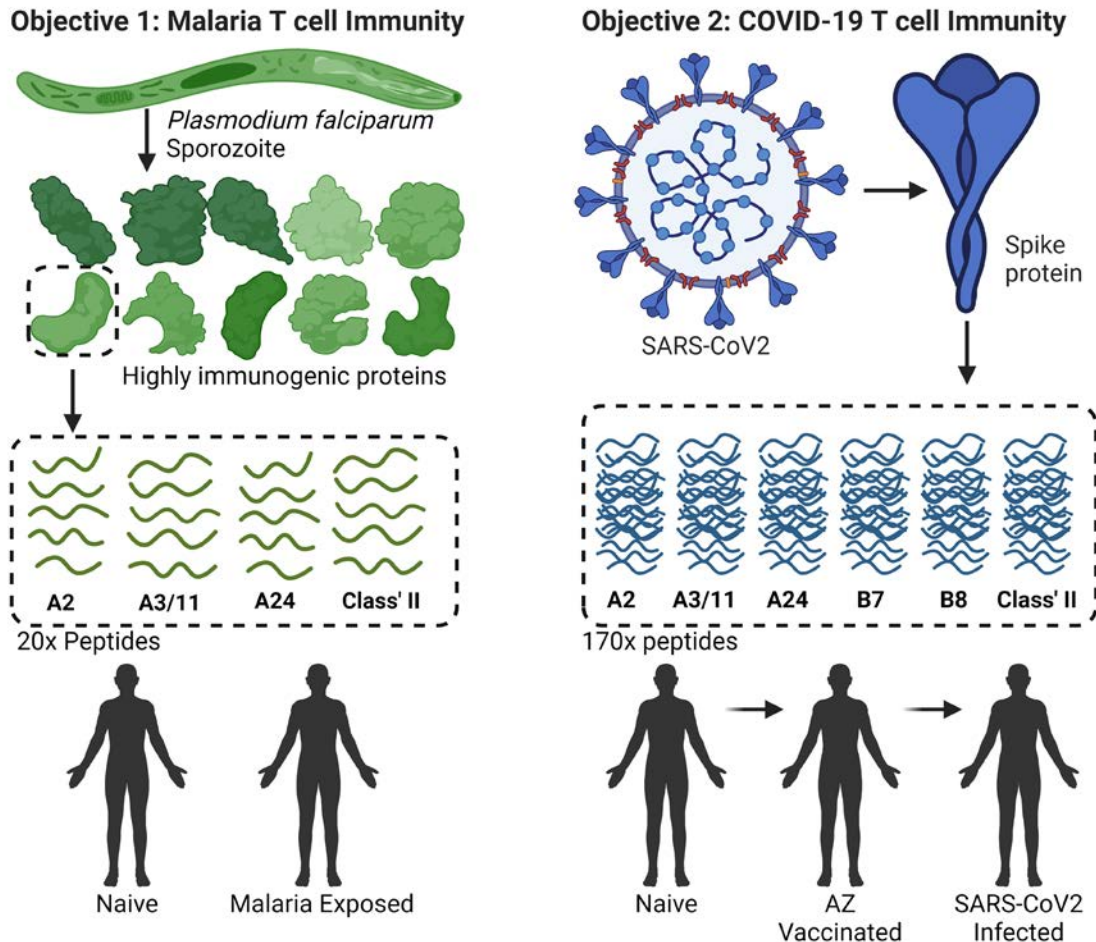
Figure 1.9. Experimental overview to identify immunodominant T cell epitopes following *Plasmodium falciparum* and SARS-CoV2 infection and vaccination. Samples for *P. falciparum* studies were from malaria naïve and malaria-exposed (previously *Plasmodium* infected) Malian donors. Samples for SARS-CoV2 studies were SARS-CoV2 naïve, AstraZeneca (AZ) COVID-19 vaccinated and subsequently SARS-CoV2-infected.

1.3.4   Experimental approach

To identify immunodominant T cell epitopes, a range of immunoassays have been developed. These assays quantitate cytokines, such as IFN-γ, and other surrogate markers of immunity produced from immune cells, such as PBMCs, which are incubated in the presence of defined peptide epitopes [350]. The protein-based IFN-γ Enzyme-linked immunosorbent assay immunoassay (IFN-γ ELIspot) has been the gold-standard to identify immunoreactive peptide epitopes [351]. Flow-cytometry is now also routinely used to identify T cell epitopes and, with

multiparametric analysis, can simultaneously define the associated specific cell populations, such as effector cell and memory cell phenotypes.

However, both IFN-γ ELIspot and flow cytometry consume high-cost reagents (*e.g.,* monoclonal antibodies) and require relatively high numbers of PBMCs to achieve sufficient sensitivity [352, 353]. Especially when considering responses from antigen reactive CD4^{+} or CD8^{+} T cells with relatively low precursor frequency [354]. PCR-based molecular diagnostics such as reverse transcription quantitative-PCR (RT-qPCR), the gold-standard transcriptome-based assay [355], allow highly sensitive and specific *ex vivo* measurements of surrogate transcriptional markers of immunity from low numbers of PBMCs [356]. Therefore, RT-qPCR could be used to screen large numbers of potentially immunoreactive peptide epitopes. However, due to costs and challenges associated with automation [357], RT-qPCR is generally considered a low throughput method. Therefore, the first goal of this thesis was to determine the suitability of RT-qPCR as a technique to determine the immunoreactivity of peptide epitopes, and then to optimise the protocol for use as a high-throughput screening (HTS) tool. Such a HTS-RT-qPCR screening tool would be capable of identifying immunoreactive epitopes from a variety of pathogens. While the original intent of this doctoral project was to investigate the immunodominance hierarchy of *Plasmodium falciparum* pre-erythrocytic stage antigens, following the outbreak of the COVID-19 pandemic, this project pivoted to investigate SARS-CoV2 immunogenicity. Therefore, this thesis has two different but related hypotheses and objectives, where the COVID aspect builds upon the malaria work.

A related aspect looked at how to optimise vaccine-induced T cell responses. We sought to explore murine T cell responses in an adenovirus vector-based vaccine delivery platform. Adenovirus vaccines are effective for induction of protective T cell responses [135], and a demonstrated efficacy and utility for deployment in malaria endemic regions as they require only refrigeration (4°C) cold-chain deployment. This project sought to optimise the detection and quantitation of specific cellular immune responses induced by vaccination, using an adenovirus-based vaccine as a proof-of-concept.

1.3.5 Thesis objective

Objective 1: Evaluate T cell dominance in malaria and define the hierarchy of T cell epitope immunodominance following **Plasmodium** *infection.*

Objective 2: Evaluate T cell dominance in COVID-19 and define the kinetics of T cell epitope immunodominance following SARS-CoV2 infection and vaccination.

1.3.6 Thesis aims

To address these overall objectives, specific aims were defined and addressed for each data chapter (**Table 1.2**), testing chapter-specific hypothesis (**Chapter Introduction: Chapters 2 to 6**).

Table 1.2. Thesis aims

Aim	Scientific aim	Chapter
1	Develop an RT-qPCR protocol with the sensitivity to delineate a T cell epitope hierarchy from 10^5 PBMCs or less.	2
2	Optimise an RT-qPCR protocol to detect and quantitate T cell epitope responses that meets high throughput screening uniformity and signal variance testing standards.	3
3	Optimise an RT-qPCR protocol to quantitate vaccine-induced T cell immunity and protection against *Plasmodium* based on stable reference gene expression.	4
4	Generate an immunodominance hierarchy of T cell peptide epitopes from *Plasmodium falciparum* in *Plasmodium*-infected subjects.	5
5	Generate an immunodominance hierarchy of T cell peptide epitopes from SARS-CoV2 S-protein in SARS-CoV2 infected and vaccinated subjects.	6

Chapter 2: An Analytically and Diagnostically Sensitive RNA Extraction and RT-qPCR Protocol for Peripheral Blood Mononuclear Cells

2.1 Chapter introduction

T cell peptide epitope immunogenicity is typically evaluated by determining the expression of cytokines, such as Interferon-gamma (IFN-γ), which serve as surrogate markers of an immune response. Standard methods to assess IFN-γ expression include flow-cytometry, cytokine-bead capture, or enzyme-linked immunosorbent spot (ELIspot) assay. These protein-based techniques are limited by the relatively high number of immune cells, such as PBMCs, which are required within each test. Molecular techniques, such as RT-qPCR offer a potential solution. As these techniques are extremely sensitive and specific, and therefore, may detect surrogate markers of immunity from very low numbers of PBMCs. However, RT-qPCR detects transcriptomic responses and is therefore not measuring the final protein effector. There is a widespread need for a comprehensive assessment and optimization of an RT-qPCR protocol to provide enough sensitivity to delineate an antigenic peptide epitope immunoreactivity hierarchy.

I hypothesised a RT-qPCR protocol could be developed with the sensitivity to delineate an epitope hierarchy from 10^5 PBMCs or less.

To test this, I addressed the following experimental aims:

1. Optimise a highly sensitive strategy to detect IFN-γ mRNA expression changes from human PBMCs.

2. Demonstrate a correlation between IFN-γ mRNA and protein quantification when delineating an epitope immunoreactivity hierarchy from less than 10^5 PBMCs.

The work presented in this chapter has been published:

Browne DJ, Brady JL, Waardenberg AJ, Loiseau C, Doolan DL. An analytically and diagnostically sensitive RNA extraction and RT-qPCR protocol for peripheral blood mononuclear cells. Front Immunol (2020) 11:402. doi: 10.3389/fimmu.2020.00402

2.2 Published manuscript

An analytically and diagnostically sensitive RNA extraction and RT-qPCR protocol for peripheral blood mononuclear cells

Daniel J. Browne[1], Jamie L. Brady[1], Ashley J. Waardenberg[1,2], Claire Loiseau[1#] and Denise L. Doolan[1,2#*]

[1] Centre for Molecular Therapeutics, Australian Institute of Tropical Health & Medicine, James Cook University, Cairns, QLD 4870, Australia

[2] Centre for Tropical Bioinformatics and Molecular Biology, Australian Institute of Tropical Health & Medicine, James Cook University, Cairns, QLD 4870, Australia

2.2.1 Abstract

Reliable extraction and sensitive detection of RNA from human peripheral blood mononuclear cells (PBMCs) is critical for a broad spectrum of immunology research and clinical diagnostics. RNA analysis platforms are dependent upon high-quality and high-quantity RNA; however, sensitive and high-quality extractions from human samples with limited PBMCs can be challenging. Furthermore, when PBMCs availability is restricted, the comparative sensitivity between RNA quantification and best-practice immune protein quantification is poorly defined. Therefore, we provide herein a critical evaluation of the wide variety of current generation of RNA-based kits for PBMCs; representative of several strategies designed to maximize sensitivity. We assess these kits with a reverse transcription quantitative PCR (RT-qPCR) assay optimized for both analytically and diagnostically sensitive cell-based RNA-based applications. Specifically, three RNA extraction kits, one post-extraction RNA purification/concentration kit, four SYBR master-mix kits, and four reverse transcription kits were tested. RNA extraction and RT-qPCR reaction efficiency were evaluated with commonly used reference and cytokine genes. Significant variation in RNA expression of reference genes was apparent, and absolute quantification based on cell number was established as an effective RT-qPCR normalization strategy. We defined an optimized RNA extraction and RT-qPCR protocol with an analytical sensitivity capable of single cell RNA detection. The diagnostic sensitivity of this assay was sufficient to show a CD8$^+$ T cell epitope hierarchy with as few as 1×10^4 cells. Finally, we compared our optimized RNA extraction and RT-qPCR protocol with current best-practice immune assays and demonstrated that our assay is a sensitive alternative to protein-based assays, especially with limited PBMCs number. This protocol with high analytical and diagnostic sensitivity has broad applicability for both primary research and clinical practice.

2.2.2 Introduction

Reliable isolation of high quality and high quantity RNA from peripheral blood mononuclear cells (PBMCs) and other cells is critical for a broad range of basic, preclinical, and clinical applications [358, 359]. RNA-based assays enable analysis of basal expression profiles and responses to antigen or mitogen stimulation [360, 361]. Human PBMCs are a common source of RNA as collection of blood is less invasive and allows in-depth monitoring of many aspects of immunobiology [359, 362] including identification, classification and prognosis of cancers [363-368], monitoring inflammation [369, 370], and evaluating therapeutic efficacy [371-374].

A range of RNA-based platforms are now available, all dependent upon high quality and high quantity RNA [359]. However, an important requirement for many applications is both excellent analytical sensitivity (*i.e.,* smallest number of cells detectable) and diagnostic sensitivity (*i.e.,* smallest detectable response to stimulation) [375]. Protein-level immunoassays (*e.g.,* flow cytometry, cytokine bead-based arrays, ELIspot) [376-379] are routinely used to detect PBMCs response to stimulation [380-382]. Indeed, ELIspot has been used extensively as the 'gold standard' immune assay given its sensitivity and has been optimized and validated as part of the global HIV/AIDS Comprehensive T Cell Vaccine Immune Monitoring Consortium [351, 383, 384]. However, these protocols are limited by the relatively high number of cells required, especially when considering targets with low frequencies [380], when collection of large blood volumes is challenging [385, 386], or when there are many experimental variables (*e.g.,* vaccine/peptide [373, 374, 387, 388] or epitope testing [389-391]). Therefore, there is an unmet need for a robust RNA extraction and transcriptomic analysis protocol from limited input cell numbers (*e.g.,* PBMCs) with high analytical and diagnostic sensitivity that meets or exceeds that of protein-level immuno-assays.

Reverse transcription quantitative PCR (RT-qPCR) remains the 'Gold Standard' for assay of gene expression as an alternate readout to protein expression [355, 392]. RT-qPCR is more sensitive than traditional RNA quantification technologies (*i.e.,* Northern blotting, nuclease protection assays, *in situ* hybridization, RNA microarrays etc) [393-395]. More recent technologies such as Sanger and next-generation sequencing (*i.e.,* RNA-Seq, single cell RNA-seq, NanoString) and advanced PCR methods (*i.e.,* digital PCR) are similarly sensitive [396, 397] but are relatively expensive or further require complex bioinformatical analysis [398, 399]. In contrast, our optimized RT-qPCR assay is designed specifically for cheap, robust, reproducible and sensitive analysis of gene expression, is available to almost any laboratory,

and serves as a sensitive and specific alternative to protein expression. Additionally, by focusing on a limited number of genes, RT-qPCR is ideal for validation of genes of interest identified from more untargeted methods such as RNAseq.

However, there is an unmet need for a robust RNA extraction and RT-qPCR protocol with excellent analytical and diagnostic sensitivity, ideally to the single cell level. An important consideration for such a protocol is that RT-qPCR normalization can be achieved by either absolute quantification of copies per reaction using a standard curve, or by semi-quantitative fold-change of relative expression normalized to reference genes [393, 400]. However, *in vitro* stimulation has been shown to modulate the expression of many commonly used reference genes [401, 402], and key assumptions underlying semi-quantitative analysis require consistent reference gene expression across experimental conditions within and amongst cell populations. An alternative is absolute quantification normalized to cell number, which minimizes this potential analytical bias [403-405].

To address this need, we developed a highly sensitive RNA extraction and RT-qPCR quantification strategy for analysis of gene expression from human PBMCs. We compared the efficiency of the latest generation of SYBR master-mixes and RNA extraction and reverse transcription kits, taking into consideration both total RNA yield and RNA concentration. We determined that ssoAdvanced™ Universal SYBR® Green Supermix provided optimal reaction efficiency, whilst SuperScript™ IV Reverse Transcriptase had the highest cDNA yields. We demonstrated significantly increased PBMC RNA recovery following extraction with the magnetic bead-based MagMAX™ *mirVana*™ kit, with no further enhancement of analytical sensitivity by including an additional step of RNA concentration. When testing the analytical sensitivity of our optimized protocol, we could detect RNA to the single cell level of highly expressed genes. Furthermore, by evaluating a hierarchy of CD8$^+$ T cell epitope responses, we demonstrated diagnostic sensitivity with as few as 1×10^4 PBMCs. This optimized RNA extraction and RT-qPCR protocol, with high analytical and diagnostic sensitivity, provides a robust alternative to protein-based immune assays.

2.2.3 Materials and equipment

PBMC stimulatory reagents

- Phorbol 12-myristate 13-acetate (PMA) (Sigma-Aldrich)

- Ionomycin (Iono) (Sigma-Aldrich)

- Phytohemagglutinin-L (PHA) (Sigma-Aldrich)

- Human cytomegalovirus, Epstein Barr virus and influenza virus synthetic peptides (**Table 2.1**)

Table 2.1. Synthetic peptides. Characteristics of synthetic peptides representing defined CD8+ T cell peptide epitopes derived from CMV, EBV and influenza virus restricted by the MHC-Class I molecules HLA-A1, -A2, -B7 and -B8.

Code	Amino acid sequence	HLA restriction	Species derived
VTE	VTEHDTLLY	A1	Cytomegalovirus
GIL	GILGFVFTL	A2	Influenza
RPH	RPHERNGFTVL	B7	Cytomegalovirus
FLR	FLRGRAYGL	B8	Epstein Barr virus

SYBR master-mix kits

- ssoAdvanced™ Universal SYBR® Green Master-Mix (Bio-Rad)

- QuantiNova SYBR® Green PCR Kit (QIAGEN)

- PowerUp SYBR® Green Master-Mix (Applied Biosystems)

- RT² SYBR® Green qPCR Master-Mix (QIAGEN)

RNA extraction kits

- RNeasy® Mini Kit (QIAGEN)

- RNeasy® MiniElute Cleanup Kit (QIAGEN)

- RNeasy® Micro Kit (QIAGEN)

- MagMAX™ *mirVana*™ Total RNA Isolation Kit (Applied Biosystems)

RNA to cDNA synthesis kits

- SuperScript™ III First-Strand Synthesis System (ThermoFisher Scientific)

- SuperScript™ IV First-Strand Synthesis System (ThermoFisher)

- iScript™ Advanced cDNA Synthesis Kit (Bio-Rad)

- High-Capacity RNA-cDNA Kit™ (Applied Biosystems)

Quantitative PCR primers

- PrimerBank™ primers (**Table 2.2**)

Antibodies

- anti-human IFN-γ monoclonal antibody (mAb) (Clone 1-D1K, MABTECH)

- anti-human IFN-γ biotinylated mAb (Clone 7-B6-1, MABTECH)

- anti-human IFN-γ-FITC mAb (Clone 4S.B3, BD Biosciences)

Equipment

- QantStudio 3 Real-Time PCR system (Applied Biosystems)

- NanoDrop 2000 Spectrophotometer (ThermoFisher)

- 2100 Bioanalyzer (Agilent Technologies)

- AID ELIspot reader system (Autoimmun Diagnostika GmbH, Germany)

- LSR Fortessa X-20 (BD Biosciences)

Software

- QuantStudio Design and Analysis Software (v1.4.3, Applied Biosystems)

- ProcartaPlex Analyst Software (v1.0, ThermoFisher)

- FlowJo Software (v10.4, BD Biosciences)

- GraphPad Prism (v7, GraphPad)

Table 2.2. Primer list. Characteristics of primers acquired from PrimerBank™ database.

Transcript	GenBank accession number	PrimerBank™ ID	Forward sequence (5′-3′)	Reverse sequence (5′-3′)	Amplicon size (bp)
			Reference genes		
RPLA13a	NM_012423	14591905c2	GCCCTACGACAAGAAAAAGCG	TACTTCCAGCCAACCTCGTGA	117
SDHA	NM_004168	156416002c3	TGGCATTTCTACGACACCGTG	GCCTGCTCCGTCATGTAGTG	77
TBP	NM_003194	285026518c2	CCCGAAACGCCGAATATAATCC	AATCAGTGCCGTGGTTCGTG	80
			Cytokine gene		
IFN-γ	NM_000619.2	56786137c1	TCGGTAACTGACTTGAATGTCCA	TCGCTTCCCTGTTTTAGCTGC	93

2.2.4   Methods

Samples

PBMCs

Blood was collected from healthy donors or buffy coats (n=12) provided by the Australian Red Cross Blood Service, under a protocol approved by the James Cook University Human Research Ethics Committee (#H6702). PBMCs were isolated by density gradient centrifugation and cryopreserved in FBS 10% DMSO. Prior to use, samples were thawed rapidly at 37°C, treated with DNAase I (1 µg/mL; StemCell), and rested for 18 hours at 2×10^6 cells/mL in media (RPMI-1640, 10% FBS, 100 U/mL penicillin/streptomycin) at 37°C and 5% CO_2. Viable PBMCs were counted prior to downstream analysis.

HLA typing

Genomic DNA was isolated from PBMCs using the QIAamp DNA Mini Kit (QIAGEN) according to manufacturer's instructions. High-resolution class I and class II HLA typing was performed by the Australian Red Cross Transplant and Immunological Services (Melbourne, Australia) using the MIA FORA NGS FLEX HLA typing kit (Immunocor) and Illumina MiSeq and MiniSeq platforms.

Cell stimulation

PBMCs were resuspended in RPMI-1640 supplemented with 10% human serum, 100 U/mL penicillin/streptomycin, 2 mM glutaMAX (ThermoFisher Scientific), 10mM HEPES (ThermoFisher Scientific), and 5×10^{-5} M β-Mercaptoethanol (Sigma-Aldrich) (complete media). Synthetic peptides (10 µg/mL) representing defined CD8$^+$ T cell epitopes from human cytomegalovirus, Epstein Barr virus or influenza virus (**Table 2.1**) were tested alongside PMA/Iono (50 ng/mL PMA, 1,000 ng/mL Iono) and PHA (PHA; 1 µg/mL) mitogen controls as well as media-only negative control. PBMCs were stimulated for 6, 12, 16, 24 or 48 hours at 2×10^6 cells/mL in 200 µL in 96-well U-bottom plates (qPCR, ELIspot and multiplexed bead array) or at 1×10^6 cells/mL in 3 mL in 12-well flat-bottom plates (flow cytometry).

Quantitative PCR

Assay setup

qPCR was conducted using the QuantStudio 3 Real-Time PCR system running QuantStudio Design and Analysis Software (v1.4.3, Applied Biosystems). A standard curve, combined calibration sample, and no template negative controls were included on each plate. All samples

were run in technical triplicate in accordance with MIQE guidelines [400]. cDNA synthesis was conducted on a SimpliAmp™ thermocycler (ThermoFisher Scientific). Unless specifically noted, all reaction conditions and protocols were performed as recommended by the manufacturer. Copies/reaction were determined by absolute quantification.

SYBR master-mix testing: Amplicon standard

Four SYBR master-mix kits were evaluated: ssoAdvanced™ Universal SYBR® Green Master-Mix (Bio-Rad), QuantiNova SYBR® Green PCR Kit (QIAGEN), PowerUp SYBR® Green Master-Mix (Applied Biosystems) and RT² SYBR® Green qPCR Master-Mix (QIAGEN). *RPL13a*, *SDHA*, *TBP* and *IFN-γ* primer (**Table 2.2**) amplicons were purified by Wizard SV Gel & PCR CleanUp System (Promega) and quantified by NanoDrop 2000 Spectrophotometer (ThermoFisher). Master-mix reaction efficiency was calculated by amplification of amplicons titrated from 10^7 to 10^1 copies/reaction, with primers at 250 nM, 500 nM or 750 nM [400].

SYBR master-mix testing: cDNA standard

The four SYBR master-mix kits were further evaluated with efficiency titrations of cDNA standards. Briefly, RNA was extracted from 1×10^6 unstimulated PBMCs using the RNeasy® Mini Kit (QIAGEN). 7 µL of extracted RNA was converted to cDNA using the SuperScript™ III First-Strand Synthesis System kit (Invitrogen). Master-mix reaction efficiency was calculated from $\log_{10}$ diluted cDNA (10^4-10^1 cells/reaction) with *RPL13a*, *SDHA*, *TBP* and *IFN-γ* primers at 500 nM.

Reference gene stability testing

1×10^6 PBMCs were stimulated for 6, 12, 16, 24 or 48 hours with or without PMA/Iono as described above. RNA was extracted with RNeasy® Mini Kit (QIAGEN). 7 µL of extracted RNA was reverse transcribed with SuperScript™ III First-Strand Synthesis System kit (Invitrogen). qPCR was run with ssoAdvanced™ master-mix, *RPL13a*, *SDHA*, *TBP* and *IFN-γ* primers at 500 nM and samples at 10^2 cells/reaction.

Evaluation of RNA extraction kits

To evaluate RNA yield and quality, three RNA extraction kits: RNeasy® Mini Kit (QIAGEN), RNeasy® Micro Kit (QIAGEN), and MagMAX™ *mirVana*™ Total RNA Isolation Kit (Applied Biosystems); and one post-extraction RNA purification and concentration kit, RNeasy® MiniElute Cleanup Kit (QIAGEN), were evaluated. All extractions included genomic DNA removal. RNA was extracted from 1×10^6 PBMCs incubated for 6 hours with or without PMA/Iono, with the exception of the RNeasy® Micro Kit where 0.5×10^6 PBMCs was used (per

manufacturer's recommendation). To evaluate concentration, kit eluates were concentrated using the RNeasy® MiniElute. All elution's were performed in the smallest recommended volume. The yield of extracted RNA was quantified using a NanoDrop 2000 Spectrophotometer (ThermoFisher). RNA yield (*i.e.,* total RNA extracted), calculated RNA quality was assessed by RNA integrity number (RIN) by the Australian Genome Research Facility (Brisbane, Australia) using a 2100 Bioanalyzer (Agilent Technologies). Subsequently, 7 μL of RNA was converted to cDNA using the SuperScript™ III First-Strand Synthesis System kit (Invitrogen) alongside negative reverse transcriptase controls. qPCR was run with ssoAdvanced™ master-mix, *RPL13a*, *SDHA*, *TBP* and *IFN-γ* primers at 500 nM and sampled at 10^2 cells/reaction.

Evaluation of reverse transcription kits

Four reverse transcription kits were evaluated: SuperScript™ III First-Strand Synthesis System (ThermoFisher Scientific), SuperScript™ IV First-Strand Synthesis System (ThermoFisher), iScript™ Advanced cDNA Synthesis Kit (Bio-Rad) or High-Capacity RNA-cDNA Kit™ (Applied Biosystems). Kits were evaluated using RNA extracted using the MagMAX™ *mirVana*™ Total RNA Isolation Kit (MagMAX) with or without the RNeasy® MiniElute Cleanup Kit. Briefly, 1×10^6 PBMCs were incubated for 6 hours with or without PMA/Iono as described above. 7 μL of RNA extracted by MagMAX was used for each cDNA synthesis kit. Alternatively, the maximum recommended input of RNA extracted by MagMAX in association with the RNeasy® MiniElute Cleanup Kit was used (*i.e.,* Superscript™ III 7 μL, Superscript™ IV 10 μL, iScript™ 14 μL and High-Capacity 9 μL). qPCR was run with ssoAdvanced™ master-mix, *RPL13a*, *SDHA*, *TBP* and *IFN-γ* primers at 500 nM and sample diluted to 10^2 cells/reaction; except when considering concentration, when the samples were run undiluted.

Analytical and diagnostic sensitivity

For determination of analytical sensitivity, RNA was extracted from a $\log_{10}$ serial dilution of unstimulated PBMCs (10^6-10^0 cells/extraction), using the MagMAX kit with or without the RNeasy® MiniElute Cleanup Kit. A media-only extraction control was processed in parallel. For determination of diagnostic sensitivity, RNA was extracted using the MagMAX kit from titrated PBMCs (4×10^5, 1×10^5, 2.5×10^4 and 1×10^4) incubated for 6 hours with or without PMA/Iono or HLA-matched peptide. For sensitivity evaluations, 10 μL of RNA was converted to cDNA using the SuperScript™ IV First-Strand Synthesis System (Invitrogen). qPCR used undiluted sample with ssoAdvanced™ master-mix, *RPL13a*, *SDHA*, *TBP* and *IFN-γ* primers at 500 nM.

Protein quantification assays

Enzyme-linked immunospot (ELIspot) assay

IFN-γ ELIspot assays were performed as previously described [406, 407]. Briefly, $4x10^5$ PBMCs were plated in triplicate onto 96-well multi-screen filtration plates (#MAIP S45-10, Merck) pre-coated with anti-human IFN-γ monoclonal antibody (mAb) (Clone 1-D1K, MABTECH) and stimulated for 24 hours with or without peptide, PMA/Iono, PHA or media. After washing, IFN-γ secreting cells were stained with 1 µg/mL of anti-human IFN-γ biotinylated mAb (Clone 7-B6-1, MABTECH) followed by streptavidin alkaline phosphatase (MABTECH). The assay was developed using the AP Conjugate Substrate Kit (BioRad). IFN-γ-spot-forming cells were counted using AID ELIspot reader system (Autoimmun Diagnostika GmbH, Germany).

Multiplex cytokine bead array

Supernatant was collected from $4x10^5$ PBMCs incubated for 6 hours with or without peptide, PMA/Iono or media. 50 µL supernatant was analysed using the ProcartaPlex Immunoassay (ThermoFisher) per manufacturer's protocol. Cytokine concentration was calculated from a standard curve using the ProcartaPlex Analyst 1.0 Software (ThermoFisher).

Flow cytometry

$3x10^6$ PBMCs were incubated for 6 hours with or without peptide, PMA/Iono or media. 5µg/mL brefeldin A (BD Biosciences) was added after one hour. Cells were then stained with Fixable Viability Stain 510 (BD Bioscience) and permeabilizated with the Cytofix/Cytoperm kit (BD Biosciences) before staining with anti-human IFN-γ-FITC (Clone 4S.B3, BD Biosciences) mAb. Data were acquired on a LSR Fortessa X-20 driven by FACSDiva software (BD Biosciences) and analysed using FlowJo software (version 10.4).

2.2.5   Data analysis

RT-qPCR, bioanalyzer and NanoDrop data were analysed using a repeated-measures two-way ANOVA with Bonferroni-corrected multiple comparisons test comparing test to control mean. Correlation between RT-qPCR and protein quantification was test with linear regression analysis. Analysis was conducted using GraphPad Prism version 7.0 (GraphPad). Unless reported otherwise, p values of less than 0.05 were considered significant.

2.2.6 Results

ssoAdvanced™ Universal SYBR® Green Master-Mix provided the highest reaction efficiency

Four master-mixes – ssoAdvanced™ Universal SYBR® Green Master-Mix (Bio-Rad), QuantiNova SYBR® Green PCR Kit (QIAGEN), PowerUp SYBR® Green Master-Mix (Applied Biosystems) and RT² SYBR® Green qPCR Master-Mix (QIAGEN) – were evaluated using two methods of preparing reference standards: i) standards derived from $\log_{10}$ diluted amplicon; and ii) standards generated from $\log_{10}$ diluted cDNA (**Fig. 2.1A**). Reaction efficiency was quantified using four primer sets: three sets targeted reference genes known to have high (60S ribosomal protein L13a; *RPL13a*), moderate (Succinate dehydrogenase complex, subunit A; *SDHA*) and low (TATA-binding protein; *TBP)* expression; and one set targeted a cytokine gene (interferon gamma; *IFN-γ*) [402]. When considering an acceptable reaction efficiency range (90 to 110%), 35.4% of the amplicon-derived standards (**Table 2.3**) and 43.8% of the diluted cDNA standards (**Table 2.4**) failed. Primer concentration did not significantly affect mean deviation from 100% reaction efficiency. Strikingly, when comparing SYBR master-mix kits with cDNA standards, the use of ssoAdvanced™ had 0% failure (efficiency*: RPL13a* 93.7%, *SDHA* 98.3%, *TBP* 95.9% and *IFN-γ* 96.1%), the largest dynamic range (10^{0-4} copies/reaction), and the lowest mean deviation from 100% (**Table 2.4**). The coefficient of determination of the standards ($R^2 \geq 0.97$) were consistent for all primers tested, at all concentrations. Together, these data identify ssoAdvanced™ master-mix as providing the highest reaction efficiency for qPCR from PBMC cDNA.
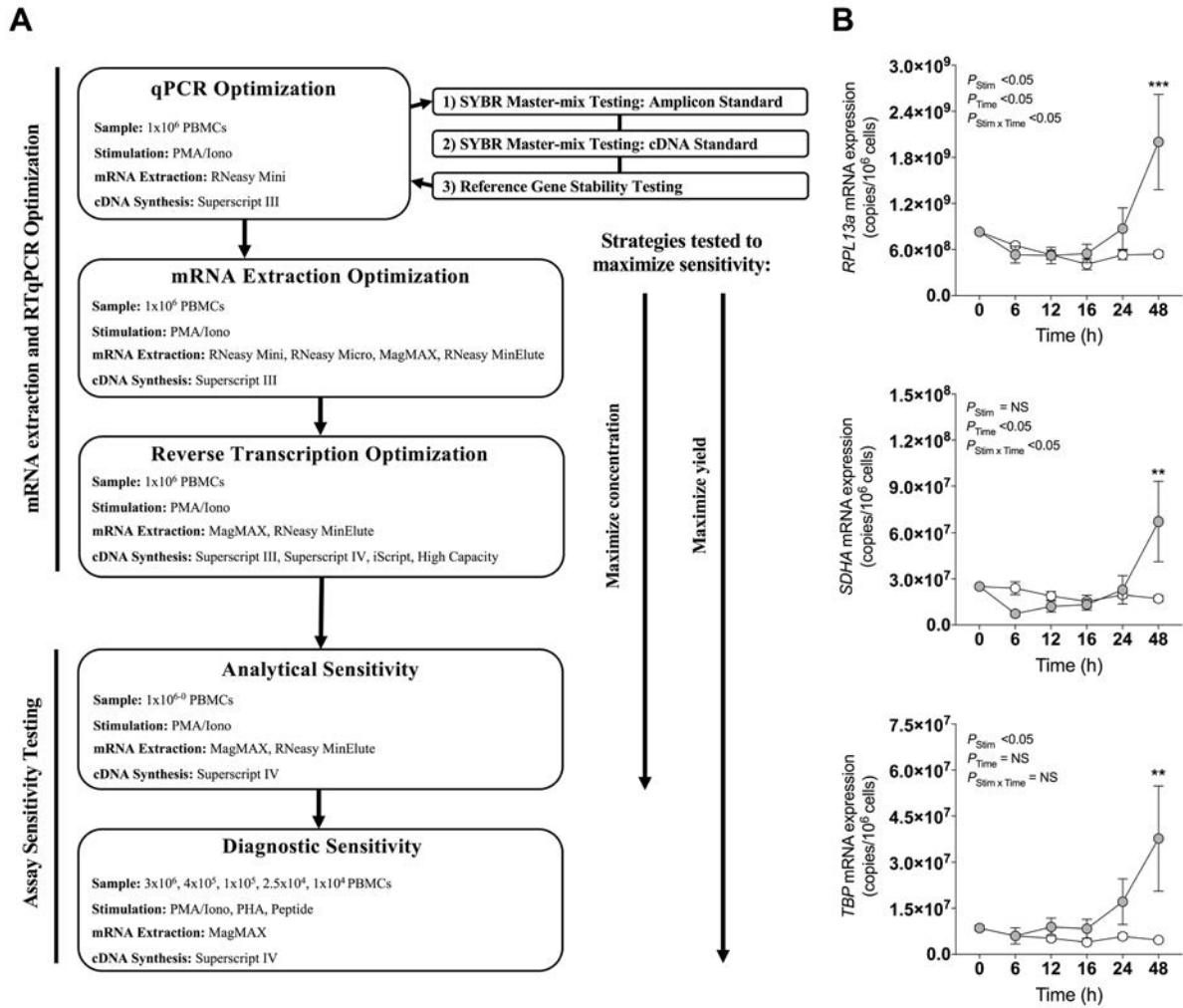
Figure 2.1. qPCR optimisation. **(A)** Experimental workflow for qPCR optimisation. **(B)** Effect of stimulation on mRNA expression of reference genes *RPL13a*, *SDHA*, and *TBP*. 1×10^6 PBMCs paired samples were cultured with complete media (white), or stimulated with PMA/Iono control (grey) for 0, 6, 12, 16, 24 or 48 hours. RNA was extracted using the RNeasy® Mini (Mini) Kit, and reverse transcribed with reverse transcribed with Superscript™ III (Invitrogen). RNA expression was determined by absolute quantitative RT-qPCR wherein number of gene copies per reaction was quantified by standard curve and normalized to cell number. Data were compared with a two-way ANOVA with post-hoc Bonferroni's multiple-comparisons test (**, $P \leq 0.01$; ***, $P \leq 0.001$). Biological replicate (n=3) single RNA extractions with single reverse transcription reactions per extraction were performed. Sample mean calculated from technical triplicate qPCR. Biological mean ± biological SEM are shown.

Table 2.3. Evaluation of commercial qPCR master-mixes by amplicon derived standards. Commercial qPCR master-mixes were evaluated in combination with three primer concentrations (250 nM, 500 nM and 750 nM) with logarithmically-diluted amplicon derived standards (10^6 to 10^1 copies amplicon per reaction). Assay performance *i.e.,* reaction efficiency (E'), limit of detection (LOD) and standard coefficient of determination (R^2) determined as per MIQE guidelines. Amplicons were purified once and measured in qPCR technical triplicate. E', Dynamic Range and R^2 were calculated from the mean of the qPCR technical triplicates. Failure rate calculated as percentage outside acceptable E' (90-110%).

[Primer]	Transcript	QIAGEN R^2 SYBR Master-mix			QIAGEN QuantiNOVA SYBR Master-mix			Bio-Rad ssoAdvanced SYBR Master-mix			Applied Biosystems PowerUp SYBR Master-mix			[Primer] failure rate
		E' (%)	LOD (copies/ reaction)	R^2	E' (%)	LOD (copies/ reaction)	R^2	E' (%)	LOD (copies/ reaction)	R^2	E' (%)	LOD (copies/ reaction)	R^2	
250 nM	*RPLA13a*	92.2	10^1	0.99	94.9	10^2	0.99	89.1	10^1	0.99	92.0	10^1	0.99	31.3%
	SDHA	107.2	10^1	0.99	102.1	10^1	0.99	94.3	10^1	0.99	94.5	10^1	0.99	
	TBP	86.1	10^1	0.99	94.7	10^1	0.99	90.0	10^1	0.99	89.7	10^1	0.99	
	IFN-γ	93.6	10^1	0.99	85.8	10^1	0.98	83.9	10^2	0.99	99.7	10^1	0.98	
250 nM failure rate		25.0%			25.0%			50.0%			25.0%			
500 nM	*RPLA13a*	88.8	10^1	0.99	96.9	10^1	0.99	86.0	10^2	0.99	92.7	10^1	0.99	37.5%
	SDHA	93.8	10^1	0.99	93.5	10^2	0.99	92.4	10^1	0.99	90.8	10^1	0.99	
	TBP	88.6	10^1	0.99	82.6	10^2	0.99	89.2	10^1	0.99	98.4	10^1	0.99	
	IFN-γ	93.5	10^1	0.99	87.1	10^2	0.99	92.4	10^1	0.99	95.2	10^1	0.99	

[Primer] Transcript	QIAGEN R^2 SYBR Master-mix			QIAGEN QuantiNOVA SYBR Master-mix			Bio-Rad ssoAdvanced SYBR Master-mix			Applied Biosystems PowerUp SYBR Master-mix			[Primer] failure rate
	E' (%)	LOD (copies/ reaction)	R^2	E' (%)	LOD (copies/ reaction)	R^2	E' (%)	LOD (copies/ reaction)	R^2	E' (%)	LOD (copies/ reaction)	R^2	
500 nM failure rate	50%			50%			50%			0%			
RPLA13a	98.2	10^1	0.99	87.7	10^2	0.99	96.8	10^1	0.99	94.0	10^1	0.99	
SDHA	98.0	10^1	0.99	104.2	10^1	0.99	102.1	10^1	0.99	92.3	10^2	0.97	
750 nM *TBP*	86.7	10^2	0.99	89.2	10^1	0.99	87.2	10^1	0.99	85.5	10^2	0.99	37.5%
IFN-γ	94.4	10^1	0.99	84.0	10^1	0.99	92.3	10^1	0.99	96.3	10^1	0.99	
750 nM failure rate	25.0%			75.0%			25.0%			25.0%			
Master-mix failure rate	33.3%			50.0%			41.7%			16.7%			
Overall failure rate	35.4%												

Table 2.4. Evaluation of commercial qPCR master-mixes by cDNA derived standards. Commercial qPCR master-mixes were evaluated with logarithmically diluted PBMC cDNA (10^4 to 10^1 cell cDNA equivalent per reaction). Assay performance, *i.e.,* reaction efficiency (E'), limit of detection (LOD) and standard coefficient of determination (R^2) determined as per MIQE guidelines. Biological replicate (n=3) RNA extractions were extracted; with single reverse transcription reactions per extraction and measured in qPCR technical triplicate. RNA extractions were repeated (2x). E', Dynamic Range and R^2 calculated from a representative (1x) technical extraction replicate (n=3) calculated from the mean of the qPCR technical replicates Data representative of two independent technical reproductions. Failure rate calculated as percentage outside acceptable E' (90-110%).

Transcript	QIAGEN R^2 SYBR Master-mix			QIAGEN QuantiNOVA SYBR Master-mix			Bio-Rad ssoAdvanced SYBR Master-mix			Applied Biosystems PowerUp SYBR Master-mix		
	E' (%)	Dynamic range (cells/reaction)	R^2	E' (%)	Dynamic range (cells/reaction)	R^2	E' (%)	Dynamic range (cells/reaction)	R^2	E' (%)	Dynamic range (cells/reaction)	R^2
RPL13a	95.2	10^0-10^3	0.99	78.9	10^0-10^3	0.99	93.7	10^0-10^4	0.99	104.9	10^0-10^3	0.99
SDHA	79.9	10^0-10^3	0.99	85.7	10^0-10^3	0.99	98.3	10^0-10^4	0.99	121.5	10^0-10^3	0.99
TBP	134.7	10^2-10^4	0.99	99.1	10^2-10^4	0.99	95.9	10^1-10^4	0.99	109.7	10^2-10^4	0.99
IFN-γ	88.3	10^1-10^3	0.99	91.2	10^1-10^3	0.99	96.1	10^1-10^4	0.99	121.9	10^0-10^3	0.99
Master-mix failure rate	75.0%			50.0%			0.0%			50.0%		
Overall failure rate	43.8%											

83

Mitogen stimulation induced changes in RPL13a, SDHA and TBP gene expression

The expression stability of three commonly used reference genes [402, 408, 409], *RPL13a*, *SDHA* and *TBP*, previously reported as stable in PBMCs following stimulation [402], were evaluated by RT-qPCR within PBMCs stimulated with PMA/Iono for 6, 12, 18, 24 or 48 hours. Expression of all three genes changed over time with cell culture, and significantly increased at 48 hours post-stimulation as compared to baseline ($P < 0.001$, $P < 0.01$ and $P < 0.01$, respectively; **Fig. 2.1B**). These data establish that the expression of common reference genes is significantly affected by stimulation, emphasizing the importance of absolute quantification normalized to cell numbers, rather than relative quantification.

Magnetic bead-based extraction significantly increased RNA yield and concentration

Next, RNeasy® Mini and Micro silica columns (both QIAGEN) and MagMAX™ *mirVana*™ (MagMAX) Total RNA Isolation (Applied Biosystems) kits were tested for 1) RNA yield and 2) concentration with or without a post-extraction RNA concentration step using the RNeasy® MiniElute Cleanup Kit (QIAGEN). In each case, PBMCs were incubated with or without PMA/Iono for 6 hours. RIN assessment demonstrated that RNA integrity was high (>7) and consistent across all kits (**Fig. 2.2A, left panel**). RNA yield was significantly increased using MagMAX as compared to the RNeasy® Mini silica column extraction kit, for both stimulated and unstimulated PBMCs (mean yield ($\mu g/10^6$ cells): 0.87 *vs.* 1.36, $P < 0.05$ and 0.82 *vs.* 1.42, $P < 0.01$, respectively) (**Fig. 2.2A, middle panel**). Moreover, the concentration of RNA extracted from both stimulated and unstimulated PBMCs significantly increased with the MagMAX-RNeasy® MiniElute combination (mean RNA concentration (ng/μL): 23.5 *vs.* 83.9, $P < 0.0001$ and 24.8 *vs.* 76.6, $P < 0.0001$, respectively) (**Fig. 2.2A, right panel**). The RNeasy® Micro extraction kit had no impact on RIN, RNA yield or concentration.
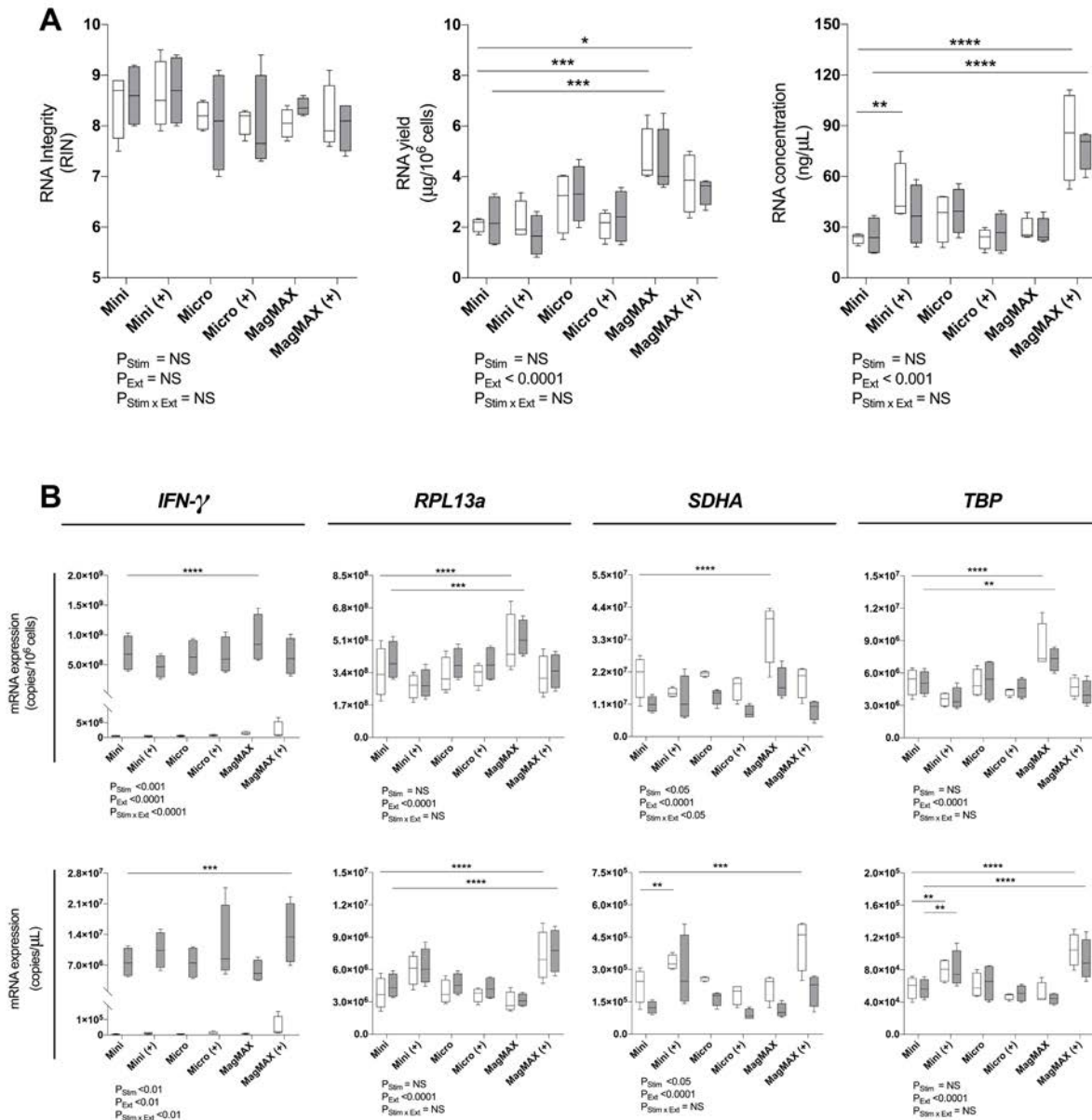
Figure 2.2. RNA extraction evaluation. **(A)** Bioanalyzer analysis of RNA Integrity Number (RIN), and nanospectrophotometer analysis of yield and concentration were obtained using three commercially-available extraction kits with (+) or without post-extraction RNA purification and concentration. **(B)** RT-qPCR analysis of *IFN-γ*, *RPL13a*, *SDHA* and *TBP* expression normalized to cell number (copies/10^6 cells) or cDNA concentration (copies/µL). 1×10^6 PBMCs paired samples were cultured with complete media (white) or PMA/Iono (grey) for 6 hours. RNA was extracted using the RNeasy® Mini (Mini) Kit, RNeasy® Micro (Micro) Kit (both QIAGEN), or MagMAX™ *mirVana*™ (MagMAX) Total RNA Isolation Kit (Applied Biosystems), with concentration step performed using the RNeasy® MiniElute Cleanup Kit (QIAGEN). All samples were reverse transcribed with Superscript™ III (Invitrogen). Data were analysed using a two-way ANOVA with post-hoc Bonferroni's multiple-comparisons test (*, $P \leq 0.05$; **, $P \leq 0.01$; ***, $P \leq 0.001$; ****, $P \leq 0.0001$). Biological replicate (n=4), triplicate RNA extractions, with single reverse transcription reactions per extraction

were performed. Sample mean calculated from the mean of the technical RNA extractions calculated from the mean of the technical triplicate qPCR reactions. Biological mean ± biological SEM are shown.

Magnetic bead-based extraction significantly increased RT-qPCR gene expression signal measurements

RNA extraction kit eluates were subsequently reverse transcribed using Superscript™ III (ThermoFisher) and *RPL13a*, *SDHA*, *TBP* as well as *IFN-γ* quantified by RT-qPCR. Data were normalised to either RNA yield (copies/10^6 cells) or concentration (copies/µL). When considering both yield and concentration, RT-qPCR signal was significantly affected by extraction technique (P_{Ext}<0.01 for all tested genes; **Fig. 2.2B**). Consistent with our findings that *SDHA* expression was reduced following 6 hours of exposure to PMA/Iono (**Fig. 2.1B**), stimulation significantly reduced *SDHA* expression ($P < 0.05$; **Fig. 2.2B**). Similarly, consistent with our findings that RNA yield was optimal with MagMAX (**Fig. 2.2A**), we found significantly increased gene expression using MagMAX when compared to RNeasy® Mini, for both unstimulated (mean copies/10^6 cells: $3.4x10^8$ *vs.* $4.9x10^8$, $P < 0.0001$ *RPL3a*; $2.1x10^7$ *vs.* $3.6x10^7$, $P < 0.0001$ *SDHA*; $5.2x10^6$ *vs.* $8.3x10^6$, $P < 0.001$ *TBP*; **Fig. 2.2B**) and stimulated (mean copies/10^6 cells: $6.9x10^8$ *vs.* $9.3x10^8$, $P < 0.0001$ *IFN-γ*; $4.0x10^8$ *vs.* $5.2x10^8$ $P < 0.001$ *RPL13a*; $5.1x10^6$ *vs.* $7.3x10^6$, $P < 0.01$ *TBP*; **Fig. 2.2B**) PBMCs. Likewise, there was a significant increase in RNA concentration following RT-qPCR using the MagMAX-RNeasy® MiniElute combination when compared to RNeasy® Mini, for both unstimulated (mean copies/µL$_{RT:}$ $3.8x10^6$ *vs.* $7.2x10^6$, $P < 0.0001$ *RPL13a*; $2.3x10^5$ *vs.* $4.2x10^5$, $P < 0.001$ *SDHA*; $5.8x10^4$ *vs.* $1.0x10^5$, $P < 0.001$ *TBP*; **Fig. 2.2B**) and stimulated (mean copies/µL$_{RT:}$ $7.7x10^6$ *vs.* $1.4x10^7$, $P < 0.001$ *IFN-γ*; $4.5x10^6$ *vs.* $7.7x10^6$, $P < 0.0001$ *RPL13a*; $5.7x10^4$ *vs.* $9.2x10^4$, $P < 0.0001$ *TBP*; **Fig. 2.2B**) PBMCs. RNA yield and concentration were not significantly affected by the RNeasy® Micro extraction kit. When assessing technical reproducibility, extraction method also did not significantly affect standard deviation amongst replicate extractions (**Supp Table S2.1**). These data establish that magnetic bead-based extraction significantly enhanced RT-qPCR signal, as compared to silica column extractions.

Superscript™ IV significantly increased RT-qPCR gene expression signal measurements

To identify the optimal reverse transcription kit, Superscript™ III, Superscript™ IV (both ThermoFisher), iScript™ Advanced (Bio-Rad) and High-Capacity (Applied Biosystems) kits were tested in conjunction with MagMAX (**Fig. 2.3A**) and MagMAX-RNeasy® MiniElute

(**Fig. 2.3B**). A statistically significant enhancement of RT-qPCR signal was observed with Superscript™ IV as compared to Superscript™ III for both unstimulated (mean copies/10^6 cells: 1.1×10^7 *vs.* 1.3×10^7 $P < 0.05$ *SDHA*; 4.1×10^6 *vs.* 5.6×10^6, $P < 0.001$ *TBP*; **Fig. 2.3A**) and stimulated (mean copies/10^6 cells: 5.8×10^8 *vs.* 6.9×10^8, $P < 0.001$ *IFN-γ*; 5.9×10^8 *vs.* 6.8×10^8, $P < 0.05$ *RPL13a*; 3.5×10^6 *vs.* 4.5×10^6, $P < 0.05$ *TBP*; **Fig. 2.3A**) PBMCs. Similarly, Superscript™ IV produced the highest RT-qPCR signal following MagMAX-RNeasy® MiniElute extraction-concentration for both unstimulated (mean copies/µL: 1.3×10^7 *vs.* 2.5×10^7, $P < 0.05$ *RPL13a*; **Fig. 2.3B**) and stimulated (mean copies/µL: 1.7×10^7 *vs.* 3.4×10^7, $P < 0.05$ *IFN-γ*; 1.1×10^7 *vs.* 2.2×10^7, $P < 0.001$ *RPL13a*; **Fig. 2.3B**) PBMCs. When assessing technical reproducibility, extraction had no statistically significant effect on variation between replicate extractions (**Supp Table S2.2**). These data identify Superscript™ IV as the superior reverse transcriptase kit irrespective of yield or concentration strategy.
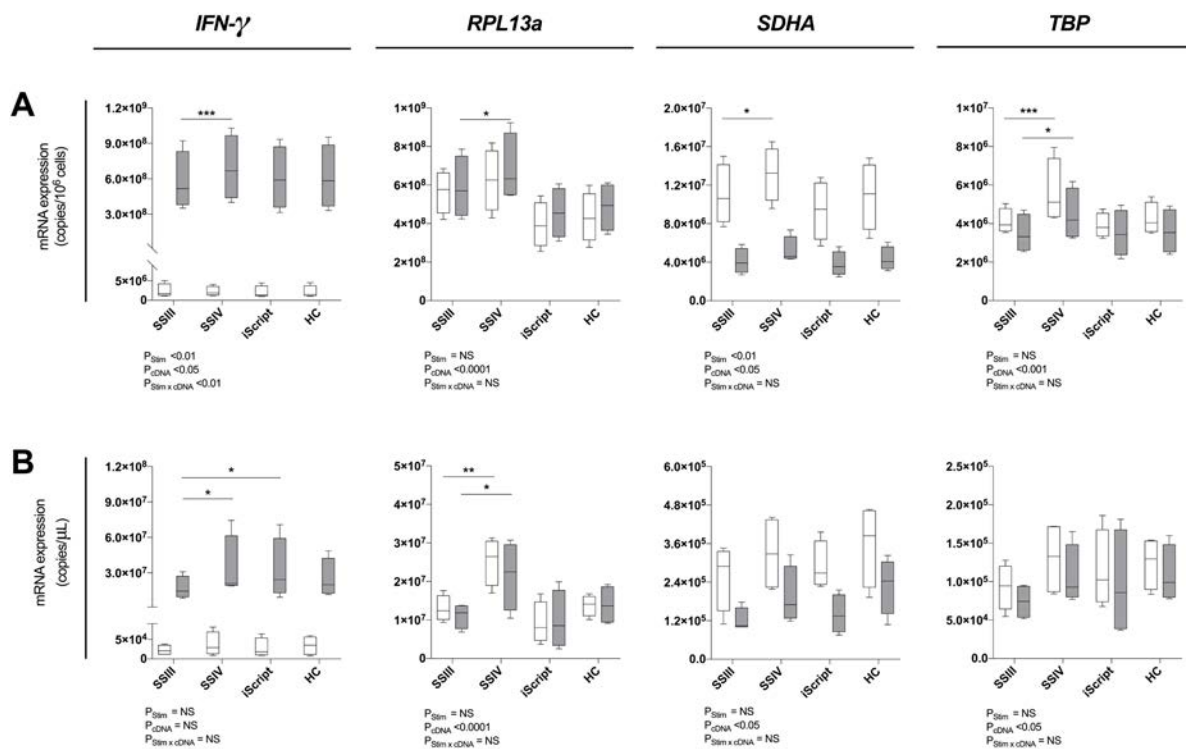
Figure 2.3. Reverse transcription evaluation. Four reverse transcription kits were evaluated for relative qPCR signal for (**A**) maximal RNA yield, or (**B**) maximal RNA concentration. When maximizing RNA yield, RNA was extracted with MagMAX™ *mirVana*™ (MagMAX) Total RNA Isolation Kit (Applied Biosystems); when maximizing concentration, RNA was concentrated with RNeasy® MiniElute Cleanup Kit (QIAGEN). RNA was reverse transcribed with either Superscript™ III (SSIII), Superscript™ IV (SSIV) (both Invitrogen), iScript™ Advanced (iScript) (BioRad) or High-Capacity (HC) (ThermoFisher) reverse transcription kits. RNA was extracted from 1×10^6 PBMCs pared

samples, cultured with complete media (white) or PMA/Iono (grey) for 6 hours, then *IFN-γ*, *RPL13a*, *SDHA* and *TBP* mRNA expression was quantified. Data were compared with a two-way ANOVA (*, $P \leq 0.05$; **, $P \leq 0.01$; ***, $P \leq 0.001$ for post-hoc Bonferroni's multiple-comparisons test). Biological replicate (n=4), single RNA extractions, with triplicate reverse transcription reactions per extraction were performed. Sample mean calculated from the mean of the reverse transcription reactions calculated from the mean of the technical triplicate qPCR reactions. Biological mean ± biological SEM are shown.

Single cell analytical sensitivity of RPL13a was observed following magnetic bead-based RNA extraction

We next evaluated the analytical sensitivity of our optimized protocol using MagMAX extraction kit (**Fig. 2.4A**) and MagMAX-RNeasy® MiniElute extraction-concentration kit (**Fig. 2.4B**). RNA was extracted from a $\log_{10}$ serial dilution of unstimulated PBMCs and expression of *IFN-γ*, *RPL13a*, *SDHA* and *TBP* determined by absolute quantification. The highly expressed *RPL13a* gene was detected at single-cell level from both MagMAX (0.88 $\log_{10}$copies/reaction; **Fig. 2.4A**) and MagMAX-RNeasy® MiniElute combination (0.90 $\log_{10}$copies/reaction; **Fig. 2.4B**) extractions. Extraction technique did not influence *IFN-γ*, *RPL13a* or *TBP* expression; whilst variability in *SDHA* expression ($P_{Ext}<0.05$) was driven by increased RT-qPCR signal at 10^5 and 10^4 PBMCs per extraction. These data establish that our optimized protocol is capable of extracting and quantifying RNA of a highly expressed gene from a single cell. Importantly, the additional step of RNeasy® MiniElute Cleanup did not further enhance analytical sensitivity.
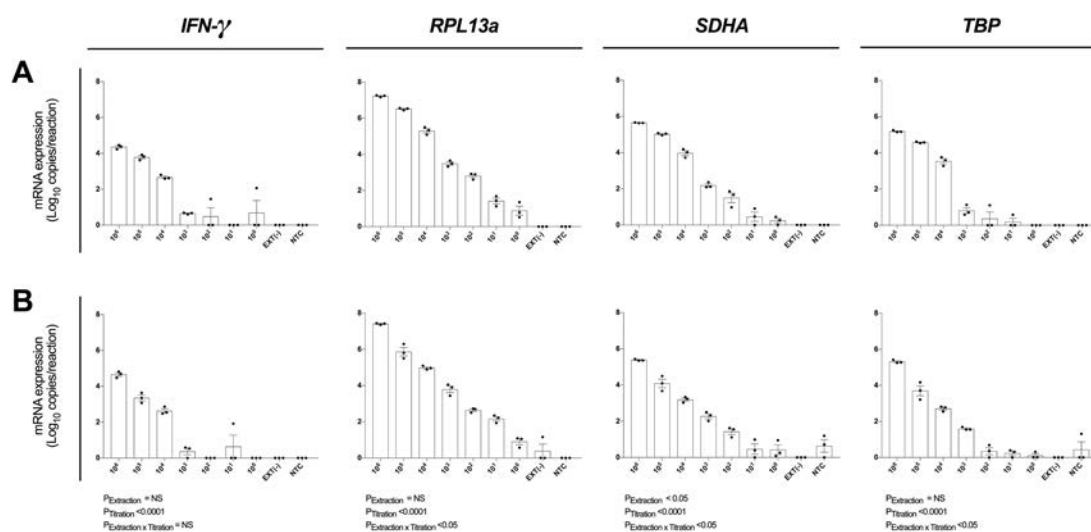
Figure 2.4. Assay analytical sensitivity. Relative RT-qPCR signal for *IFN-γ*, *RPL13a*, *SDHA* and *TBP* mRNA expression from $\log_{10}$ dilutions of unstimulated PBMCs when **(A)** maximizing RNA yield, or

(B) maximizing RNA concentration. When maximizing RNA yield, RNA was extracted with MagMAX™ *mirVana*™ (MagMAX) Total RNA Isolation Kit (Applied Biosystems); when maximizing concentration, RNA was concentrated with RNeasy® MiniElute Cleanup Kit (QIAGEN). All samples were reverse transcribed with Superscript™ IV (Invitrogen). mRNA expression was determined by absolute-quantitative RT-qPCR and gene copy number per reaction was normalized to $\log_{10}$ copies per reaction. Biological replicate (n=3), single RNA extractions, with single reverse transcription reactions per extraction were performed. Sample mean calculated from the mean of the technical triplicate qPCR reactions. Biological mean ± biological SEM are shown.

RT-qPCR protocol diagnostic sensitivity correlates significantly with protein level quantification of epitope-specific stimulation from as few as $1x10^4$ PBMCs

Next, we determined the diagnostic sensitivity of our optimized RNA extraction and RT-qPCR protocol to confirm that it accurately reflected data generated using protein-level assays. We evaluated the epitope-specific stimulatory response for four $CD8^+$ T cell epitopes restricted by different MHC molecules, quantifying IFN-γ production by flow cytometry, cytokine bead array and ELIspot; and *IFN-γ* mRNA by our optimized protocol. A limited epitope-specific IFN-γ response was demonstrated by flow cytometry (**Fig. 2.5A**) and bead arrays (**Fig. 2.5B**) whereas all samples were observed to respond to stimulation by ELIspot (**Fig. 2.5C**). Importantly, our RT-qPCR protocol (**Fig. 2.6**), was able to replicate the ELIspot results but with significantly reduced cell numbers (HLA-A1 $2.5x10^4$, -A2 $1x10^5$, -B7 $1x10^4$, -B8 $1x10^5$; 48-fold, 12-fold, and 48-fold and 12-fold respectively; **Fig. 2.5D**)
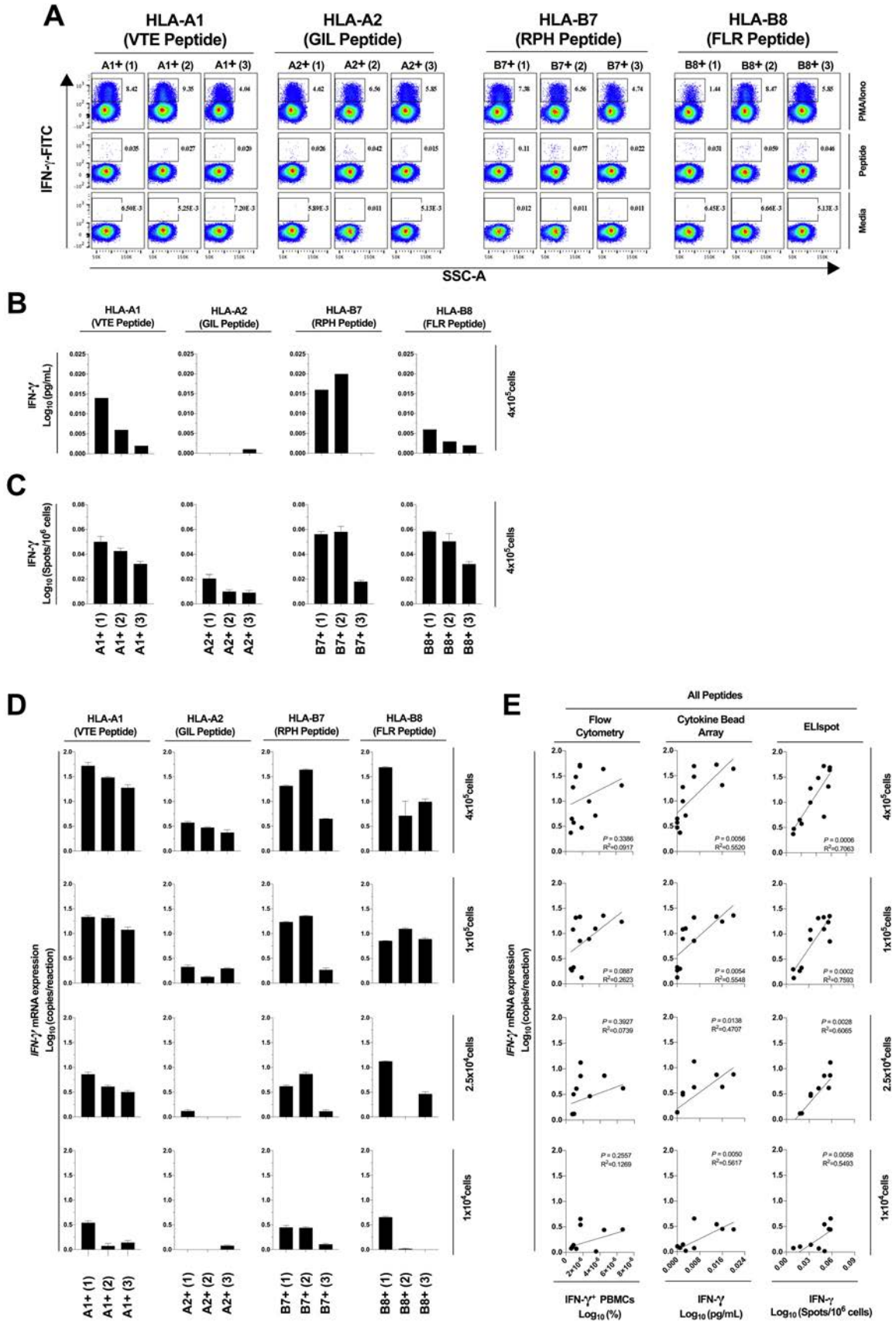
Figure 2.5. Assay diagnostic sensitivity. Production of IFN-γ protein was determined by flow cytometry **(A)**, bead-based multiplex assay (MagPIX) **(B)**, IFN-γ ELIspot **(C)**; or *IFN-γ* mRNA

expression by absolute RT-qPCR (**D**). *IFN-γ* mRNA expression was correlated to measurements of protein production by flow cytometry, MagPIX or IFN-γ ELIspot (**E**; left, middle and right panel, respectively). Biological replicate (n=3) per HLA-A1 (A1$^+$(1-3)) or HLA-A2 (A2$^+$(1-3)) or HLA-B7 (B7$^+$(1-3)) or HLA-B8 (B8$^+$(1-3)) positive PBMCs (*i.e.,* n=12 total; in groups 3x HLA matched) were stimulated with synthetic HLA-matched peptides representing CMV, Influenza or EBV CD8$^+$ T cell epitopes 'VTE', 'GIL', 'RPH' or 'FLR' (black), respectively. All samples were cultured with media negative control or PMA/Iono positive control. *IFN-γ* mRNA expression was determined by absolute quantification RT-qPCR of titrated PBMCs ($4x10^5$, $1x10^5$, $2.5x10^4$ and $1x10^4$); gene copy number per reaction was quantified by standard curve and log_{10} transformed. Single RNA extractions, with single reverse transcription reactions per n were performed. qPCR performed in technical triplicate replicates. Flow cytometry and MagPIX performed in single replicates. ELIspot performed in technical triplicate replicates. Sample mean calculated from the mean of the technical single or triplicates. Biological mean ± technical SEM above background are shown.
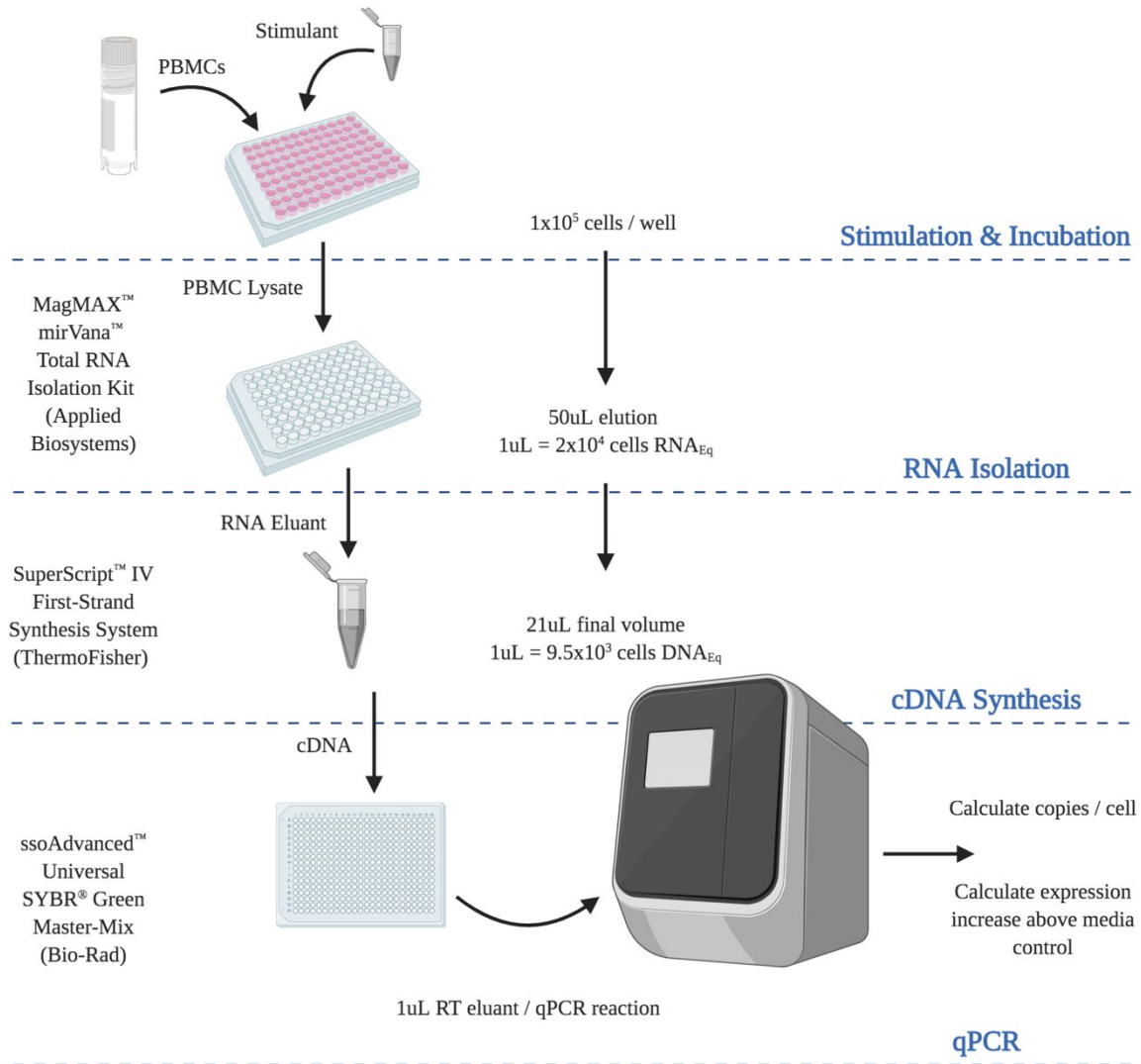
Figure 2.6. Final optimized RT-qPCR assay. Steps and calculations required for the use of this analytically and diagnostically sensitive RNA extraction and RT-qPCR protocol. Specifically designed for the sensitive detection of RNA from peripheral blood mononuclear cells, and thus transcriptomic response to stimulation. (RNA_{EQ} RNA equivalent; DNA_{EQ} DNA equivalent). Figure created with BioRender.com.

Optimized RT-qPCR assay correlated with best-practice protein-based immunoassays

Next, we assessed correlation between results obtained using our optimized RT-qPCR protocol and current best-practice immunoassays. The correlation between our RT-qPCR protocol and ELISpot was significant at all cell numbers tested ($P = 0.0006$, $R^2 = 0.7063$ (4×10^5); $P = 0.0002$, $R^2 = 0.7593$ (1×10^5); $P = 0.0028$, $R^2 = 0.6065$ (2.5×10^4); $P = 0.0058$, $R^2 = 0.5493$ (1×10^4); **Fig. 2.5E** right panel). The correlation was also significant with MagPIX ($P = 0.0056$, $R^2 =$

0.5520 (4×10^5); P = 0.0054, R^2 = 0.5548 (1×10^5); P = 0.0138, R^2 = 0.4707 (2.5×10^4); P = 0.0050, R^2 = 0.5617 (1×10^4); **Fig. 2.5E** middle panel), but non-significant (albeit with a similar trend) with flow cytometry (**Fig. 2.5E** left panel). Thus, data generated using our optimized RT-qPCR assay are consistent with best practice protein-based immunoassays. Furthermore, our assay is capable of defining an epitope-specific response hierarchy from as few as 1×10^4 cells, representing a clinically and diagnostically meaningful reduction in cell number.

Taken together, we report here a highly sensitive RNA extraction and RT-qPCR quantification strategy using the MagMAX RNA extraction kit, Superscript™ IV reverse-transcription kit and ssoAdvanced™ SYBR master-mix (**Supp Table S2.3**). This assay is sensitive to the single cell level, can define an epitope hierarchy of response from as few as 1×10^4 cells, and represents a sensitive and robust alternative to protein quantification for research, diagnostic and clinical applications.

2.2.7 Discussion

Herein, we describe an optimised RNA extraction and RT-qPCR protocol requiring low PBMC numbers, with high analytical and diagnostic sensitivity, whilst maintaining high correlation to protein-level quantification that is typically reliant on much larger cell numbers for detection.

Precise RT-qPCR results are typically dependent on reactions maintaining efficiency close to 100% [400]. Both assay design (*e.g.,* primer concentration, master-mix) and sample (*e.g.,* co-extracted inhibitors) may influence PCR efficiency. We made use of the open-access database PrimerBank™ since those primers have been designed for use under consistent conditions (*i.e.,* optimal Tm 60°C) and cover most known human and mouse genes [410]. We found primer concentration titrations did not impact reaction efficiency, whereas the SYBR master-mix had a significant impact. PCR inhibitors, including haemoglobin, lactoferrin, anticoagulants, IgG, polysaccharides, and proteases, can be co-extracted in PBMC preparations [411, 412]. It is known that some DNA-polymerase variants and PCR buffer 'enhancers' have improved reaction efficiency in the presence of such inhibitors [411, 413]. The ssoAdvanced™ master-mix, identified herein as optimal of those tested, appears to be one such master-mix facilitating PCR efficiency in the presence of co-extracted inhibitors. Optimization of master-mix reagents will likely continue to be important in improving blood-based PCR analysis and diagnostics [414, 415]; especially for accurate amplification of relatively low abundant targets, comparisons between populations with high variability, or amplification from inhibitor-enriched mediums (*i.e.,* whole blood extractions) [368, 414].

We tested three RNA extraction kits by evaluating extraction quality and efficiency: RNeasy® Mini Kit, RNeasy® Micro Kit, RNeasy® and MagMAX™ *mirVana*™ Kit; in combination with the RNA purification and concentration kit: MiniElute Cleanup Kit. When extracting identically controlled samples, all kits yielded RNA with equivalent RIN scores and low technical variability between replicates. Importantly, RNA yield from PBMCs was significantly increased using MagMAX as compared to silica-column technologies. Additionally, when compared to silica-column extractions, we found MagMAX was more cost and time efficient when running larger number of samples (*e.g.,* 96 samples in ~2 hours). We therefore expect magnetic bead-based extractions will become increasingly common within blood-based nucleic acid isolations [414, 416, 417]. In addition to extraction techniques (*e.g.,* silica column, phase separation), other factors that could impact RNA quality, yield and concentration include sample collection, storage, and transportation.

Four reverse transcriptase (RT) kits were also evaluated: SuperScript™ III First-Strand Synthesis System, SuperScript™ IV First-Strand Synthesis System, iScript™ Advanced cDNA Synthesis Kit and High-Capacity RNA-cDNA Kit™. Of those, Superscript™ IV was associated with the highest qPCR signal. A previous study evaluating RNA extracted from PBMCs using earlier-generation RT kits reported >128-fold increased qPCR signal between kits [359]. We speculate that the reduced variability that we observed between RT kits tested in our study reflects consistent kit quality, purity of the RNA extracted by MagMAX, or a combination thereof.

Both analytical sensitivity and diagnostic sensitivity are key criteria for any RT-qPCR protocol. We show that the analytical sensitivity of our assay is to the level of single cell RNA detection for relatively highly expressed RPL13a. Sample concentration and clean-up has been suggested to remove inhibitors and increase sensitivity [418, 419]. Unexpectedly, we found this step did not improve our analytical sensitivity, and was time-consuming, expensive and reduced sample volume. Nevertheless, if concentration is warranted under specific experimental situations, our data suggest that it is technically feasible while retaining high analytical sensitivity. Diagnostic sensitivity determined using MagMAX showed that an epitope response hierarchy could be detected with as few as $1x10^4$ PBMCs. It is well known that there is no absolute correlation between RNA expression and protein translation. Indeed, correlations between transcript and protein expression would be markedly reduced under situations of epigenetic, post-transcriptional or post-translational modification of the gene of interest [420]. Nevertheless, we correlated our optimized RT-qPCR assay with commonly used protein-level immunoassays

(flow cytometry, cytokine bead arrays, and ELIspot) and showed a very high correlation with the gold-standard protein-level assay, ELIspot, as well as the commonly used MagPIX bead-based cytokine assay, at all tested PBMC concentrations. This highlights that our protocol represents a robust alternative to protein-based assays (e.g., when measuring changes in cytokine mRNA expression in PBMCs in response to specific *in vitro* stimulation). This work will significantly improve analytical capacity of studies relying on irreplaceable, relatively small, or costly human samples (*e.g.,* neonatal PBMCs) [421, 422].

Another important outcome of our work is the finding that absolute quantification of transcripts and subsequent normalization to cell numbers is the most appropriate analysis strategy for RNA/RT-qPCR quantification from PBMCs [400, 403]. We observed significant alterations in gene expression of commonly used reference genes *RPL13a*, *SDHA* and *TBP* following stimulation. This is not unexpected as reference genes have been described as variable across cell types, tissues, and experimental and stimulatory conditions [381, 402, 423, 424].

In summary, we report herein the development of an optimized PBMC RNA extraction and RT-qPCR protocol. We employed a qPCR strategy of absolute quantification utilizing PrimerBank™ primers and ssoAdvanced™ Universal SYBR® Green Master-Mix. PBMC RNA was isolated with MagMAX™ *mirVana*™ Total RNA Isolation Kit and reverse transcribed with SuperScript™ IV First-Strand Synthesis System. Our assay provided single cell analytical sensitivity and a diagnostic sensitivity that could define response hierarchy from 1×10^4 cells. This assay offers an alternative to current best practice protein-based immunoassays, especially for limited PBMC numbers. This work has broad applicability for both clinical and primary research practice.

Acknowledgements

Funding

Authorship contributions

DJB and CL performed experiments. DJB, JLB, CL and DLD designed experiments. DJB, JLB, AJW, CL and DLD, analysed and interpreted the data. DJB, CL and DLD wrote the manuscript, with input from JLB and AJW.

Conflicts of interest

The authors declare that the research was conducted in the absence of any commercial or financial relationships that could be construed as a potential conflict of interest.

Data availability statement

All datasets for this study are available upon request.

2.2.8 Supplementary material

Supplementary Table S2.1. Technical and biological variability of RNA extraction kits. The mean standard deviation of technical (kit variability) and biological (sample variability) replicates from RT-qPCR analysis of *IFN-γ*, *RPL13a*, *SDHA* and *TBP* expression as determined following RNA extraction kit testing. 1×10^6 PBMCs were cultured with complete media (Non-Stim) or stimulated (Stim) with PMA/Iono for 6 hours. RNA was extracted using the RNeasy® Mini (Mini) Kit, the RNeasy® Micro (Micro) Kit (both QIAGEN), and the MagMAX™ *mirVana*™ (MagMAX) Total RNA Isolation Kit (Applied Biosystems), with concentration step performed using the RNeasy® MiniElute (+) Cleanup Kit (QIAGEN). All samples were reverse transcribed with Superscript™ III (Invitrogen). Data $\log_{10}$ transformed standard deviation of RNA expression of mean (copies/10^6cells) and (copies/μL). Change in standard deviation ($\Delta \text{Log10}(\sigma)$) calculated as biological variability over technical variability. Data were analysed using a two-way ANOVA with post-hoc Bonferroni's multiple-comparisons test. * Technical variability greater than biological variability.

	Technical Variability Mean Log$_{10}$(σ)		Biological Variability Mean Log$_{10}$(σ)		Δ Log$_{10}$(σ)	
IFN-γ	Non-Stim	Stim	Non-Stim	Stim	Non-Stim	Stim
Mini	0.210*	0.038	0.182	0.197	-0.027	0.159
Mini (+)	0.235	0.058	0.313	0.183	0.078	0.125
Micro	0.194*	0.053	0.090	0.222	-0.103	0.169
Micro (+)	0.144	0.051	0.228	0.248	0.084	0.196
MagMAX	0.221*	0.069	0.126	0.184	-0.095	0.116
MagMAX (+)	0.264	0.072	0.396	0.230	0.132	0.158
	P_{Ext} = NS					
RPL13a	Non-Stim	Stim	Non-Stim	Stim	Non-Stim	Stim
Mini	0.142	0.024	0.214	0.106	0.072	0.082
Mini (+)	0.045	0.066	0.110	0.116	0.066	0.050
Micro	0.051	0.039	0.120	0.089	0.068	0.051
Micro (+)	0.048	0.038	0.083	0.102	0.035	0.064
MagMAX	0.041	0.074	0.130	0.077	0.089	0.003
MagMAX (+)	0.069	0.064	0.139	0.118	0.070	0.054
	P_{Ext} = NS					
SDAH	Non-Stim	Stim	Non-Stim	Stim	Non-Stim	Stim
Mini	0.180	0.095	0.244	0.103	0.065	0.007
Mini (+)	0.057*	0.292*	0.045	0.099	-0.012	-0.193
Micro	0.100*	0.218*	0.025	0.078	-0.075	-0.140
Micro (+)	0.208*	0.061	0.166	0.111	-0.042	0.051
MagMAX	0.375*	0.102	0.186	0.129	-0.189	0.027
MagMAX (+)	0.150*	0.741*	0.149	0.431	-0.001	-0.310
	P_{Ext} = NS					
TBP	Non-Stim	Stim	Non-Stim	Stim	Non-Stim	Stim
Mini	0.130	0.036	0.206	0.100	0.076	0.063
Mini (+)	0.072	0.089	0.084	0.115	0.013	0.027
Micro	0.079	0.069	0.135	0.129	0.056	0.060
Micro (+)	0.054	0.043	0.067	0.094	0.012	0.051
MagMAX	0.058	0.065	0.225	0.072	0.166	0.006
MagMAX (+)	0.054	0.074	0.084	0.119	0.030	0.045
	P_{Ext} = NS					

Supplementary Table S2.2. Technical and biological variability of cDNA kits. The mean standard deviation of technical (kit variability) and biological (sample variability) replicates from RT-qPCR analysis of IFN-γ, RPL13a, SDHA and TBP expression as determined following RNA extraction kit testing. $1x10^6$ PBMCs were cultured with complete media (Non-Stim) or stimulated (Stim) with PMA/Iono for 6 hours. RNA was reverse transcribed with either Superscript™ III (SSIII), Superscript™ IV (SSIV) (both Invitrogen), iScript™ Advanced (iScript) (BioRad) or High-Capacity (HC) (ThermoFisher) reverse transcription kits. Data log10 transformed standard deviation of RNA expression of mean (copies/106 cells) and (copies/μL). Change in standard deviation (Δ Log10(σ)) calculated as biological variability over technical variability. Data were analysed using a two-way ANOVA with post-hoc Bonferroni's multiple-comparisons test.

	Technical Variability Mean $Log_{10}(\sigma)$		Biological Variability Mean $Log_{10}(\sigma)$		$\Delta Log_{10}(\sigma)$	
IFN-γ	Non-Stim	Stim	Non-Stim	Stim	Non-Stim	Stim
SSIII	0.139	0.055	0.258	0.210	0.119	0.155
SSIV	0.139	0.080	0.260	0.217	0.121	0.137
iScript	0.123	0.092	0.312	0.301	0.189	0.209
HC	0.162	0.065	0.251	0.205	0.088	0.140
	$P_{Ext} = NS$					
RPL13a	Non-Stim	Stim	Non-Stim	Stim	Non-Stim	Stim
SSIII	0.074	0.065	0.132	0.079	0.057	0.013
SSIV	0.085	0.076	0.167	0.134	0.082	0.058
iScript	0.118	0.115	0.203	0.207	0.085	0.092
HC	0.075	0.082	0.129	0.102	0.055	0.019
	$P_{Ext} = NS$					
SDAH	Non-Stim	Stim	Non-Stim	Stim	Non-Stim	Stim
SSIII	0.106	0.082	0.118	0.113	0.012	0.031
SSIV	0.081	0.106	0.104	0.106	0.023	0.000
iScript	0.120	0.107	0.189	0.204	0.068	0.097
HC	0.094	0.105	0.122	0.119	0.028	0.014
	$P_{Ext} = NS$					
TBP	Non-Stim	Stim	Non-Stim	Stim	Non-Stim	Stim
SSIII	0.079	0.065	0.122	0.118	0.044	0.052
SSIV	0.074	0.075	0.140	0.137	0.067	0.062
iScript	0.090	0.088	0.137	0.245	0.046	0.157
HC	0.072	0.079	0.101	0.113	0.029	0.034
	$P_{Ext} = NS$					

Supplementary Table S2.3. Technical guideline for PBMC RNA quantification via RT-qPCR. Summary of optimization results for human peripheral blood mononuclear cell (PBMC) RNA extraction and quantification with reverse transcription quantitative PCR (RT-qPCR). This assay allows single cell analytical sensitivity and a diagnostic sensitivity that can define immunodominant hierarchy from 1×10^4 cells.

Workflow Order	Protocol Step		Optimal Kit	Pros	Cons
1	PBMC RNA Extraction		MagMAX™ *mirVana*™ Total RNA Isolation Kit (Applied Biosystems)	- PBMC RNA yield and concentration significantly increased - Low variability between technical replicates - Time and cost efficient - Amendable to automation	- Beads bind total nucleic acid (requires DNase) - Requires specialist equipment (*i.e.* plate shaker and magnetic stand)
2	RNA to cDNA Synthesis		SuperScript™ IV First-Strand Synthesis System (ThermoFisher)	- PBMC RNA yield and concentration significantly increased - Low variability between technical replicates	- Expensive relative to other cDNA synthesis kits
3	qPCR	Reaction Master-mix	ssoAdvanced™ Universal SYBR® Green Master-Mix (Bio-Rad)	- Optimal reaction efficiency and largest dynamic range	- Expensive relative to other SYBR chemistry master-mix kits
		Primer Selection	PrimerBank™	- Minimal primer optimization required - Designed to provide optimal binding at 60°C - Covers most known human and mouse genes	- May not cross introns - May not be as efficient as manually designed primers
		Quantification Strategy	Absolute quantification based on standard curve	- Remove potential reference gene bias post PBMC stimulation	- May introduce technical error if experiment is inappropriately controlled

Chapter 3: A High-Throughput Screening RT-qPCR Assay for Quantifying Surrogate Markers of Immunity from PBMCs

3.1 Chapter introduction

We next sought to miniaturise and cost-optimise our sensitive RT-qPCR protocol to develop a protocol specifically designed for high-throughput screening (HTS).,

I hypothesised the sensitive RT-qPCR protocol could be optimised to create an assay which met high throughput screening uniformity and signal variance testing standards.

To test this, I addressed the following experimental aims:

1. Miniaturise and cost-optimise the assay.
2. Confirm high throughput screening uniformity and signal variance of the optimised assay.
3. Define the analytical and diagnostic sensitivity of the assay.

This chapter has been published:

Browne, D. J., Kelly, A. M., Brady, J. L., & Doolan, D. L. (2022). A high-throughput screening RT-qPCR assay for quantifying surrogate markers of immunity from PBMCs. Frontiers in Immunology, 13, 962220.

3.2 Published manuscript

A high-throughput screening (HTS) RT-qPCR assay for quantifying surrogate markers of immunity from PBMCs

Running head: HTS RT-qPCR protocol for PBMCs

Daniel J. Browne[1], Ashton M. Kelly[1], Jamie L. Brady[1] and Denise L. Doolan[1*]

[1] Centre for Molecular Therapeutics, Australian Institute of Tropical Health and Medicine, James Cook University, Cairns, QLD 4878, Australia

3.2.1 Abstract

Immunoassays that quantitate cytokines and other surrogate markers of immunity from peripheral blood mononuclear cells (PBMCs), such as flow cytometry or Enzyme-Linked Immunosorbent Spot (ELIspot), allow highly sensitive measurements of immune effector function. However, those assays consume relatively high numbers of cells and expensive reagents, precluding comprehensive analyses and high-throughput screening (HTS). To address this issue, we developed a sensitive and specific reverse transcription-quantitative PCR (RT-qPCR)-based HTS assay, specifically designed to quantify surrogate markers of immunity from very low numbers of PBMCs. We systematically evaluated the volumes and concentrations of critical reagents within the RT-qPCR protocol, miniaturizing the assay and ultimately reducing the cost by almost 90% compared to current standard practice. We assessed the suitability of this cost-optimized RT-qPCR protocol as an HTS tool and determined the assay exceeds HTS uniformity and signal variance testing standards. Furthermore, we demonstrate this technique can effectively delineate a hierarchy of responses from as little as 50,000 PBMCs stimulated with CD4$^+$ or CD8$^+$ T cell peptide epitopes. Finally, we establish that this HTS-optimized protocol has single-cell analytical sensitivity and a diagnostic sensitivity equivalent to detecting 1:10,000 responding cells (*i.e.,* 100 Spot Forming Cells/10^6 PBMCs by ELIspot) with over 90% accuracy. We anticipate this assay will have widespread applicability in preclinical and clinical studies, especially when samples are limited, and cost is an important consideration.

3.2.2 Graphic abstract
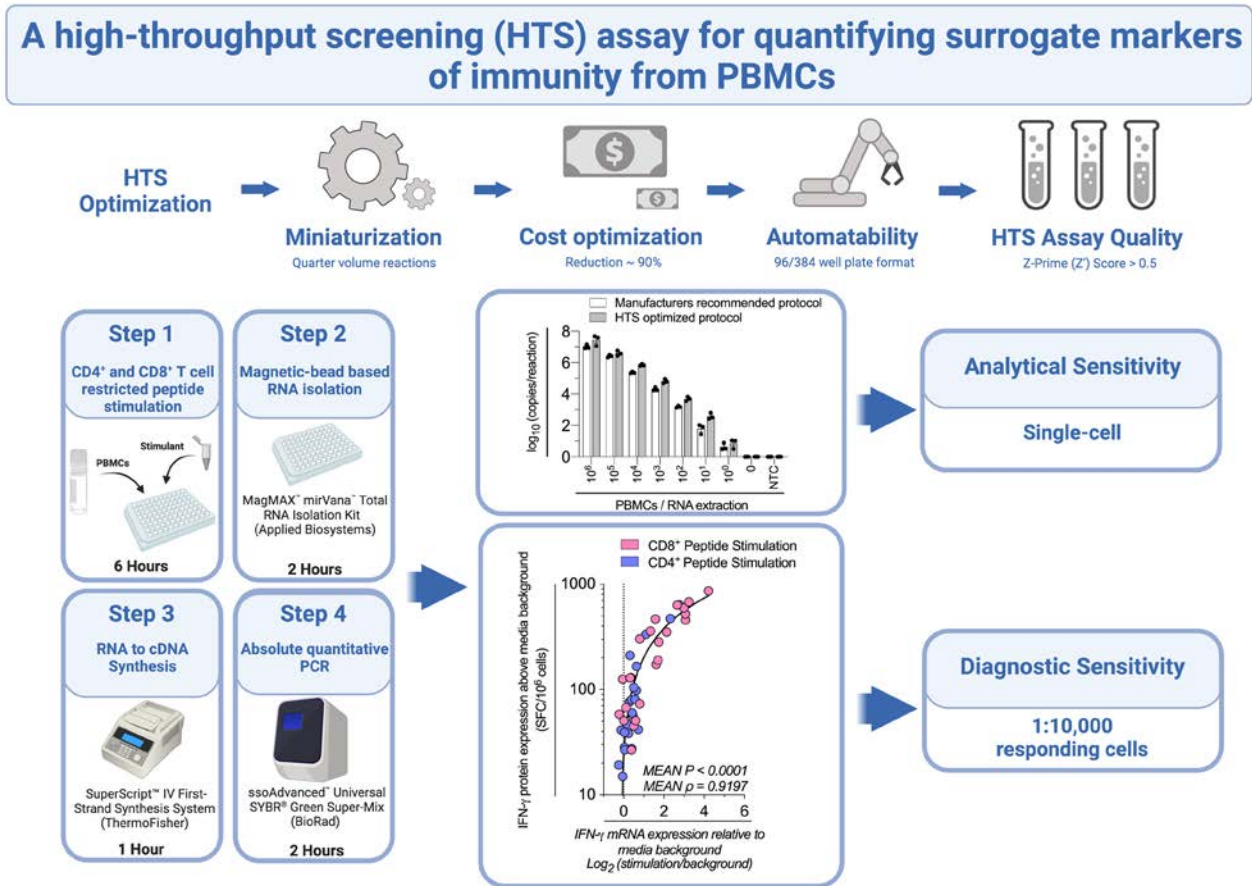
3.2.3   Introduction

Ex vivo measurements of surrogate markers of immunity have informed immunobiological processes [425], provided disease biomarkers [426], and delivered measures of the effectiveness of candidate drugs and vaccines [427]. These assays typically incubate peripheral blood mononuclear cells (PBMCs) in the presence of defined antigenic or mitogenic stimulants and quantitate protein production of effector molecules (*e.g.,* cytokines) using immunoassays such as flow cytometry or Enzyme-Linked Immunosorbent Spot (ELIspot) [350]. ELIspot and flow cytometry both consume high-cost reagents (*e.g.,* monoclonal antibodies) and require relatively high numbers of PBMCs to achieve sufficient sensitivity [352, 353]; especially when considering responses from sub-populations within PBMCs, such as antigen-reactive $CD4^+$ or $CD8^+$ T cells with relatively low precursor frequency [354]. These factors pose severe constraints which preclude comprehensive immune evaluation and high-throughput screening (HTS) experiments.

PCR-based molecular diagnostics present a potential solution; in particular, reverse transcription quantitative-PCR (RT-qPCR), the gold-standard transcriptome-based assay [355], allows highly sensitive and specific *ex vivo* measurements of surrogate transcriptional markers of immunity from low numbers of PBMCs [356]. However, due to costs and challenges associated with automation, RT-qPCR is generally considered a low throughput method [357]. Ideally, an RT-qPCR-based HTS assay for quantifying surrogate markers of immunity would enable measurements from low numbers of PBMCs and use techniques that are cost-effective and amenable to both miniaturization and automation [428].

We have recently published a systematic evaluation of RNA extraction and reverse transcription kits to maximize the quantity and quality of isolated RNA and synthesized cDNA from human PBMCs [356]. We found the mRNA expression of a key surrogate marker of immunity interferon-gamma (IFN-γ) correlated strongly to IFN-γ protein production measured by ELIspot [356]. *Ex vivo* assays that quantify mRNA as a surrogate marker of immunity are typically limited by low genome-wide mRNA-protein correspondence rates [429]. Nevertheless, certain classes of proteins, such as IFN-γ and other rapidly produced and secreted cytokines are much more highly correlated [356, 430], and therefore, may provide an mRNA target with comparable accuracy to protein-based immunoassays. Since each stage of this RT-qPCR assay is conducted in 96-well or 384-well format, the protocol is potentially suitable as

an HTS assay. However, RT-qPCR is limited by cost, especially for studies involving many thousands of conditions that are typical of HTS [431].

To facilitate comprehensive HTS of surrogate markers of immunity from PBMCs, we present herein an HTS-optimized, highly sensitive and specific RT-qPCR protocol. This protocol reduces the cost of the RT-qPCR by almost 90%, is amenable to both miniaturization and automation, and achieved a ranking of excellent (Z′ factor >0.5 [432]) when evaluated for HTS uniformity and signal variance. When considering the analytical sensitivity (*i.e.,* smallest number of cells detectable) and diagnostic sensitivity (*i.e.,* smallest detectable response to stimulation) of our optimized protocol [375], we established single-cell analytical sensitivity and a diagnostic sensitivity equivalent to detecting 1:10,000 responding cells (*i.e.,* 100 SFC/10^6 PBMCs by ELIspot) with over 90% accuracy. As a proof-of-concept for high-throughput *in vitro* PBMC functional testing, we applied this assay to investigate antigen-specific cytokine gene expression kinetics across 12 hours, with hourly resolution. Robust peptide-specific IFN-γ mRNA expression responses were detected between 3-9 hours post-stimulation, which we determined peaked at 6 hours post-stimulation when correlated to IFN-γ protein production across a larger number of peptides. This protocol provides a robust, scalable, and cost-effective RT-qPCR-based assay for high-throughput quantification of surrogate markers of immunity.

3.2.4   Materials and equipment

PBMC stimulatory reagents

- Phorbol 12-Myristate 13-Acetate (PMA), (Sigma-Aldrich)

- Ionomycin (Iono), (Sigma-Aldrich)

- Human cytomegalovirus, Epstein Barr virus, polyomavirus, and influenza virus Synthetic peptides (**Supp Table S3.1**).

SYBR master-mix kits

- ssoAdvanced™ Universal SYBR® Green Master-Mix (Bio-Rad)

RNA extraction kits

- MagMAX™ *mirVana*™ Total RNA Isolation Kit (Applied Biosystems)

RNA to cDNA synthesis kits

- SuperScript™ IV First-Strand Synthesis System (ThermoFisher)

Quantitative PCR primers

- PrimerBank™ primers (**Supp Table S3.2**)

Antibodies

- anti-human IFN-γ monoclonal antibody (mAb) (Clone 1-D1K, MABTECH)

- anti-human IFN-γ biotinylated mAb (Clone 7-B6-1, MABTECH)

Equipment

- QuantStudio 5 Real-Time PCR system (Applied Biosystems)

- AID ELIspot reader system (Autoimmun Diagnostika GmbH, Germany)

Software

- QuantStudio Design and Analysis Software (v1.4.3, Applied Biosystems)

- ProcartaPlex Analyst Software (v1.0, ThermoFisher)

- GraphPad Prism (v7, GraphPad)

3.2.5 Methods

Samples

PBMCs

PBMCs from healthy donors were isolated by standard density gradient centrifugation and cryopreserved in 90%FBS/10%DMSO. Before use, samples were thawed rapidly at 37°C, treated with DNase I (100 μg/mL; StemCell Technologies), and rested for 18 hours at $2x10^6$cells/mL in RPMI-1640 supplemented with 10% heat-inactivated AB human serum (Sigma-Aldrich), 100U/mL penicillin/streptomycin (ThermoFisher Scientific), 1xMEM non-essential amino acids (ThermoFisher Scientific), 2mM glutaMAX (ThermoFisher Scientific), 10mM HEPES (ThermoFisher Scientific), and $5x10^{-5}$M β-Mercaptoethanol (Sigma-Aldrich)

(R10 media) at 37°C and 5% CO_2. Viable PBMCs were counted with a CASY™ Cell Counter (OLS-OMNI Life Science).

Cell stimulation

Synthetic peptides (10 μg/mL) representing $CD4^+$ and $CD8^+$ T cell predicted epitopes from influenza virus, Epstein-Barr virus and cytomegalovirus (**Supp Table S3.1**) were tested alongside PMA/Iono (50ng/mL PMA, 1,000ng/mL Ionomycin) mitogen positive-control and a media-only negative-control. For RT-qPCR analysis; PBMCs were stimulated in 200 μL R10 media in 96-well U-bottom plates. For IFN-γ ELIspot analysis, 4×10^5 PBMCs per well were stimulated for 24 hours in 96-well ELIspot plates.

RT-qPCR optimization

RNA extraction and reverse transcription

RNA was extracted as previously described [356], with MagMAX™ *mirVana*™ Total RNA Isolation Kit (Applied Biosystems) following manufacturer's instructions. Extracted RNA was converted to cDNA with SuperScript™ IV First-Strand Synthesis System (ThermoFisher) following manufacturer's instructions unless otherwise stated. For 'Full Volume' protocols, all reagents were used at the volume recommended by the manufacturer. For 'Half Volume' or 'Quarter Volume' protocol, all reagents were used at 50% or 25% of the volume recommended by the manufacturer, respectively. DEPC-Treated H_2O (Invitrogen) was substituted to maintain equal reaction volume when evaluating presence, absence, or titration of reagents.

Quantitative PCR (qPCR)

qPCR was conducted as previously described [356]. Briefly, mRNA copies/reaction were determined with absolute quantification based on a standard curve. *IFN-γ*, *TNF-α* and *IL-2* specific desalt-grade (Sigma-Aldrich) primers (**Supp Table S3.2**), obtained from PrimerBank™ [410] were used at 500 nM using ssoAdvanced™ Universal SYBR® Green Master-Mix (Bio-Rad). All reactions were run in technical triplicate in accordance with MIQE guidelines [400] at either 10 μL or 5 μL total volume. For 10 μL reaction volumes, 1 μL undiluted reverse transcription eluent was added per reaction. For 5 μL reaction volumes, 1 μL of reverse transcription eluent diluted 1:2 in Ultra-Pure™ H_2O (Invitrogen) was added. Data was acquired using a QuantStudio5 Real-Time PCR system running QuantStudio Design and Analysis Software (v1.4.3, Applied Biosystems). Primer reaction efficiency was calculated by amplification of logarithmically diluted cDNA. A detailed final HTS-optimized RT-qPCR protocol is available (**Supplementary Protocol: Cost-Optimized Protocol).**

HTS uniformity and signal variance testing

Validation of uniformity and signal variance was conducted in accordance with the 'HTS Assay Validation' chapter of the National Institute of Health (NIH) 'Assay Guidance Manual' [433]. Briefly, the coefficient of variation (CV) values and Z-Prime values were calculated from the mean and the standard deviation of the qPCR cycle threshold values for the 'Min', 'Mid' and 'Max' signals. *"Min" Signal* was the 'media only' stimulation, the *"Max" Signal* was 'PMA/Iono stimulation', and the *"Mid" Signals* was KGI and ARS peptide stimulations.

Protein analysis

IFN-γ enzyme-linked immunospot (ELIspot) assay

IFN-γ ELIspot assays were performed as previously described [356]. Briefly, 4×10^5 PBMCs were plated in triplicate into 96-well MAIPS45-10 plates (Merck) and stimulated for 24 hours with or without peptide, PMA/Iono or media.

Analytical and diagnostic sensitivity testing

For determination of analytical sensitivity, mRNA was extracted from $\log_{10}$ serially diluted unstimulated PBMCs (10^6-10^0 cells/extraction) with a media-only extraction control processed in parallel. mRNA, cDNA synthesis and qPCR was conducted using either the manufacturers recommended protocol as previously described [356], or the HTS-optimized RT-qPCR protocol. Two strategies were tested for determining diagnostic sensitivity, where false negatives (FN) were considered mRNA values ≤ 0 or <1 where the matched ELIspot data was >0 or ≥ 100 respectively; and true positives (TP) were considered mRNA values >0 or ≥ 1 where the matched ELIspot data was >0 or ≥ 100 respectively. Assay accuracy was calculated as ((TP+TN)/(TP+TN+FP+FN)).

Data analysis

The strength of the association between RT-qPCR *IFN-γ* mRNA gene expression and ELIspot IFN-γ protein expression was tested by Pearson's correlation on log-transformed data. *P* values and Pearson's correlation coefficient (ρ) were reported. Analytical sensitivity was analysed with $\log_{10}$ transformed data using a repeated-measures two-way ANOVA. GraphPad Prism version 8.3.0 (GraphPad Software) was used and *P* values <0.05 were considered statistically significant.

3.2.6   Results

A high correlation between IFN-γ mRNA and IFN-γ protein ELIspot quantification persisted following RT-qPCR reagent miniaturization

To develop a sensitive and specific HTS tool to quantify surrogate markers of immunity from PBMCs, we first stimulated either 4×10^5, 1×10^5 or 0.5×10^5 PBMCs with CD4$^+$ T cell peptide epitopes. *IFN-γ* mRNA expression was quantified by RT-qPCR [356] and correlated with IFN-γ protein production quantified by 'gold-standard' ELIspot. When tested with a Spearman's rank correlation coefficient (ρ), we found a high correlation between mRNA and protein, which decreased with stimulated cell number (**Supp Fig. S3.1A**). When correlating *IFN-γ* mRNA expression with IFN-γ protein production, we modelled logarithmically (Log$_2$) transformed mRNA data against linear protein data presented on a logarithmic scale [434]. Log$_2$ transformation allowed visualization of protein measurements approaching the limit of ELIspot sensitivity (*i.e.,* <100 SFC/10^6 PBMCs) [435]. This graphical presentation did not change the ρ or *P* values (**Supp Fig. S3.1B**). Given the high correlation between gene and protein expression observed, we chose to progress with testing using 1×10^5 stimulated PBMCs.

We next sought to systematically reduced the volume and concentration of the reverse transcription (RT), qPCR and RNA isolation reagents. We therefore stimulated 1×10^5 PBMCs with a portfolio of well-characterized CD8$^+$ and CD4$^+$ T cell restricted peptide epitopes and evaluated IFN-γ mRNA expression from quarter volume RT reactions and RNA isolations, and from 5 μL total volume qPCR reactions. When considering the mean ρ of the triplicate replicates, mRNA expression retained a high correlation with protein expression at all conditions tested (**Fig. 3.1 (A1)**: *P* < 0.0001, ρ $= 0.8139$; *vs.* **Fig. 3.1 (A4)**: *P* < 0.0001, ρ $= 0.8914$). When considering the ρ of the individual triplicate experimental technical replicates, multiple comparisons testing found a significantly increased correlation between IFN-γ mRNA and protein following the use of quarter-volume RNA extractions (**A1** *vs.* **A4** *P = 0.0110*, **Supp Fig. S3.2A**). When considering the cycle threshold value of all measured samples (*i.e.,* inclusive of controls), the RT-qPCR protocol measurements correlated highly between all test conditions (ρ > 0.98, **Supp Fig. S3.2A**). Overall, these data demonstrate that all stages of our RT-qPCR protocol are amenable to miniaturization without loss of sensitivity.
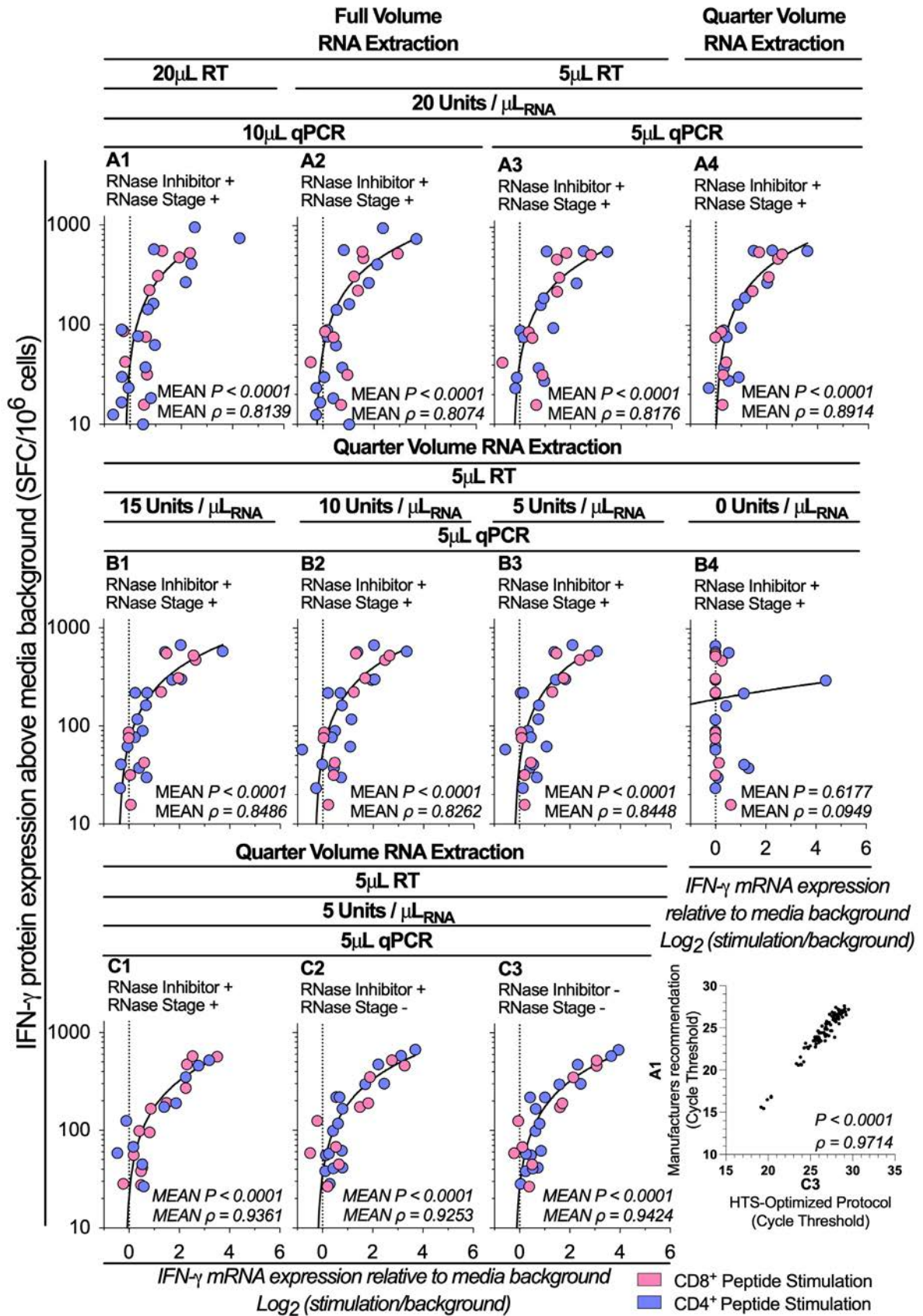
Figure 3.1. Assay optimization. IFN-γ mRNA expression by RT-qPCR correlated to IFN-γ protein production by ELIspot across various test conditions denoted A1-A4, B1-B4 and C1-C3 following stimulation of PBMCs (1×10^5; n=5) with peptides representing two well-defined CD4$^+$ (Blue Dots) T cell peptide epitopes (Influenza$_{57-71}$ KGILGFVFTLTVPSE and Influenza$_{260-284}$ ARSALILRGSVAHKSCLPACVYGP) and two CD8$^+$ (Pink Dots) T cell peptide epitopes (Influenza$_{58-76}$ GILGFVFTL and Epstein Barr Virus$_{280-288}$ GLCTLVAML). Conditions A1-A3 were evaluating the correlation between RNA isolation, cDNA synthesis and qPCR reagent miniaturizations; B1-B4 were evaluating the correlation between reverse transcription (RT) reactions containing 15, 10, 5, and 0 units/µL$_{RNA}$; and C1-C4 were evaluating the correlation between reverse transcription (RT) reactions including RNase Inhibitors and a post-cDNA synthesis RNase digestion stage, and reactions excluding the RNase digestion stage; and RT reactions excluding the RNase digestion stage and RT reactions excluding both the RNase digestion stage and RNase Inhibitors. Shown are the mean gene copy number of technical triplicate RT-qPCR assays correlated to mean of triplicate IFN-γ spot forming cells (SFC) by ELIspot, with both mRNA and protein measurements corrected for background. The technical means of qPCR cycle threshold values (Ct value) combined (for all tests and controls) were correlated between test conditions A1 and C3. ELIspot data <10 SFC/10^6 were graphically omitted. The strength of each association was tested by Pearson's correlation on log-transformed data, with *P* values and Pearson's correlation coefficient (ρ) reported.

A high degree of correlation between mRNA and protein was maintained following a four-fold reduction in the concentration of SuperScript™ IV RT enzyme

We next sought to determine whether reducing the concentration of the SuperScript™ IV RT enzyme impacted the correlation between *IFN-γ* mRNA and IFN-γ protein quantification. We titrated the SuperScript™ IV RT enzyme concentration from 15 to 5 units/µL$_{RNA}$. We found the correlation between the RT-qPCR protocol and ELIspot was statistically significant across all RT reactions which contained enzyme (**Fig. 3.1 (B3)**: $P < 0.0001$, ρ = 0.8448). When considering the ρ of the triplicate experimental technical replicates, reducing the concentration of the RT enzyme did not impact the high correlation between IFN-γ mRNA and protein (**Supp Fig. S3.2B**). When considering the cycle threshold value of all measured samples, the RT-qPCR protocol measurements correlated highly between all tested conditions which contained enzyme (10 *vs.* 5 units/µL$_{RNA}$: $P < 0.0001$, ρ = 0.9969; **Supp Fig. S3.2B**), but not against the no-enzyme control (5 *vs.* 0 units/µL$_{RNA}$: $P = 0.1072$, ρ = 0.1681; **Supp Fig. S3.2B**). These data demonstrate that highly accurate measurements of epitope-specific *IFN-γ* mRNA stimulatory responses can be achieved with RT reactions containing the SuperScript™ IV enzyme at a concentration as little as 5 units/µL$_{RNA}$.

RNase inhibitors and RNase treatment are not required to maintain a high correlation between mRNA and protein measurements

We next sought to investigate the impact of RNase inhibitors and post-cDNA synthesis Ribonuclease H (RNaseH) digestion on the correlation between IFN-γ mRNA and IFN-γ protein measurements. When stimulating $1x10^5$ PBMCs with a range of CD8$^+$ and CD4$^+$ T cell restricted peptide epitopes, we found the correlation between the RT-qPCR protocol and ELIspot was statistically significant across all conditions regardless of the presence of RNase inhibitor or RNaseH ($P < 0.0001$, $\rho = 0.9424$; **Fig. 3.1 (C3)**). When considering the ρ of the triplicate experimental technical replicates, there was no statistically significant change in the correlation between IFN-γ mRNA and protein either when the RNase digestion was eliminated or when the RNase inhibitors were absent (**Supp Fig. S3.2C**); and the cycle threshold values of all measured samples correlated highly between all tested conditions ($\rho>0.99$; **Supp Fig. S3.2C**). These data demonstrate that omitting RNase inhibitors or RNaseH had no impact on the correlation between IFN-γ mRNA and protein measurements. When considering the cycle threshold value of all measured samples (*i.e.,* inclusive of controls), the RT-qPCR protocol measurements correlated highly between the manufacturers recommended protocol and the HTS-optimized protocol ($P < 0.0001$, $\rho = 0.9714$; **Fig. 3.1 A1** *vs.* **C3**). Taken together, the protocol miniaturization and modifications described above resulted in a reduction of the overall cost of the RT-qPCR by almost 90%.

HTS assay quality assessment

We next sought to assess the uniformity and signal variability of this optimized assay to demonstrate its suitability as an HTS tool. We stimulated $1x10^5$ PBMCs with CD4$^+$ T cell peptide epitopes in technical triplicate inter-day tests and compared IFN-γ mRNA expression as measured with the above-optimized protocol to IFN-γ protein production measured by ELIspot. The correlation between the RT-qPCR protocol and ELIspot was statistically significant across all three technical replicates (**Supp. Fig. S3.3**). When validating the uniformity and signal variance between these replicates, all tested coefficient of variation (CV), values were well below the NIH's 20% acceptance criteria threshold (between 1.20%-1.49%, 2.48%-4.45% and 1.02%-2.60% for the *Min*, *Mid* and *Max* signals, respectively; **Table 3.1**). The Z-prime score (Z′) of the replicates ranged from 0.548-0.630, all above the NIH's 0.5 threshold for 'Excellent HTS Assay' [432]. These data demonstrate that this assay has uniformity and signal variability that passes the initial HTS assay quality assessment.

Table 3.1. Assay uniformity and quality assessment

EXPT	MEDIA ONLY (*Min Signal*)			KGI (*Mid Signal 1*)			ARS (*Mid Signal 2*)			PMA/Iono (Max *Signal*)			
	Mean	**SD**	**CV(%)**	**Mean**	**SD**	**CV(%)**	**Mean**	**SD**	**CV(%)**	**Mean**	**SD**	**CV(%)**	**Z′**
1	28.239	0.671	1.37%	26.697	2.056	4.45%	26.959	1.626	3.48%	19.937	0.353	1.02%	0.630
2	28.454	0.732	1.49%	26.445	1.716	3.75%	27.365	1.173	2.48%	18.364	0.827	2.60%	0.548
3	27.088	0.563	1.20%	25.318	1.148	2.62%	26.253	1.542	3.39%	17.466	0.564	1.86%	0.627

Mean: Mean of cycle threshold value (Ct); SD: Standard deviation of Ct values; n=5

Pass: Coefficient of variation (CV) < 20%; Z-prime score (Z′) > 0.4

The highest magnitude of response following peptide epitope stimulation occurs between 3 and 6-hours post-stimulation

We next sought to determine the optimal time point post-stimulation for correlating mRNA expression to protein production by assessing the kinetics of cytokine expression. We evaluated the kinetics of IFN-γ, *IL-2,* and *TNFα* mRNA expression each hour across 12 hours from 1×10^5 PBMCs stimulated with a range of CD8$^+$ and CD4$^+$ T cell restricted peptide epitopes. Donor-specific peak IFN-γ mRNA expression was peptide-specific (**Fig. 3.2A**). The profile of *IL-2* mRNA expression was similar to IFN-γ, but the *TNFα* peak tended to be slightly delayed (**Supp Fig. S3.4**). When correlating *IFN*-γ mRNA expression to IFN-γ protein production by ELIspot, we found a high correlation was retained across many time points, with the highest occurring at the 3 hours post-stimulation timepoint (3-hours: $P < 0.0001$, ρ = 0.9478; **Fig. 3.2B**). These data suggested that although no single timepoint is optimal for all peptides, as peak IFN-γ mRNA expression is donor and peptide-specific, the highest magnitude of IFN-γ mRNA response to peptide stimulation (*i.e.,* expression relative to media background) generally occurs between 3- and 9-hours post-stimulation.
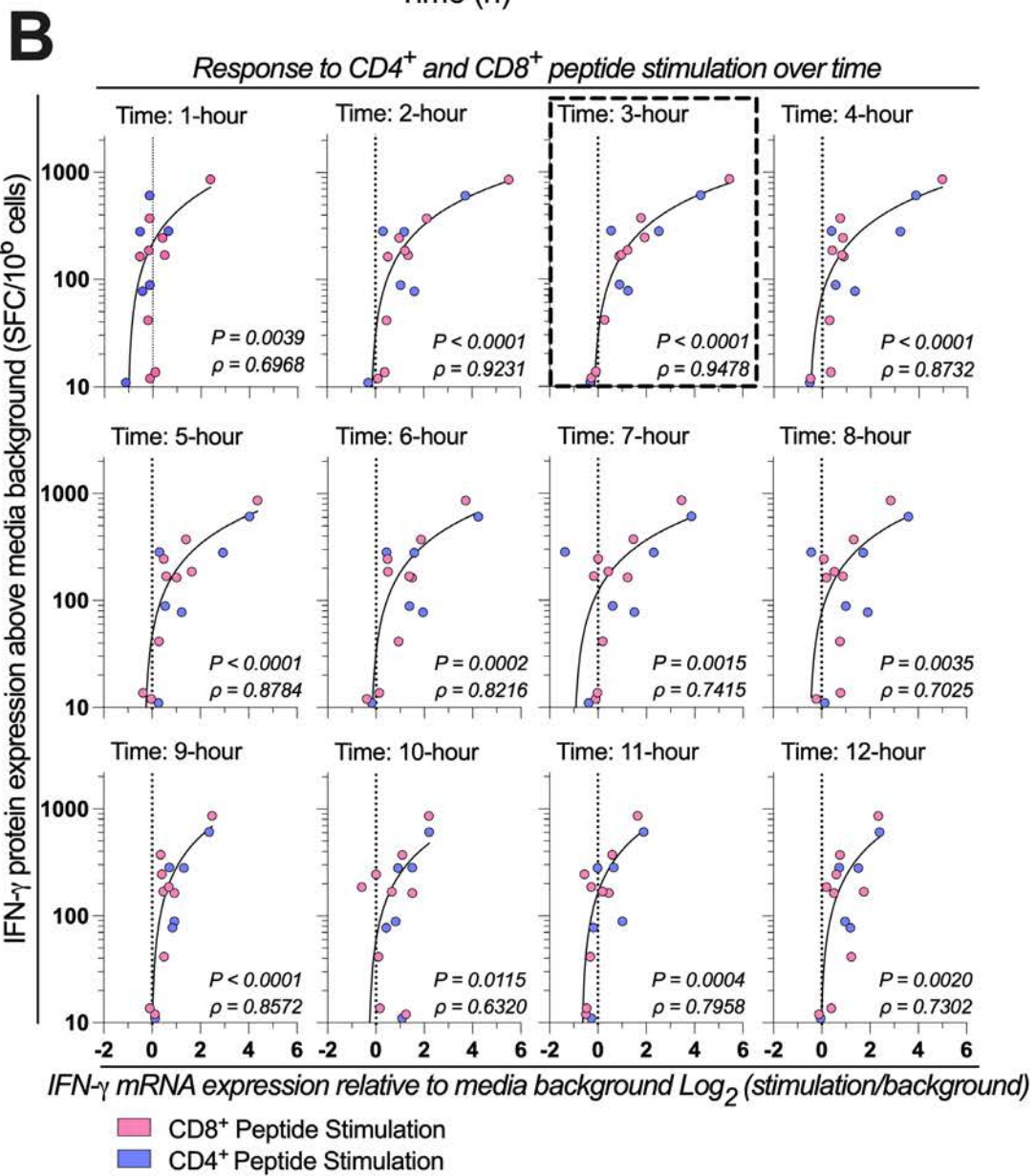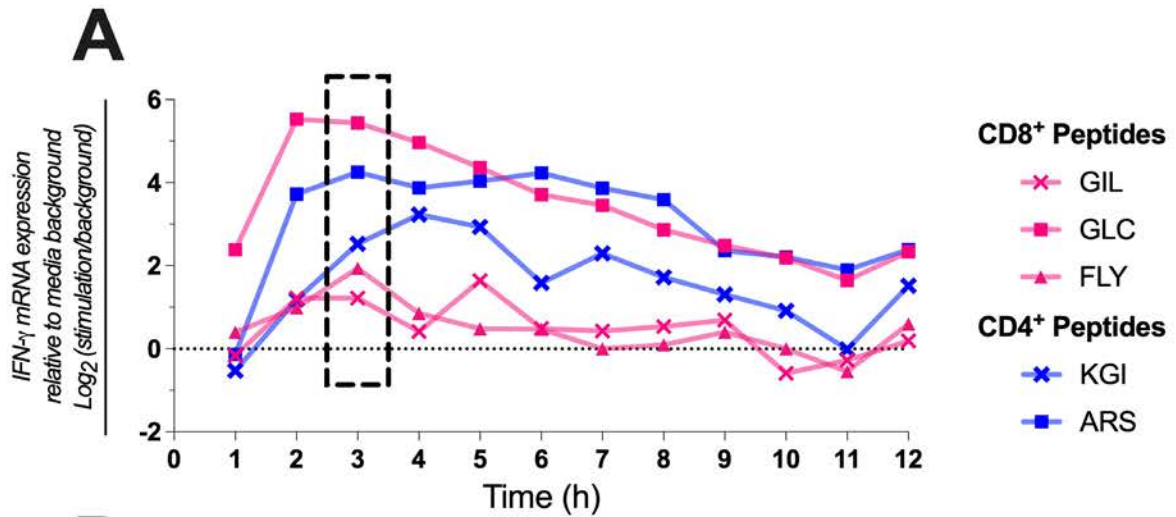
Figure 3.2. Response to CD4$^+$ and CD8$^+$ T cell peptide epitope stimulation over time. **(A)** IFN-γ mRNA expression by absolute-quantitative HTS-optimized RT-qPCR in response to stimulation with two CD4$^+$ (Influenza$_{57-71}$ KGI and Influenza$_{260-284}$ ARS) and three CD8$^+$ (Influenza$_{58-76}$ GIL, Epstein Barr Virus$_{356-364}$ FLY and Epstein Barr Virus$_{280-288}$ GLC) peptides representing well-defined T cell epitopes across 1-12 hours post-stimulation. Shown is a representative sample. **(B)** IFN-γ mRNA expression by RT-qPCR correlated to IFN-γ protein production by ELIspot in response mRNA expression. Single RNA extractions, with single reverse transcription reactions per n (n=3) per stimulation were performed, with qPCR and ELIspot performed in technical triplicate. Technical mean of gene copy number or spot forming cells (SFC) corrected for background are shown. The strength of the association between RT-qPCR *IFN-γ* mRNA gene expression and ELIspot IFN-γ protein expression was tested by Pearson's correlation on log transformed data. ELIspot data <10 SFC/10^6 were graphically omitted. The 3-hour timepoints are highlighted (dashed box). *P* values and Pearson's correlation coefficient (ρ) reported.

The HTS-optimized protocol has single-cell analytical sensitivity and a diagnostic sensitivity equivalent to at least 100 SFC/106 by ELIspot

Finally, we sought to investigate the analytical sensitivity (*i.e.,* smallest number of cells detectable) and diagnostic sensitivity (*i.e.,* smallest detectable response to stimulation [375]) of this HTS-optimized assay. To assess the analytical sensitivity, RNA was extracted from a log$_{10}$ serial dilution of unstimulated PBMCs, and the expression of IFN-γ and the reference gene *60S ribosomal protein L13a* (RPL13a) were determined using the HTS-optimized protocol in comparison to the manufacturer's recommended protocol (**Fig. 3.3A**). *RPL13a* expression was detected in all tested biological replicates at the single-cell level in both protocols. These data establish that the HTS-optimized protocol can quantify RNA to the single-cell level. IFN-γ expression was detected when extracted from cell numbers typical of PBMC stimulation assays for both protocols (10^6-10^4 PBMCs per stimulation; **Fig. 3.3A**) [356].

To assess the diagnostic sensitivity of the assay, we stimulated 1x10^5 PBMCs with a range of CD8$^+$ and CD4$^+$ T cell restricted peptide epitopes, and compared IFN-γ mRNA expression from 3-hours and 6-hours to IFN-γ protein production measured by ELIspot. Data were pooled from three inter-day experiments, each performed in technical triplicate replicate. The combined mRNA/protein correlation was statistically significant (*P* < 0.0001, **Fig. 3.3B**) at 3-hour and 6-hour time points in agreement with previously acquired data. The combined CD4$^+$ and CD8$^+$ peptide mRNA/protein correlation were highest at the 6-hour time point (ρ = 0.8716

vs. $\rho = 0.9197$; 3 hours *vs.* 6 hours; **Fig. 3.3B**). Additionally, we found the RT-qPCR true-positive rate (*i.e.,* inverted ratio of false-negative (FN) RT-qPCR results relative to the true-positive (TP) RT-qPCR results) compared to ELIspot at 3- and 6-hours crossed 95% (*i.e.,* FN<5% of total RT-qPCR results) at 50.8 and 41.7 SFC/10^6 PBMCs respectively (**Supp Fig. S3.5**). When considering the ρ of the inter-day technical replicates, the IFN-γ mRNA and protein correlation varied between experiments and time ($P_{\text{EXPT}} < 0.0001$; $P_{\text{Time}} < 0.0001$; **Fig. 3.3C**). The interaction was also statistically significant ($P_{\text{EXPTxTime}} < 0.0001$; **Fig. 3.3C**), which demonstrates the optimal timepoint for correlating IFN-γ mRNA expression and protein production is both donor- and peptide-specific. However, when considering large numbers of peptides and samples, these data demonstrate that 6-hours post-stimulation produces a marginally higher correlation.

To determine the diagnostic sensitivity of the HTS-optimized RT-qPCR protocol, we stimulated 1×10^5 PBMCs with 30 CD8$^+$ cell restricted peptide epitopes and compared IFN-γ mRNA expression from 6-hours to IFN-γ protein production measured by ELIspot (**Supp Fig. S3.6**) and combined these data with all above qPCR and ELIspot responses when RT-qPCR data were collected with the HTS-optimized protocol. When considering a threshold of positivity as responses greater than 0, the assay accuracy was calculated as 73.3% (**Fig. 3.3D**). When considering IFN-γ protein expression equivalent to or greater than 100 SFC/10^6 PBMC, and a $\log_2$ relative increase of IFN-γ mRNA equivalent to or greater than 1 (*i.e.,* a doubling of IFN-γ mRNA expression), the assay accuracy was calculated as 90.8% (**Fig. 3.3D**). Taken together, these data establish that our HTS-optimized protocol has single-cell analytical sensitivity and a diagnostic sensitivity conservatively estimated to be at least equivalent to detecting 1:10,000 responding cells (*i.e.,* 100 SFC/10^6 PBMCs) with 90% accuracy.
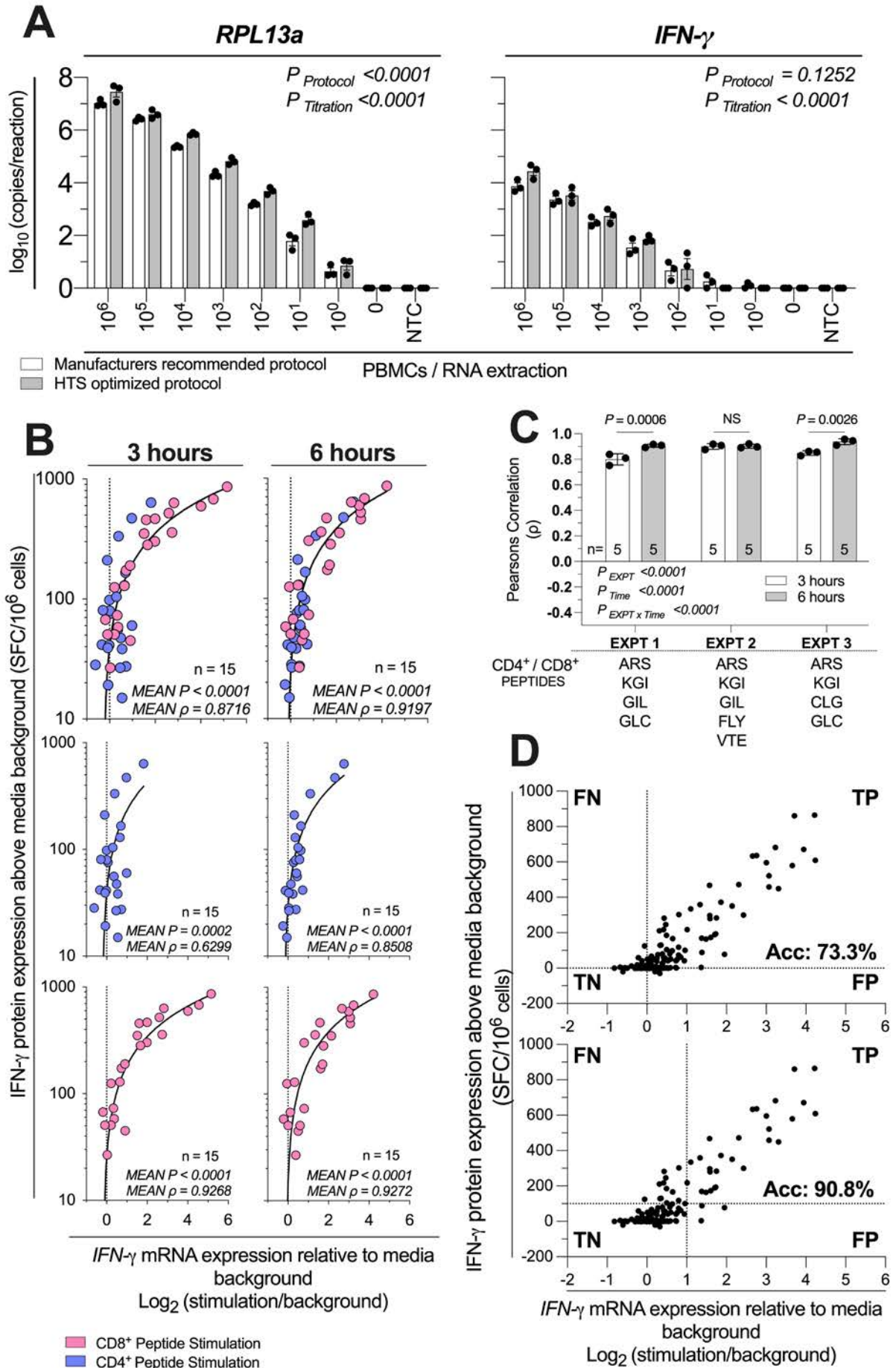
Figure 3.3. HTS-optimized RT-qPCR analytical and diagnostic sensitivity. **(A)** Assay analytical sensitivity of IFN-γ and RPL13a mRNA copies per reaction from $\log_{10}$ dilutions of unstimulated PBMCs from 10^6 to 0. Samples were tested alongside blank extraction control (0) and qPCR no template control (NTC). mRNA expression was determined by absolute-quantitative RT-qPCR with manufacturer's recommended protocol (White Bars) or HTS optimized protocol (Grey Bars), with gene copy number per reaction normalized to $\log_{10}$ copies per reaction. Biological replicates (n = 3), single RNA extractions, with single reverse transcription reactions per extraction were performed. Sample mean calculated from the mean of the technical triplicate qPCR reactions. Biological mean ± biological SEM shown. Significant differences due to protocol or PBMC titration were analysed by two-way ANOVA. **(B)** IFN-γ mRNA expression by RT-qPCR correlated to IFN-γ protein production by ELIspot across 3-hours or 6-hours post-stimulation of PBMCs (1×10^5; n=15) stimulated with peptides representing two well-defined CD4$^+$ T cell peptide epitopes (Influenza$_{57\text{-}71}$ KGI and Influenza$_{260\text{-}284}$ ARS; blue) and CD8$^+$ T cell peptide epitopes (Influenza$_{58\text{-}76}$ GIL and Epstein Barr Virus$_{280\text{-}288}$ GLC, Epstein Barr Virus$_{300\text{-}309}$ FLY, Epstein Barr Virus$_{300\text{-}309}$ VTE, or Epstein Barr Virus$_{300\text{-}309}$ CLG; pink). Shown are the mean gene copy number of technical triplicate RT-qPCR assays correlated to the mean of triplicate IFN-γ spot forming cells (SFC) by ELIspot; then data separated by CD4$^+$ or CD8$^+$ restriction. Data from three independent inter-day experiments, with both mRNA and protein measurements corrected for background. ELIspot data <10 SFC/10^6 were graphically omitted. The strength of each association was tested by Pearson's correlation on log-transformed data, with *P* values and Pearson's correlation coefficient (ρ) reported. **(C)** The RT-qPCR assay was performed in technical triplicate, with each replicate individually correlated to the mean IFN-γ SFC by ELIspot, with the ρ shown. The technical variability of ρ between inter-day experiments (EXPT), the 3- or 6-hour timepoints (Time), and their interaction (EXPT x Time) was tested with a Two-Way ANOVA with a Bonferroni corrected multiple comparisons test. Shown are the technical mean ± technical SEM; and the peptides used in each experiment. **(D)** A confusion matrix demonstrating true-positive (TP), false-positive (FP), true-negative (TN) and false-negative (FN) rate of the HTS-optimized RT-qPCR protocol relative to ELIspot results. Data are inclusive of all above CD4$^+$ and CD8$^+$ peptide stimulation responses and additional (n=3) samples stimulated with (30x) CD8$^+$ T cell peptide epitopes. Shown are the mean gene copy number of technical triplicate RT-qPCR assays correlated to the mean of triplicate IFN-γ spot forming cells (SFC) by ELIspot.

3.2.7 Discussion

This report describes an HTS-compatible RT-qPCR-based assay specifically designed to provide a high-throughput, robust, scalable, and cost-effective alternative to protein-based *in*

vitro immunoassays. With this protocol, the cost per sample has been reduced by almost 90% compared to standard practice, and the assay consumes 10-300 fold fewer PBMCs than commonly used immunoassays [356]. This assay has single-cell analytical sensitivity and a diagnostic sensitivity capable of detecting 1:10,000 responding cells with an accuracy greater than 90%. We demonstrate a very high mRNA/protein correlation between our HTS-optimized RT-qPCR protocol and ELIspot. ELIspot is often considered the 'gold-standard' PBMC immunoassay [351] and has been extensively optimized for global consistency as part of the HIV/AIDS Comprehensive Cellular Vaccine Immune Monitoring Consortium (CCVIMC)[383]. Our RT-qPCR-based protocol effectively delineated a hierarchy of IFN-γ stimulation responses for different CD4$^+$ and CD8$^+$ T cell peptide epitopes and defined 6-hours post *in vitro* stimulation as the optimal timepoint for IFN-γ immune readout. However, this may not be universal for all cytokines, and other target surrogate markers of immunity should be validated independently.

Our assay was optimized for analysis using cryopreserved PBMCs since these are common sample sources for human immunoassays [436], as blood collection is less-invasive [359] and PBMC isolation is relatively technically straightforward [437] and cost-efficient [438]. Additionally, cryopreserved PBMCs can be shipped globally [439] for batched testing [440] or long-term storage in biobanks [441]. It is reasonable to expect an even higher diagnostic sensitivity than reported herein could be achieved using our cost-optimized RT-qPCR protocol with fresh PBMCs, as cryopreservation can profoundly influence surface marker and antigen-specific T cell responses [352, 436]. Additionally, we speculate that our cost-optimized assay can be readily adapted to a wide range of cell types. Moreover, although results were reported herein for only *IFN-γ, IL-2* and *TNF-a* mRNA, this assay can be readily adapted to a broad range of effector function markers by using different primer sets. When assessing cytokine expression kinetics, peak mRNA expression was stimulant, cytokine, and donor-dependent. To the best of our knowledge, ours is the first study of *IFN-γ*, *IL-2* and *TNF-α* mRNA expression kinetics post-stimulation with hourly resolution across a 12-hour timeframe. Despite this variability, when considering the correlation between *IFN-γ* mRNA gene expression and protein production, we defined 6 hours post *in vitro* stimulation as optimal for all donors and peptide epitopes.

RT-qPCR-based HTS protocols which screen a broad range of samples and targets have been previously described; including screens for anti-parasitic drugs [428], bioactive small molecules [431, 442], or disease diagnostics [443]. Those assays are limited by the cost of

generating the high-quality and high-purity sample required for optimal qPCR. We have previously demonstrated the automatable technologies used in this protocol produce high quality and quantity RNA and cDNA [356]. Herein, we demonstrate no statistically significant loss in the correlation between mRNA and protein quantification post assay miniaturization and cost-optimization. We speculate that with automated technologies capable of accurate ultra-low volume (*i.e.,* <0.1uL) dispensing, both cost-optimization and miniaturization could be extended further.

When assessing the confusion matrix between RT-qPCR and ELIspot results, we tested two thresholds of positivity: (i) all results above background for both assays (*i.e.,* mRNA >0 and ELIspot SFC/10^6 >0), or (ii) a doubling of mRNA and more than 1 in 10,000 responding cells (*i.e.,* mRNA >1 and ELIspot SFC/10^6 >100). The improved accuracy (*i.e.,* 73.3% *vs.* 90.8%) observed when the threshold of positivity was increased suggests that more sophisticated strategies to define positivity (*i.e.,* statistical testing), or more stringent positivity criteria (*i.e.,* a change of 2 of more standard deviations), may further increase assay accuracy in larger screens. ELIspot is generally considered positive above a threshold (*i.e.,* 40-100 SFC/10^6) [435]. However, a threshold strategy for qPCR may overlook low level mRNA responses from antigen reactive cells. We expect that defining an experimental threshold of positivity for a RT-qPCR-based HTS immune-assay will be dependent upon sample, stimulation, and desired experimental outcome.

We expect that this study will be of broad interest to a diverse number of researchers by facilitating comprehensive laboratory and field studies. One example where high-throughput functional immunoassays may provide critical experimental information is during vaccine candidate testing [94, 444, 445]. This assay would allow more comprehensive preclinical or clinical studies, with either more samples or more parameters per sample, without requiring additional engineering or modification steps such as those required for luciferase or other luminescence-based reporter screens [446]. Additionally, high-throughput transcriptome profiling of RNA-based biomarkers of disease have been reported for a broad range of malignancies including lung [447], skin [448] and breast [449] carcinomas, and other diseases such as rheumatoid arthritis [450]. An assay with high analytical and diagnostic sensitivity which allows cost-efficient isolation and quantification of PBMC RNA is likely to be highly beneficial.

When considering transcription-based molecular diagnostics, RT-qPCR is highly sensitive and specific and is relatively cheap and uncomplicated to analyse [393, 419]. Other transcription-based techniques include Northern blotting [451], *in situ* hybridization [452], RNA microarrays [453], NanoString™ [392], Sanger and Next-Generation Sequencing (NGS) [454] and advanced PCR techniques (*e.g.,* digital PCR [455], microsphere-multiplex PCR [414]). Higher-throughput transcription-based techniques will likely surpass RT-qPCR in cost-efficiency. Still, SYBR®-chemistry will remain the most inexpensive option for effective sensitive and specific mRNA quantitation for the foreseeable future.

In conclusion, we present herein an HTS-compatible assay with high analytical and diagnostic sensitivity, which allows cost-efficient isolation and quantification of PBMC RNA. This robust, scalable, and cost-effective alternative to protein-based *ex vivo* PBMC immunoassays addresses the limitations of cost and sample volume associated with standard immunoassay protocols. By overcoming these well-accepted constraints, we anticipate this assay will have widespread applicability in preclinical and clinical studies [456], especially when samples are limited, and cost is an important consideration.

Authorship contributions

DJB and AMK performed experiments. DJB, JLB, and DLD designed experiments. DJB, JLB, AMK, and DLD analysed and interpreted the data. DJB, and DLD wrote the manuscript with input from JLB, and AMK.

Conflicts of interest

The authors declare that the research was conducted in the absence of any commercial or financial relationships that could be construed as a potential conflict of interest.

Data availability statement

All datasets for this study are available upon request.

3.2.8   Supplementary material

Supplementary figures
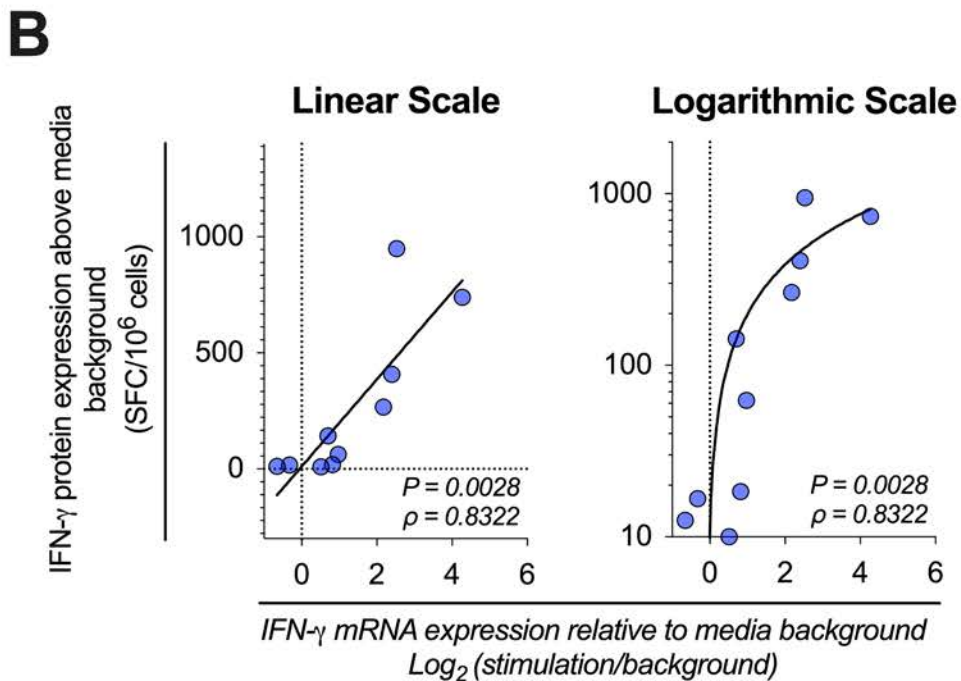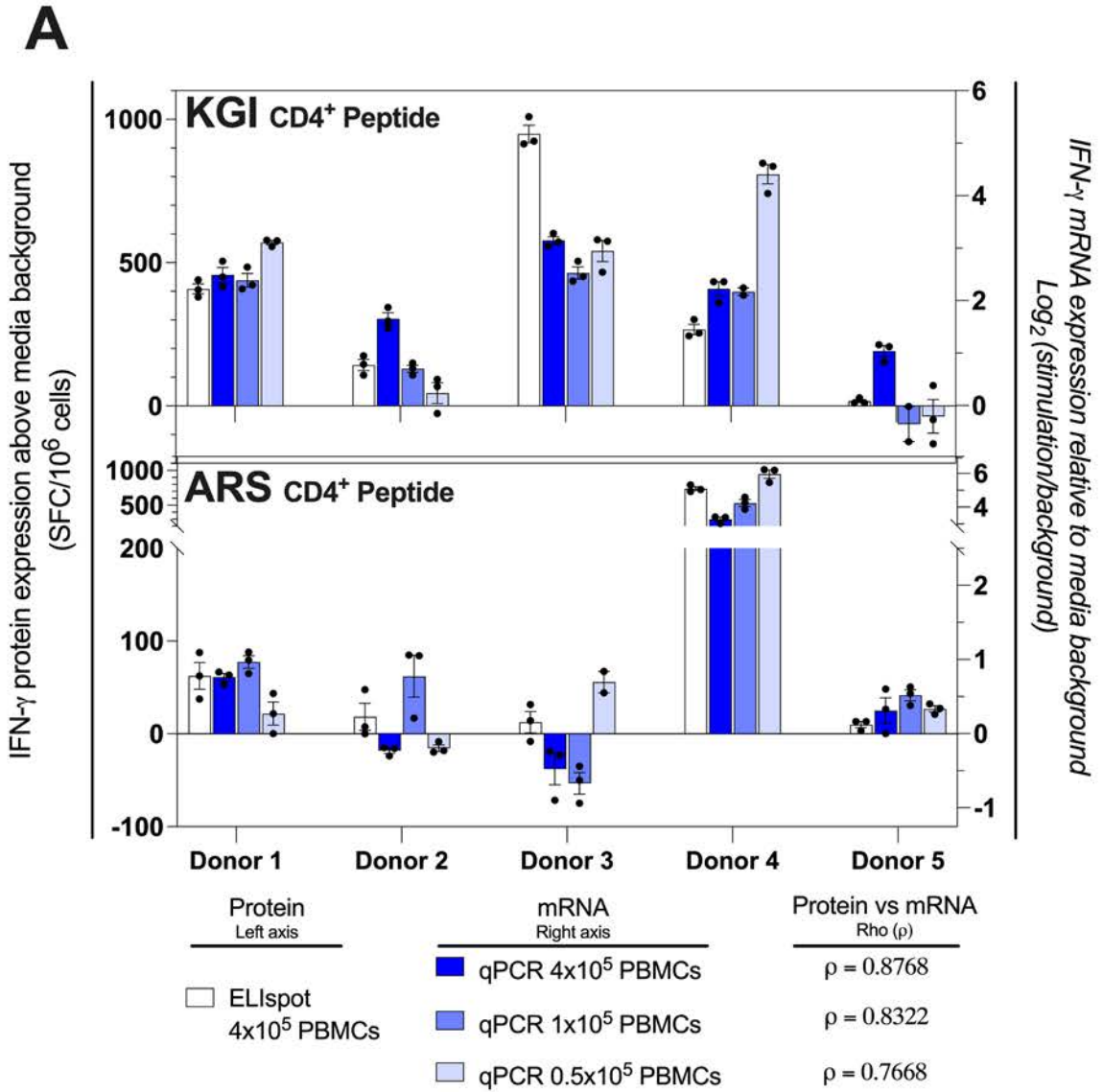
Supplementary Figure S3.1. mRNA expression correlates with protein-based quantification following stimulation of PBMCs with CD4$^+$ T cell peptide epitopes. (**A**) IFN-γ mRNA expression by RT-qPCR compared to IFN-γ protein production by ELIspot following stimulation of PBMCs ($4x10^5$, $1x10^5$ or $5x10^4$; n=5) with synthetic peptides representing two well-defined CD4$^+$ T cell peptide epitopes (Influenza$_{57-71}$ KGILGFVFTLTVPSE and Influenza$_{260-284}$ ARSALILRGSVAHKSCLPACVYGP). Spot forming cells (SFC) were quantified from technical triplicate stimulations by ELIspot. Gene copy number per reaction were quantified from single stimulations by absolute quantification RT-qPCR. Single full volume RNA extractions, with single full volume reverse transcription reactions, and qPCR in technical triplicate replicates were performed as per manufacturers recommendation. The technical mean ± technical SEM of gene copy number or SFC corrected for background are shown. (**B**) IFN-γ mRNA expression by RT-qPCR correlated to IFN-γ protein production by ELIspot graphed either on a linear or logarithmic scale, following stimulation of $1x10^5$ PBMCs (n=5). The strength of the association between RT-qPCR IFN-γ mRNA gene expression (on Log$_2$ transformed data) and ELIspot IFN-γ protein expression (linear data) was tested by Pearson's correlation. *P* values and Pearson's correlation coefficient (ρ) reported.
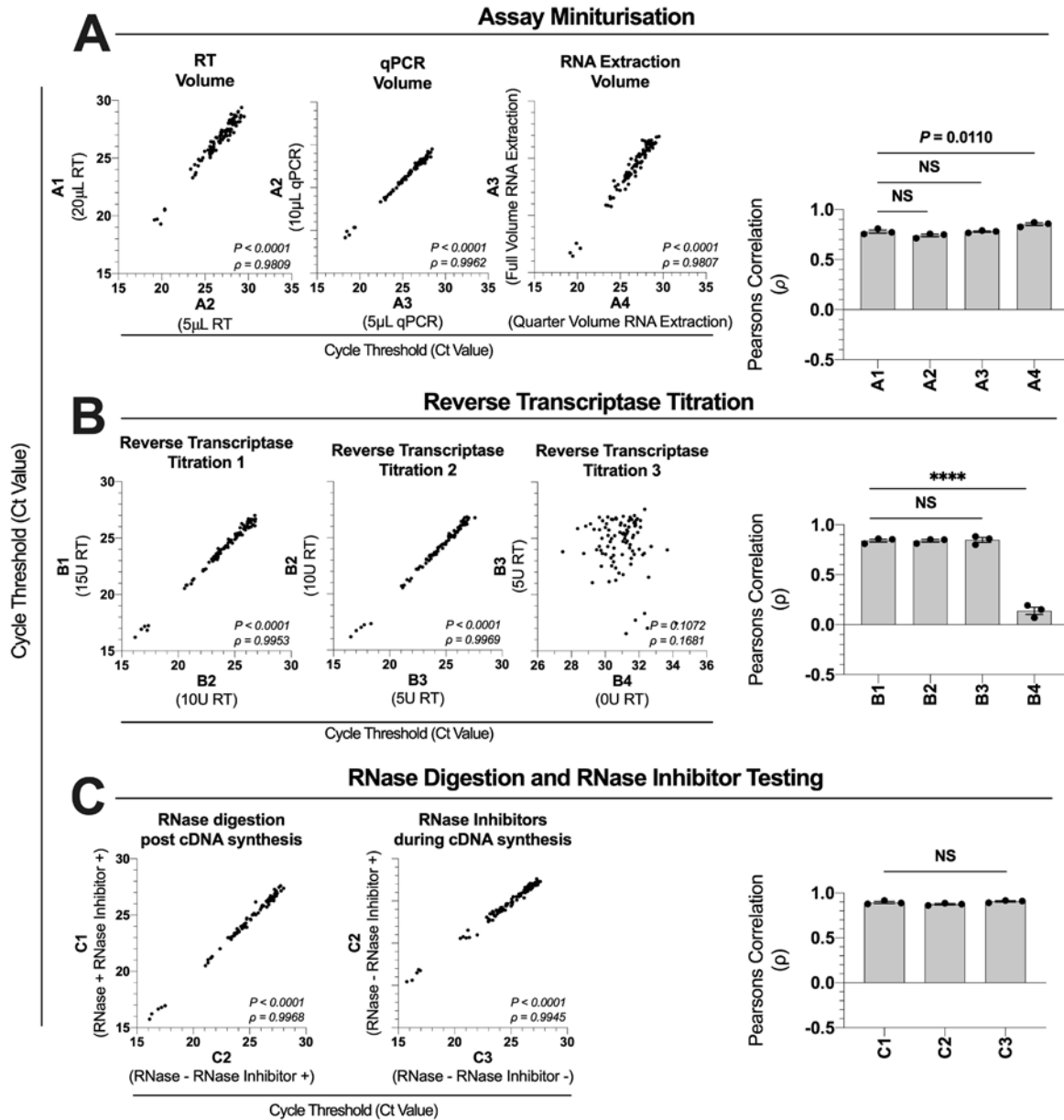
Supplementary Figure S3.2. Correlations between RT-qPCR data following assay optimization.
IFN-γ mRNA expression by RT-qPCR correlated to IFN-γ mRNA expression by RT-qPCR following
systematic adjustments the RT-qPCR protocol (left panels); and the RT-qPCR assay was performed in
technical triplicate, with each replicate individually correlated to the mean IFN-γ SFC by ELIspot (right
panel) and tested using a One-Way ANOVA with a Bonferroni corrected multiple comparisons test.
(**A**) A1, A2, A3 or A4 (top panel) were evaluating the correlation between 20 μl versus 5 μl final volume
single reverse transcription (RT) reactions containing 20 units/μL$_{RNA}$ (20U) of reverse transcriptase
enzyme; the correlation between 10 μl versus 5 μl final volume qPCR; and the correlation between full
volume and quarter volume RNA extractions. All RT reactions included RNase Inhibitors and a post-
cDNA synthesis RNase digestion stage. (**B**) B1, B2, B3 or B4 (middle panel) were evaluating the
correlation between reverse transcription (RT) reactions containing 15 units/μL$_{RNA}$ (15U) or 10

units/μL_{RNA} (10U) of reverse transcriptase enzyme; the correlation between RT reactions containing 10U versus 5U reverse transcriptase enzyme; and the correlation between RT reactions containing 5U versus 0U reverse transcriptase enzyme. All RT reactions included RNase Inhibitors and a post-cDNA synthesis RNase digestion stage. (**C**) C1, C2 and C3 (bottom panel) were evaluating the correlation between reverse transcription (RT) reactions including RNase Inhibitors and a post-cDNA synthesis RNase digestion stage, and reactions excluding the RNase digestion stage; and RT reactions excluding the RNase digestion stage and RT reactions excluding both the RNase digestion stage and RNase Inhibitors. The strength of the association between RT-qPCR IFN-γ mRNA gene expression and ELIspot IFN-γ protein expression was tested by Pearson's correlation. *P* values and Pearson's correlation coefficient (ρ) reported.
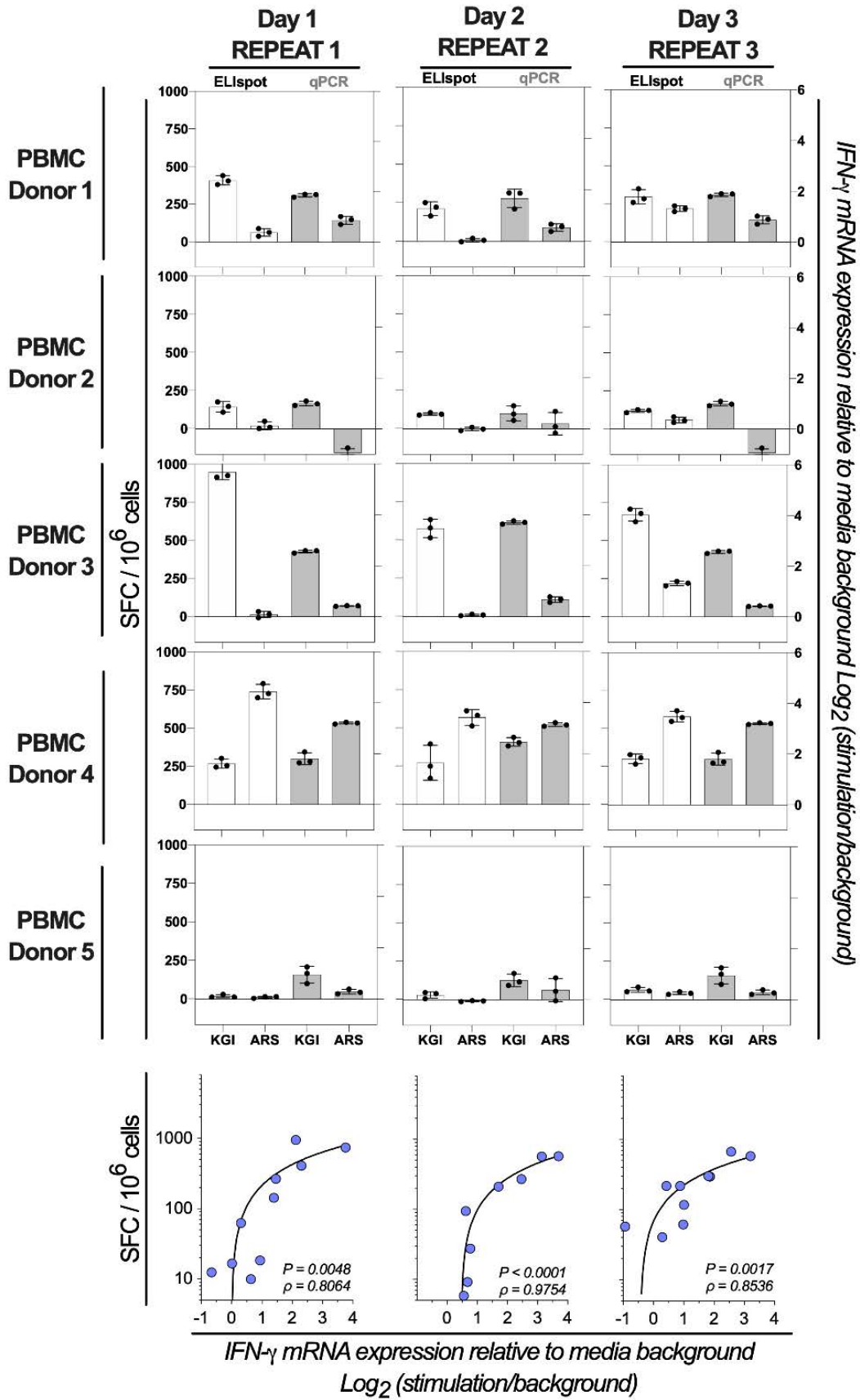
Supplementary Figure S3.3. Technical triplicate replicate inter-day testing. IFN-γ mRNA expression (Grey Bars) by RT-qPCR correlated to IFN-γ protein production (White Bars) by ELIspot following stimulation of PBMCs ($1x10^5$; n=5) with peptides representing two well-defined CD4$^+$ T cell peptide epitopes (Influenza$_{57-71}$ KGILGFVFTLTVPSE and Influenza$_{260-284}$ ARSALILRGSVAHKSCLPACVYGP) across three inter-day technical replicate experiments. Spot forming cells (SFC) were quantified from technical triplicate stimulations by ELIspot. Gene copy number per reaction were quantified from single stimulations by absolute quantification RT-qPCR. Quarter (manufacturers recommendation) volume RNA extractions, with single 5 ml final volume reverse transcription (RT) reactions containing 5 units/μL_{RNA} (5U) of reverse transcriptase enzyme per n, were performed. RT reactions were exclusive of RNase Inhibitors or a post-cDNA synthesis RNase digestion stage. 5 ml final volume qPCR was performed in technical triplicate replicate. Shown are the technical mean ± technical SEM of the technical triplicate gene copy number or spot forming cells (SFC) corrected for background. The strength of the association between RT-qPCR IFN-γ mRNA gene expression and ELIspot IFN-γ protein expression was tested by Pearson's correlation on log transformed data with *P* values and Pearson's correlation coefficient (ρ) reported. SFC≤20/$1x10^6$ PBMCs were omitted when correlating protein to mRNA. The correlation of each technical replicate was tested with One-Way ANOVA with a Bonferroni corrected multiple comparisons test reported.
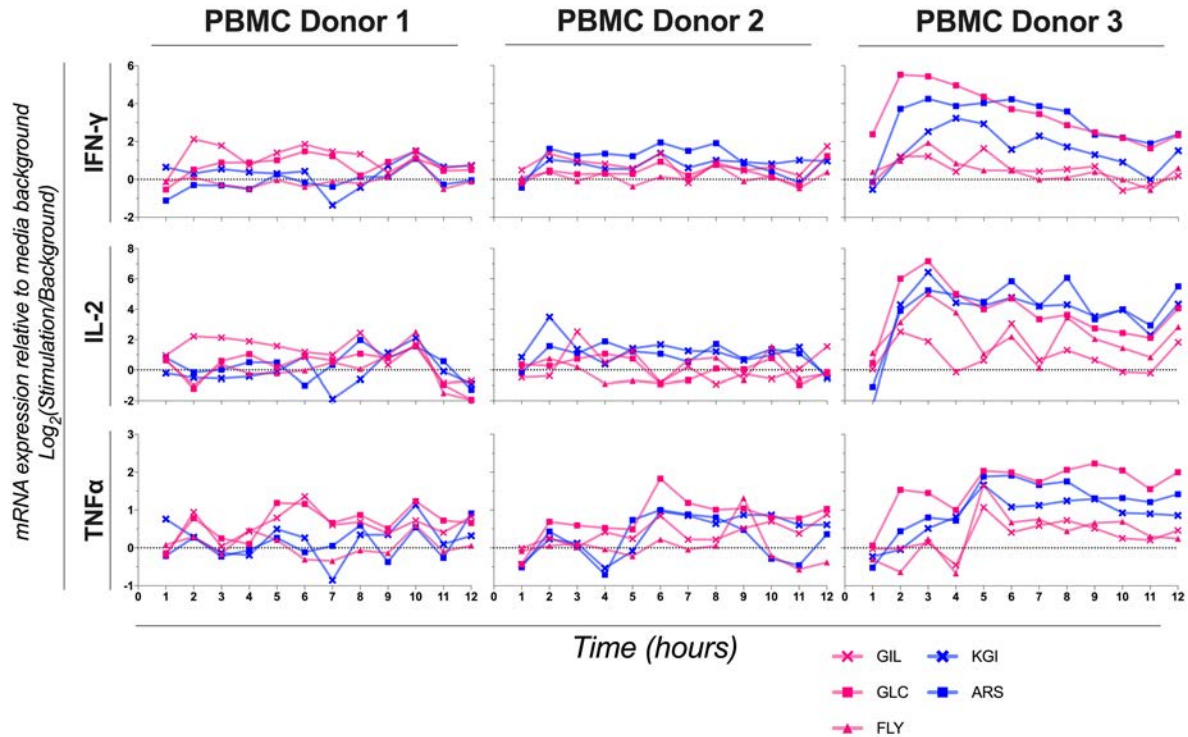
Supplementary Figure S3.4. Cytokine mRNA expression kinetics in PBMCs in response to antigen and mitogen stimulation. Hourly kinetics of *IFN-γ*, *TNF-a* and *IL-2* mRNA expression from 1×10^5 PBMCs from three individuals (PBMC Donor 1, 2 and 3) stimulated with MHC Class I CD8+ (GIL; pink cross, GLC; pink square and FLY pink triangle) or MHC Class II CD4+ (KGI; blue cross, and ARS; blue square) peptides. Mean of gene copy number relative to background are shown. Single RNA extractions, with single reverse transcription reactions per n per stimulation were performed, with qPCR performed in technical triplicate replicates. Gene copy number per reaction was quantified by absolute quantification. The sample mean was calculated from the mean of the technical triplicate replicates. All samples (n=3) were stimulated with individual peptide in parallel with media negative background control and CEF peptide pool and PMA/Iono positive controls.
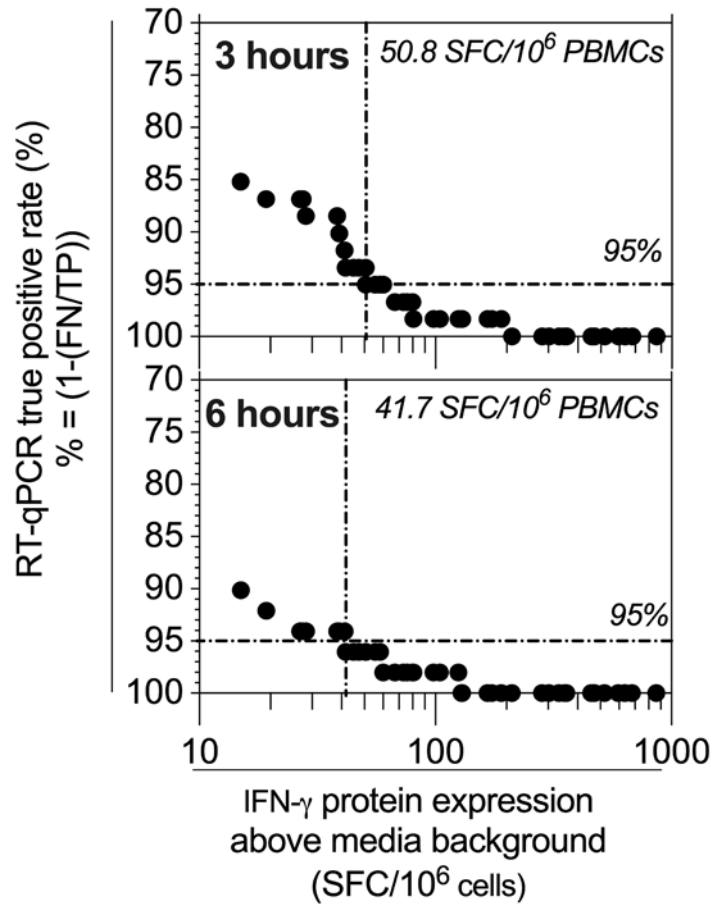
Supplementary Figure S3.5. True-positive rate of RT-qPCR compared to ELIspot at 3- and 6-hours. The true positive rate of the RT-qPCR assay was calculated as the inverse of RT-qPCR total false negatives (FN) relative to true positives (TP) compared to ELIspot. 95% diagnostic sensitivity threshold and time specific diagnostic sensitivity shown - dashed line.
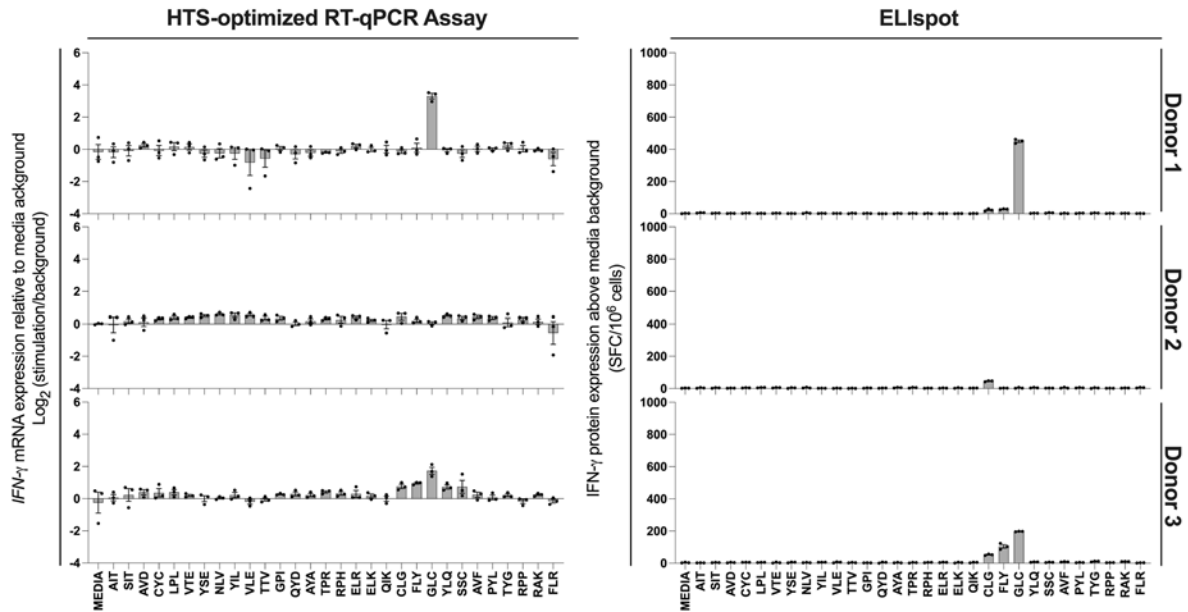
Supplementary Figure S3.6. Response to stimulation measuring a broad number of peptides epitopes. IFN-γ mRNA expression by high-throughput screening (HTS) optimized RT-qPCR and IFN-γ protein production by ELIspot following stimulation with 30x well-defined CD8⁺ peptide epitope stimulations of PBMCs (n=3). Shown are the mean ± technical SEM of gene copy number of technical triplicate RT-qPCR assays, and the mean ± technical SEM of triplicate IFN-γ spot forming cells (SFC) by ELIspot, with both mRNA and protein measurements corrected for background.

Supplementary tables

Supplementary Table S3.1. Synthetic peptides. Peptides representing defined CD8^{+} or CD4^{+} T cell peptide epitopes derived from Epstein Barr virus and influenza virus; and Anaspec CEF control peptide pool (CEFpp) representing 32 CD8^{+} T cell peptide epitopes derived from human cytomegalovirus, Epstein-Barr virus, or influenza virus.

Code	Epitope	Species derived	Antigen	Residues	MHC Class / T cell	Reference
CEFpp	Multiple[*]	Cytomegalovirus Epstein-Barr virus Influenza virus	Multiple*	Multiple*	MHC I / CD8^{+}	[457]
KGI	KGILGFVFTLTVPSE	Influenza virus	Matrix protein 1	57-71	MHC II / CD4^{+}	[458]
ARS	ARSALILRGSVAHKSCLPACVYGP	Influenza virus	Nucleoprotein	260-284	MHC II / CD4^{+}	[459]
GIL	GILGFVFTL	Influenza virus	Matrix protein 1	58-76	MHC I / CD8^{+}	[460, 461]
AIT	AITEVECFL	Polymaviruses	VP1	44-53	MHC I / CD8^{+}	[462]
SIT	SITEVECFL	Polymaviruses	VP1	36-44	MHC I / CD8^{+}	[462]
AVD	AVDTVLAKK	Polymaviruses	Large T antigen	341-349	MHC I / CD8^{+}	[463]
CYC	CYCIDCFTQW	Polymaviruses	Small T antigen	136-145	MHC I / CD8^{+}	[463]
LPL	LPLMRKAYL	Polymaviruses	Large T antigen	27-35	MHC I / CD8^{+}	[463]
VTE	VTEHDTLLY	Cytomegalovirus	pp50	245-253	MHC I / CD8^{+}	[464]
YSE	YSEHPTFTSQY	Cytomegalovirus	pp65	363–373	MHC I / CD8^{+}	[465]
NLV	NLVPMVATV	Cytomegalovirus	pp65	495–503	MHC I / CD8^{+}	[465]
YIL	YILEETSVML	Cytomegalovirus	IE-1	315-324	MHC I / CD8^{+}	[466]
VLE	VLEETSVML	Cytomegalovirus	IE-1	316–324	MHC I / CD8^{+}	[465]
TTV	TTVYPPSSTAK	Cytomegalovirus	pp150	947-957	MHC I / CD8^{+}	[467]
GPI	GPISGHVLK	Cytomegalovirus	pp65	16-25	MHC I / CD8^{+}	[467]
QYD	QYDPVAALF	Cytomegalovirus	pp65	328-337	MHC I / CD8^{+}	[468]
AYA	AYAQKIFKIL	Cytomegalovirus	IE-1	248-258	MHC I / CD8^{+}	[468]

Code	Epitope	Species derived	Antigen	Residues	MHC Class / T cell	Reference
TPR	TPRVTGGGAM	Cytomegalovirus	pp65	417–426	MHC I / CD8+	[465]
RPH	RPHERNGFTVL	Cytomegalovirus	pp65	265-275	MHC I / CD8+	[469]
ELR	ELRRKMMYM	Cytomegalovirus	IE-1	199–207	MHC I / CD8+	[470]
ELK	ELKRKMIYM	Cytomegalovirus	IE-1	199-207	MHC I / CD8+	[465]
QIK	QIKVRVDMV	Cytomegalovirus	IE-1	88–96	MHC I / CD8+	[465]
FLY	FLYALALLL	Epstein Barr virus	LMP2	356-364	MHC I / CD8+	[471]
GLC	GLCTLVAML	Epstein Barr virus	BMLF1	280–288	MHC I / CD8+	[472]
CLG	CLGGLLTMV	Epstein Barr virus	LMP2	426-434	MHC I / CD8+	[473]
YLQ	YLQQNWWTL	Epstein Barr virus	LMP1	159-167	MHC I / CD8+	[474]
SSC	SSCSSCPLSKI	Epstein Barr virus	LMP2	340–350	MHC I / CD8+	[475]
AVF	AVFDRKSDAK	Epstein Barr virus	BERF2a	399-428	MHC I / CD8+	[476]
PYL	PYLFWLAAI	Epstein Barr virus	LMP2	131-139	MHC I / CD8+	[475]
TYG	TYGPVFMCL	Epstein Barr virus	LMP2	419-427	MHC I / CD8+	[473]
RPP	RPPIFIRRL	Epstein Barr virus	EBNA 3A	881-889	MHC I / CD8+	[477]
RAK	RAKFKQLL	Epstein Barr virus	BZLF1	190–197	MHC I / CD8+	[478]
FLR	FLRGRAYGL	Epstein Barr virus	EBNA3A	325–333	MHC I / CD8+	[478]

LMP2: Latent Membrane Protein 2; BMLF1: mRNA export factor ICP27 homolog; pp50: 50K phosphoprotein; VP1: Major capsid protein VP1; pp65: 65K phosphoprotein; IE-1: Immediate Early Protein 1; 150K phosphoprotein; LMP1: Latent Membrane Protein 1; BERF2a: BamHI-E rightward reading frames 2a; EBNA-3A: nuclear antigen EBNA-3A; BZLF1: BamHI Z fragment leftward open reading frame 1

*32 x 8-12 amino acids in length

Supplementary Table S3.2. Oligonucleotide primers. Characteristics of primers acquired from the PrimerBank™ database. Primers were evaluated with logarithmically diluted PBMC cDNA wherein reaction efficiency (E′) and standard coefficient of determination (R^2) were determined per MIQE guidelines.

Transcript	GenBank accession number	PrimerBank™ ID[*]	Forward sequence (5′-3′)	Reverse sequence (5′-3′)	Amplicon size (bp)	E' (%)	R^2
RPL13a	NM_012423	14591905c2	GCCCTACGACA AGAAAAAGCG	TACTTCCAGCCA ACCTCGTGA	117	94.5	0.99
IFN-γ	NM_000619.2	56786137c1	TCGGTAACTGA CTTGAATGTCCA	TCGCTTCCCTGT TTTAGCTGC	93	99.7	0.99
TNFα	NM_000594	25952110c2	GAGGCCAAGCC CTGGTATG	CGGGCCGATTG ATCTCAGC	91	99.3	0.99
IL-2	NM_000586.3	28178861a1	AACTCCTGTCTT GCATTGCAC	GCTCCAGTTGTA GCTGTGTTT	93	91.2	0.99

* https://pga.mgh.harvard.edu/primerbank/

Supplementary protocol: Cost-optimized protocol

The below protocol complies with 'Protocol Exchange' formatting

https://protocolexchange.researchsquare.com/

Introduction

Herein we present a reverse-transcription quantitative PCR (RT-qPCR) assay specifically designed to provide a high-throughput, robust, scalable, and cost-effective alternative to protein-based *in vitro* immunoassays. This protocol is targeted towards high-throughput studies of antigen-specific immune responses in human peripheral blood mononuclear cells (PBMCs). This assay is amendable to miniaturization and automation, exceeds HTS uniformity and signal variance testing standards, and represents a cost saving of almost 90% on standard-practice assays. This HTS-optimized protocol has single-cell analytical sensitivity and a diagnostic sensitivity equivalent to detecting 1:10,000 responding cells (*i.e.,* 100 Spot Forming Cells/10^6 PBMCs by ELIspot) with 90% accuracy.

Reagents

1. Molecular grade isopropanol (Sigma-Aldrich: Catalog# I9516)
2. Molecular grade ethanol (Sigma-Aldrich: Catalog# E7023)
3. Molecular grade β-Mercaptoethanol (Sigma-Aldrich: Catalog# M3148)
4. MagMAX™ *mirVana*™ Total RNA isolation Kit (ThermoFisher: Catalog# A27828)
5. Superscript IV™ Enzyme kit (ThermoFisher: Catalog# 18090050)
6. 50 µM Random Hexamers (ThermoFisher: Catalog# N8080127)
7. 10 mM dNTPs (ThermoFisher: Catalog# R0191)
8. Ultra-Pure H_2O (ThermoFisher: Catalog# 10977015)
9. ssoAdvanced SYBR™ (BioRad: Catalog# 1725270)
10. RNaseZAP™ (Sigma-Aldrich: Catalog# R2020)
11. Desalt Grade qPCR Primers (Sigma-Aldrich) (https://pga.mgh.harvard.edu/primerbank/)

Equipment

1. 96-well U-bottom incubation plate (Falcon: Catalog# 353077)
2. CO_2 incubator: (LabGear: SCO6AD-2)
3. Benchtop Centrifuge (Beckman Coulter: Avanti J-15R)
4. p200 multichannel pipette (Eppendorf: Research Plus)
5. p10, p20, p200 and p1000 pipettes (Eppendorf: Research Plus)
6. Microplate shaker (GrantBio: PMS 100i)
7. Magnetic stand (Invitrogen: Catalog# AM10027)
8. Vortex mixer (GrantBio: PV1)
9. Benchtop mini-centrifuge (LabGear: LABG3000001)
10. 0.2 mL PCR-grade clean tube (Eppendorf: PCR grade)
11. Thermocycler (SimpliAmp™ Thermal Cycler: Catalog# A24811)
12. MicroAmp™ Optical 384-Well Reaction Plate (Thermo Fisher: Catalog# 4309849)
13. MicroAmp™ Optical Adhesive Film (Thermo Fisher: Catalog# 4311971)
14. QuantStudio™ 5 Quantitative Thermocycler (Applied Biosystems)
15. QuantStudio™ 5 Design and Analysis Software (Applied Biosystems)

Procedure

1. **Experimental cell stimulation/culture**
   a. Stimulate or culture PBMCs as per standard practice in a 96-well U-bottom incubation plate/s
      i. This assay is suitable for testing PBMCs between $1x10^6 - 1x10^0$ PBMCs per well.
      ii. A higher diagnostic sensitivity would be expected with a higher PBMC cell input.
      iii. For interferon-gamma (IFN-γ) expression, $1x10^5$ PBMCs have a diagnostic sensitivity equivalent to $100/10^6$ spot forming cells ($SFC/10^6$) by ELIspot, with an accuracy of 90%
      iv. Peak mRNA expression is stimulant and individual dependent, however 6-hours post-stimulation is generally optimal for correlating mRNA to protein

b. Prepare '*Lysis Binding Mix*' as per Protocol Table 1.

Protocol Table 1. Lysis Binding Mix		
Component	**Amount (1x)**	**Amount (____x)**
Lysis Buffer	25 μL	
Molecular Grade Isopropanol	25 μL	
β-Mercaptoethanol	1 μL	
Total	51 μL	

c. Centrifuge the 96-well U-bottom incubation plate/s at 1000 x g for 4 min

d. Remove the media, and lyse cells in 50 μL of the *Lysis Binding Mix* directly in the U-bottom incubation plate

    i. Do not disturb the cell pellet until lysis step.

    ii. Remove as much media as possible

    iii. Mechanical lysis can be achieved by pipetting up and down 5x (The cell pellet will almost immediately dissolve).

    iv. **STOP POINT** – Cell lysate can be stored in -80°C for 2 weeks without RNA degradation. When thawing from -80°C, thaw samples at 4°C (on ice).

2. RNA extraction

    i. To decontaminate the working area, gently wipe down all surfaces and equipment with lint free, non-woven, non-abrasive wipes sprayed with RNaseZAP™

    ii. Preheat Elution Buffer to 37°C

    iii. Prepare '*TURBO DNase solution*' and '*Bead Binding Mix*' as per Protocol Table 2 and 3 respectively.

Protocol Table 2. TURBO DNase solution		
Component	Amount (1x)	Amount (____x)
MagMAX TURBO DNase Buffer	12 μL	
TURBO DNase	0.5 μL	
Total	12.5 μL	

Protocol Table 3. Bead Binding Mix		
Component	Amount (1x)	Amount (____x)
RNA Binding Beads	2.5 μL	
Lysis/Binding Enhancer	2.5 μL	
Total	5 μL	

b. Cover and shake the U-bottom incubation plate on the microplate shaker for 3 min at speed 7 (700 rpm), to ensure samples are homogenous and are at room temperature.

c. Add 5 μL 'Binding Bead Mix' to each sample

d. Cover and shake the U-bottom incubation plate on the microplate shaker for 5 min at speed 6 (600 rpm)

e. Place the U-bottom incubation plate on the magnetic stand for 5 min

    i. The solution will clear

f. Carefully aspirate and discard the supernatant

    i. Do not to disturb the RNA binding beads

g. Remove the U-bottom incubation plate from the magnetic stand

h. Add 50 μL of MagMAX™ Wash Solution 1 to each sample

i. Cover and shake the U-bottom incubation plate on the microplate shaker for 1 min at speed 7 (700 rpm)

j. Place the U-bottom incubation plate on the magnetic stand for 1 min

    i. The solution will clear

k. Repeat steps f. to j. to perform a second 50 μL wash with MagMAX™ Wash Solution 2

l. Carefully aspirate and discard supernatant without disturbing the RNA binding beads

m. Shake (the uncovered) U-bottom incubation plate for 2 min at speed 12 (1200 rpm), to evaporate residual ethanol

    i. Be careful not to over dry the beads

n. Add 12.5 μL of 'TURBO DNase Solution' to each sample

o. Cover and shake the U-bottom incubation plate for 15 min at speed 11 (1100 rpm)

p. Add 12.5 μL MagMAX™ Rebinding Buffer

q. Add 25 μL molecular grade isopropanol

    i. NEVER premix these reagents – premixing these reagents will cause the RNA extraction to fail

r. Cover and shake U-bottom incubation plate for 3 min at speed 7 (700 rpm)

s. Place the U-bottom incubation plate on the magnetic stand for 3 min

    i. The solution will clear

t. Carefully aspirate and discard the supernatant

    i. Ensure not to disturb the RNA binding beads

u. Remove the U-bottom incubation plate from the magnetic stand

v. Add 50 μL of MagMAX™ Wash Solution 2 to each sample

w. Cover and shake U-bottom incubation plate for 3 min at speed 7 (700 rpm)

x. Place the U-bottom incubation plate on the magnetic stand for 1 min

    i. The solution will clear

y. Repeat steps t. to x. to perform a second 50 μL wash with MagMAX™ Wash Solution 2

z. Carefully aspirate and discard the supernatant

    i. Ensure not to disturb the RNA binding beads

aa. Shake (the uncovered) U-bottom incubation plate for 2 min at speed 10 (1200 rpm)

    i. This is to dry the plate by evaporation

    ii. Be careful not to over dry the beads

bb. Add 15 μL of (preheated) MagMAX™ Elution Buffer to each sample

    i. 10 μL can be added to increase RNA concentration

cc. Cover and shake U-bottom incubation plate for 3 min at speed 11 (1100 rpm)

dd. Place the plate on the magnetic stand for 3 min

    i.   The solution will clear

    ii.   The clear supernatant contains the samples RNA

    iii.   **STOP POINT** – Transfer supernatant to a fresh 96 well RNase Free 96 well plate for storage at -80ºC. When thawing from -80ºC, thaw samples at 4ºC (on ice).

3. cDNA synthesis

    i.   Accurate and precise pipetting is critical

    ii.   Before beginning, gently wipe down all surfaces and equipment with lint free, non-woven, non-abrasive wipes sprayed with RNaseZAP

b. Thaw and prepare the 50 µM Random Hexamers, 10 mM dNTPs, and the reagents within the Superscript IV™ Enzyme kit

    i.   Thaw reagents on ice to minimize degradation

    ii.   Once defrosted, briefly vortex and centrifuge all defrosted reagents to ensure well mixed

a. Make up '*Primer Binding Mix (MM#1)*' as per Protocol Table 4.

Protocol Table 4. Primer Binding Mix (MM#1)		
Component	1x	__x
50 µM Random Hexamers	0.25 µL	
H_2O	0.25 µL	
10 mM dNTP	0.25 µL	
Total	0.75 µL	

b. Add 0.75 µL of 'Primer Binding Mix (MM#1)' per 0.2 mL PCR Tube

c. Add 2.5 µL of eluted RNA to each tube

    i.   Normalization to RNA concentration is not required.

    ii.   Nano-spectroscopy readings are not required and are likely to highly inaccurate as RNA concentrations will be very low (<10 ng/µL)

d. Incubate tube at 65ºC for 5 minutes then cool to 4ºC for at least 1 minute

e. Prepare '*cDNA Synth Mix (MM#2)*' as per Protocol Table 5

Protocol Table 5. cDNA Synth Mix (MM#2)		
	5U	
Component	**1x**	**__x**
5 x Superscript IV™ Buffer	1 μL	
100 mM DTT	0.25 μL	
Superscript IV™ Enzyme	0.063 μL	
DEPC H$_2$O	0.438 μL	
Total	1.75 μL	

    i. A negative reverse transcription control master mix can be made by substituting the Superscript IV™ enzyme with DEPC H$_2$O

f. Add 1.75 μL of '*cDNA Synth Mix (MM#2)*' to each tube

g. Incubate in Thermocycler as per Protocol Table 6.

Protocol Table 6. cDNA synthesis conditions	
Process	Conditions
Primer Priming and RT	10 min at 23ºC
	10 min at 50ºC
Reaction Termination	10 min at 85ºC

h. cDNA is now ready for use

    i. **STOP POINT** – cDNA can be stored long-term at -20ºC

    ii. Final cDNA volume = 5 μL

4. **Quantitative PCR**

    i. Accurate and precise pipetting is critical

b. Dilute the cDNA 1:4 with Ultra-Pure H$_2$O

    i. Final volume = 20 μL

c. If performing absolute quantification prepare standard curve as per standard practice

    i. Standard curves can be made from either a plasmid containing the gene of interest, or purified amplicon.

d. Mix primers into a forward and reverse working solution where each primer is at a 5 µM concentration (F&R 5 µM Primers)

e. Prepare '*qPCR master mix*' as per standard qPCR practice using the below table.

    i. Ensure enough master mix is made for the standards, a positive control, a no-template control and triplicate replicates for each cDNA sample.

Protocol Table 7. qPCR Master mix		
Master mix	1x	___ x
2 x ssoAdvanced SYBR supermix™	2.5 µL	
5 µM F&R Primers	0.5 µL	
Ultra-Pure H2O	1 µL	
Total	4 µL	

f. Aliquot 4 µL of master mix into each reaction well MicroAmp™ optical 384-well reaction plate

g. Add 1 µL of sample (cDNA, standards, or controls) to each well

h. Cover and seal the MicroAmp™ optical 384-well reaction plate with MicroAmp™ optical adhesive film

i. Centrifuge 384-well reaction plate at 200 g for 1 second in the benchtop centrifuge

j. Run and collect data as per ssoAdvanced SYBR Supermix™ protocol and quantitative thermocycler as per standard practice

    i. If performing absolute quantification, quantitate copies per reaction.

    ii. If performing relative quantification, quantitate copies per copy of reference gene.

5. **Data analysis**

    a. Data is presented as 'mRNA expression relative to media background'

    b. From the triplicate replicates of the negative control calculate the average (AVG_{NEG}) individually for each sample

       i. For each technical qPCR replicate (x) calculate:

$$Log_2 \; (x \; / \; AVG_{NEG})$$

       ii. A value of 0 is equal to the mean of the negative media-only control

Troubleshooting

RNA extraction - Poor RNA recovery is most commonly associated with allowing the magnetic beads to over dry; to avoid this issue, ensure a quick workflow. Another common problem is adding too much sample (*i.e.,* too many cells) into the wells. This assay has been tested for between 10^0-10^6 PBMCs per well of the U-bottom plate. Adding other tissue types or increased number of cells should be carefully optimized.

cDNA Synthesis - We report herein that reducing the concentration of the Superscript IV™ enzyme by 75% to 5 U/μL_{RNA} retains high analytical and diagnostic sensitivity when generating cDNA from 10^5 PBMCs. It is likely, however, that higher enzyme concentrations will be required when synthesizing cDNA from samples containing inhibitors or a more concentrated RNA template.

SYBR chemistry qPCR - The most significant problem facing qPCR data is reproducibility across experiments and laboratories. To minimize this issue, all qPCR should be conducted and reported as per MIQE Guidelines. The protocol described herein allows normalization of data to PBMC number with absolute quantification. We promote absolute quantification when testing distinct cell numbers (e.g., PBMCs/condition). This strategy does not require reference genes for normalization and therefore eliminates issues associated with inappropriate reference gene selection. However, we stress that all MIQE guidelines must be followed to reduce the risk of making a type I or type II statistical error. This protocol would also be suitable when relative quantification is required (*e.g.,* incubations requiring cell proliferation).

Time taken

PBMC Stimulation/culture: 6 hours

RNA extractions: 96 samples can be extracted in 2 hours

cDNA synthesis: 96 samples can be prepped in 2 hours

SYBR qPCR: A 384 well plate can be loaded in 2 hours (and will take 1 hour to run with ssoAdvanced SOP on the quantitative thermocycler)

Anticipated results

If the experiment is performed correctly as described above, users should be able to quantify total copies of mRNA target and compare increased or decreased expression relative to media controls.

Chapter 4: Evaluating the Stability of Host-Reference Gene Expression and Simultaneously Quantifying Parasite Burden and Host Immune Responses in Murine Malaria

4.1 Chapter introduction

A related aspect of this project was to optimise RT-qPCR to understand vaccine-induced T cell responses using an adenovirus vector-based vaccine delivery platform as a proof-of-concept. The efficacy and immunogenicity of pre-erythrocytic stage malaria vaccines are routinely assessed in mice challenged with *Plasmodium* sporozoites, using RT-qPCR to quantify liver-stage parasite burden and host-cytokine responses. However, this quantification relies on the stable expression of endogenous host reference genes, whose consistency post-*Plasmodium* challenge or vaccination has not been previously validated. Furthermore, we anticipated antigen testing would result in partial non-sterile protection, and therefore, we established a method to define a threshold of protection and optimised a technique for quantitation of host liver T cell cytokine responses. The aim was to develop a reliable murine model for evaluating host immunity and the protective capacity of specific immunoreactive *Plasmodium* antigens.

I hypothesised that stable murine reference genes can be identified which will enable accurate quantification of Plasmodium *burden and T cell mediated immune gene expression.*

We addressed the following experimental aims:

1. Classify common reference gene expression as either stable or unstable following sporozoite challenge and subsequent adenovirus vector-based vaccination
2. Identify a set of stable reference genes that are optimal for data normalisation.
3. Optimise a process for quantitation of protection following *Plasmodium* sporozoite infection using RT-qPCR and reference gene normalisation
4. Optimise a protocol to detect cytokine expression as a measure of T cell response in the liver following *Plasmodium* sporozoite infection, in. a mouse model of malaria.

The work presented in this chapter has been published:

Browne, D. J., Kelly, A. M., Brady, J., Proietti, C., Sarathkumara, Y. D., Pattinson, D. J., & Doolan, D. L. (2023). Evaluating the stability of host-reference gene expression and simultaneously quantifying parasite burden and host immune responses in murine malaria. Scientific Reports, 13(1), 21071. https://doi.org/10.1038/s41598-023-48066-9

4.2 Published manuscript

Evaluating the stability of host-reference gene expression and simultaneously quantifying parasite burden and host immune responses in murine malaria

Daniel J. Browne[1], Ashton M. Kelly[1,2], Jamie Brady[1], Carla Proietti[2,3], Yomani D. Sarathkumara[1,2], David J. Pattinson[1#] and Denise L. Doolan[1,2,3#]

[1] Centre for Molecular Therapeutics, Australian Institute of Tropical Health & Medicine, James Cook University, Cairns, QLD 4870, Australia

[2] Institute for Molecular Bioscience. The University of Queensland, St Lucia, QLD 4067, Australia

[3] Centre for Tropical Bioinformatics and Molecular Biology, Australian Institute of Tropical Health & Medicine, James Cook University, Cairns, QLD 4870, Australia

4.2.1 Abstract

The efficacy of pre-erythrocytic stage malaria antigens or vaccine platforms is routinely assessed in murine models challenged with *Plasmodium* sporozoites. Relative liver-stage parasite burden is quantified using reverse transcription quantitative PCR (RTqPCR), which relies on constitutively expressed endogenous control reference genes. However, the stability of host-reference gene expression for RTqPCR analysis following *Plasmodium* challenge and immunization has not been systematically evaluated. Herein, we evaluated the stability of expression of twelve common RTqPCR reference genes in a murine model of *Plasmodium yoelii* sporozoite challenge and DNA-adenovirus IV 'Prime-Target' immunization. Significant changes in expression for six of twelve reference genes were shown by one-way ANOVA, when comparing gene expression levels among challenge, immunized, and naïve mice groups. These changes were attributed to parasite challenge or immunization when comparing group means using post-hoc Bonferroni corrected multiple comparison testing. *Succinate dehydrogenase* (*SDHA*) and *TATA-binding protein* (*TBP*) were identified as stable host-reference genes suitable for relative RTqPCR data normalisation, using the RefFinder package. We defined a robust threshold of 'partial-protection' with these genes and developed a strategy to simultaneously quantify matched host parasite burden and cytokine responses following immunisation or challenge. This is the first report systematically identifying reliable host reference genes for RTqPCR analysis following *Plasmodium* sporozoite challenge. A robust RTqPCR protocol incorporating reliable reference genes which enables simultaneous analysis of host whole-liver cytokine responses and parasite burden will significantly standardise and enhance results between international malaria vaccine efficacy studies.

4.2.2 Background

Pre-erythrocytic stage malaria vaccine candidates and vaccination platforms are routinely evaluated pre-clinically by quantifying liver-stage *Plasmodium* burden in mouse models [81, 406, 479]. Reverse [81, 406, 479] transcription quantitative PCR (RT-qPCR) is the gold-standard transcriptome-based diagnostic tool [355] and is used to quantify liver-stage parasite burden [479-487]. RT-qPCR analysis of *Plasmodium* liver burden allows the determination of the degree of pre-erythrocytic stage non-sterile protective immunity following sporozoite challenge [481, 488, 489]. In contrast, quantifying parasitemia following sporozoite challenge with blood-stage diagnostics (*i.e.,* Giemsa-Wright stain microscopy [490], flow cytometry [491], or blood-stage RT-qPCR [492]) typically represents an 'all-or-nothing' response, and is unable to determine the degree of protection during the liver-stage [479].

RT-qPCR has very high analytical sensitivity and specificity [356, 392]. However, inter-study RT-qPCR-based results can be inconsistent or irreproducible [400, 419]. Variables including sample extraction, RNA isolation and storage, cDNA synthesis and PCR amplification efficiencies may influence RT-qPCR measurements [400, 402]. These factors can be controlled by reference gene-based relative normalisation. However, a fundamental limitation of relative normalisation is the use of inappropriate or inadequately justified reference genes [356, 402, 493], or the selection of a single reference gene [400]. Indeed, robust and reproducible RT-qPCR depends upon multiple endogenous reference genes maintaining consistent expression across all experimental conditions [494]. Many conventional reference genes, such as *Glyceraldehyde 3-phosphate dehydrogenase* (*GAPDH*) or *β-actin* (*βACT*), are differentially expressed under certain stimulatory or stressful cellular conditions [402], including vaccination [495]. Therefore, reference gene validation across all experimental conditions is crucial for reproducible RT-qPCR. Despite previous publications describing [479-481, 496, 497] and using [406, 498-500] RT-qPCR-based liver-stage *Plasmodium* detection strategies, no publication has yet provided a set of stable host reference genes following *Plasmodium* infection or vaccination.

Additionally, this study describes an integrated dual whole-liver parasite burden and host-cytokine RTqPCR analysis strategy. The ability to use RTqPCR to simultaneously determine important host *in vivo* immunological responses to challenge and vaccination, as well as quantify matched liver-stage *Plasmodium* burden from an individual animal, is a valuable tool for vaccine development. For example, RTqPCR can measure the transcriptional response to

Plasmodium challenge of critical immunomodulatory cytokines, such as Interferon-gamma (IFN-γ), Interleukin 2 (IL-2), and Interleukin 10 (IL-10), which are associated with host-protection [501-503]. Unbiased RNA sequencing [504-506] and RTqPCR protocols [507, 508], have been developed to analyse mRNA responses to *Plasmodium* infection in whole liver, isolated splenocytes [498] and liver lymphocytes [509]. However, these protocols require additional processing, which preclude matched assessment of parasite burden, did not identify differences in critical protective immunomodulatory cytokines, or have been described following repeated or large sporozoite challenges, which may not be optimal for vaccine antigen testing.

Herein we report the first assessment of host whole-liver reference gene expression stability for RTqPCR analysis of *Plasmodium* parasite burden. Additionally, we provide an optimised protocol that allows the simultaneous assessment of parasite burden and host-cytokine mRNA responses. Specifically, as a representative immunisation strategy, BALB/c mice were immunised with a DNA prime and intravenous adenovirus 'Prime-Target' strategy [324], and challenged intravenously with 1,000 *P. yoelii* sporozoites. We developed a robust SYBR® chemistry-based protocol for relative quantification of matched parasite burden and host-cytokine mRNA responses. We identified unstable reference genes with high expression variability between naïve, parasite-challenged, and immunised mice. However, two reference genes *Succinate dehydrogenase (SDHA)* and *TATA-binding protein (TBP),* were stable across conditions. Additionally, we found that both challenge and vaccination significantly influenced cytokine expression of several host immunomodulatory cytokines, including *IFN-γ*, *IL-12p40* and *IL-10*. This study provides an optimised protocol that allows simultaneous quantification of host-parasite burden and immune responses to sporozoite challenge and vaccination.

4.2.3   Materials and methods

Mouse model and sample generation

Immunogens

Full-length *Plasmodium yoelii* Circumsporozoite protein (CSP) was synthesised commercially (Genscript, USA) and cloned into a pVR1020 plasmid DNA vector (Vical Inc, USA) downstream from a human cytomegalovirus immediate-early promoter and in-frame with the tissue plasminogen activator signal peptide. Plasmids were purified using an EndoFree plasmid gigaprep kit (Qiagen). A human adenovirus serotype 5 (AdHu5) vector was constructed with a *Py*CSP antigen using pAd/PL-DEST™ Gateway vector system and Gateway LR clonase

enzyme (Invitrogen) following the manufacturer's protocol. Linearised plasmids were transfected into Microbix HEK293 cells (Microbix Biosystems Inc., Canada) using a FuGENE HD transfection reagent (Promega, Australia). The virus was then cultured and purified by ultracentrifugation over a caesium chloride gradient, as previously described [510].

Immunisations and parasite challenge

Female BALB/c H-2Dd mice aged 5-7 weeks obtained from the Animal Resource Centre (ARC, Australia) were immunised by intramuscular injection (IM) into the anterior tibialis muscle (50 µl/leg) with 100 µg plasmid DNA (Prime) followed 12 days later with an intravenous injection (IV) into the lateral tail vein (200 µl) of 1×10^8 infectious units (IFU) of respective AdHu5 virus (Target). At 5 weeks post-boost, as tissue resident memory T cells are present [324], mice were challenged by IV injection of 1,000 cryopreserved *Plasmodium yoelii* 17XNL sporozoites (Sanaria Inc., USA) diluted in 200 µl PBS with 2% naïve mouse serum. Unchallenged and unimmunised (Naïve), sporozoite-challenged infection control (IC), and Prime-Target immunised and challenged (*Py*CSP) mice were studied. All experiments were approved by the Animal Ethics Committee of James Cook University (#A2549), and all procedures were conducted following the 2007 Australian Code of Practice for the Care and Use of Animals for Scientific Purposes, which adheres to the ARRIVE guidelines.

Liver harvesting and RNA extraction

All livers were processed identically as previously described [479, 481]; however, MagMAX™ *mirVana* Total RNA Isolation Kit (Applied Biosystems) was used for RNA extraction to increase RNA yield [356]. Briefly, whole livers were harvested at 42 h post-challenge in 5 mL MagMAX™ lysis buffer (Applied Biosystems) containing 1% β-2-mercaptoethanol (Sigma-Aldrich, Australia) and homogenised with a TissueRuptor II (Qiagen) homogeniser for 1 min. The lysate was stored at -80°C. RNA was extracted from 50 µL of liver lysate diluted 1:1 in MagMAX™ lysis buffer, following the manufacturer's recommendations with DNase treatment and elution in 50 µL elution buffer.

cDNA synthesis

Extracted mRNA was quantified using a NanoPhotometer® N60 (Implen, München, Germany). RNA (0.4 µg) was then converted to cDNA using the SuperScript™ IV First-Strand Synthesis System (Invitrogen) in 10 µL total volume reactions with random hexamers only with the following modifications from the manufacturer's protocol: cDNA synthesis was conducted

with the SuperScript™ reverse transcriptase at half the manufacturers recommended concentration (10U/μL$_{RNA}$), as previously described [511].

Quantitative PCR (qPCR)

Assay setup

qPCR was performed using ssoAdvanced SYBR® Supermix (BioRad) following the manufacturer's recommendations (hot start 2 min at 95°C, followed by 40 cycles of 15 sec at 95°C and 30 sec at 60°C) [356]. Reactions were run at 5 μL total volume amplifying 1 μL sample, as previously described [511]. Reactions were measured by QuantStudio 5 Real-Time PCR Machine running QuantStudio Design and Analysis Software (v1.4.3, Applied Biosystems), using technical triplicates and no template negative controls. Amplification efficiencies were calculated for all qPCR primers by calculating calibration curves from log diluted cDNA of pooled (n=5) naïve whole mouse liver, or pooled (n=5) infection control whole mouse liver when testing Py18s primers, as per MIQE guidelines [400] (**Table 4.1**). Cycle threshold values (Ct) were determined with the threshold set in exponential phase amplification at ΔRn0.3. All reactions were followed by a melt curve analysis ensuring primer specificity and contained desalt-grade PrimerBank™ [410] primers (Sigma-Aldrich) run at 500 nM. Reference gene expression stability and whole liver protectivity were evaluated by directly comparing Ct as amplified from 25 ng cDNA per reaction. The host-cytokine response to infection and immunisation was assessed by amplifying 50 ng cDNA per reaction, as per the optimised protocol.

Quantification of host-cytokine expression and parasite burden

Host-cytokine expression was calculated with the standard delta-delta cycle threshold ($2^{-\Delta\Delta Ct}$) method relative to the geometric mean of the endogenous control reference genes *SDHA* and *TBP*, as previously described [494], using naïve mice as the control group. Parasite burden was analysed using a modified 'Fold-reduction' approach, wherein several adaptations were made to the standard $2^{-\Delta\Delta Ct}$ protocol. Briefly, since the parasite burden of test groups would be expected to be equal or less than IC mice, the fold-change (*i.e.,* $2^{-\Delta\Delta Ct}$) calculation was inverted to fold-reduction (*i.e.,* $2^{\Delta\Delta Ct}$) using IC mice set as the control group. Since a standard deviation (σ) of *P. yoelii 18s* expression within the IC group was equal to 1 Ct (*i.e.,* $1\sigma = 0.957$ Ct), the threshold of 'partial protection' was set 2σ (*i.e.,* 2 Ct) from the mean. Since the inclusion of qPCR data with Ct >35 may increase false positive pathogen detection [494, 512], the limit of detection (LOD) of the qPCR assay was set to Ct = 35. Therefore, 'partial protection' is between

2 σ from the mean of the infection control, to the LOD of the assay. 'Sterile protection' is defined as a greater than the LOD of the assay. Both the 'partial protection' and LOD were normalised relative to the experimental geometric mean of endogenous control reference genes *SDHA* and *TBP*.

Table 4.1. Primer characteristics. Gene-specific forward and reverse primers acquired from Primer Bank™ database or literature. Assay performance determined as per MIQE guidelines.

Transcript	GenBank accession number	PrimerBank ID / Reference	Forward sequence (5′-3′)	Reverse sequence (5′-3′)	Size (bp)	E' (%)	R²
Reference genes							
18s	X00686.1	[513]	GTAACCCGTTGAACCCCATT	CCATCCAATCGGTAGTAGCG	151	110.6	0.99
GAPDH	NM_008084	126012538c3	TGGCCTTCCGTGTTCCTAC	GAGTTGCTGTTGAAGTCGCA	178	97.1	0.99
ACTβ	X03672.1	[513]	ACTATTGGCAACGAGCGGTT	ACACTTCATGATGGAATTGAATGTAGT	110	97.9	0.99
RPL13a	NM_009438	334688867c2	AGCCTACCAGAAAGTTTGCTTAC	GCTTCTTCTTCCGATAGTGCATC	129	100.0	0.99
PGK1	NM_008828	6679291a1	ATGTCGCTTTCCAACAAGCTG	GCTCCATTGTCCAAGCAGAAT	164	97.0	0.99
ALAS1	NM_020559	23956102a1	TCGCCGATGCCCATTCTTATC	GGCCCCAACTTCCATCATCT	109	101.4	0.99
SDHA	NM_025333	31560262a1	GCGGTGGTCACCTTGATCC	CCTCTGTAGAAGCGTCTGAATG	101	99.9	0.99
IPO8	NM_001081113	20071797a1	ACGTGACAGTAGATACCAACGC	GCATAGCACTCGGCATCTTCT	115	106.9	0.99
B2M	NM_008249	6680223a1	GGCCCATCTTGCATTCTAGGG	CAGGCAACGGCTCTATATTGAAG	100	102.8	0.99
HPRT1	NM_013556	7305155a1	TCAGTCAACGGGGGACATAAA	GGGGCTGTACTGCTTAACCAG	142	101.8	0.99
HMBS	NM_013551	30794512a1	AAGGGCTTTTCTGAGGCACC	AGTTGCCCATCTTTCATCACTG	78	97.5	0.99
TBP	NM_020614	10181156a1	CTTCCTGCCACAATGTCACAG	CCTTTCTCATGCTTGCTTCTCTG	118	99.8	0.99

Transcript	GenBank accession number	PrimerBank ID / Reference	Forward sequence (5′-3′)	Reverse sequence (5′-3′)	Size (bp)	E' (%)	R^2
Cytokine genes							
IFN-γ	NM_008337	33468859a1	ATGAACGCTACACACTGCATC	CCATCCTTTTGCCAGTTCCTC	182	99.1	0.96
TNFα	NM_013693	7305585a1	CCCTCACACTCAGATCATCTTCT	GCTACGACGTGGGCTACAG	61	107.3	0.98
IL-2	NM_008366	1504135a1	TGAGCAGGATGGAGAATTACAGG	GTCCAAGTTCATCTTCTAGGCAC	120	68.8	0.99
IL-6	NM_031168	13624311a1	TAGTCCTTCCTACCCCAATTTCC	TTGGTCCTTAGCCACTCCTTC	76	126.3	0.98
IL-12p40	NM_008352	6680397a1	TGGTTTGCCATCGTTTTGCTG	ACAGGTGAGGTTCACTGTTTCT	123	86.1	0.96
IL-1β	NM_008361	118130747c1	GAAATGCCACCTTTTGACAGTG	TGGATGCTCTCATCAGGACAG	116	101.7	0.99
IL-10	NM_010548	6754318a1	GCTCTTACTGACTGGCATGAG	CGCAGCTCTAGGAGCATGTG	105	81.8	0.99
IL-13	NM_008355	6680403a1	CCTGGCTCTTGCTTGCCTT	GGTCTTGTGTGATGTTGCTCA	116	65.6	0.94
TGF-β	NM_011577	6755774c1	CCACCTGCAAGACCATCGAC	CTGGCGAGCCTTAGTTTGGAC	91	89.6	0.96
17XNL *Plasmodium yoelii* gene							
18s	XR_004618869.1	[514]	GGGGATTGGTTTTGACGTTTTTGCG	AAGCATTAAATAAAGCGAATACATCCTTAT	104	103.2	0.98

E' Reaction efficiency, R^2 standard coefficient of determination

Flow-cytometric assessment of parasitemia

Parasitemia was assessed using the flow cytometric assessment of blood (FCAB) assay [491] from day five post-challenge until the infection had resolved. Briefly, blood from the tail vein was stained with anti-CD71-PE (BioLegend, USA), fixed with PBS containing 4% w/v paraformaldehyde and 0.0067% w/v saponin and then resuspended in buffer containing 0.5 µg/ml bisbenzimide Hoechst 33342 (Sigma-Aldrich, USA). Flow cytometric analysis was performed on an LSR Fortessa (BD Biosciences, NSW, Australia) using a high-throughput sampler. Post-acquisition data analysis was performed with FlowJo software version 9.4 (Treestar Inc., Ashland, OR, USA). Below 2% Red blood cell (RBC) parasitemia was considered background autofluorescence.

Statistical analysis

Reference gene expression stability of Ct values was analysed using an Ordinary One-way ANOVA with a Bonferroni-corrected multiple comparisons test against naïve mice. All data were tested for Gaussian distributions were tested with a Shapiro–Wilk normality test. Reference gene expression stability was analysed with RefFinder software as previously described [402]. Briefly, three packages (BestKeeper, geNorm and NormFinder) employed individual statistical approaches to assess reference gene expression stability, which was ranked and tabulated by RefFinder. Host-cytokine expression (Fold-change; $2^{-\Delta\Delta Ct}$) were analysed using a Kruskal-Wallis ANOVA with a Dunn's multiple comparisons test. Analysis was conducted using GraphPad Prism version 7.0 (GraphPad). In all statistical analyses, a $P < 0.05$ was considered significant.

4.2.4 Results

The expression of host reference genes is impacted by Prime-target immunisation and **Plasmodium** *sporozoite challenge*

We determined the stability of expression of twelve commonly reported reference genes [402] (**Table 4.1**) in murine livers following 'Prime and Target' immunisation and *P. yoelii* sporozoite challenge. We found the optimum cDNA concentration to measure reference gene expression was of 25ng or lower, to avoid inhibitory effects seen at higher concentrations (Reaction efficiency (E') > 100%; **Supp Fig. S4.1**). A one-way ANOVA identified significant variation in reference gene expression was found in *βACT* ($P = 0.0223$), *PGK1* ($P = 0.0456$), *ALAS1* ($P = 0.0157$), *IPO8* ($P = 0.0284$), *HPRT1* ($P = 0.0449$) and *HMBS* ($P = 0.0334$; **Fig.**

4.1). Post-hoc analysis found reference gene transcript variation following sporozoite challenge between naïve and IC mice for *βACT* ($P = 0.0455$), *PGK1* ($P = 0.0342$), *ALAS1* ($P = 0.0187$), *IPO8* ($P = 0.0168$) and *ALAS1* ($P = 0.0187$) genes; and between naïve and *Py*CSP mice for *βACT* ($P = 0.0211$). These data demonstrate that both immunisation and *Plasmodium* challenge impact reference gene expression.
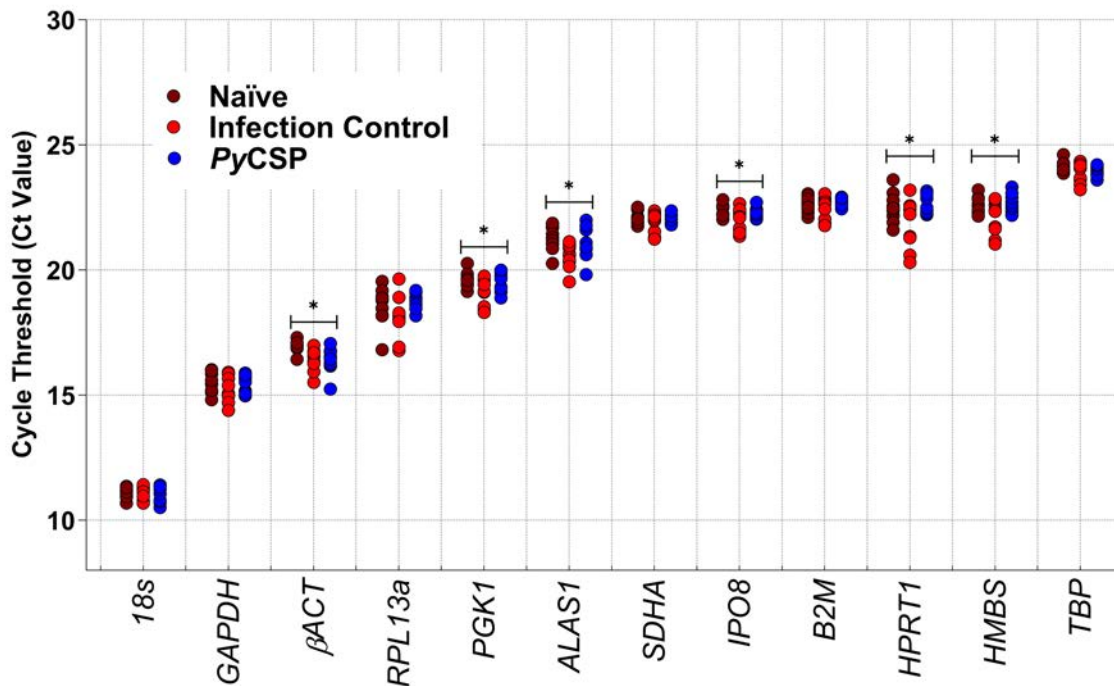
Figure 4.1. Reference gene stability following 'Prime-Target' immunisation and *Plasmodium* sporozoite challenge. Groups of BALB/c mice (n=10/group) included naïve unchallenged (Naïve), naïve with sporozoite challenge (Infection Control), and *Plasmodium yoelii* Circumsporozoite protein immunised and sporozoite challenged (*Py*CSP). Where appropriate, mice were intramuscularly immunised with plasmid DNA (Prime), followed 12 days later with an intravenous injection of the respective AdHu5 virus (Target). RNA was extracted from the homogenised whole liver at 5 weeks post-immunisation and 42 h post-challenge with 1,000 *Py*17XNL sporozoites. Cycle threshold (Ct) values were determined from the mean of triplicate replicate qPCR reactions, with the threshold set in exponential phase amplification at ΔRn0.3. Ct values of twelve candidate reference genes from two independent experimental replicates (n=5/replicate) are shown. Data were analysed using one-way ANOVA with a Bonferroni-corrected multiple comparisons test comparing each group to the naïve mice (* $P < 0.05$).

SDHA and TBP were identified as the most suitable reference genes for RT-qPCR analysis of **Plasmodium** *liver-burden and host-cytokine response*

To identify the most suitable reference genes for determining both *Plasmodium* liver burden and host-cytokine responses in the liver post-challenge, Ct values for each reference gene (**Fig. 4.1**), were ranked for their stability with the RefFinder software package [515], combining geNorm, NormFinder and BestKeeper analysis (**Table 4.2**). *SDHA* and *TBP* were ranked as the most stable genes and, therefore, the most suitable reference genes and had a combined geNorm M stability value of 0.14 which falls below the established threshold of 0.15 for requiring additional reference genes [516]. Therefore, the inclusion of further reference genes beyond the two genes SDHA and TBP was not required. Notably, all packages ranked *SDHA* and *TBP* as the most stable genes, and *RPL13a* as the least stable gene. The most widely used reference gene *GAPDH* [479] was ranked 6th, 8th, and 9th most stable by geNorm, NormFinder and BestKeeper, respectively.

Table 4.2. Reference gene expression stability as determined by RefFinder. The reference gene stability of 12 potential reference genes was calculated for naïve, sporozoite-challenged, and *Plasmodium yoelii* CSP immunised and sporozoite-challenged BALB/c mice (n=10/group) by RefFinder software.

	SDHA	TBP	IPO8	PGK1	B2M	HMBS	18s	GAPDH	βACT	HPRT1	ALAS	RPL13a
Rank [*]	1	1.68	3.46	4.05	4.9	6.12	7.11	7.17	8.91	9.72	10.74	12
GM [C_t] [#]	21.99	24.01	22.21	19.40	22.57	22.47	10.99	15.34	16.55	22.31	21.01	18.45
AM [C_t] [#]	22.00	24.01	22.22	19.40	22.57	22.48	11.00	15.35	16.56	22.32	21.02	18.46
Min [C_t] [#]	21.24	23.21	21.35	18.30	21.78	21.04	9.04	14.39	15.24	20.30	19.53	16.79
Max [C_t] [#]	22.51	24.61	22.82	20.27	23.04	23.32	11.42	16.02	17.30	23.61	21.99	19.64
SD [± C_t] [#]	0.23	0.24	0.25	0.34	0.26	0.38	0.31	0.40	0.35	0.50	0.50	0.55
CV [%C_t] [#]	1.07	0.99	1.12	1.74	1.17	1.71	2.78	2.60	2.11	2.24	2.36	2.95
Min [x-fold] [#]	-1.69	-1.73	-1.82	-2.14	-1.73	-2.71	-3.85	-1.93	-2.47	-4.02	-2.79	-3.16
Max [x-fold] [#]	1.43	1.52	1.52	1.83	1.39	1.80	1.35	1.60	1.68	2.45	1.97	2.29
SD [± x-fold] [#]	1.18	1.18	1.19	1.26	1.20	1.31	1.24	1.32	1.27	1.41	1.41	1.46
S	0.073	0.144	0.177	0.163	0.264	0.222	0.333	0.326	0.451	0.443	0.604	0.631
M	-	0.149	0.181	0.216	0.201	0.272	0.301	0.244	0.344	0.38	0.432	0.478

[*] RefFinder overall rank, [#] BestKeeper Statistics, S stability value by NormFinder, M stability value by geNorm GM, geometric mean; AM arithmetic mean; C_t cycle threshold; SD standard deviation; CV coefficient of variation. Decreasing Rank, M, and S values signifies increased expression stability.

The threshold for partial protection is defined as two standard deviations below the mean of the infection control

When infection was allowed to progress to the blood-stage all IC mice and one in five *Py*CSP mice developed parasitemia (**Fig. 4.2A**). Using RT-qPCR relative quantification of parasite rRNA in the liver, we could determine both sterile protection (*i.e.,* the absence of *P. yoelii* 18s (*Py18s*) rRNA) and a reduction in parasite burden indicating partial protection (**Fig. 4.2B**). A high liver-stage parasite burden was found in all IC mice (*Py18s* Ct mean = 24.78 with σ = 0.96; **Fig. 4.2B**), which passed normal-distribution testing (Shapiro–Wilk test; *P* = 0.5882). We defined the LOD of the assay as Ct = 35, which provided a fold-reduction dynamic range of the assay (relative to the IC) as $2^{\Delta\Delta CT}$ = 1189. Furthermore, we defined 2 σ from the *Py18s* Ct mean of the IC as the threshold of partial protection (*i.e.,* Threshold Ct = 26.70 or $2^{\Delta\Delta CT}$ = 3.77; **Fig. 4.2B**), which demonstrated five PyCSP mice were partially protected, and five PyCSP mice were sterilely protected (**Fig. 4.2B**). This RT-qPCR protocol detected degrees of liver-stage parasite burden, allowing for the interpretation of partial protection.
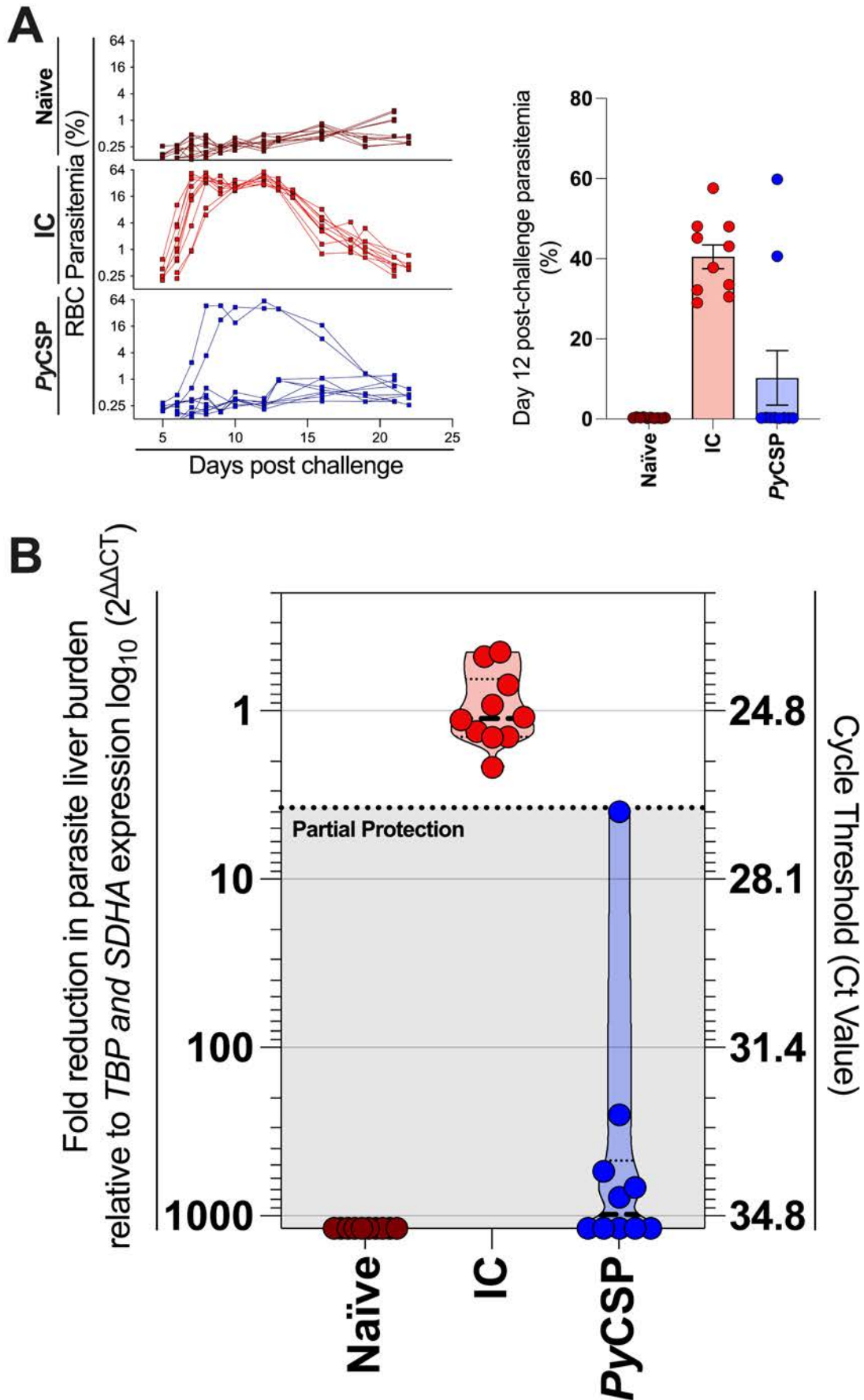
Figure 4.2. The threshold of 'partial protection' in the liver stage. BALB/c mice (n=10/group) were immunised and challenged as described above (Figure 4.1 legend): naïve (brown), infection control (IC) sporozoite challenged (red), and PyCSP immunised and sporozoite challenged (blue). Parasitemia over the duration of infection and at day 12 post-challenge **(A)** was measured by flow cytometry using the FCAB assay. Liver-stage parasite burden of individual mice was measured at 42 h post-challenge by technical triplicate RT-qPCR **(B)**. The Ct was determined from the mean of triplicate replicate, with data calculated based on Fold-reduction (2ΔΔCt) relative to the Ct geometric mean of the reference genes TBP and SDHA. Protection was defined as two standard deviations (2 σ = 1.91 Ct) below the mean Ct of the IC (dotted line). The limit of detection (LOD) is Py18s Ct = 35 (2ΔΔCt = 1189). Data are pooled from two independent experimental replicates (n=5/replicate).

Whole-liver host-cytokine expression responds to both immunisation and challenge

To detect clinically relevant cytokines in the host-whole liver using relative mRNA quantification, we found the optimum concentration of cDNA in the qPCR to detect *IFN-γ* was 50 ng of cDNA per reaction (**Supp Fig. S4.1**). A non-parametric Kruskal-Wallis ANOVA found that the expression of *IFN-γ, TNFα, IL-2, IL-12p40, IL-1β* and *IL-10* was significantly influenced by treatment ($P = 0.0103$, $P = 0.0052$, $P = 0.0250$, $P = 0.0005$, $P < 0.0001$ and $P < 0.0001$ respectively; **Fig. 4.3**). Dunn's multiple comparisons testing identified increased expression of *IFN-γ, IL-1β* and *IL-10* in IC mice ($P = 0.0363$, $P = 0.0027$, $P = 0.0010$, respectively; **Fig. 4.3**) relative to naïve mice. Likewise, increased expression of *IFN-γ, TNFα, IL-12p40, IL-1β* and *IL-10* was identified in *Py*CSP mice ($P = 0.0096$, $P = 0.0030$, $P = 0.0002$, $P < 0.0001$, and $P < 0.0001$ respectively; **Fig. 4.3**) relative to naïve mice. Taken together, these data demonstrate a robust SYBR® chemistry-based RT-qPCR protocol for liver-stage *Plasmodium* infection burden testing with matched host-cytokine mRNA response quantification.
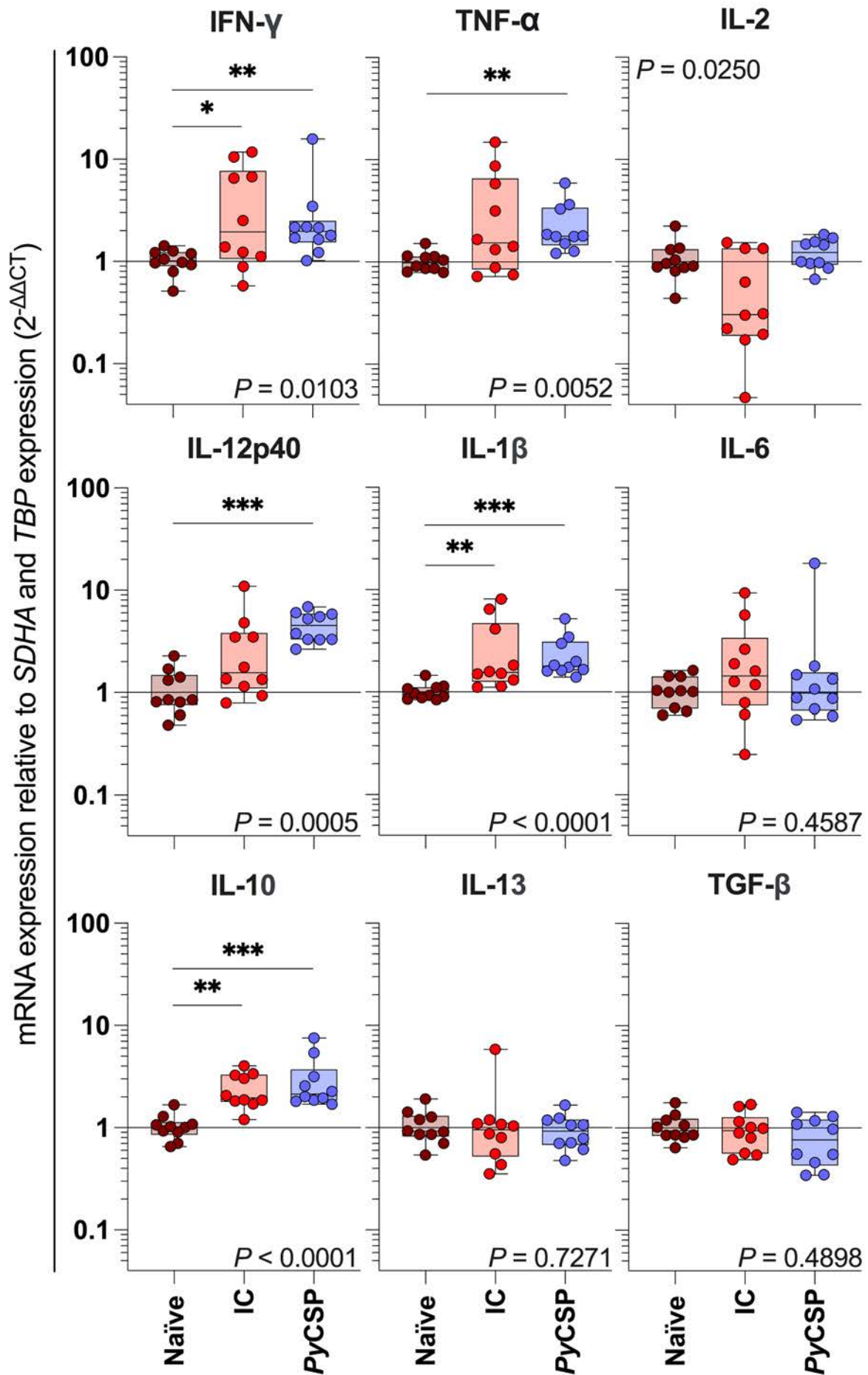
Figure 4.3. Cytokine expression following Prime-Target immunisation and *Plasmodium yoelii* sporozoite challenge. BALB/c mice (n=10/group) were immunised with a Prime-Target regimen and challenged with *Py*17XNL sporozoites as previously described (Figure 4.1 legend). mRNA expression was assessed by RT-qPCR in liver extracts harvested at 42 h post-challenge from naïve, infection control (IC) sporozoite-challenged (red), *Py*CSP-immunised and sporozoite-challenged (blue) BALB/c mice (n=10/group). Data are pooled from two independent experimental replicates (n=5/replicate). Fold-change was determined within each experiment with the delta-delta cycle threshold ($2^{-\Delta\Delta Ct}$) method relative to the Ct geometric mean of the reference genes *TBP* and *SDHA*. Data were compared with a non-parametric Kruskal-Wallis one-way ANOVA with *P*-value displayed and a post-hoc Dunns-corrected multiple comparisons test comparing test groups to the mean of naïve mice (*, $P \leq 0.05$; **, $P \leq 0.01$; ***, $P \leq 0.001$; ****, $P \leq 0.0001$).

4.2.5   Discussion

Herein, we describe a *Plasmodium yoelii 18s* (*Py18s*) rRNA-specific RT-qPCR-based detection strategy with an optimised reference gene selection. This protocol defines 'partial protection' in the liver-stage following a sporozoite challenge and allows matched quantification of host whole-liver cytokine responses. Our assay provides an important update for pre-erythrocytic stage whole-liver *Plasmodium* parasite burden molecular diagnostics.

The inappropriate selection of reference genes is a major contributor to the lack of reproducibility of RT-qPCR data [400, 419]. Previously published RT-qPCR-based relative quantification strategies of *Plasmodium* liver burden are derived from a single reference gene [500]. Indeed, routine or habitual RT-qPCR reference gene selection is common across multiple disciplines [517, 518]. Using inappropriate reference genes for normalisation may result in the incorrect identification of fully or partially protected animals and misrepresentation of cytokine expression profiles. By analysing the variability of Ct values from 12 commonly cited host reference genes, we identified half were differentially expressed following immunisation and infection, emphasising the importance of systematic reference gene assessment. Although we have established that TBP and SDHA as highly suitable for RTqPCR relative normalisation in our model of *P. yoelii* sporozoite challenge and adenovirus vector-based 'Prime-Target' immunization, it is likely that other stably expressed reference genes may be identifiable with unbiased screening in other models [504-506]. *TBP* and *SDHA* have been identified as stable reference genes for human leukocyte RT-qPCR analysis studies [402].

It is widely acknowledged that reference gene expression stability testing must include all experimental conditions [400, 419], including vaccination [495] and challenge [519], as these influence reference gene expression. Our study found statistically significant whole-liver reference gene expression instability in the expression of the commonly cited reference gene *β-actin (βACT)* following a 'Prime & Target' immunisation regimen and parasite challenge. *βACT* can be differentially expressed under inflammatory conditions [520]; therefore, we speculate that the differential expression we observed in whole-liver *βACT* expression may result from antigen-independent adenovirus vector-based inflammation [324]. We found several reference genes were differentially expressed in infection control mice (*i.e., IPO8, PGK1* and *ALAS1*) in response to sporozoite challenge. While many key host-parasite liver-stage immunological interactions remain unresolved [521], innate or innate-adaptive interface immune responses to *P. yoelii* challenge may be driving differential whole-liver cytokine expression. Whilst we have assessed the 'Prime-Target' regimen followed by a 1000 *P. yoelii* sporozoite challenge, other vaccine regimens or challenges involving different sporozoite species or numbers, or other mouse strains will likely require an independent assessment of reference gene expression stability.

A significant advantage of liver-stage parasite burden RT-qPCR quantification is the determination of the degree of pre-erythrocytic stage non-sterile protective immunity following sporozoite challenge. To provide a robust method to analyse parasite liver burden data and define 'partial protection' from sporozoite challenge, we made several key adaptations to the standard fold change ($2^{-\Delta\Delta Ct}$) method. The first adaptation was to invert the method from fold-change to fold-reduction ($2^{-\Delta\Delta Ct}$ *vs* $2^{\Delta\Delta CT}$) relative to the infection control group. The second adaptation was to define the LOD as Ct = 35. The theoretical LOD (*i.e.,* the lowest amount of measurable analyte) of qPCR is between one and three copies [400], which under ideal conditions (*i.e.,* a reaction efficiency of 100%) typically reaches cycle threshold (Ct) around cycle 35. Including results >35 Ct significantly increases the false-positive rate when performing pathogen detection qPCR [494, 512]. We set our fold-reduction (*i.e.,* $2^{\Delta\Delta CT}$) data analysis strategy LOD to Ct = 35 and found a 1189-fold dynamic range from the mean of the IC. The third adaptation was to use this calculated fold dynamic range to provide values to samples from which no amplification occurred. As fold-change RT-qPCR analysis is incapable of including 'u*ndefined*' samples [494], an 'u*ndefined*' or $2^{\Delta\Delta CT} > 1189$ result was therefore given a value of $2^{\Delta\Delta CT} = 1189$. This strategy avoids the use of setting non-detect Ct values to a threshold (*i.e.,* Ct = 35), which can introduce substantial bias during normalisation [522].

The final method adaption was to define a threshold of partial protection. We found the standard deviation (σ) of IC liver parasitemia (*Py18s*) was 0.96 Ct, and the *Py18s* of the IC and the reference genes of all groups were normally distributed. This consistency suggested the I.V. transmissibility of the sporozoites was high. Two standard deviations from the mean typically cover 95% of all intra-group data when normally distributed. Therefore, we defined 'partial protection' as 2 σ from the mean *Py18s* of the IC group to appropriately identify mice with a clinically relevant reduction of parasite liver burden. We did not employ any method to remove technical replicate outliers, as no obvious inappropriate technical variability was observed. However, care must be taken to ensure that results are not biased by high replicate variability, and methods to identify and remove replicate outliers must be reported.

We have optimised a SYBR®-chemistry fold change ($\Delta\Delta$Ct)-based strategy to quantify the whole-liver expression of immunologically important cytokines to facilitate matched host-response and parasite burden assessment. We found the *Py18s* rRNA-specific SYBR® qPCR primers amplified non-specifically in the absence of *Py18s* in the sample. As reported, these readings were excluded based on an incorrect melt curve. It is likely a TAQ-polymerase probe-based assay could eliminate the detection of this non-specific amplification, however, these results demonstrate that careful optimisation is required to ensure the probe does not bind to the non-specific amplicon. We utilised the $\Delta\Delta$Ct method due to its prevalent use in evaluating whole liver parasitemia [406, 479-481, 496-500]. Although, normalisation methods like the Pfaffl method, which account for primer efficiency, could offer a more rigorous analysis of gene expression data [523].

The simultaneous quantification of liver parasite burden and host-cytokine response in a standardised protocol is an important addition to pre-erythrocytic stage vaccine development, as this technique will increase the reproducibility of studies investigating the host immune response elicited during the pre-erythrocytic stage to vaccination and challenge [509]. The critical effector molecule of adaptive immunity to sporozoite challenge appears to be Interferon-gamma (IFN-γ) released by CD8^{+} T cells [67, 69], and Th1 CD4^{+} T cells secreting IFN-γ and Interleukin-2 (IL-2) [310-312]. The mRNA expression profiles of IFN-γ and many other rapidly produced and secreted cytokines are relatively highly correlated to protein production [511]. Therefore, transcriptomic quantification of host-cytokine responses will inform functional efforts to understand the immunological response following vaccination. A protocol that can evaluate mRNA expression of essential host effector genes following a

challenge of 1,000 *P. yoelii* sporozoites is expected to provide the sensitivity required for most *P. yoelii* vaccine challenge models. Furthermore, it is anticipated that a similar strategy to quantify whole organ cytokine response could be applied to other immunisation, mouse strain, *Plasmodium* species, or other pathogen challenge rodent models.

We present a protocol for the robust analysis of primary liver-stage *Plasmodium* infection and pre-erythrocytic stage immunity burden testing. We demonstrate that *P. yoelii* infection and 'Prime-Target' immunisation influence reference gene expression and identify *SDHA* and *TBP* as optimal reference genes for relative RTqPCR normalisation. We have established a criterion for defining partially protective immunity to infection and provide a customised fold-reduction method to provide a LOD and account for 'u*ndefined*' measurements. This assay is suitable for studying whole-liver host-cytokine mRNA responses, which are matched with a parasite-burden readout. This protocol is designed to be broadly adaptable across various murine models. While we anticipate the need for reference gene optimization may vary depending on the specific model, the protocol presented herein offers a systematic framework for identifying stable RTqPCR reference genes in mouse whole liver, determining 'partial' and 'sterile' protection, and assessing the expression of critical matched host immunomodulatory genes. This report provides an important update for further trials evaluating pre-erythrocytic stage whole-liver *Plasmodium* parasite burden and host response and highlights the importance of thorough selection of reference genes for RTqPCR.

Acknowledgments

Author contributions

DJB, DJP and DLD designed the study. DJB, AMK, JB, DJP, and YDS performed experiments. DJB, and CP analysed the data. DJB, DJP, and DLD wrote the manuscript, with editorial input from all authors.

Data availability statement

All data supporting the findings of this study are available within the paper and its Supplementary Information.

Additional information

The authors declare that the research was conducted in the absence of any commercial or financial relationships that could be construed as a potential conflict of interest.

4.2.6 Supplementary material
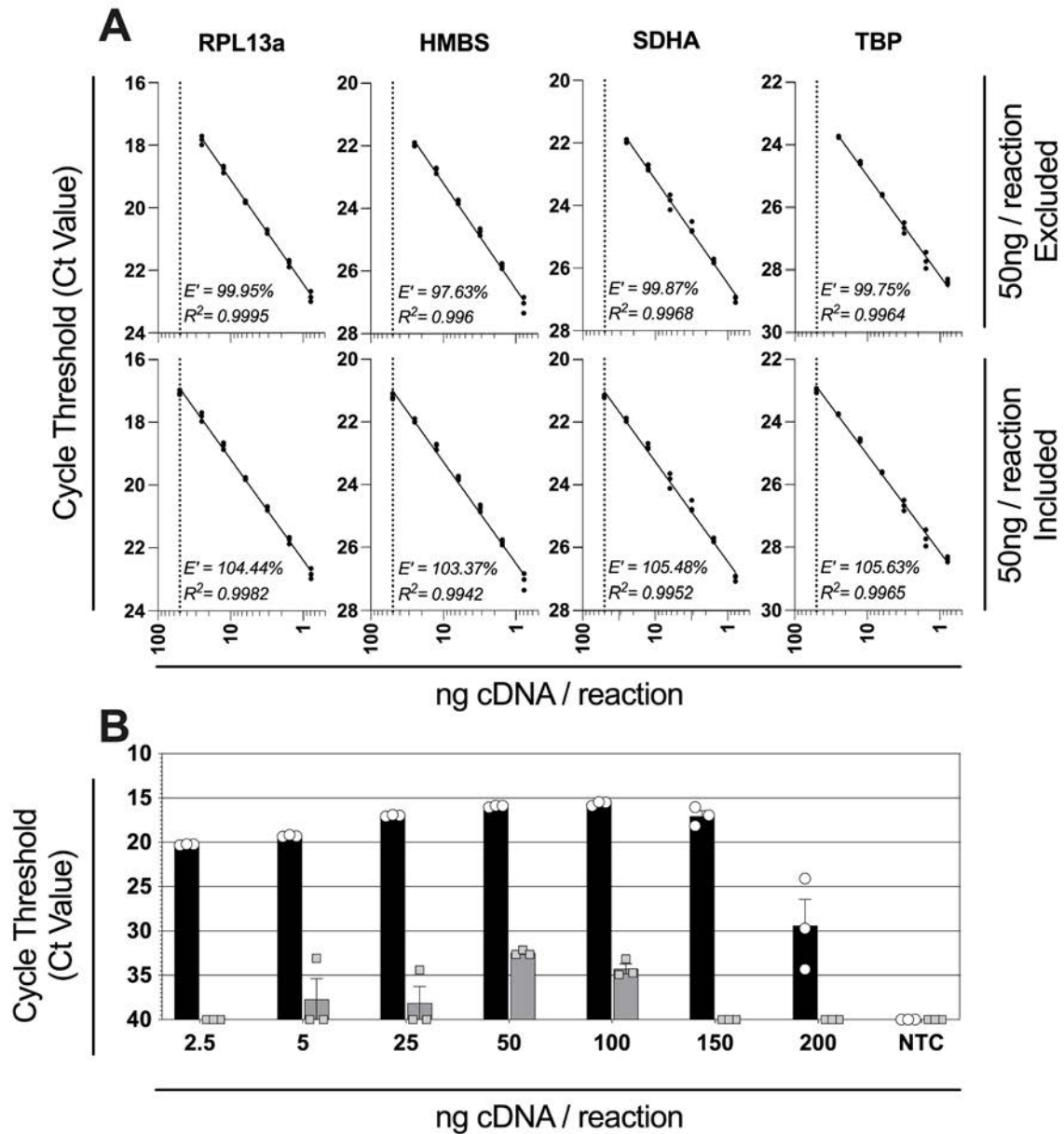
Supplementary Figure S4.1. Optimisation of cDNA concentration in reaction for reference gene assessment and cytokine detection. (**A**) The reaction efficiency (E') and the coefficient of determination (R^2) were calculated as per the MIQE guidelines from Log titrations of cDNA testing reference genes RPL13a, HMBS, SDHA and TBP with 50ng included (bottom) and 50ng excluded (top). (**B**) mRNA expression of reference gene RPL13a (black bars, white spots) and cytokine IFN-γ (grey bars, grey squares) from pooled (n=5) naïve whole mouse liver; and no-template negative control (NTC). Shown is the cycle threshold value (Ct Value), with undetermined values receiving a value of 40, as measured by RT-qPCR. Individual technical replicates (spots and squares) are shown alongside the technical replicate mean (bars) ± technical SEM.

Chapter 5: Evaluating Immunoreactivity to *Plasmodium falciparum* CD8+ and CD4+ T cell Epitopes in a Malian Cohort

5.1 Chapter introduction

After successfully optimising a HTS-RT-qPCR protocol to identify immunoreactive antigens and T cell peptide epitopes, and refining an approach to assess the protective efficacy of such antigens in a murine model, we sought to apply those tools to investigate the immunoreactivity of previously identified immunoreactive T cell peptide epitopes. We sought firstly to more thoroughly investigate *P. falciparum* antigens which were identified as immunoreactive in malaria-naïve controls. We next sought to investigate the antigens which were identified as immunoreactive in Papua New Guinan (PNG) adults with clinical immunity to malaria. We aimed to deconvolute the *P. falciparum* peptide pools to identify specific epitopes responsible for the immunoreactivity. This study demonstrated our HTS-RT-qPCR protocol produced robust and reproducible results which were closely correlated with matching protein responses from ELIspot assays.

I hypothesised that the immunodominance hierarchy previously established by the Doolan Laboratory in PNG donors would match the hierarchy in Malian donors

We attempted to address the following experimental aims:

1. Validate the *P. falciparum* T cell antigen immunoreactivity observed in naïve donors in a new naïve cohort.
2. Validate the T cell antigen immunoreactivity observed in clinically immune PNG subjects in a Malian cohort.
3. Identify the peptide epitopes responsible for immunoreactivity.

5.2 Draft Manuscript

Evaluating immunoreactivity to *Plasmodium falciparum* CD8^{+} and CD4^{+} T cell epitopes

Daniel J. Browne[1] and Denise L. Doolan[1,2*]

[1] Centre for Molecular Therapeutics, Australian Institute of Tropical Health and Medicine, James Cook University, Cairns, QLD 4878, Australia

[2] Institute for Molecular Bioscience, The University of Queensland, St Lucia, QLD 4067, Australia

5.2.1 Abstract

Malaria is a major public health concern that affects millions of people worldwide. A vaccine which can induce robust host T-cell responses during the liver-stage of a *Plasmodium* infection is expected to provide a critical tool for controlling the disease. The Doolan research group has previously leveraged 'Omic'-datasets to identify a comprehensive set of 1,500 parasite antigens expressed during the liver-stage of the malaria parasite's life cycle which were expected to provoke potent T-cell responses. The group subsequently predicted CD8$^+$ and CD4$^+$ T-cell peptide epitopes within these antigens *in silico* and ranked the immunogenicity of the antigens following *in vitro* stimulation of peripheral blood mononuclear cells (PBMCs) from malaria-experienced Papua New Guinean donors with pools of antigen-specific peptides. In this doctoral study, we sought to test if other populations would respond to the top ten prioritized immunoreactive antigens, and to deconvolute the peptide pools to identify the T-cell epitopes responsible for the immunoreactivity. Using an optimized high-throughput real-time quantitative PCR (HTS-RT-qPCR) protocol and gold-standard IFN-γ enzyme-linked immunospot (ELIspot) we found the previously identified liver-stage *P. falciparum* CD8$^+$ and CD4$^+$ T cell antigen peptide pools which were highly immunoreactive in PNG had limited immunogenicity in Malian donors. Further studies with freshly acquired Malian and PNG donors will be required to draw further conclusions from this study. Nonetheless, this study demonstrates our optimized HTS-RT-qPCR protocol combined with ELIspot validation allows identification of immunoreactive antigens and their corresponding T cell epitopes, which may aid in the development of effective vaccines against malaria.

5.2.2 Introduction

Malaria, a disease caused by infection with *Plasmodium* spp. parasites [3], is a major public health concern that affects millions of people worldwide [524]. The development of a vaccine targeting the liver-stage of the *Plasmodium* life cycle would represent a critical advance in controlling the disease, as such a vaccine would prevent both clinical disease and transmission which occurs in the subsequent blood and sexual stages. [94, 113, 200]. A pre-erythrocytic stage vaccine would ideally induce robust T-cell responses, as T-cells are the critical immune effector cells during the liver-stage of a *Plasmodium* infection [67, 69, 76, 272, 294]. However, previous malaria vaccine development efforts have either focused on inducing strong antibody-responses to blood-stage antigens [198, 525], or selected pre-erythrocytic sporozoite and liver-stage antigens in an *ad-hoc* manner [32, 94]. The selection of appropriate liver-stage vaccine antigens is challenging as *Plasmodium spp* parasites are complex eukaryotic pathogens with a large proportion of genes devoted to immune evasion and host-parasite interaction [526]. The Doolan research group have addressed this issue by identifying 1,500 *Plasmodium falciparum* proteins expressed during the liver-stage using a systems-biology approach which combined genomic, transcriptomic, and proteomic (omic)-datasets (*See: 1.3.3: Foundational Data*). The Doolan research group aimed to prioritise the identified antigens as potential liver-stage vaccine candidates based on their ability to elicit a strong T-cell response in peripheral blood mononuclear cells (PBMCs) obtained from individuals from Papua New Guinea (PNG) with prior malaria exposure. Furthermore, the group aimed to investigate fundamental aspects of the host-parasite relationship, including epitope immunodominance [84] and potential mechanisms of immune evasion by the malaria parasite [128].

While approximately 30% of the tested proteome was reproducibly recognized in donors from PNG (unpublished data, D. Doolan, with permission; **Fig. 1.8**), the immunogenicity of these peptides in populations beyond PNG had not been tested. Therefore, the intent of this doctoral study was to evaluate the recognition of the top 10 immunoreactive antigens by adults in Mali, Africa, and use the HTS-RT-qPCR strategy to deconvolute the pool of 20 peptides to identify the specific peptide epitopes recognized by the PNG adults. However, the outbreak of the SARS-CoV2 pandemic [527] limited availability of additional PNG donors as well as Mali sample sources, thus restricted experimentation. In this study, we aimed to address these challenges by using a combination of our optimized high-throughput real-time quantitative PCR (HTS-RT-qPCR) protocol [356] and gold-standard enzyme-linked immunospot (ELIspot) [351] to measure the immunoreactivity of the top 10 prioritised antigens in PBMCs from adult

malaria-experienced Malian donors. Firstly, we characterized the 'cross-reactive' T cell responses from the antigens that were found in the foundational studies by the Doolan group to be immunoreactive to malaria-naïve healthy controls to identify the most immunoreactive peptide epitope (peptide 12) and corresponding HLA restriction element. Secondly, we deconvoluted the peptide pool for the top-10 peptides identified as immunoreactive in PNG by testing each of the 20 peptides individually. Overall, this study demonstrated that the optimized HTS-RT-qPCR protocol and ELIspot methodology hold promise to identify immunoreactive antigens and their corresponding T cell epitopes.

5.2.3 Foundational Data

Data in this section, which form the foundation for this doctoral study, pertaining to antigens identified as the most immunoreactive in PNG donors (*i.e.,* 'specific antigens') or antigens identified as the most immunoreactive in malaria naïve donors (*i.e.,* 'cross-reactive antigens') were collected previously by Ms. Joanne Roddick, Ms. Lea Lekieffre, Dr. Carla Proietti, and Prof. Denise Doolan. Of the ten *P. falciparum* antigens identified in the foundational studies as the most immunoreactive in PNG donors (Specific antigen ID#: 853, 1068, 307, 535, 533, 638, 101, 606, 610, and 76; unpublished and confidential) all were immunoreactive in ten of ten donors. Of the five *P. falciparum* antigens identified as the most immunoreactive in malaria naïve donors (Cross-Reactive Antigen ID#: 789, 437, 497, 703, and 707; [342]) 789 and 437 were immunoreactive in nine of ten donors, 497 and 703 were immunoreactive in eight of ten donors, and 707 was immunoreactive in five of ten donors.

5.2.4 Methods

Peripheral blood mononuclear cell (PBMC) processing

All work reported in this chapter was performed according to the principles of the *Declaration of Helsinki*. All samples were collected and processed in compliance with all applicable federal regulations governing protection of human subjects, and all methods were performed in accordance with institutional guidelines and regulations.

Malaria naïve PBMCs

PBMCs from healthy malaria-naïve donors were obtained from the Australian Red Cross. Ethics approval for work with malaria-naive PBMCs was obtained from James Cook University Human Research Ethics Committee (#H7886). Informed consent was obtained from

all participants and donors were questioned about their history of exposure to malaria. The inclusion criteria for the study were that participants were over the age of 18 and were well and able to donate in adherence with Queensland Health policies had no known prior exposure to malaria. PBMCs were isolated by standard density gradient centrifugation and cryopreserved in 90%FBS/10%DMSO as previously described [356]. PBMCs were thawed at 37°C, treated with DNase I (100 μg/mL; StemCell Technologies), and rested for 18 hours at 2×10^6 cells/mL in RPMI-1640 supplemented with 10% heat-inactivated AB human serum (Sigma-Aldrich), 100U/mL penicillin/streptomycin (ThermoFisher Scientific), 1x MEM non-essential amino acids (ThermoFisher Scientific), 2mM glutaMAX (ThermoFisher Scientific), 10 mM HEPES (ThermoFisher Scientific), and 5×10^{-5}M β-Mercaptoethanol (Sigma-Aldrich) (R10 media) at 37°C and 5% CO_2.

Malaria experienced PBMCs

Cryopreserved PBMCs collected in 2009 from asymptomatic malaria-experienced individuals from the Kambila region of the Republic of Mali by Dr Peter Crompton (Laboratory of Immunogenetics; National Institute of Health, USA) in collaboration with Dr Boubacar Traore (Malaria Research and Training Center; University of Sciences, Techniques and Technologies of Bamako, Mali) were also used. Malian PBMCs collection was approved by the Ethics Committee ((FWA #00001769) of the Faculty of Medicine, Pharmacy and Dentistry at the University of Sciences, Techniques and Technologies of Bamako (#2011/37/FMPOS and 2018/181/FMPOS) and the Institutional Review Board of the National Institute of Allergy and Infectious Diseases, National Institutes of Health (#07-I-N141, #11-I-N126 and OHSRP #12362), the Queensland Institute of Medical Research Human Research Ethics Committee (#P1111), and the James Cook University Human Research Ethics Committee (#H7735).

PBMCs were thawed following *The International Maternal Pediatric Adolescent AIDS Clinical Trials* (IMPAACT) network standard operating procedure [528]. Briefly, PBMCs were thawed rapidly at 37°C, washed twice with R10 Media containing 50U/mL of Benzonase® Nuclease (Sigma Aldrich). Live and dead cells were counted on a hemocytometer following Trypan blue staining. Live and dead cells were isolated with Lymphoprep™ (STEMCELL) density gradient separation fo0llowing manufacturer's instructions and rested for 18 hours at 2×10^6 cells/mL in R10 Media. Before stimulation, viable malaria naïve and experienced PBMCs were counted with a CASY™ Cell Counter (OLS-OMNI Life Science).

Cell stimulation

Pools or individual synthetic peptides (10 or 2 μg/mL) representing well-characterized CD8$^+$ T cell epitopes from influenza virus, Epstein-Barr virus and cytomegalovirus (**Chapter 3: Supplementary Table S3.1**), CD4$^+$ T cell epitopes from SARS-CoV2 (**Chapter 6: Supplementary Table S6.1**) or predicted CD4$^+$ and CD8$^+$ T cell epitopes from *Plasmodium falciparum* (Commercial in Confidence) were tested alongside PMA/Iono (50ng/mL PMA, 1,000ng/mL Ionomycin) mitogen positive-control and a media-only negative-control. For RT-qPCR analysis; PBMCs were stimulated in 200 μL R10 media (described above) in 96-well U-bottom plates. For IFN-γ ELIspot analysis, 4x10^5 PBMCs per well were stimulated for 24 hours in 96-well ELIspot plates, following standard procedures. For some studies different batched of Human serum (Sigma-Aldrich) were investigated: Batches: SLBN8825V, SLCD5598, SLCF0693, SLCF0694 and SLCF0695; and Foetal bovine serum (FBS) from (Sigma-Aldrich).

High-throughput screening reverse transcription quantitative PCR (HTS-RT-qPCR)

RNA extraction and reverse transcription

RNA was extracted and converted to cDNA using a 'High-Throughput Screening (HTS) optimised protocol' as previously described [356]. Briefly, RNA was isolated using a MagMAX™ *mirVana*™ Total RNA Isolation Kit (Applied Biosystems) and converted to cDNA with SuperScript™ IV First-Strand Synthesis System (ThermoFisher) following manufacturer's instructions, where all reagents were used at 25% of the volume recommended by the manufacturer, respectively; and the Superscript™ IV reverse transcriptase enzyme was used at 5 U/μL RNA.

Quantitative PCR (qPCR)

qPCR was conducted as previously described, using either absolute [356] or relative [400] quantification. Briefly, mRNA copies/reaction were determined with a standard curve, or fold-change expression were determined relative to the expression of the reference gene *RPL13a* for absolute and relative quantification, respectively. *IFN-γ*, *TNF-α, IL-2* and *RPL13a* specific desalt-grade (Sigma-Aldrich) primers (**Chapter 3: Supplementary Table S3.2**) obtained from PrimerBank™ [410] were used at 500 nM using ssoAdvanced™ Universal SYBR® Green Master-Mix (Bio-Rad). All reactions were run in technical triplicate in accordance with MIQE guidelines [400] at 5 μL total volume with 1 μL of reverse transcription eluent diluted 1:4 in Ultra-Pure™ H$_2$O (Invitrogen). Data was acquired using a QuantStudio5 Real-Time PCR system running QuantStudio Design and Analysis Software (v1.4.3, Applied Biosystems).

Protein analysis

IFN-γ enzyme-linked immunospot (ELIspot) assay

IFN-γ ELIspot assays were performed as previously described [356]. Briefly, 4×10^5 PBMCs were plated in triplicate into 96-well MAIPS45-10 plates (Merck) and stimulated for 24 hours with or without peptide, PMA/Iono or media.

Data analysis

ELIspot and RT-qPCR stimulation responses were analysed using either an ordinary one-way, or repeated-measures two-way or three-way ANOVA with Bonferroni-corrected multiple comparisons testing comparing test to non-stimulated control mean. The strength of the association between RT-qPCR *IFN-γ* mRNA absolute and relative gene expression was tested by Pearson's correlation on log-transformed data. *P* values and Pearson's correlation coefficient (ρ) were reported. GraphPad Prism version 8.3.0 (GraphPad Software) was used and *P* values <0.05 were considered statistically significant.

5.2.5 Results 1

Only two of eight individuals responded to 'cross-reactive' antigen peptide pool stimulation

To further characterise 'cross-reactive' T cell responses identified by previous members of the Doolan team [342] (*See: 1.3.3: Foundational Data*), we stimulated 4×10^5 PBMCs with pools of CD4$^+$ and CD8$^+$ T cell peptide epitopes predicted from antigens recognised by malaria-naïve individuals (*see section: 5.2.3 Foundational Data*), alongside a Cytomegalovirus, Epstein-Barr virus, and Influenza virus control peptide pool of 23 different peptides covering 11 HLA types (CEF), which is expected to elicit a response from approximately 80% of donors with at least one of these common HLA [529], and positive control individual peptides (NLV and FLR). When quantifying IFN-γ protein expression with ELIspot, we defined a positive response as >40 Spot Forming Cells per million Peripheral Blood Mononuclear Cells (SCF/10^6 PBMCs) above the media control. We found seven of the eight samples responded to the CEF and broad immunogenicity against NLV and FLR (**Fig. 5.1**); however, only two of eight individuals responded to any of the 'cross-reactive' antigen peptide pools (**Arrows, Donor 3 and 7; Fig 5.1**), where the highest SFC response was against the Antigen 707 peptide pool (707: 156.3 and 45.0 mean SFC/10^6 PBMCs; Donor 3 and Donor 5 respectively; **Arrow; Fig. 5.1**). These results were not consistent with data previously collected by members of the Doolan Laboratory, where the mean reactivity of individuals against 'cross-reactive' antigen peptide

pools was often >100 SFC/10^6 (unpublished) [342]. We therefore sought to optimise our assay to increase PBMC immunoreactivity.
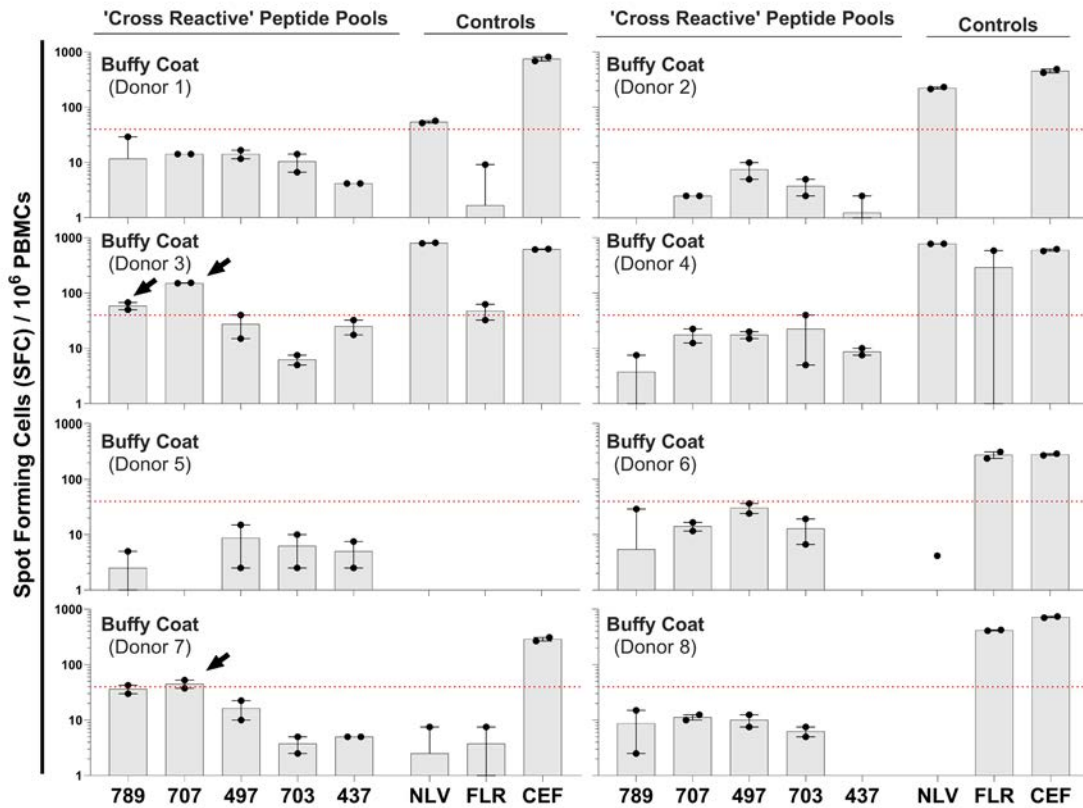
Figure 5.1. Initial screen for donors responsive to 'cross-reactive' peptide pools. 4×10^5 PBMCs were stimulated with pools of $CD4^+$ and $CD8^+$ T cell peptide epitopes predicted from antigens 789, 707, 497, 703, and 437 recognised by malaria-naïve individuals ('Cross-Reactive' Peptide Pools), alongside a Cytomegalovirus, Epstein-Barr virus, and Influenza virus control peptide pool (CEF) and single peptide (NLV and FLR) positive controls (Controls). Spot Forming cells SCF/10^6 PBMCs measured by IFN-γ ELIspot. A positive response was considered >40 SFC/10^6 (Red dotted line). Each point indicates a technical replicate stimulation. Data relative to media only background. Mean +/- SEM shown. **Arrow** indicates a positive response in the NS Peptide pools

Sera batch did not influence PBMC immunoreactivity

To optimise the assay to increase PBMC immunoreactivity, we first sought to investigate if the sera batch of the R10 media was influencing PBMC immunoreactivity. We stimulated 4×10^5 PBMCs with 'cross-reactive' antigen peptide pools, CEF and three single peptide controls (GIL, FLR and KGI) in R10 medias with various baches of human sera, which could influence immunogenicity [530]. Human sera baches tested were SLBN8825V, SLCD5598, SLCF0693,

SLCF0694 and SLCF0695, alongside Foetal bovine serum (FBS). When considering the immunoreactivity of each serum, a two-way ANOVA found stimulation, but not sera, significantly influenced immunogenicity ($P_{Stim} = 0.0038$, $P_{Sera} = 0.6974$; **Fig 5.2**). These data demonstrate PBMC immunoreactivity was not influenced by the R10 media serum. We chose to use Sera 3 for all subsequent studies (SLCD5598; Dashed box; **Fig. 5.2**).
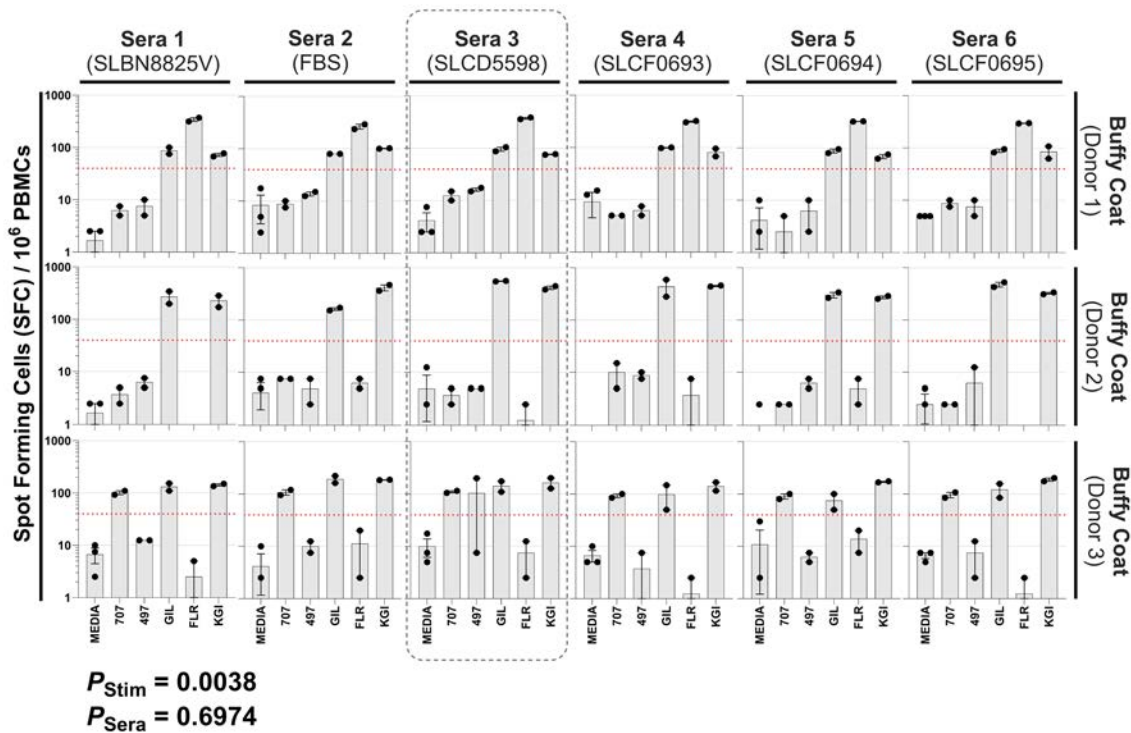
Figure 5.2. Screening sera to optimise the assay to increase PBMC immunoreactivity. $4x10^5$ PBMCs were stimulated with pools of CD4$^+$ and CD8$^+$ T cell peptide epitopes predicted from antigens 707 and 497, alongside single peptide (GIL, FLR and KGI) positive controls. Spot Forming cells SCF/10^6 PBMCs measured by IFN-γ ELIspot. A positive response was considered >40 SFC/10^6 (Red dotted line). Each point indicates a technical replicate stimulation. Data presented without background correction. Mean +/- SEM shown. Combined data were analysed with a repeated measures two-way ANOVA testing stimulation (Stim) and sera batch (Sera) with *P* values shown. **Dashed box** indicates sera that was selected for future experiments.

Resting PBMCs before stimulation and removing β-mercaptoethanol from the R10 media improved immunoreactivity

To investigate if post-thawing overnight resting (REST), or the use of β-mercaptoethanol (βME) in the R10 media influenced PBMC immunoreactivity, we stimulated $1x10^5$ PBMCs from Donor 3 with 707, and a range of CD8$^+$ (GIL, NLV, FLY, and FLR) and CD4$^+$ (KGI and

ARS) T cell restricted peptide epitopes, a pool of these peptides (HOME) and CEF. We evaluated IFN-γ mRNA expression with our HTS-RT-qPCR protocol, as we had limited remaining cells from Donor 3. When analysed with a three-way ANOVA stimulation, REST and βME were all found to have significantly influenced sample immunoreactivity ($P_{Stim} <$ 0.0001, $P_{REST} = 0.0038$ and $P_{βME} = 0.0211$; **Fig. 5.3**). These data were limited to a single n (Donor 3). Nevertheless, these data strongly suggest that consistent with best-practice for conduct of human T cell studies, including post-thawing overnight resting and excluding βME the R10 media increases PBMC immunoreactivity.
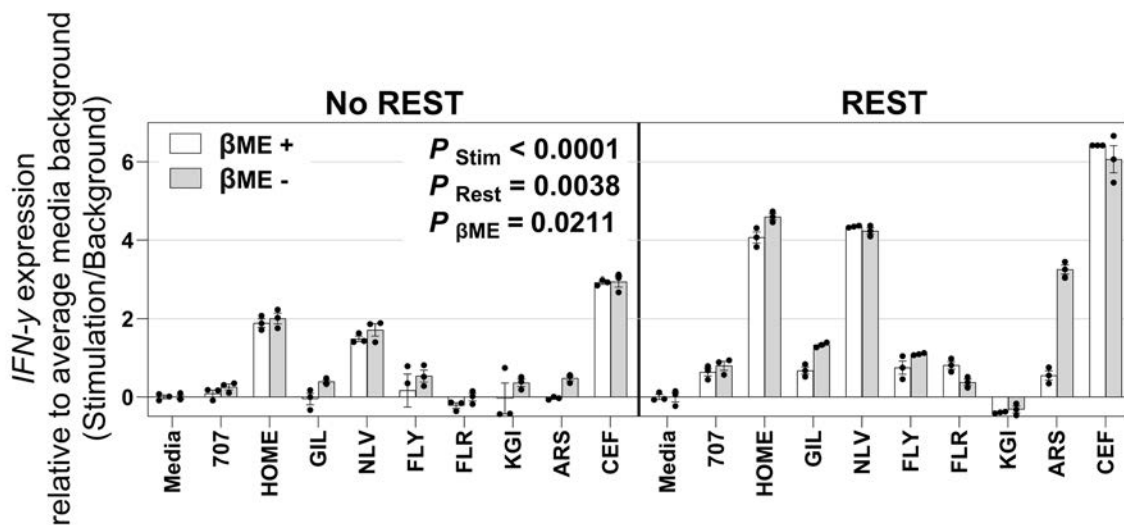
Figure 5.3. Resting 'Donor 3' PBMCs before stimulation and removing β-mercaptoethanol. $1x10^5$ PBMCs were stimulated with pools of $CD4^+$ and $CD8^+$ T cell peptide epitopes predicted from antigens 707, single peptides GIL, NLV, FLY, FLR, KGI, ARS, a pool of these 6 peptides (HOME) and CEF. IFN-γ mRNA expression relative to the media control was determined with HTS-RT-qPCR. Each point indicates a technical replicate stimulation. Mean +/- SEM shown. Combined data were analysed with a three-way ANOVA testing stimulation (Stim) resting PBMCs overnight (Rest) and including β-mercaptoethanol in the media (β ME) with *P* values shown. Media containing β ME (White Bars) or no β ME (Grey Bars) tested.

Freezing and thawing CD4+ or CD8+ peptides in RPMI does not influence immunoreactivity

Preparing antigenic peptide stimulation dilutions on the day of stimulation may be impractical, especially when conducting high throuput screens. Therefore, we next sought to identify if pre-stimulation peptide preparation influenced the immunoreactivity of stimulated PBMCs. To investigate if diluted working stocks of antigenic peptides lost immunoreactivity if stored

overnight in RPMI at -20°C (Storage), we stimulated either 4×10^5 or 1×10^5 PBMCs with fresh or frozen and thawed CD4$^+$ and CD8$^+$ peptides and assessed IFN-γ protein and mRNA production with ELIspot or HTS-RT-qPCR respectively. A two-way ANOVA found that stimulation significantly influenced immunogenicity (P_{Stim} = 0.0010 and 0.0062, RT-qPCR and ELIspot respectively; **Fig 5.4**); while storage of peptides overnight in RPMI at -20°C did not significantly influenced immunogenicity ($P_{Storage}$ = 0.9707 and 0.9158, RT-qPCR and ELIspot respectively; **Fig 5.4**). These data demonstrate that the immunoreactivity of CD4$^+$ or CD8$^+$ T cell epitope peptides is not influenced when the peptides are diluted in RPMI, frozen at -20°C, and thawed the morning of the stimulation.
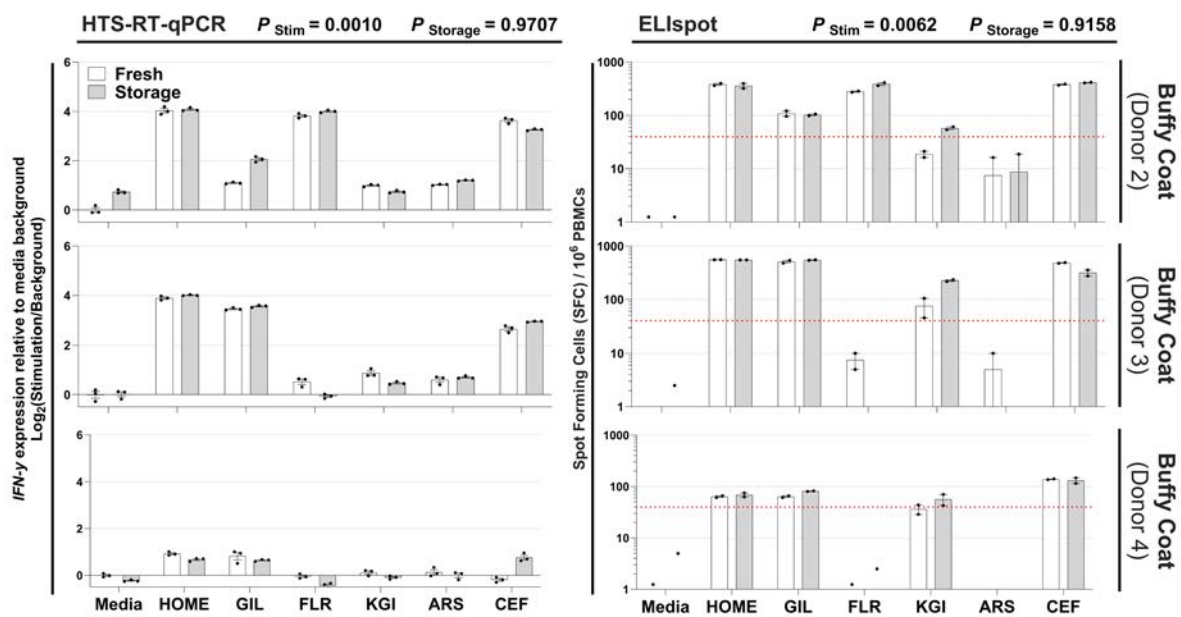
Figure 5.4. Optimisation of stimulation preparation. 4×10^5 or 1×10^5 PBMCs were stimulated with single peptides GIL, FLR, KGI and ARS, a pool of these 4 peptides (HOME) and CEF. IFN-γ mRNA expression relative to the media control was determined with HTS-RT-qPCR. Spot Forming cells SCF/10^6 PBMCs measured by IFN-γ ELIspot. Each point represents a technical replicate. Mean +/- SEM shown. HTS-RT-qPCR and ELIspot data were individually analysed with a repeated measures two-way ANOVA testing stimulation (Stim) and storage of peptides overnight at -20°C in RPMI (Storage) with *P* values shown. Peptides used immediately after mixing (White Bars) or peptides stored overnight at -20°C (Grey Bars) tested.

Peptide 12 is responsible for the immunoreactivity to Antigen 707 peptide pool observed following Donor 3 stimulation

We next sought to apply our optimised assay to perform a peptide deconvolution. We stimulated either 4×10^5 or 1×10^5 PBMCs from Donor 3 with 707, individual 707 antigenic peptides (1 to 20) and CEF for screening with ELIspot or HTS-RT-qPCR respectively. PBMC thawing and stimulation were performed with the HTS-optimised protocol inclusive of the immunoreactivity optimisation modifications (R10 media did not contain β-mercaptoethanol and used human sera batch: SLCD5598). The CEF was positive in HTS-RT-qPCR (7.147 Relative IFN-γ expression) and too many to count (TMTC) in ELIspot (>1000 SFC/10^6PBMCs) and was therefore omitted from statistical analysis. A one-way ANOVA found stimulation was statistically significant ($P < 0.0001$; both HTS-RT-qPCR and ELIspot; **Fig. 5.5**), and multiple comparisons testing relative to media control (Media) identified 707 and peptide 12 as statistically significantly reactive in ELIspot ($P < 0.0001$ both 707 and peptide 12; **Fig. 5.5**), and HTS-RT-qPCR ($P = 0.0107$ and $P = 0.0037$ for 707 and peptide 12 respectively; **Fig. 5.5**). All other stimulation conditions were not statistically significantly different to media. This experiment consumed the last of the PBMCs available from Donor 3, and therefore, this sample was unavailable for future experiments. Nonetheless, these data demonstrate the immunoreactivity optimised protocol can identify immunoreactive peptides following a peptide deconvolution stimulation experiment.
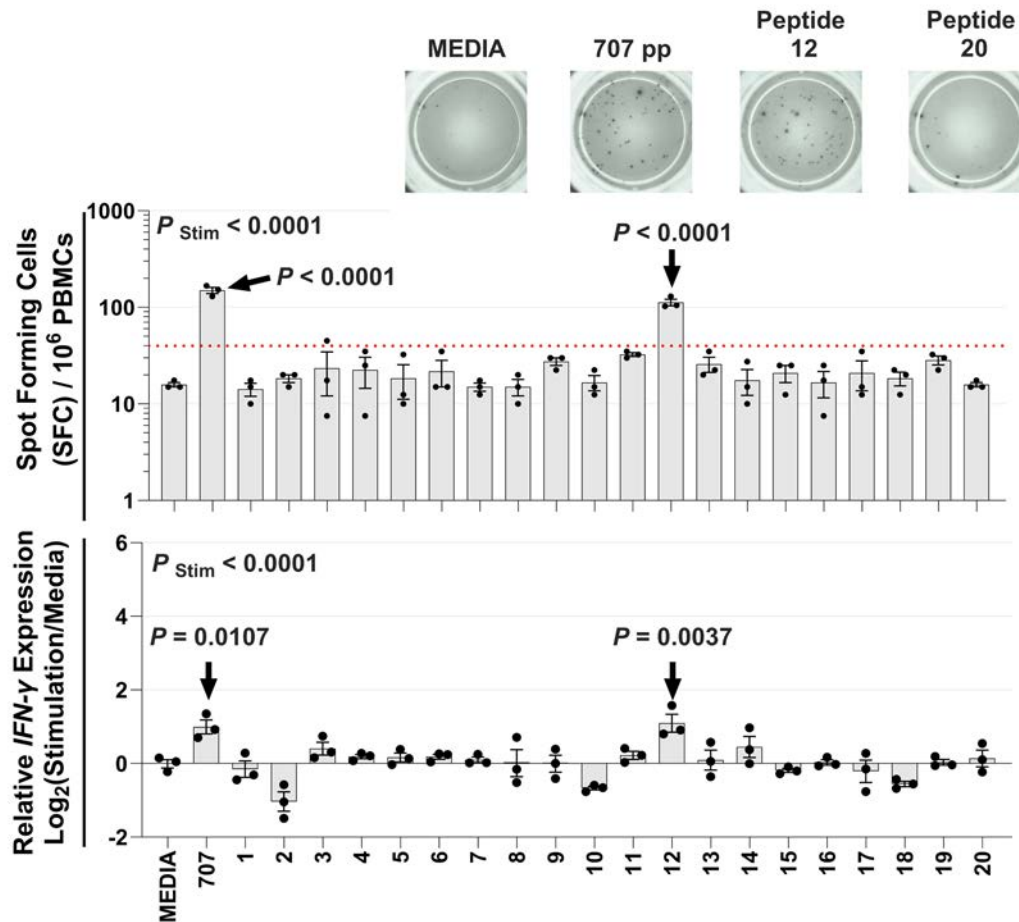
Figure 5.5. Peptide deconvolution of Donor 3's T cell response to Antigen 707. 4×10^5 or 1×10^5 PBMCs were stimulated with a pool of peptides predicted from antigen 707 (707) and single $CD4^+$ and $CD8^+$ T cell peptide epitopes (1 to 20). Spot Forming Cells $SCF/10^6$ PBMCs measured by IFN-γ ELIspot and IFN-γ mRNA expression relative to the media control was determined with HTS-RT-qPCR. Each point represents a technical replicate. Mean +/- SEM shown. HTS-RT-qPCR and ELIspot data were individually analysed with an ordinary one-way ANOVA testing stimulation (Stim), with Bonferroni corrected multiple comparisons compared to the media only control (Media). Statistically significant multiples comparisons (black arrows) and *P* values shown.

Limited donor immunoreactivity to the 'cross-reactive' antigens could be identified

We next sought to screen additional PBMCs to identify immunoreactive donors' responsive to the 'cross-reactive' antigens. We stimulated 4×10^5 PBMCs from eight additional malaria naive donors (Donors 9 to 16) with the 'cross-reactive' antigens 789, 707, 497, 703, and 437 and CEF and assessed IFN-γ protein production with ELIspot. One donor with high media background (108 SFC/10^6PBMCs; Donor 15) was omitted from analysis. A one-way ANOVA

found stimulation statistically significantly influenced IFN-γ protein production (P_{Stim} < 0.0001 ELIspot; **Fig. 5.6**). Multiple comparisons identified only CEF was statistically significantly different to background (P < 0.0001 ELIspot; **Fig. 5.6**). When considering >40 SFC/10^6PBMCs as positive (Dotted red line; **Fig 5.6**), one donor responded each to 789, 497 and 437 (61.25, 45.0, and 73.75 SFC/10^6PBMCs above background for Donor 13, Donor 12, and Donor 13 respectively; **Fig 5.6**). In parallel, we stimulated $1x10^5$ PBMCs of the eight additional donors with antigens 789, individual 789 antigenic peptides (1 to 20) and CEF for analysis of IFN-γ mRNA response to stimulation with HTS-RT-qPCR. The donor with high background identified by ELIspot was omitted from analysis. A one-way ANOVA found stimulation significantly influenced *IFN-γ* mRNA production (P_{Stim} < 0.0001 HTS-RT-qPCR; **Fig. 5.6**), while multiple comparisons identified the CEF as the only statistically significant stimulation (P < 0.0001 HTS-RT-qPCR; **Fig. 5.6**). When considering a threshold of positivity as responses greater than 2, as previously described [511], one donor responded to peptide 8 and 20 (2.16, and 2.14 Log_2 (Stimulation/Background) for Donor 14 and Donor 13 respectively; **Fig 5.6**). Given the expectation that 100% of donors would respond to 789 and 437, 90% to 497 and 703, and 50% to 707 (*see section: 5.2.3 Foundational Data*), these data establish we did not observe the expected immunoreactivity to the 'cross-reactive' antigens.
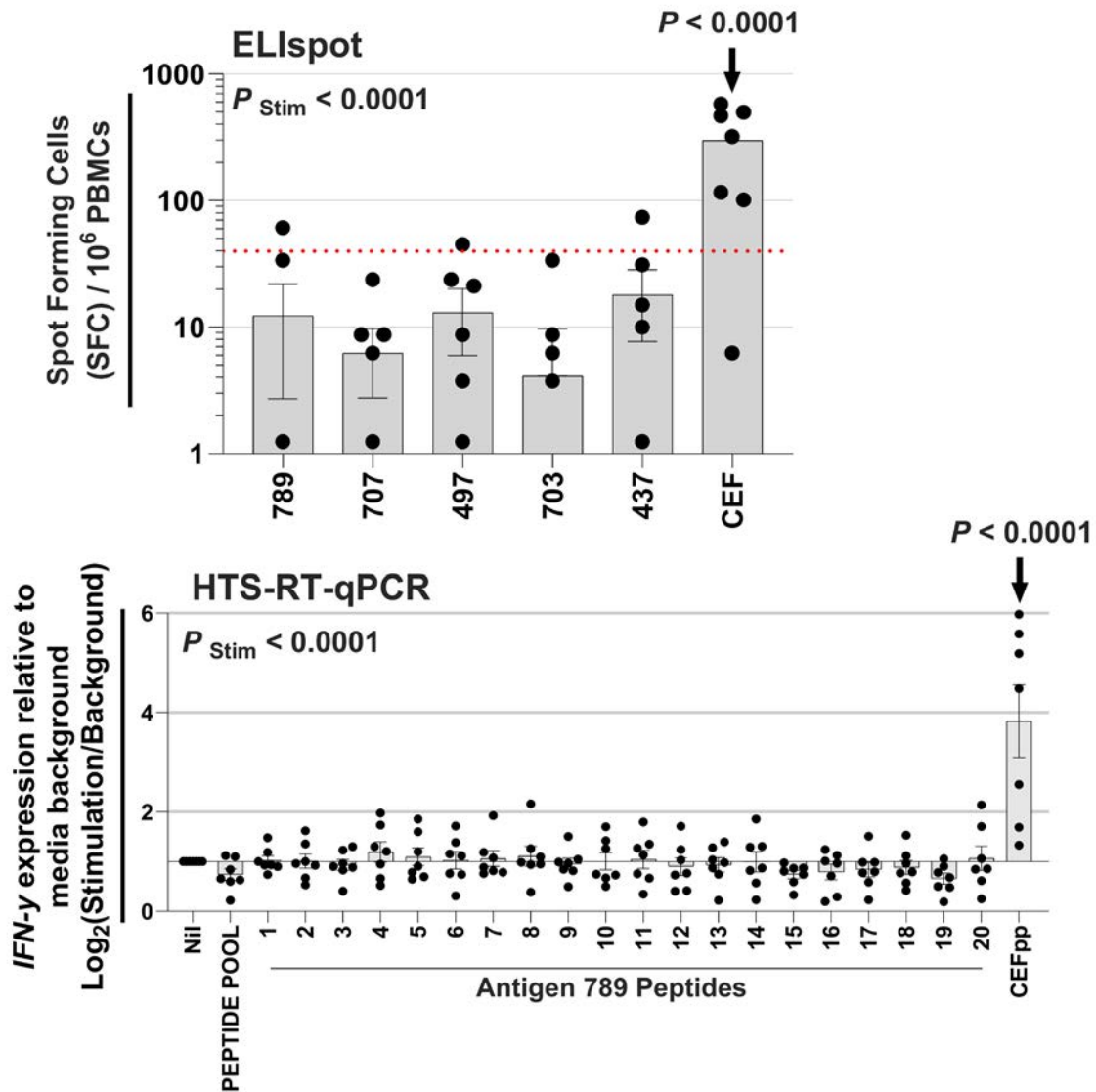
Figure 5.6. Screening to identify donors immunoreactive to the 'cross-reactive' antigens. 4×10^5 or 1×10^5 PBMCs were stimulated with pools and single CD4$^+$ and CD8$^+$ T cell peptide epitopes predicted from antigen 789, 707, 497, 703 and 437. Spot Forming cells SCF/10^6 PBMCs were measured by IFN-γ ELIspot and *IFN-γ* mRNA expression relative to the media control was determined with HTS-RT-qPCR. Each point represents a biological replicate (n=7) with mean +/- SEM shown. HTS-RT-qPCR and ELIspot data were individually analysed with an ordinary one-way ANOVA testing stimulation (Stim), with Bonferroni corrected multiple comparisons compared to the media only control (Media). Statistically significant multiples comparisons (black arrows) and *P* values shown.

Re-synthesis of 'cross-reactive' antigen peptides did not improve immunogenicity

We hypothesised that the peptides may have lost immunogenicity since the original synthesis, which was approximately 10 years prior. Therefore, the panel of 20 peptides which constitute the 'cross-reactive' antigens 789, 707, 497, 703, and 437 were commercially re-synthesised. We stimulated 4×10^5 PBMCs from the eight additional freshly acquired samples (Donors 9 to 16) with the freshly synthesised 'cross-reactive' antigen-peptide pools, and as positive controls: pooled CD4$^+$ SARS-CoV2 spike protein antigenic peptide pools (SARS-CoV2 Class II), and known immunoreactive individual peptides GIL and VTE, CEF, and PMA/Iono. While the vaccination status of the donors was unknown, given recent Australian vaccination rates, we expected approximately 80% to respond to the SARS-CoV2 peptides. When considering > 16 SFC/well above media as positive, (equivalent to >40 SFC/10^6 PBMCs), we found PMA/Iono was TMTC, and 8/8 (100%), 3/8 (37.5%), 4/8 (50%), and 4/8 (50%) of donors responded to CEF, VTE, GIL, and the SARS-CoV2 Class II peptides, respectively (**Fig. 5.8**). In contrast, 0/8 (0.0%) of donors responded to 'cross-reactive' antigen peptide pool stimulation, regardless of antigen (**Fig. 5.8**). These data demonstrate that peptide re-synthesis did not resolve the problem of unexpectedly poor immunogenicity of the 'cross-reactive' antigen peptide pools. Nonetheless, taken together, our data demonstrate that HTS-RT-qPCR is a robust tool to identify immunoreactive CD8$^+$ and CD4$^+$ T cell epitopes derived from the *Plasmodium falciparum* parasite.
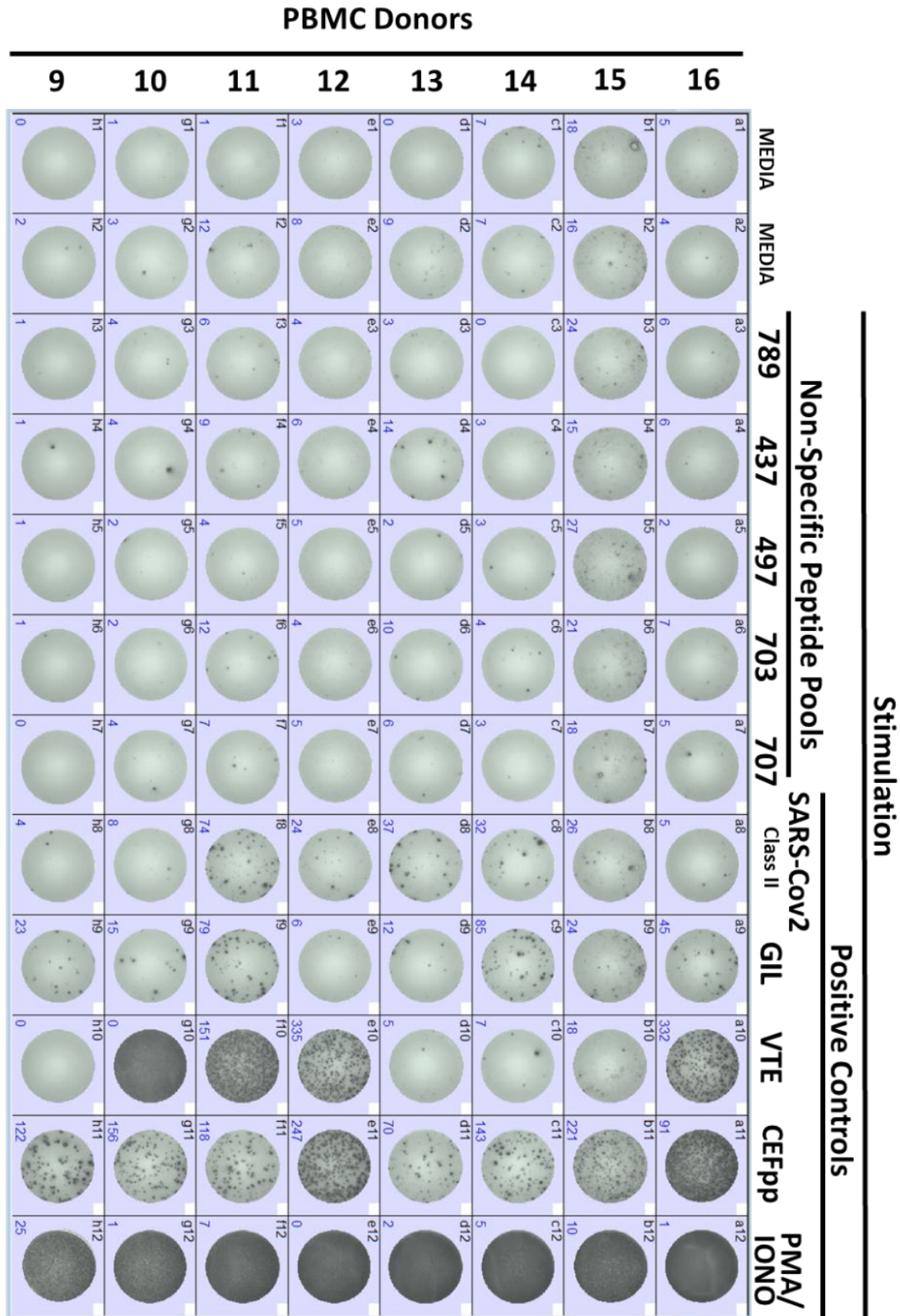
Figure 5.7. ELISpot screen with freshly synthesised 'cross-reactive' peptide pools. 4×10^5 PBMCs were stimulated with pools and single CD4$^+$ and CD8$^+$ T cell peptide epitopes predicted from antigen 789, 437, 497, 703, 707, SARS-CoV2 Spike protein (Class II) and CEF peptides; alongside GIL and VTE single peptide controls. Spot Forming cells SCF (Blue Numbers) measured by IFN-γ ELISpot.

5.2.6   Results 2

Malaria-experienced Malian PBMCs were heavily degraded

To identify immunoreactive liver-stage *P. falciparum* CD8$^+$ and CD4$^+$ T cell epitopes, we first sought to stimulate malaria-experienced Malian PBMCs with antigenic peptide pools representing CD4$^+$ and CD8$^+$ T cell epitopes predicted from the top immunoreactive antigens recognised by malaria-experienced individuals (**Figure 1.8**). The quantity and viability of the Malian PBMCs was, however, much lower than anticipated (**Fig. 5.9**), with between 0.4–2.8x10^6 viable PBMCs recovered per vial, from an anticipated 5-10x10^6 PBMCs/vial. Moreover, contaminating cell debris from the degraded cells was readily apparent.

(A)   **(B)**
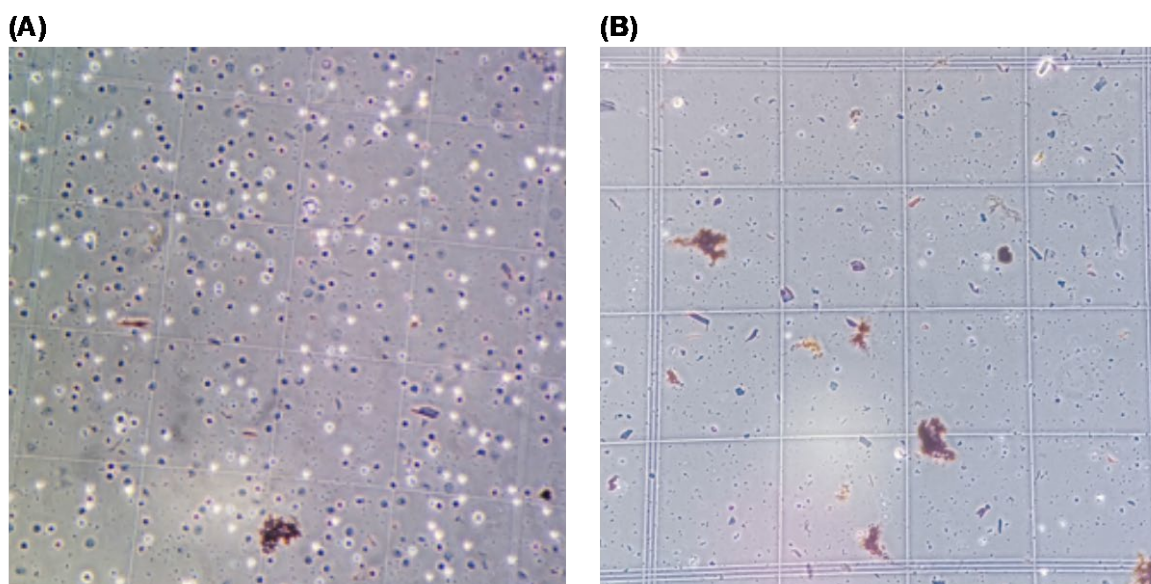
Figure 5.8. Low PBMC viability and abundance as visualised on a hemocytometer cell. PBMCs were diluted 1:2 with trypan blue for visualisation at a magnification of 40X. White spots are viable cells while blue dots are non-viable cells, viability was expected to be >95%. Two representative samples with either low viability **(A)**, or low cell number **(B)** shown.

Benzonase is suitable as a digestion nuclease to process heavily degraded PBMC samples

To maximise post-rest PBMC recovery from degraded Malian samples, we thawed and rested the cells using the highly optimised standard operating procedure reported by the *The International Maternal Pediatric Adolescent AIDS Clinical Trials* (IMPAACT) network [528]. IMPAACT uses Benzonase nuclease digestion, a density gradient isolation to remove dead cells and debris, and only 'rests when necessary'. There was no information available on

whether Benzonase would impact HTS-RT-qPCR signal, or whether the density gradient step would result in enhanced nonspecific background. To determine if Benzonase digestion and gradient isolation interfered with HTS-RT-qPCR, we stimulated $1x10^5$ PBMCs from a well-characterised malaria-naïve local donor with a range of $CD8^+$ T cell restricted peptide epitopes (VTE, ELR, FLR and RAK), a pool of these peptides (HOME), and CEF. A two-way ANOVA analysis identified both stimulation and nuclease can influence qPCR signal ($P_{Stim} < 0.0001$ and $P_{Nuclease} < 0.0001$; **Fig. 5.9**), which demonstrated that when considering the two nucleases tested, DNase was optimal for maximising qPCR signal. Nevertheless, when considering a threshold of positivity as responses greater than 2, as previously described, both DNase and Benzonase digestion identified the expected immunoreactive stimulants. These data demonstrate that despite a statistically significant loss of signal following Benzonase treatment, IFN-γ mRNA expression can be determined with our HTS-RT-qPCR protocol. Therefore, Benzonase is suitable as a digestion nuclease to process heavily degraded PBMC samples.
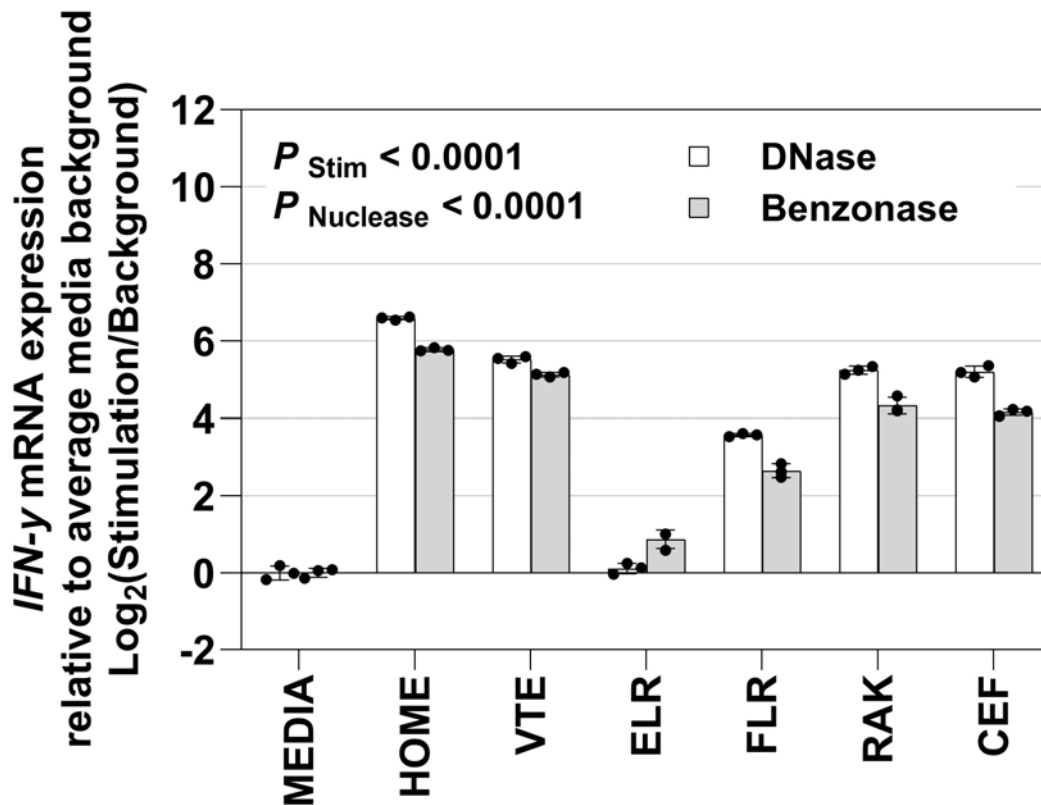
Figure 5.9. Benzonase endonuclease digestion influence on qPCR Signal. $1x10^5$ PBMCs from a well-characterised malaria naïve donor (n = 1) were stimulated with single peptides VTE, ELR, FLR, and RAK, a pool of these 4 peptides (HOME), and CEF. IFN-γ mRNA expression relative to the media control was determined with HTS-RT-qPCR. Three technical replicates per test, mean +/- SEM shown.

Data were analysed with a two-way ANOVA testing stimulation (Stim) and choice of nuclease (Nuclease) with *P* values shown. DNase (White Bars) or Benzonase (Grey Bars) tested.

ΔΔCT quantification is a suitable method to determine relative IFN-γ mRNA expression from antigenic peptide stimulated PBMCs

To address the high variability in cell number between samples, we tested if relative quantification (ΔΔCT) could be used to reliably quantify IFN-γ mRNA expression by HTS-RT-qPCR from PBMCs following antigenic peptide stimulation. The relative expression of IFN-γ to the stable reference gene 60S ribosomal protein L13a (*RPL13a*) [356] was quantified from PBMCs stimulated with a range of CD8$^+$ and CD4$^+$ T cell restricted peptide epitopes from a previous experiment (**Chapter 3: HTS Optimisation**). We found a strong statistically significant correlation between absolute and relative reference-gene based quantification strategies (*P* < 0.0001, ρ = 0.9424; **Fig. 5.10**). These data demonstrate that ΔΔCT quantification can be used to determine relative IFN-γ mRNA expression from antigenically stimulated PBMCs and may help reduce variability introduced from absolute quantification from PBMCs with low viability.
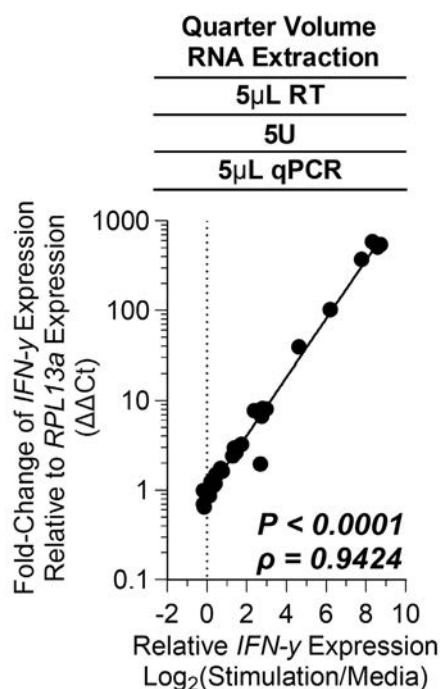
Figure 5.10. Relative correlated to absolute IFN-γ mRNA quantification. IFN-γ mRNA expression by HTS-RT-qPCR determined by absolute quantification correlated to the same data determined by relative quantification. Relative quantification was normalised to cell number while relative quantification was normalised to expression of RPL13a (ΔΔCt). 1x10^5 PBMCs were stimulated with

single peptides KGI, ARS, GIL and GLC, CEF and PMA/Iono. The strength of the association was tested by Pearson's correlation on log-transformed data, with *P* values and Pearson's correlation coefficient (ρ) reported.

No significant antigenic response was detected in Malian PBMCs stimulated with liver-stage P. falciparum *CD8+ and CD4+ T cell epitopes when measured with HTS-RT-qPCR*

Finally, we sought to determine if Malian PBMCs were immunogenically responsive to the top ten 'Highly immunoreactive antigens' identified in the foundational studies (**Table. 5.1**). Archived Malian PBMCs (24 Malian donors) were thawed and rested following the IMPAACT SOP, and $1x10^5$ PBMCs were stimulated with peptide pools, single peptides or CEF. *IFN-γ* mRNA expression was quantified following the HTS-RT-qPCR protocol with the exception that fold-change (ΔΔCT) quantification relative to *RPL13a* expression was used (**Fig 5.10**). Malian donor 5, 6, 8, and 17 did not respond to the PMA/Iono mitogen positive control and were therefore removed from analysis. When considering antigen peptide pool stimulation, a one-way ANOVA found that stimulation significantly influenced *IFN-γ* mRNA production (*P* Stim < 0.0209; **Fig. 5.11 A**). Multiple comparisons testing found that only CEF was significantly different to the media negative control (*P* < 0.0350; **Fig. 5.11 A**). Of the remaining 20 samples, when considering a threshold of positivity as IFN-γ mRNA expression increase greater than 2, two donors (10%) responded to stimulation with 853 and 101, and 1 donor (5%) responded to stimulation with 535, 638 and 606 antigen peptide pools (**Fig. 5.11 A**). Approximately one half (9 of 20) of donors responded to the CEF. These data demonstrate that these Malian samples had a lower response rate to the 100% response rate observed in the PNG donors (*see section: 5.2.3 Foundational Data*). However, with only half of donors responding to CEF, these data suggest that these PBMCs were not optimally immunoreactive.

When considering single peptide stimulations, each antigen peptide deconvolution was tested with a one-way ANOVA without considering the CEF control. Stimulation did not influence *IFN-γ* mRNA production across any antigen peptide deconvolution (*P* Stim = 0.5835, 0.7887, 0.7571, 0.5692, 0.6077, 0.2210, 0.4078, 0.9853, 0.3252, and 0.3221 Antigens 853, 1068, 307, 535, 533, 638, 101, 606, 610, and 76 respectively; **Fig. 5.11 B**). When considering a mRNA expression increase greater than 2 as responsive, at least one donor responded to a peptide in each antigen peptide pool. The most immunogenicity was detected in Antigen 1068, with 11 of 20 peptides having at least one responsive donor. The least responsive were Antigen 638, 610, and 76 which only one donor responded to one peptide (**Fig. 5.11 B**). This immunogenicity

was far lower than the previously reported 100% response rate to observed in the PNG donors (*see section: 5.2.3 Foundational Data*). These data demonstrate that we were unable to detect significant IFN-γ mRNA responses from Malian PBMCs to liver-stage *Plasmodium falciparum* CD8^{+} and CD4^{+} T cell epitopes recognised by Papua New Guineans.
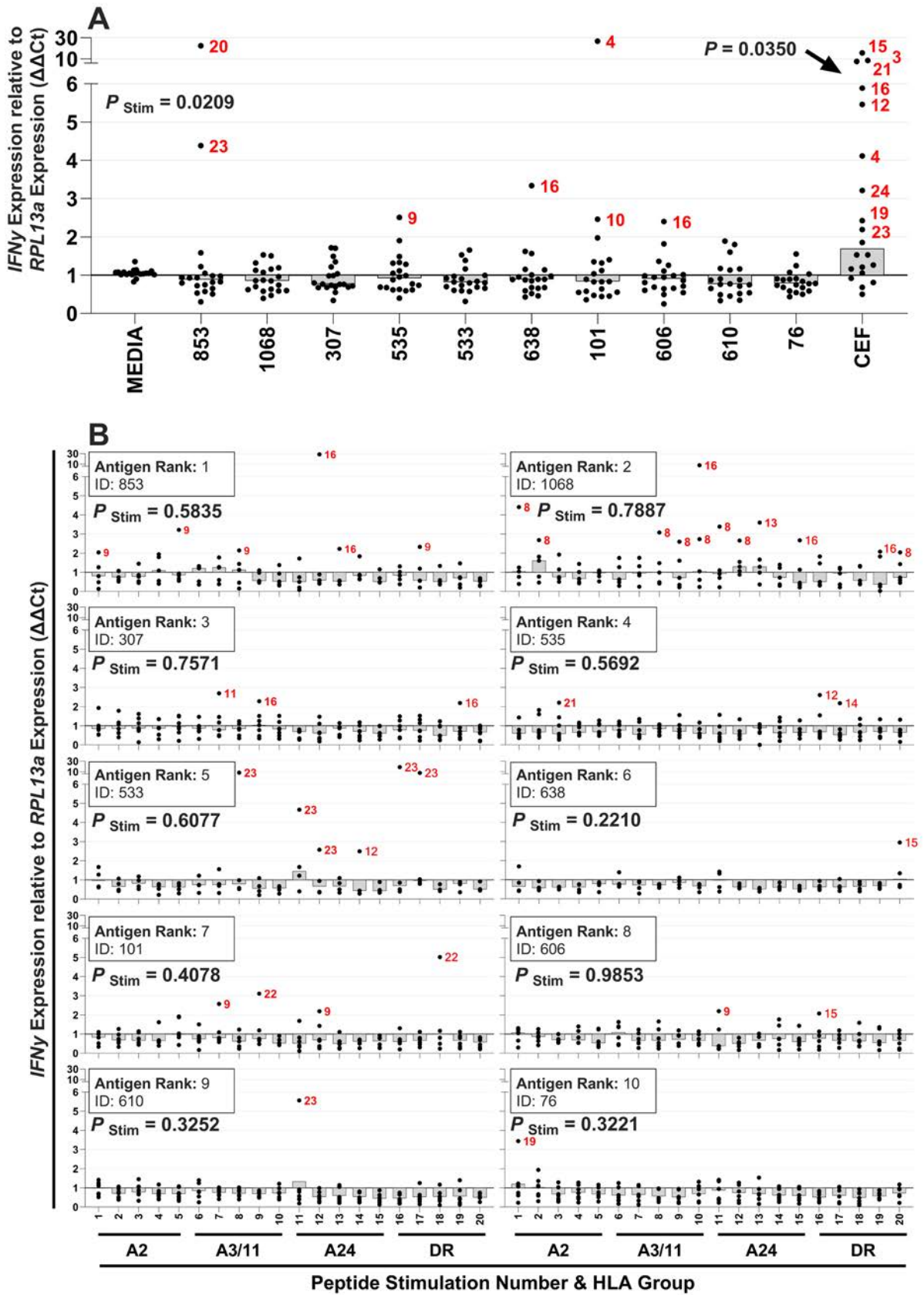
Figure 5.11. Antigenic response of Malian PBMCs stimulated with liver-stage *P. falciparum* CD8^{+}

and CD4^{+} T cell epitopes measured with HTS-RT-qPCR . 1x10^{5} PBMCs were stimulated with (**A**)

pools or (**B**) single CD4$^+$ and CD8$^+$ T cell peptide epitopes predicted from the top ten immunoreactive antigens. IFN-γ mRNA expression normalised to expression of RPL13a (ΔΔCt). was determined with HTS-RT-qPCR. Spot Forming cells SCF/10^6 PBMCs measured by IFN-γ ELIspot. Each point represents a biological replicate (n=20) with median shown. Donor number shown (Red numbers) next to data when IFN-γ mRNA expression increase greater than 2. Data were analysed with an one-way ANOVA testing stimulation (Stim). Statistically significant multiples comparisons (black arrows) and *P* values shown.

No significant antigenic response was detected in Malian PBMCs stimulated with liver-stage P. falciparum *CD8$^+$ and CD4$^+$ T cell epitopes when measured with ELIspot*

We sought to validate the Malian response to stimulation with gold-standard IFN-γ ELIspot. Additionally, the above stimulatory experiments were conducted with peptides synthesised in 2022; and therefore, we sought to test if there were differences between the immunogenicity of the peptides originally synthesised by the Doolan group in 2009. Malian PBMCs were thawed, rested, and stimulated as above and IFN-γ protein production was measured with ELIspot. When considering >40 SFC/10^6 as positive, four of five (80%) of the Malian samples responded to CEF stimulation, while none responded to antigen peptide pool stimulation (**Fig. 5.12**). These data demonstrate the Malian PBMCs did not respond to the antigens synthesised in 2009 as PNG PBMCs had previously. Similarly, the Malian PBMCs did not respond to the antigens resynthesized in 2022. Taken together, Result 2 data demonstrate that the Malian PBMCs had low viability, and subsequently, did not respond to antigen peptide pool stimulation. It is likely that the poor viability of the Malian PBMCs available for testing contributed to this outcome.
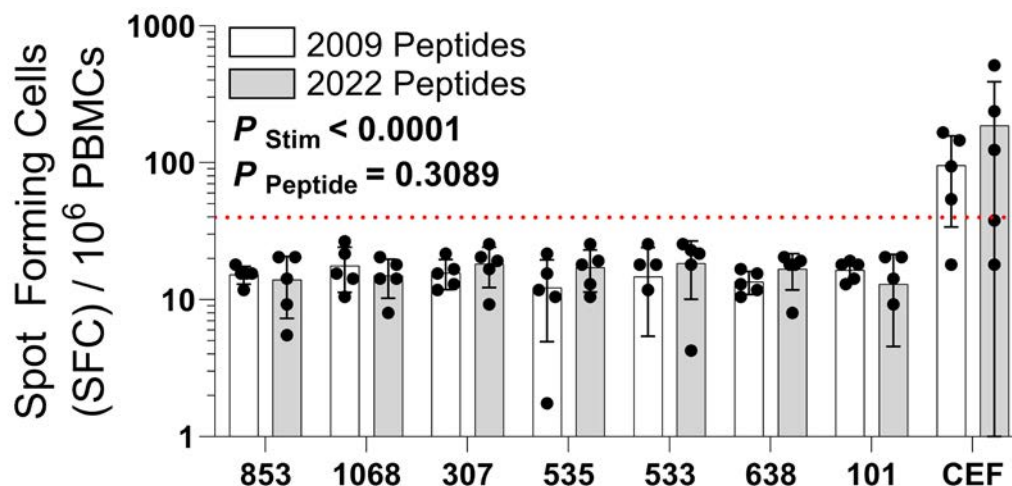
Figure 5.12. Antigenic response of Malian PBMCs stimulated with liver-stage *P. falciparum* CD8⁺ and CD4⁺ T cell epitopes antigen peptide pools measured with ELIspot. 4×10^5 PBMCs FROM Malian donors were stimulated with pools of freshly synthesised (2022 Peptides) and original synthesis (2009 Peptides) peptide pools from antigen 853, 1068, 307, 535, 533, 638, 101, and CEF peptides; Spot Forming cells (SCF) measured by IFN-γ ELIspot. Data were analysed with a two-way ANOVA testing stimulations (Stim) and the 2022 Peptides (Grey Bars) and 2009 peptides (White Bars) synthesis (Peptide) with *P* values shown.

5.2.7   Discussion

In this study, we sought to assess the ability of peptide epitope from liver-stage *Plasmodium falciparum* antigens which had previously been identified as highly immunoreactive in Papua New Guinean (PNG) donors to induce a T-cell response in Malian PBMCs (unpublished data; data in confidence). Additionally, we sought to investigate the immune response of individuals who have not been previously exposed to malaria but have T cells that can react to several of these immunoreactive antigens (unpublished data; data in confidence). Due to the limited availability of malaria-experienced donor samples [527], we used a combination of gold-standard IFN-γ ELIspot [351], and our optimized high-throughput real-time quantitative PCR (HTS-RT-qPCR) protocol which allows detection of antigenic responses from very low numbers of cells [511].

In the first half of this study, we identified several donors who were relatively weakly immunoreactive to stimulation with the 'cross-reactive' antigen peptide pools; which was significantly less immunoreactivity that expected [342]. Therefore, several strategies were investigated to increase the immunogenicity of antigenic and mitogenic stimulations. We found resting PBMCs before stimulation and removing β-mercaptoethanol from the R10 media

improved PBMC immunoreactivity. Despite this optimisation, we were unable to identify any other malaria-naïve donors who were immunoreactive to the 'cross-reactive' antigens.

In the second half of the study, we focused on assessing the response of malaria-experienced Malian PBMCs to stimulation with liver-stage *P. falciparum* CD8+ and CD4+ T cell epitopes previously identified as immunoreactive in PNG donors. We found the Malian PBMCs were heavily degraded, which resulted in the use of the IMPAACT thawing protocol which included Benzonase thawing and ΔΔCT quantification to reduce technical variability. However, despite this, no significant antigenic response was detected in the Malian PBMCs stimulated with liver-stage *P. falciparum* CD8+ and CD4+ T cell epitopes. These data suggest that PBMCs from Malian adults do not respond to antigens recognised by PNG adults. However, the poor viability of the Malian PBMC is likely to have contributed to the subsequent poor peptide immunogenicity. Any number of technical issues encountered during the collection, cryopreservation and storage of the samples may have contributed to this outcome [530]. Since we were unable to acquire fresh sources of PBMC samples due to the COVID-19 pandemic [527], no side-by side comparison could be performed to rule out these potential confounders. Further studies with freshly acquired non-degraded parallel peripheral blood mononuclear cells (PBMCs) from Malian and PNG donors will be required to draw further conclusions from this study.

It has been hypothesised that the 'cross-reactive' *P. falciparum* antigens which were previously identified as immunoreactive in malaria-naïve individuals may constitute evidence of a *Plasmodium* spp. immune evasion strategy [342]. The affinity between TCRs and MHC-peptides is degenerate [531], allowing a single TCR to recognize multiple epitopes and a single epitope to be recognized by various TCRs. Cross-reactive antigens may contain epitopes that are immunogenic for T cells previously activated by epitopes from other endemic human pathogens. *Plasmodium* spp. proteome contains antigens which can influence the human immune response favourably for the parasite [98, 532, 533]. It is possible the 'cross-reactive' antigens represent immunoreactive proteins designed to direct the host immune response away from otherwise immunodominant antigens that may confer host protection. *P. falciparum* has been co-evolving with humans for at least 10,000 years [48], while other *Plasmodium* spp. have been co-evolving with human ancestors for millions of years [52]. This long co-evolutionary history has facilitated the development of extremely complex immune evasion mechanisms in *Plasmodium* spp., such as antigenic variation [534], and immune-suppression and manipulation [535]. However, the complex host-parasite interactions which lead to these immune evasion

outcomes are not fully understood. It is possible we were unable to identify reactivity to the 'cross-reactive' antigens due to an unknown host interaction or condition implicit of the donors used in this study.

Unknown or unappreciated human variation may also explain why Malian donors did not respond to the antigens identified as highly immunoreactive when stimulating PNG donors. The Immune Epitope Database (IEDB; www.iedb.org) is an effective predictor of T cell epitope immunodominance based on a peptides binding affinity to variable MHC alleles [536]. However, there are many other factors which influence epitope immunodominance and the possibility of the establishment of a population of responsive T cells against any specific epitope [334, 537, 538]. Antigen intrinsic qualities such as abundance and peptide-MHC processing capacity can significantly influence immunodominant epitope choice in a complex process that remains incompletely understood [341]. Host-intrinsic qualities such as genetics, prior exposure to other antigens, and T-cell repertoire can also influence immunodominant antigens, and subtle variations can lead to great differences between dominant and subdominant epitopes between populations irrespective of the affinity of a MHC-peptide binding complex and the prevalence of MHC alleles in a population [330-332].

Unknown or unappreciated technical variation may explain the reduced immunogenicity from the 'cross-reactive' antigens or the lack of response from Malian PBMCs. Assays stimulating PBMCs with antigenic and mitogenic stimulants are common in immunology research, and significant efforts have been undertaken to standardise inter-laboratory practise to reduce immunoreactivity variation [351, 383, 384]. Despite these efforts, PBMC immunoreactivity can vary significantly due to cell viability and purity which is influenced by PBMC collection, cryopreservation, thawing, and stimulation [440, 530]. In this study, we observed a significant loss of viability in Malian PBMCs, even when using the IMPAACT thaw procedure. Following Benzonase and density gradient thawing, and overnight resting, only one-third of the Malian PBMCs responded to the CEF peptide pool control. It is possible that Malian PBMCs with higher viability would have responded to peptide stimulation. We believe that the loss of viability in our Malian PBMCs may be due to long-term cryopreservation.

Without conducting a direct comparison of the immunogenicity of the antigen peptide pools between PNG and Malian PBMCs, drawing significant conclusions is challenging. However, if the immunodominant *P. falciparum* antigens recognized by donors from PNG and Mali differ significantly, this would have significant implications for developing an efficacious liver-stage

malaria vaccine [539, 540]. Our work suggests that the peptide epitopes recognized by PNG donors differ fundamentally from those recognized by Malian donors. Thus, this work implies that vaccines designed to induce host T-cell responses to liver-stage antigens may need to be customized to specific populations or *P. falciparum* strains [541]. Screening freshly sourced Malian PBMCs with the 1,500 antigen peptide pools may identify if alternative antigens are immunodominant in this population. Notably, it remains possible that the antigens remain immunodominant between Malian and PNG donors, and it is the epitopes that differ between populations. To investigate this possibility further, PBMCs from globally sourced populations should be evaluated in parallel. Antigen-wide epitope mapping from leading immunodominant antigens should be investigated across populations as has recently been performed against the SARS-CoV2 virus [125]. Ideally, these studies would be linked with human leukocyte antigen (HLA) genotyping and T-cell receptor (TCR) repertoire data [542]. Such a large-scale screening study is now feasible using the HTS-RT-qPCR protocol developed and utilised within this study [511], which allows high-throughput screening of thousands of antigen stimulations. Combined with gold-standard IFN-γ ELIspot validation, this methodology represents an exciting tool to identify population-specific immunoreactive liver-stage antigens and their corresponding T-cell epitopes.

In summary, we investigated several *P. falciparum* liver-stage antigens previously identified as highly immunoreactive in PNG donors or cross-reactive with malaria-naïve donors. Our findings revealed limited immunoreactivity to the cross-reactive antigens in malaria-naïve individuals, as only one individual responded, which is much lower response rate than previously reported [342]. Additionally, we observed limited antigenic responses in malaria-exposed Malian PBMCs stimulated with liver-stage antigen T cell epitopes which were previously found to be highly immunoreactive in PNG donors. These results suggest that Malians may not exhibit immunoreactivity to the same liver-stage *P. falciparum* T cell epitopes as PNG donors, but we could not rule our technical concerns. Further studies using fresh samples from Malian and PNG donors are necessary to resolve those concerns.

Overall, data presented in this chapter study established that the HTS-RT-qPCR protocol, especially when validated with gold-standard IFN-γ ELIspot, enables large studies with limited sample to be conducted and has great potential for identifying immunoreactive antigens and their corresponding T cell epitopes. This approach could facilitate the identification of optimal target antigens for malaria vaccines by providing crucial insights into the most optimal liver-stage antigens that stimulate protective immune responses against the *Plasmodium* parasite.

Chapter 6: Differential Reactivity of SARS-CoV2 S-Protein T-cell Epitopes in Vaccinated versus Naturally Infected Individuals

6.1 Chapter introduction

With the declaration of COVID-19 as a pandemic on 31st December 2019, we seized the opportunity to apply our optimised sensitive and specific HTS-RT-qPCR assay to provide further insights into this pathogen. In collaboration with Prof. Corey Smith from the QIMR Berghofer Medical Research Institute (QIMRB), we obtained matched PBMCs from donors collected before the COVID-19 pandemic, following COVID vaccination, and after a subsequent infection with the SARS-CoV2 virus. Our goal was to employ our HTS-RT-qPCR assay to identify immunoreactive peptide epitopes from the Spike-protein (S-protein), the SARS-CoV2 antigen on which most COVID-19 vaccines were based. We sought to simultaneously study the magnitude, and kinetics of T cell reactivity to a large number of T cell peptide epitopes in pre-vaccinated, post-vaccinated, and post-SARS-Cov2 infected individuals.

I hypothesized that infection would enhance the immunoreactivity of peptide epitopes that were immunoreactive following vaccination.

To test this, we addressed the following experimental aims:

1. Identify a putative list of immunodominant peptide epitopes from the S-protein.

2. Determine the immunoreactivity of these peptide epitopes in pre-vaccination, post-vaccination, and post infected individuals.

6.2 Draft Manuscript

Differential reactivity of SARS-CoV2 S-protein T-cell epitopes in vaccinated versus naturally infected individuals

Running head: SARS-CoV2 T cell epitope reactivity

Daniel J. Browne[1], Pauline Crooks[2], Catherine M. Miller[3], Corey Smith[2,4], and Denise L. Doolan[1,5*]

[1] Centre for Molecular Therapeutics, Australian Institute of Tropical Health and Medicine, James Cook University, Cairns, QLD 4878, Australia

[2] QIMR Berghofer Centre for Immunotherapy and Vaccine Development and Translational and Human Immunology Laboratory, Department of Immunology, QIMR Berghofer Medical Research Institute, Brisbane, QLD 4006, Australia.

[3] College of Medicine and Dentistry, James Cook University, Cairns, QLD 4878, Australia

[4] Faculty of Medicine, The University of Queensland, Brisbane, QLD 4067, Australia.

[5] Institute for Molecular Bioscience, The University of Queensland, St Lucia, QLD 4067, Australia

6.2.1 Graphic abstract
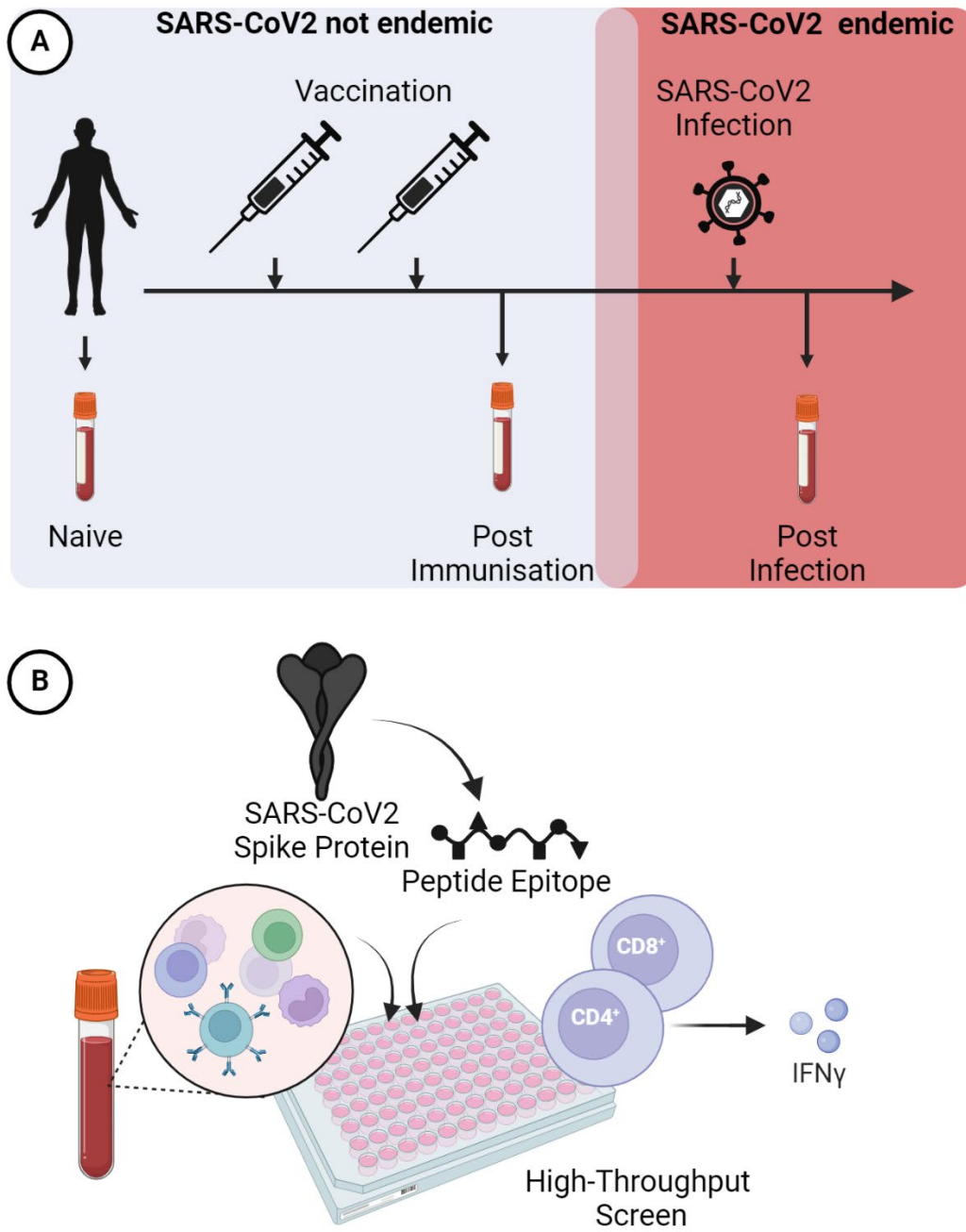
6.2.2 Abstract

Vaccine-induced protective immunity against SARS-CoV2 has proved difficult to sustain. Robust T cell responses are thought to play an important role but T cell responses against the SARS-CoV2 Spike-protein (S-protein), the core vaccine antigen, following vaccination or natural infection are incompletely understood. Herein, the reactivity of 170 putative SARS-CoV2 S-protein CD8^{+} and CD4^{+} T-cell peptide epitopes in individuals pre- or post-COVID19 vaccination and following subsequent natural infection were assayed using a high-throughput reverse transcription-quantitative PCR (HTS-RT-qPCR) assay. The profile of immunoreactive SARS-CoV2 S-protein epitopes differed between vaccination and natural infection. Vaccine-induced immunoreactive epitopes were localized primarily into two extra-domanial regions. In contrast, epitopes recognised following natural infection were spread across the antigen. Furthermore, T cell epitopes in naïve individuals were primarily recognised in association with HLA-A, while natural infection shifted epitope associations towards HLA-B, particularly the B7 supertype. This study provides insight into T cell responses against the SARS-CoV2 S-protein following vaccination and subsequent natural infection.

6.2.3 Introduction

The SARS-CoV2 coronavirus, the causative agent of COVID-19 [543], is now endemic throughout the world, despite the rapid development of effective vaccines that induce robust immunity against the virus [544]. While vaccination against SARS-CoV2 has substantially reduced the mortality and morbidity associated with COVID-19 [545-547], the effectiveness of the available vaccines decreases relatively rapidly [548, 549], and multiple novel viral variants have emerged that can evade vaccine-induced protection [124]. By 2023, individuals who received the original wild-type COVID-19 vaccines were found to have minimal protection against severe disease requiring hospital admission [550]. This waning immunity contrasts with the sustained protection provided by many vaccines included in global adolescent immunization schedules, such as measles, mumps, rubella, and hepatitis B [27, 28]. Following convalescence from exposure to SARS-CoV2, natural immunity provides robust protection against reinfection and COVID-19-related hospitalisation, with this protection remaining relatively high over a longer period than vaccination [126, 551-553]. Indeed, hybrid immunity, resulting from vaccination followed by subsequent natural infection, appears to provide the highest level of protection [553].

Many COVID-19 vaccines, including the Pfizer-BioNTech mRNA vaccine (BNT162b2) and the Moderna mRNA vaccine (mRNA-1273), were intended to induce high levels of neutralizing antibodies [554]. Conversely, the AstraZeneca vaccine (ChAdOx1 nCoV-19) was designed to induce a balanced immune response that includes activated T -cells responses in addition to antibody responses [555, 556]. Both vaccine strategies proved effective at inducing robust antibody and T cell responses, but vaccine-induced efficacy decreased relatively quickly for both [557]. Promoting robust cellular immunity and cellular immune memory, particularly T cell-mediated immunity, is expected to enhance the development of long-term protection and maintain protection against novel viral variants [327, 558, 559]. Broadly, CD8$^+$ T cells can eliminate virally infected host cells [560], while T helper CD4$^+$ T cells play a multipurpose role, including assisting in the production of high affinity neutralizing antibodies, or promoting immune activation, regulation, and memory formation [561]. However, the specificity, magnitude, and kinetics of T cell reactivity to SARS-CoV2 in relation to vaccination or natural infection are incompletely understood.

The magnitude of T cell responses has been associated with the effectiveness of host immunity to SARS-CoV-2 infection [562]. Perturbations to T cell populations and circulating numbers [563] and a decline in naïve T cell number and diversity [564] have been all associated with poor COVID-19 clinical outcomes. Several HLA alleles have been identified as beneficial for immunity to SARS-CoV2 [553, 565], while others have been found to be detrimental [566-568] to patient outcomes. Immunodominance is the 'choice of the immune system' to develop immunity to any specific antigen or epitope [569], and only a fraction of potential peptide epitopes induce measurable cellular immunity [570]. The tripartite interaction of expressed HLA alleles, antigen and peptide epitope chemistry, and the repertoire of available naïve T cells is the dominant paradigm which is believed to determine epitope immunodominance [571]. Understanding T cell immunodominance during a SARS-CoV-2 infection following vaccination and subsequent natural infection may provide insight to develop more efficacious vaccines.

Currently, all licenced COVID-19 vaccines are based on the SARS-CoV2 Spike-Protein (S-Protein) antigen. The S-protein is a large homotrimer transmembrane glycoprotein that facilitates SARS-CoV2 entry by binding to the human AE2 receptor. Each trimer consists of between 1273-1300 amino acids, depending on the viral variant [572], which allows for a large number of potential T cell epitopes and abundant T cell peptide epitope HLA presentation [573]. Various studies have explored S-protein epitope immunodominance or reactivity

following vaccination [574-576], and in infected or convalescent patients [125, 568, 577-581]. However, relatively few have assessed epitope reactivity in the same individuals across these timepoints [582]. Pre-existing T cell immunity to SARS-CoV-2 in COVID-19 naïve individuals is another notable phenomenon observed during the COVID-19 pandemic [578, 583], pre-existing presumably from exposure to other endemic coronaviruses [584]. Further developing an understanding of which SARS-CoV2 S-protein T cell epitopes are immunodominant in pre-existing immunity, following vaccination, and following an infection may provide critical insight for future vaccine design.

The identification of immunodominant T cell epitopes within the SARS-CoV2 S-protein involves analysis of peptide-stimulation reactivity by human peripheral blood mononuclear cells (PBMCs), quantified by measuring markers of activation such as the secretion of interferon-gamma (IFN-γ) [585]. T cell epitopes can be identified by screening large panels of overlapping peptides representing the complete protein or a more focused panel of putative peptide epitopes predicted using software such as the T cell epitope NetMHCpan HLA-Peptide binding prediction tool [586] within the Immune Epitope Database (IEDB) [349]. In this study, 170 CD8$^+$ and CD4$^+$ T cell peptide epitopes were identified from the SARS-CoV2 S-protein, based on prediction to bind with high affinity to a range of class I and class II HLA alleles using the IEDB NetMHCpan algorithm. Thousands of peptides were identified, overall, and were subsequently prioritised by reported immunogenicity [125, 558, 578, 583, 587, 588] (as well as HLA-peptide binding affinity) to define a subset of putative T cell epitopes for study.

Peptide epitopes are typically screened for immunoreactivity with conventional assays including IFN-γ ELISpot, intracellular cytokine staining (ICS), or activation-induced marker (AIM) assay [356, 383, 589]. These assays typically require high number of PBMCs, especially when screening the large number of potential peptide epitopes available within the SARS-CoV2 S-protein. To address this limitation, we developed a sensitive and specific high-throughput screening reverse transcription-quantitative PCR (HTS-RT-qPCR) assay to screen large panels of putative T cell epitope peptides from low numbers of PBMCs [511]. Herein, we applied this assay to identify immunoreactive T cell epitopes from SARS-CoV2 recognised by humans naïve to SARS-CoV2 (pre-existing immunity, cross-reactive to other viruses), following COVID vaccination, and following SARS-CoV2 infection. We used our HTS-RT-qPCR assay to evaluate the immunoreactivity of these peptide epitopes in donors either naïve to the S-protein, vaccinated with the S-protein, or following a subsequent natural infection. Where available, matched PBMCs collected from donors pre-exposure, post-vaccination, and

post-infection were tested. This study contributes to the understanding of vaccine epitope immunodominance and kinetics, while highlighting the utility of HTS-RT-qPCR for peptide epitope immunoreactivity testing.

6.2.4 Methods

Peptides

CD8^{+} epitope prediction and selection

Over 7,500 CD8^{+} T cell peptide epitope-HLA allele combinations with a HLA-binding score >0.2 were predicted from the S protein of Wuhan reference strain of SARS-CoV2 (GenBank: YP_009724390.1) using the Immune Epitope Database (IEDB) NetMHCpan EL 4.1 algorithm [586] (**Supp Fig. S6.1**). A prioritised list of 145 peptides was defined by sorting epitopes into affinity of binding to HLA-A2, -A3/11, -A24, -B7, and -B8 Class I supertypes, ordering by the sum of the response as reported from Tarke *et al*, 2021 [125] and, subsequently, the IEDB predicted binding score (**Supp Table S6.1**). Other peptides reported in the literature to be immunoreactive were also included [558, 578, 587] (**Supp Table S6.1**).

CD4^{+} epitope selection

Twenty-five CD4^{+} T cell S protein peptide epitopes reported as immunogenic following exposure to SARS-CoV-2 were selected from the literature [125, 583, 588] (**Supp Table S6.1**).

In silico predicted CD8^{+} peptide epitope cross-HLA binding affinity analysis

The capacity of predicted CD8^{+} T cell peptide epitopes to bind degenerately to multiple HLA alleles (cross-HLA binding affinity) was determined using the Immune Epitope Database (IEDB) NetMHCpan EL 4.1 algorithm [586] queried to predict a binding score of each peptide across 27 common alleles within the HLA-A1, A2, A3/11, A24, A3/01, B7, B8, B44, B58, and B62 HLA-supertypes (**Supp Fig. S6.2**).

In silico CD4^{+} and CD8^{+} T cell epitope homology analysis

Variant defining consensus nonsynonymous mutations in SARS-CoV2 S-protein relative to the Wuhan consensus sequence were provided by CoVarients [590] (accessed October 2023) using data from the *Global Initiative on Sharing All Influenza Data* (GISAID). Each peptide (**Supp Fig. S6.3)** and the Alpha (B.1.1.7; GenBank: QWE88920.1), Beta (B.1.351; GenBank: QRN78347.1), Gamma (B.1.1.28.1; GenBank: QVE55289.1), Delta (B.1.617.2; GenBank: QWK65230.1), and Omicron (B.1.1.529; GenBank: UFO69279.1) strains; and SARS-CoV1(YP_009825051.1), MERS (GenBank: YP_009047204.1), CovNL63 (GenBank: YP_003767.1), Cov229E (GenBank: AAK32191.1), Cov43 (GenBank: QXL74886.1), and

CovHKU1 (GenBank: YP_173238.1) species of coronavirus were aligned to the SARS-CoV2 Wuhan strain (GenBank: YP_009724390.1) using the Multiple Sequence Comparison by Log-Expectation (MUSCLE; European Bioinformatics Institute) alignment tool with standard settings [591].

Peptides

T cell peptide epitopes from SARS-CoV2 S-protein were synthesised at 95% purity (Mimotopes, Melbourne, AUS), and resuspended in dimethyl sulfoxide (DMSO) at a concentration of 20 mg/mL [592]. A positive control CEF peptide-pool representing well-characterized CD8^{+} T cell epitopes from Influenza virus, Epstein-Barr virus and Cytomegalovirus (CEF (HLA Class I Control) Peptide Pool) was purchased commercially (Stem Cell Technologies).

Samples

Ethical approval

This study was performed according to the principles of the Declaration of Helsinki. Ethics approval to undertake the research was obtained from QIMR Berghofer Medical Research Institute Human Research Ethics Committee (HREC: P2282). Informed consent was obtained from all participants. The inclusion criteria for the study were that participants were over the age of 18 and were well and able to donate in adherence with Queensland Health policies. All methods were performed in accordance with institutional guidelines and regulations.

Samples

PBMCs were collected from 11 individuals at three timepoints: i) Pre-2019 (SARS-CoV2-naïve), ii) Four-weeks post double homologous AstraZeneca™ (ChAdOx1 nCoV-19) vaccination (Vaccinated), and iii) four-weeks post subsequent SARS-CoV2 infection (Naturally Infected). Information about which variant each donor was infected with was not available, but the dominant variant circulating during the sampling period was the original Wuhan strain, followed by the Delta and Omicron variants. There were no mortality or severe outcomes (*i.e.,* hospitalisation) during convalescence for all naturally infected donors. Human leukocyte antigen (HLA) typing was performed by AlloSeq Tx17 (CareDx Pty Ltd, Fremantle, Australia) (**Supp Table S6.2**). PBMCs were isolated by standard density gradient centrifugation and cryopreserved in 90% FBS / 10% DMSO as previously described [356]. PBMCs were thawed at 37°C, rested for 18 hours at $2x10^6$ cells/mL in RPMI-1640 supplemented with 10% heat-inactivated AB human serum (Sigma-Aldrich), 100U/mL

penicillin/streptomycin (ThermoFisher Scientific), 2mM GlutaMAX (ThermoFisher Scientific), 10 mM HEPES (ThermoFisher Scientific) (R10 Media), at 37°C and 10% CO_2.

T cell assays

PBMCs were stimulated in 50 µL R10 media in 96-well U-bottom plates for 6 hours, before cells were lysed in MagMAX Lysis Buffer, as previously described [511]. The number of PBMCs stimulated was normalised across kinetic timepoints but varied between donors (3.4 – 11.5 x10^5 PBMCs/Stimulation; **Supp Table S6.2**). Predicted SARS-CoV2 T cell peptides and CEF peptide pool at 2 µg/mL, were tested alongside a 50ng/mL PMA, 1,000ng/mL Ionomycin mitogen positive-control and a media-only negative-control.

Reverse transcription quantitative PCR

RNA was extracted and converted to cDNA using our 'High-Throughput Screening (HTS) optimised protocol' as previously described [511]. Briefly, RNA was isolated using a MagMAX™ *mirVana*™ Total RNA Isolation Kit (Applied Biosystems) and converted to cDNA with SuperScript™ IV First-Strand Synthesis System (ThermoFisher) following the manufacturer's instructions, except that all reagents were used at 25% of the volume recommended by the manufacturer, respectively; and the Superscript™ IV reverse transcriptase enzyme was used at 5 U/µL RNA. Due to the variable numbers of stimulated PBMCs across donors (**Supp Table S6.2**), relative quantification was used for qPCR, as previously described [400]. Briefly, the fold-change expression of *Interferon gamma* (IFN-γ) were determined relative to the expression of the reference gene *Ribosomal protein L13a (RPL13a).* Fold change was normalised relative to the negative control (media only) stimulation. *IFN-γ*, and *RPL13a* specific desalt-grade (Sigma-Aldrich) previously optimised primers[356], obtained from PrimerBank™ [410] were used at 500 nM using ssoAdvanced™ Universal SYBR® Green Master-Mix (Bio-Rad). All reactions were run in technical triplicate in accordance with MIQE guidelines [400] at 5 µL total volume with 1 µL of reverse transcription eluent diluted 1:4 in Ultra-Pure™ H_2O (Invitrogen). Data was acquired using a QuantStudio5 Real-Time PCR system running QuantStudio Design and Analysis Software (v1.4.3, Applied Biosystems).

Data analysis

To examine the immunoreactivity of peptide epitopes, stimulations were classified as either positive or negative, and these categorical data were tested with Fisher's exact testing. Further categorical data, including epitope homology (Homologous *vs.* Not Homologous), and immunoreactive epitope localisation (within region *vs.* outside region), were also tested with a

Fisher's exact test. Kinetic data examining the strength of immunoreactivity of peptide epitopes across donor-matched timepoints were tested with a non-parametric Kruskal-Wallis test, followed by Dunns corrected multiple comparisons testing. GraphPad Prism version 10.2.0 (GraphPad Software) was used, and in all cases, P values < 0.05 were considered statistically significant.

6.2.5 Results

The number of immunoreactive epitopes were generally consistent across donor immune status

We defined a list of 170 putative SARS-CoV2 S-protein peptide epitopes (**Supp Table S6.1**) from a total of 7,500 identified CD8$^+$ T cell peptide epitope-HLA allele combinations (**Supp Fig. S6.1**); test peptides were generally restricted to either the HLA-A2, -A3/11, -A24, -B7, or -B8 MHC Class I (**Supp Fig. S6.2**) or Class II HLA-DR or -DQ supertypes. These peptide epitopes were derived from the Wuhan reference strain and analysis of sequence similarity for other SARS-CoV2 variants was assessed and showed that the peptide epitope sequences were mostly homologous to clinically relevant circulating SARS-CoV2 variants but not homologous to other circulating coronaviruses (**Supp Fig. S6.3**).

To study the magnitude and kinetics of T cell reactivity to these peptide epitopes in pre-vaccinated, post-vaccinated, and post-SARS-CoV2 infected individuals, we used our published HTS-RT-qPCR assay [511] to determine the expression of *IFN-γ* mRNA from PBMCs stimulated with these peptides. Defining the threshold of positivity as a doubling of IFN-γ expression (ΔΔCt>2), we identified 65 / 170 epitopes were immunoreactive in at least one donor. Robust T cell epitope reactivity was identified in SARS-CoV-2 S-protein naïve individuals (17.0% positive: 29/170 epitopes, n=9; **Table 6.1**), following vaccination (14.7% positive: 25/170 epitopes, n=10; **Table 6.1**), and following subsequent natural exposure (16.5% positive: 28/170 epitopes, n=8; **Table 6.1**), which was generally consistent with previously reported peptide immunogenicity amongst donors of similar immune status (**Supp Table S6.3**).

No significant differences were detected in the number of positive epitopes between naïve, vaccinated, or naturally infected donors (Peptide Epitope Immunoreactivity: $P = 0.6565$ (Naïve *vs.* Vaccinated), $P > 0.9999$ (Naïve *vs.* Naturally Infected), and $P = 0.7652$ (Vaccinated *vs.* Naturally infected); **Table 6.1**). When considering individual donors, the number of reactive epitopes amongst donor-matched PBMCs were generally consistent (**Fig. 6.1A**), although

some significance differences were detected. Specifically, when tested with a Fisher's exact test, there was a statistically significant increase in the number of reactive epitopes between naïve and naturally infected PBMCs (P = 0.0353) and a decrease in the number of reactive epitopes between naïve and vaccinated PBMCs (P = 0.0366) from Donor 3 and 8 respectively (**Supp Table S6.4**). Taken together these data demonstrate that the number of immunoreactive epitopes were generally consistent across donor immune status.

Table 6.1. Categorical analysis of SARS-CoV2 S-protein epitope immunoreactivity and kinetics in matched donors following vaccination and natural infection.

Immunoreactive epitopes	Immune status	Positive	Negative	Total	Positive (%)	P value vs. naive	P value vs. vaccination
Peptide epitope immunoreactivity							
Background	Naïve	29	141	170	17.0%	-	-
	Vaccinated	25	145	170	14.7%	0.6565	-
	Naturally infected	28	142	170	16.5%	>0.9999	0.7652
Positive epitope kinetics						P value vs. immune status	P value vs. background
Naïve	Vaccinated	9	20	29	31.0%	-	0.0570
	Naturally infected	2	27	29	6.9%	0.0411	0.2634
Vaccinated	Naïve	9	16	25	36.0%	-	0.0330
	Naturally infected	6	19	25	24.0%	0.5380	0.3965
Naturally Infected	Naïve	2	26	28	6.9%	-	0.3997
	Vaccinated	6	22	28	24.0%	0.2516	0.2631

PBMCs (n=12) were collected from donors which were either SARS-CoV-2 S-protein naïve (Naïve), following COVID-19 vaccination (Vaccinated), or following infection with SARS-CoV2 (Naturally infected). The discovery rate of positive epitopes (% Positive) across all stimulations (Background) was determined from the relative number of reactive stimulations to non-reactive stimulations. Positive epitope kinetics tested if positive epitopes were consistently positive across classes of immune status by comparing the discovery rate of positive epitopes to background.
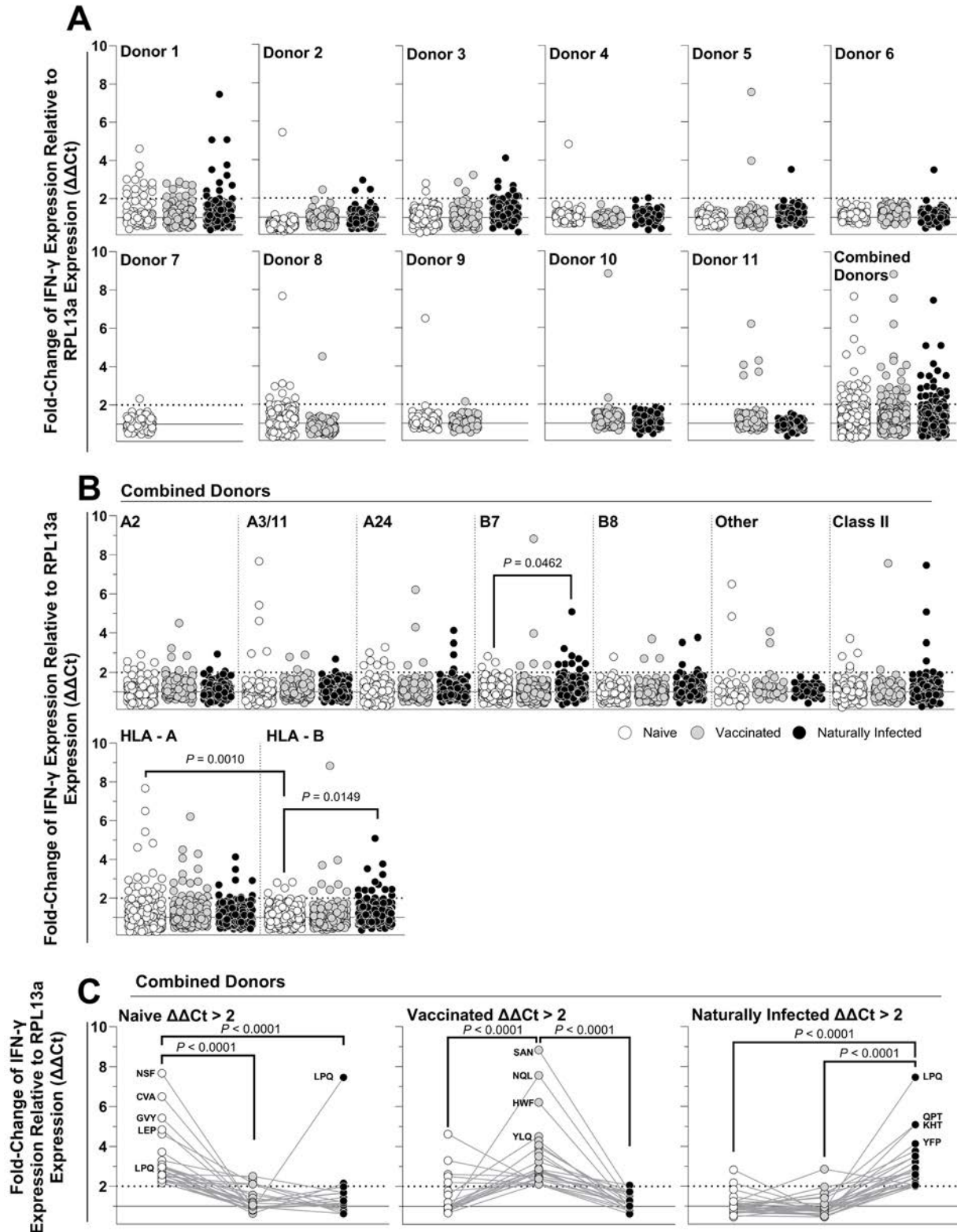
Figure 6.1. Peptide epitope immunoreactivity in PBMCs isolated from individuals naïve to the SARS-CoV2, as well as following vaccination and natural infection. *Interferon gamma* (IFN-γ) expression quantified through a high-throughput RT-qPCR (HTS-RT-qPCR) assay with fold change (ΔΔCt) determined relative to the endogenous control reference gene *Ribosomal Protein L13a*

(RPL13a) of Peripheral Blood Mononuclear Cells (PBMCs) isolated from 12 individuals naïve to SARS-CoV-2 S-protein (Naïve; white dots), following homologous AstraZeneca COVID-19 vaccination (Vaccinated; grey dots), and following infection with SARS-CoV2 (Naturally Infected; black dots) stimulated with 170 SARS-CoV2 S-protein peptide epitopes. Shown are data sorted by donor (**A**), sorted into HLA A2, A3/11, A24, B7, B8, other, and Class II supertype classifications (**B**), and data showing matched peptide kinetics tracking immunoreactive epitopes ($\Delta\Delta$Ct>2) across the naïve, vaccinated and naturally infected (**C**). Epitopes with $\Delta\Delta$Ct between 0-10 shown graphically while all data were considered for statistical analysis. Selected immunoreactive peptides shown with three letter codes.

High-affinity HLA-A epitopes are more immunoreactive in the naïve while HLA-B epitopes are more immunoreactive post-natural infection

When considering the HLA supertype restriction element of the tested peptides (**Fig. 6.1B**), there was no statistically significant increase in the number of reactive epitopes in HLA-matched peptides as determined by Fisher's exact test (**Supp Table S6.5**), except for an increase in immunoreactive HLA-B7-supertype epitopes between naïve and naturally infected PBMCs ($P = 0.0462$; **Fig. 6.1B**). For epitopes predicted to bind with high affinity to any of the HLA-A gene alleles, there was no statistically significant differences in the number of immunoreactive epitopes across donor immune status by Fisher's exact testing (**Supp Table S6.5**). However, for epitopes predicted to bind with high affinity to HLA-B gene alleles, there was a statistically significant increase in the number of immunoreactive epitopes between the naïve and the naturally infected ($P = 0.0149$; **Fig. 6.1B**). Furthermore, when comparing across HLA-genes, there was a statistically significant decrease in the number of immunoreactive epitopes in the naïve between HLA-A *vs.* HLA-B associated epitopes ($P = 0.0010$; **Fig. 6.1B**). These data demonstrate that type of epitope recognised altered from HLA-A restricted epitopes being predominantly immunoreactive in the naïve to HLA-B restricted epitopes being predominantly immunoreactive following natural infection, with a particular focus on HLA-B7 supertype epitopes.

Peptide epitopes immunoreactive following vaccination were more likely to be immunoreactive in the naïve, but not following natural infection

We examined the kinetics of epitope immunoreactivity across donor-matched naïve, vaccinated, or naturally-exposed samples (**Fig. 6.1C**). There was a statistically significant decrease ($P < 0.0001$, in all cases) in immunogenicity for epitopes that were found to be

immunoreactive in the naïve (Naïve $\Delta\Delta$Ct > 2), vaccinated (Vaccinated $\Delta\Delta$Ct > 2) or naturally infected (Naturally Infected $\Delta\Delta$Ct > 2) subjects, as determined by a non-parametric Kruskal-Wallis test. Dunns corrected multiple comparisons testing found there was a statistically significant decrease in immunogenicity at all matched kinetic timepoints ($P < 0.0001$ in all cases; **Fig. 6.1C**). These data demonstrated that the immunoreactivity of epitopes varied between immune statuses.

To investigate if there was an association between positive epitopes across immune status, we next investigated if epitopes that were positive at one kinetic timepoint were also positive at another. Among the 29 epitopes identified as positive in the naïve, nine (31.0%) were also positive in the vaccinated, while two (6.9%) were positive in the naturally infected (Positive Epitope Kinetics: **Table 6.1**). This difference was statistically significant by Fisher's exact testing (Positive (%): 31.0% *vs.* 6.9%, $P < 0.0411$; **Table 6.2**), while neither were significantly different to the background rate of detection (Positive (%): 17.0% *vs.* 31.0% $P = 0.0570$ (Vaccinated); 14.7% *vs.* 6.9% $P = 0.2634$ (Naturally Infected)). Of the 25 epitopes that were immunoreactive in the vaccinated, nine (31.0%) were also immunoreactive in the naïve, while six (24.0%) were immunoreactive in the vaccinated. This difference was not statistically significant by Fisher's exact test (Positive (%): 31.0% *vs.* 6.9%, $P < 0.5380$; **Table 6.2**), while there was a significant increase in the rate of positive epitopes between the background rate of detection and epitopes positive in the naïve and vaccinated (Positive (%): 17.0% *vs.* 36.0% $P = 0.0330$; **Table 6.2**), but not in the vaccinated and naturally infected (Positive (%): 16.5% *vs.* 24.0% $P = 0.3965$; **Table 6.2**). There was no statistically significant difference between the rates of detection of the six (24.0%) or two (6.9%) of 28 epitopes that were immunoreactive in the naturally infected and immunoreactive in the naïve or vaccinated respectively (Positive (%): 24.0% *vs.* 6.9%, $P < 0.2516$; **Table 6.1**), and no significant difference in these rates of detection when compared to background. There were no epitopes identified that were immunoreactive at all three timepoints. These data demonstrate there was a consistency of epitopes that were immunoreactive between matched donors that were SARS-CoV2 spike-protein naïve and who had been vaccinated.

Given this consistency of epitopes between the naïve and vaccinated donors, we sought to investigate if the epitopes immunoreactive in donors of various immune statuses were associated with SARS-CoV2 variant homology. Of the epitopes selected for this study, 38 of 170 (22.3%) had less than 100% homology to all clinically circulating SARS-CoV2 variants (**Supp Fig. S6.3**), while 8 of 29 (27.6%), 8 of 25 (32.0%), and 10 of 27 (37.0%) peptides that induced an immunogenic response in the naïve, vaccinated and naturally infected respectively

did not have 100% homology (**Supp Table S6.6**). There was no significant difference in the number of epitopes with imperfect homology by Fisher's exact testing, either when compared to the total peptides, or across donor immune status. These data suggest that 100% epitope sequence homology did not play a significant role in determining epitope immunogenicity.

Table 6.2. Categorical analysis of immunoreactive epitope localization within SARS-CoV2 S-protein domains and regions following vaccination and natural infection.

Domain	Immune status	Epitope in domain	Epitope outside domain	Total	In domain (%)	P value vs. naive	P value vs. vaccination
NTD	Naïve	13	17	30	43.3%	-	
	Vaccinated	4	22	26	15.4%	0.0401	-
	Naturally infected	10	19	29	34.5%	0.5959	0.1302
RBD	Naïve	5	25	30	16.7%	-	
	Vaccinated	3	23	26	11.5%	0.7116	-
	Naturally infected	3	26	29	10.3%	0.7065	>0.9999
VC1	Naïve	4	26	30	13.3%	-	
	Vaccinated	7	19	26	26.9%	0.3130	-
	Naturally infected	4	25	29	13.8%	>0.9999	0.3153
VC2	Naïve	5	25	30	16.7%	-	
	Vaccinated	11	15	26	42.3%	0.0426	-
	Naturally infected	4	25	29	13.8%	>0.9999	0.0321
VC1 / VC2 Combined	Naïve	9	21	30	30.0%	-	
	Vaccinated	18	8	26	69.2%	0.0068	-
	Naturally infected	8	21	29	27.6%	>0.9999	0.0029

The location of immunoreactive epitopes ($\Delta\Delta Ct > 2$) were tested relative to the number of epitopes inside and outside of domains across combined (n=12) donors of various immune statuses. Tested were the N-terminus domain (13-304aa; NTD), the Receptor Binding (319-541aa; RBD), Vaccination

Cluster 1 (590-730aa; VC1), Vaccination Cluster 2 (905-1115aa; VC2), and epitopes within both VC1 and VC2 (Combined).

The localisation of immunoreactive peptide epitopes within the SARS-CoV2 S-protein is dependent upon immune status

We next sought to determine if there was variation in the location of immunoreactive epitopes along the SARS-CoV2 S-protein amino acid sequence amongst donors of either naïve, vaccinated, or naturally-exposed immune status. Broadly, epitopes appeared to cluster, especially in the vaccinated (**Fig. 6.2**). This contrasted with the spread of the 170 selected peptide epitopes which were generally spread across the S-protein sequence (**Supp Fig. S6.1**). Fisher's exact testing found there was a statistically significant decrease in the number of immunoreactive epitopes in the N-terminus domain (NTD) following vaccination. Specifically, of the 30 stimulations that were immunoreactive in the naïve, 13 (43.3%) were from peptide epitopes found in the NTD. While of the 26 stimulations identified as immunoreactive following vaccination only 4 (15.4%) epitopes were in the NTD (In Domain (%): 43.3% *vs.* 15.4%, $P = 0.0401$; **Table 6.2**). There was no significant difference in the number of immunoreactive epitopes in the NTD between the naturally infected and naïve (In Domain (%): 34.5% *vs.* 43.3%; $P = 0.5959$; **Table 6.2**) or the naturally infected and vaccinated (In Domain (%): 34.5% *vs.* 15.4%; $P = 0.1302$; **Table 6.2**). Furthermore, there were no significant differences in epitope location amongst donors of differing immune status within the Receptor Binding Domain (**Table 6.2**), or any other previously defined tested domains (**Supp Table S6.7**). These data demonstrate that while epitope localisation differed in the vaccinated, it was generally not associated with previously defined domains.

As the immunoreactive epitopes within the vaccinated appeared to generally cluster in two regions (**Fig. 6.2**), we defined these regions as Vaccination Cluster 1 (590-730aa; VC1), and Vaccination Cluster 2 (905-1115aa; VC2). Fisher's exact testing found there were no significant differences between the 7 of 26 (26.9%) epitopes located within VC1 that were immunoreactive in the vaccinated compared to the 4 of 30 (13.3%) in the naïve (In Domain (%): 26.9% *vs.* 13.3%; $P = 0.3130$; **Table 6.2**), and 4 of 29 (13.8%) in the naturally infected (In Domain (%): 26.9% *vs.* 13.8%; $P = 0.3153$; **Table 6.2**). In contrast, the 11 of 26 (42.3%) immunoreactive epitopes in the vaccinated that were located within VC2 were statistically significantly more than the 5 of 30 (16.7%) in the naïve (In Domain (%): 42.3% *vs.* 16.7%; *P*

= 0.0426; **Table 6.2**), and the 4 of 29 (13.8%) in the naturally infected (In Domain (%): 42.3% *vs.* 13.8%; $P = 0.0321$; **Table 6.2**). When combined, 18 of 26 (69.2%) immunoreactive epitopes in the vaccinated were located within either VC1 or VC2, which was statistically significantly more than the 9 of 30 (30.0%) in the naïve (In Domain (%): 69.2% *vs.* 30.0%; $P = 0.0068$; **Table 6.2**), and the 8 of 29 (27.6%) in the naturally infected (In Domain (%): 69.2% *vs.* 27.6%; $P = 0.0029$; **Table 6.2**). There was no significant difference in the number of immunoreactive epitopes located within VC1, VC2, or when combined between the naïve and naturally infected ($P > 0.9999$ in all cases; **Table 6.2**). These data demonstrate that vaccination significantly altered the localization of immunoreactive epitopes on the SARS-CoV2 S-protein, causing them to cluster predominantly in two specific regions.

Taken together, this study established that the most immunoreactive epitopes varied following vaccination and subsequent natural infection, shifting from HLA-A in the naïve to HLA-B in the naturally infected. Furthermore, although there was consistency between specific immunoreactive epitopes in naïve and vaccinated donors, vaccination significantly altered the localization of immunoreactive epitopes, promoting epitopes that clustered within two extra-domanial regions, while subsequent natural infection generally promoted novel epitopes.
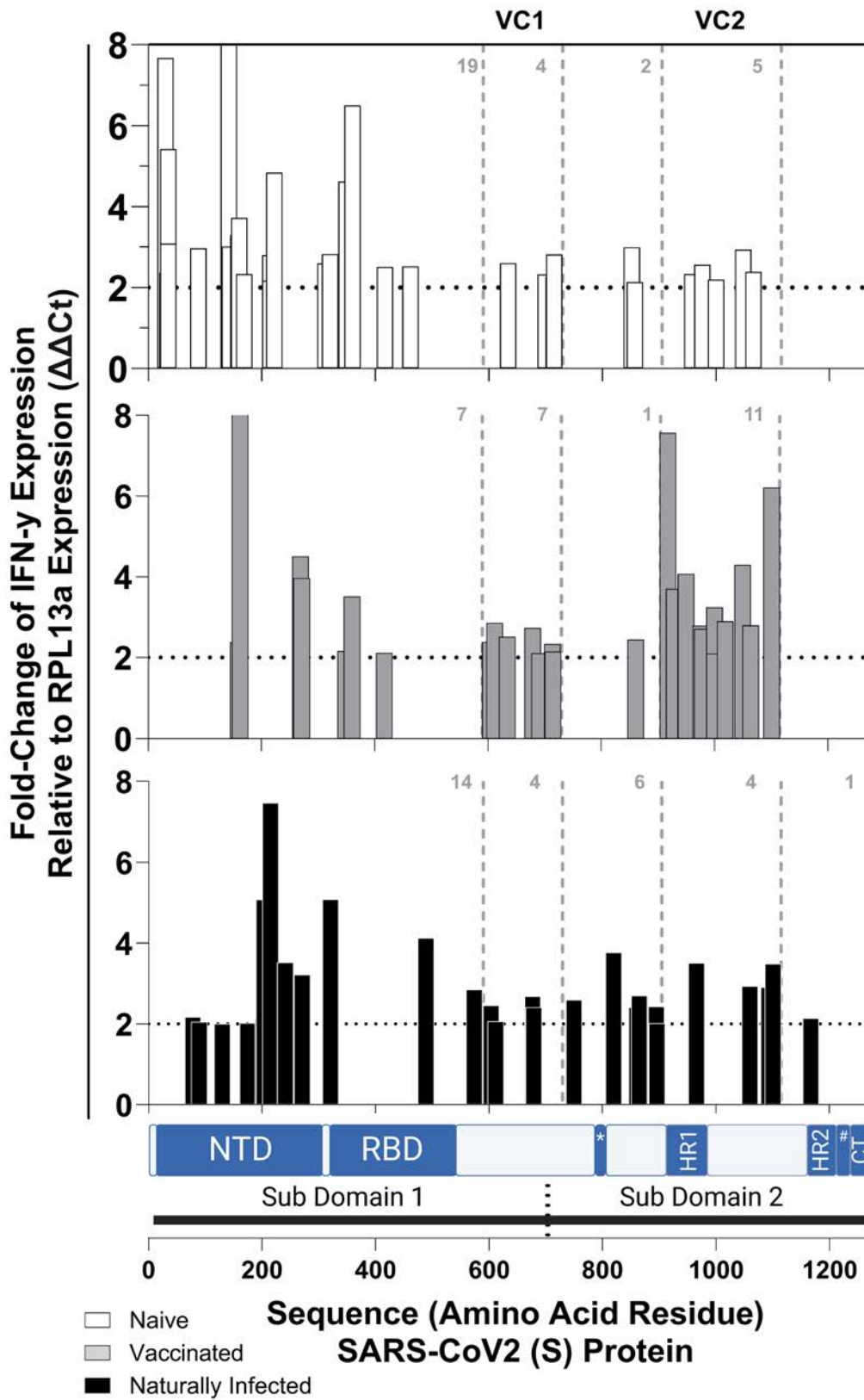
Figure 6.2. Immunoreactive peptide epitope locations along the SARS-CoV2 Spike (S) protein amino acid sequence. Immunoreactivity was determined as *Interferon gamma* (IFN-γ) expression quantified through a high-throughput RT-qPCR (HTS-RT-qPCR) assay with fold change (ΔΔCt)

relative to the endogenous control reference gene *Ribosomal Protein L13a* (RPL13a) of Peripheral Blood Mononuclear Cells (PBMCs) isolated from 12 individuals naïve to SARS-CoV-2 S-protein (Naïve; white bars), following homologous AstraZeneca COVID-19 vaccination (Vaccinated; grey bars), and following infection with SARS-CoV2 (Naturally Infected; black bars) stimulated with 170 SARS-CoV2 S-protein peptide epitopes. Discreet locations shown along the amino acid sequence are Sub-Domain 1 (1-681), and Sub-Domain 2 (686-1273aa), and the N-terminus (13-304aa; NTD), Receptor Binding (319-541aa; RBD), internal fusion peptide (816-833; *), Heptad Repeat 1 (981-983aa; HR1), Heptad Repeat 2 (1162-1203aa; HR2), transmembrane (1213 to 1237aa; #); Cytoplasmic Tail (1274 to the end of the protein; CT) domains. Vaccination Cluster 1 (590-730aa; VC1) and Vaccination Cluster 2 (905-1115aa; VC2) were experimentally defined by a high density of immunoreactive epitopes in these regions in donors following vaccination (Grey Bars). Numbers shown are total immunoreactive (ΔΔCt >2) epitopes identified within VC1 and VC2 defined regions.

6.2.6   Discussion

In this study, we analysed the immunoreactivity of SARS-CoV2 S-protein peptide epitopes in donors across multiple kinetic timepoints from SARS-CoV2 S-protein naïve, following Astra-Zeneca double homologous vaccination, and subsequent natural exposure to SARS CoV2. The results of this study suggested the most immunoreactive SARS-CoV2 S-protein epitopes varied following vaccination and subsequent natural infection. Immunoreactive epitopes in the naïve were predominantly associated with HLA-A, with nearly half clustering in the N-terminal domain. After vaccination, there was a shift in the localization of immunoreactive epitopes to two extra-domanial regions. Subsequent natural infection induced novel epitopes that were dispersed across the antigen and primarily associated with HLA-B, specifically the B7 supertype.

The immunoreactivity of SARS-CoV-2 S-protein T cell epitopes has been extensively studied [125, 593], and many well-characterised epitopes have been identified as immunoreactive across naïve, vaccinated, and naturally infected donors (**Table 6.2**). Nevertheless, herein, we report immunoreactivity in several epitopes in immune status groups for the first time. For example, we report the A*02:01 epitope GLTVLPPLL was immunoreactive in a naïve donor, whereas previously this epitope has only been found to be immunoreactive following natural infection [125]. In other epitopes, we report immunoreactivity which is in agreement with some of the literature. For example, we report the A*02:01 epitope VLNDILSRL was immunoreactive in a naïve and vaccinated donor, but we found no immunoreactivity following natural infection. Studies have reported immunogenicity of VLNDILSRL in naïve individuals

[594, 595], others have not [596], while some studies have reported immunogenicity only in naturally infected individuals [568], or reported immunogenicity only following certain immunisation strategies [580, 597]. Indeed, many of the epitopes we identified as immunoreactive have inconsistent findings on IEDB (**Table 6.2**). Such inconsistencies are frequent in human studies, due to the significant environmental and genetic variation inherent in human donors. These inconsistencies may also stem from the influence and interaction of underreported technical variation, such as during PBMC collection, cryopreservation, thawing, and culture [530].

We found there was a statistically significant increase in the number of HLA-B7 supertype epitopes which were immunogenic following natural infection. HLA-B genes have a reported strong association with viral infections [598, 599], including in COVID-19 [600], especially the B7 supertype allele HLA-B*15:01, which has been associated with asymptomatic SARS-CoV-2 infections [601], and HLA-B*07:02 which is associated with a high degree of pre-existing cross-reactive memory T cells [602]. Nevertheless, it remains unclear as to how increasing HLA-B7 allele immunogenicity influences patient outcomes, as HLA-B7 supertype alleles have been associated with increased disease susceptibility [603, 604]. It is also unclear why peptide epitopes associated with HLA-A genes would be prominently immunoreactive in the naïve. There is significant peptide overlap amongst common S-protein epitopes and endogenous tumour associated epitopes [605], which may be activated during healthy immune homeostasis, and core amino acid anchors of epitopes immunoreactive in the naive have found broad anchor homology in seasonal coronavirus. It remains unclear if this pre-existing immunity is irrelevant or related to beneficial or detrimental patient outcomes [606]. Our analysis revealed that sequence homology was not correlated with epitope immunogenicity. This finding aligns with existing literature, which indicates that CD4$^+$ and CD8$^+$ T cell responses in convalescent COVID-19 patients or recipients of the COVID-19 mRNA vaccines were not significantly impacted by mutations present in SARS-CoV2 variants [607]. However, given the thousands of possible epitopes available within the S-protein, more extensive studies are needed to definitively determine the relationship between sequence homology, viral variants, vaccines, and epitope immunogenicity.

Our study identified the localization of immunoreactive epitopes in two extra-dominal regions, between 590-730aa and 905-1115aa of the S-protein following vaccination. Other studies have shown dynamic changes in epitope localization among donors with varying immune statuses. For example, one study found that individuals previously infected with SARS-CoV2 develop

more distinct T cell immune memory compared to those who are only vaccinated [608]. Another study observed that, in naïve patients, both the C- and N-terminal regions of the ORF1 protein contain fewer T cell epitopes, and in agreement with this study, reported similar epitope localization in convalescent and naïve patients [596]. It is unclear why such localisation of T cell epitopes would occur in donors of various immune statuses.

The only post-vaccination samples assessed in this study were PBMCs collected from donors following a double homologous AstraZeneca ChAdOx1 nCoV-19 (AZ) vaccination regimen. The AZ vaccine has been found to induce potent CD4$^+$ and CD8$^+$ T cell responses [135, 609]. Heterologous boosting with other vaccines, such as the BNT162b2 Pfizer BioNTech (Pfizer) vaccine may induce stronger immune responses than a homologous regimen [556]. Investigating the reactivity of peptide epitopes across varying homologous and heterologous vaccine regimens may provide further insight into improving vaccine induced T cell immunogenicity against SARS-CoV2. Post-vaccination and -infection samples were collected between 1-4 months following convalescent and therefore the T cell reactivity observed in this study was more likely associated with long-term immune memory cells [610]. However, flow-cytometry reactive cell phenotyping would be required to identify which cells are responsible for the immunoreactivity. It is possible investigating the kinetics of acute phase peptide epitope immunoreactivity and subsequent long-term memory formation may provide insight into development of long-term cellular immunity. Furthermore, this study exclusively assessed donors vaccinated before natural infection. To clarify the impact of prior vaccination on epitope immunoreactivity, future studies should include individuals who were naturally infected without prior vaccination.

The *in vivo* development a T cell peptide epitope immunodominance hierarchy is a complex process which remains incompletely understood [611]. However, several aspects of the formation of immunodominance, such as the relationship between immunogenicity and MHC binding affinity, are relatively well established. Indeed, the binding affinity of peptide epitopes to variable MHC alleles is described as the most selective stage of the formation of an epitope immunodominance hierarchy [570], and a binding affinity threshold of 500 nM for peptide-MHC interactions has been experimentally established as necessary to initiate T cell immunity [612]. We found the Immune Epitope Database (IEDB) HLA-peptide binding score did identify peptide epitopes found to be highly immunoreactive in convalescent COVID-19 patients [125]. However, the predictive binding affinity of a putative peptide epitope for a given HLA molecule should not be used as the sole predictor of immunodominance [613, 614]. Variables

including previous exposure to homologous epitopes, antigen abundance following vaccination and infection, antigen processing, peptide-HLA binding competition and T cell receptor (TCR) repertoire can all influence the immunodominance hierarchy [611]. We found abundant cross HLA binding affinities in our prioritized peptide epitopes (**Supp Fig. S6.2**). To investigate how the cross-HLA binding affinities of peptides predicted from the SARS-CoV2 S-protein impact epitope immunogenicity, a validated immunodominance hierarchy of S-protein epitopes would need to be constructed across variably HLA-matched donors and compared to HLA-peptide binding scores.

Variance in peptide epitope immunogenicity between post-vaccinated and -infected individuals can be partially explained by exposure to viral variants carrying epitope mutations within the S-protein. We found variant defining mutations crossed several of our peptide epitopes, with the Omicron variant carrying the largest number of S-protein non-synonymous mutations, mostly within the receptor binding domain (**Supp Fig. S6.3**). By late 2023, the most dominant variant circulating globally was Omicron, and due to its global distribution, many sub-variants are now circulating, each with defining mutations [615]. Interestingly, Omicron sub-variants are undergoing convergent evolution, as several areas in the RBD have appeared as mutational hotspots [616]. While the cause remains unknown, it is likely both humoral and cellular immunity are applying selective pressure to these strains. It is likely that genomic surveillance of viral lineages amongst PBMC donors would provide significant insight into how variants can influence epitope immunogenicity, and how this may relate the variant evolution [617].

In summary, herein we have investigated the immunogenicity of 170 immunodominant peptide epitopes from the S-protein of SARS-CoV2 in pre-vaccinated, post-vaccinated, and post-infected individuals. Our investigation revealed that immunoreactivity was not confined to a select few immunodominant epitopes; instead, it was widely distributed among numerous epitopes. Immunoreactive epitopes in the naïve were predominantly associated with HLA-A, which shifted to primary HLA-B following natural infection. Vaccination promoted epitopes that were immunoreactive in the naïve, but primarily within two regions, and naturally infection generally promoted novel epitopes that were dispersed across the S-protein antigen.

6.2.7   Supplementary material

Supplementary figures
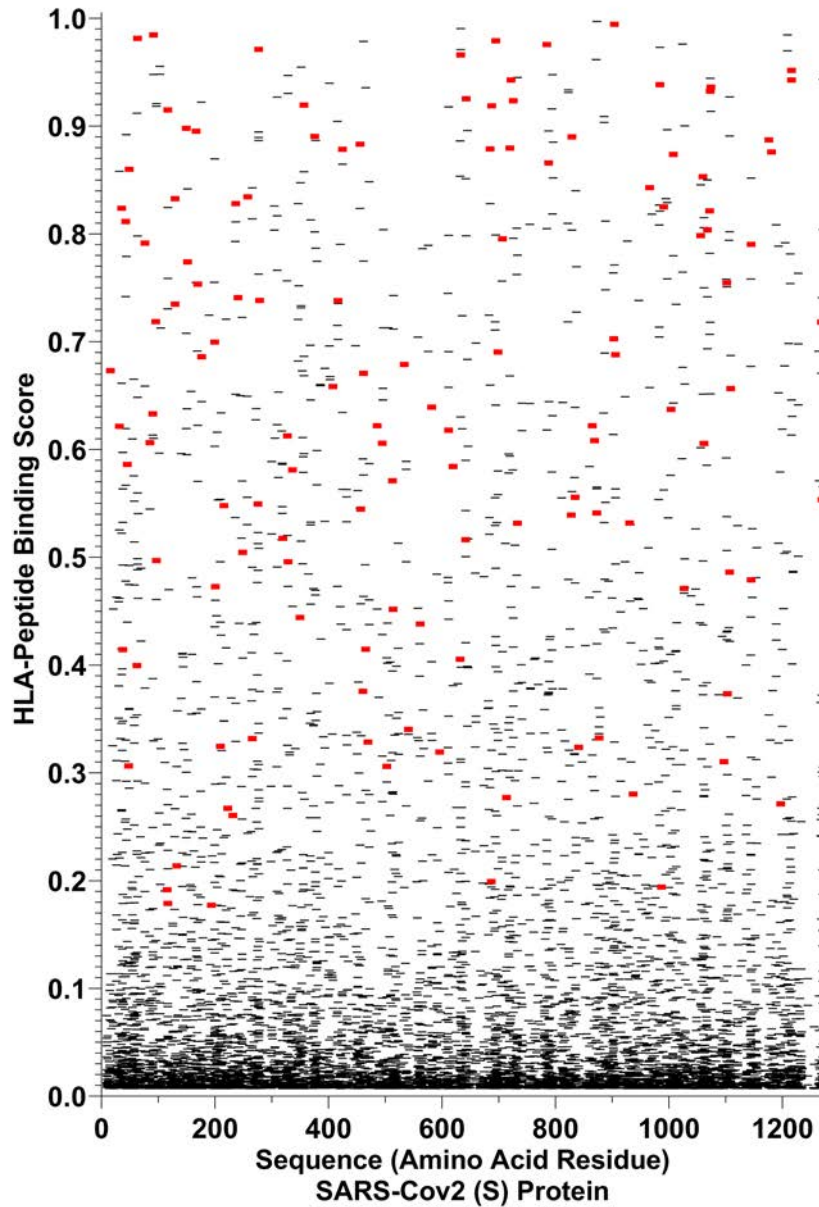
Supplementary Figure S6.1. Selection of a putative list of CD8^{+} T cell SARS-CoV2 S-protein peptide epitopes from IEDB predicted epitopes. A putative list of MHC Class I SARS-CoV2 S-protein epitopes predicted to bind with high affinity to any allelic variant of the HLA-A or -B genes contained 7749 MHC Class I peptide epitopes identified with a HLA-peptide binding score > 0.007 were distributed across the sequence of the SARS-CoV2 S-protein (Black lines). A final list of 170 peptides were selected (139 Class I shown; Red lines) prioritised by binding to HLA supertype A2, A3/A11, A24, B7 and B8, and further prioritised by identification as immunoreactive in the literature [580].
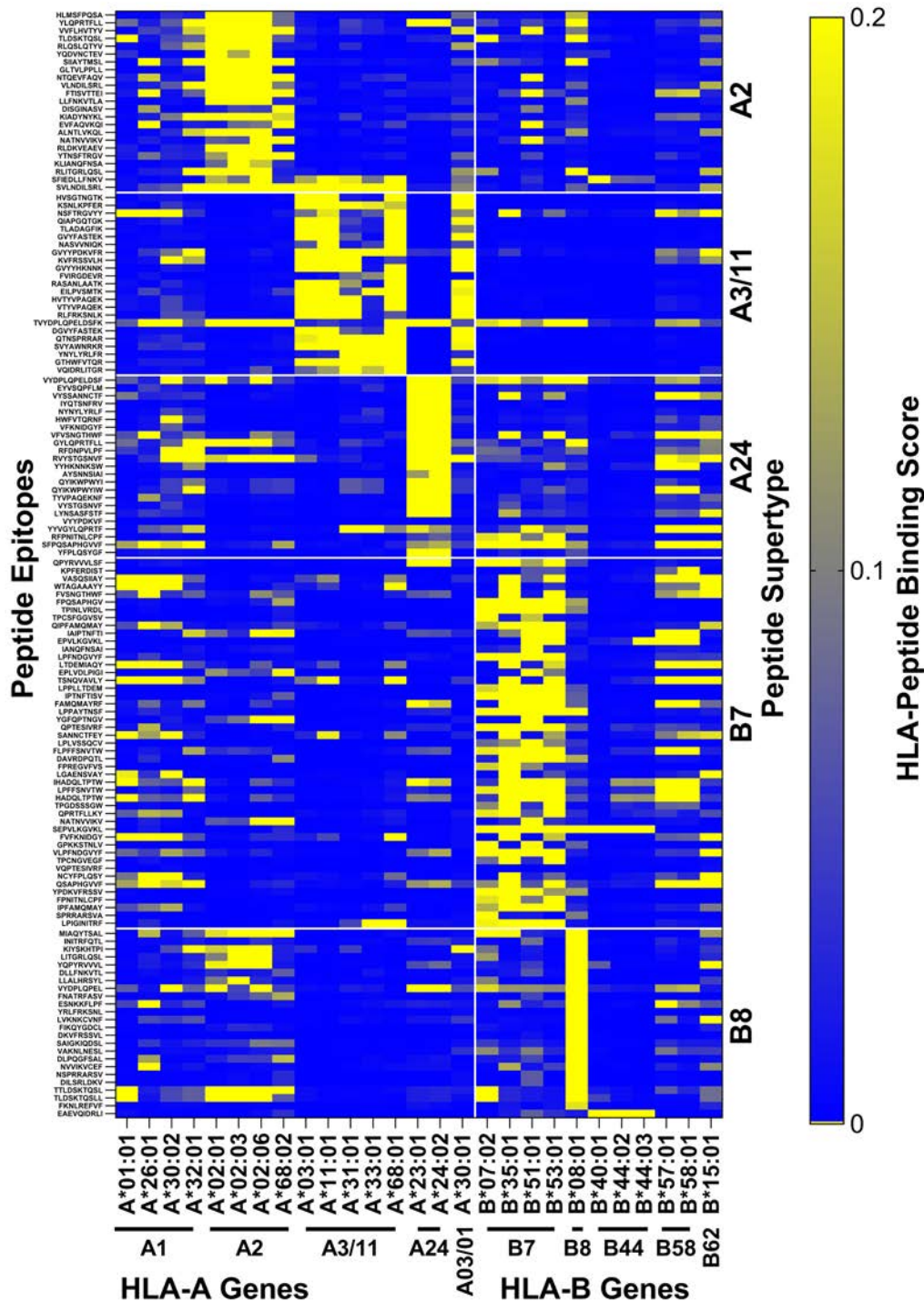
Supplementary Figure S6.2. Predicted CD8^{+} peptide epitope HLA affinity. A heatmap visualisation of the *in silico* cross-HLA binding affinity of our prioritized CD8^{+} peptide list by querying IEDB to predict a binding score of each peptide across 27 common HLA alleles. Relatively strong peptide-HLA interactions (HLA binding scores >0.2) were typically predicted between most HLA alleles within a supertype. Heatmap organised with SARS-CoV2 S-protein peptide epitopes (y-axis; left) sorted into HLA A2, A3/11, A24, B7, B8, supertype classifications (y-axis; right). Yellow is a relatively high binding score while blue is a relatively low binding score.
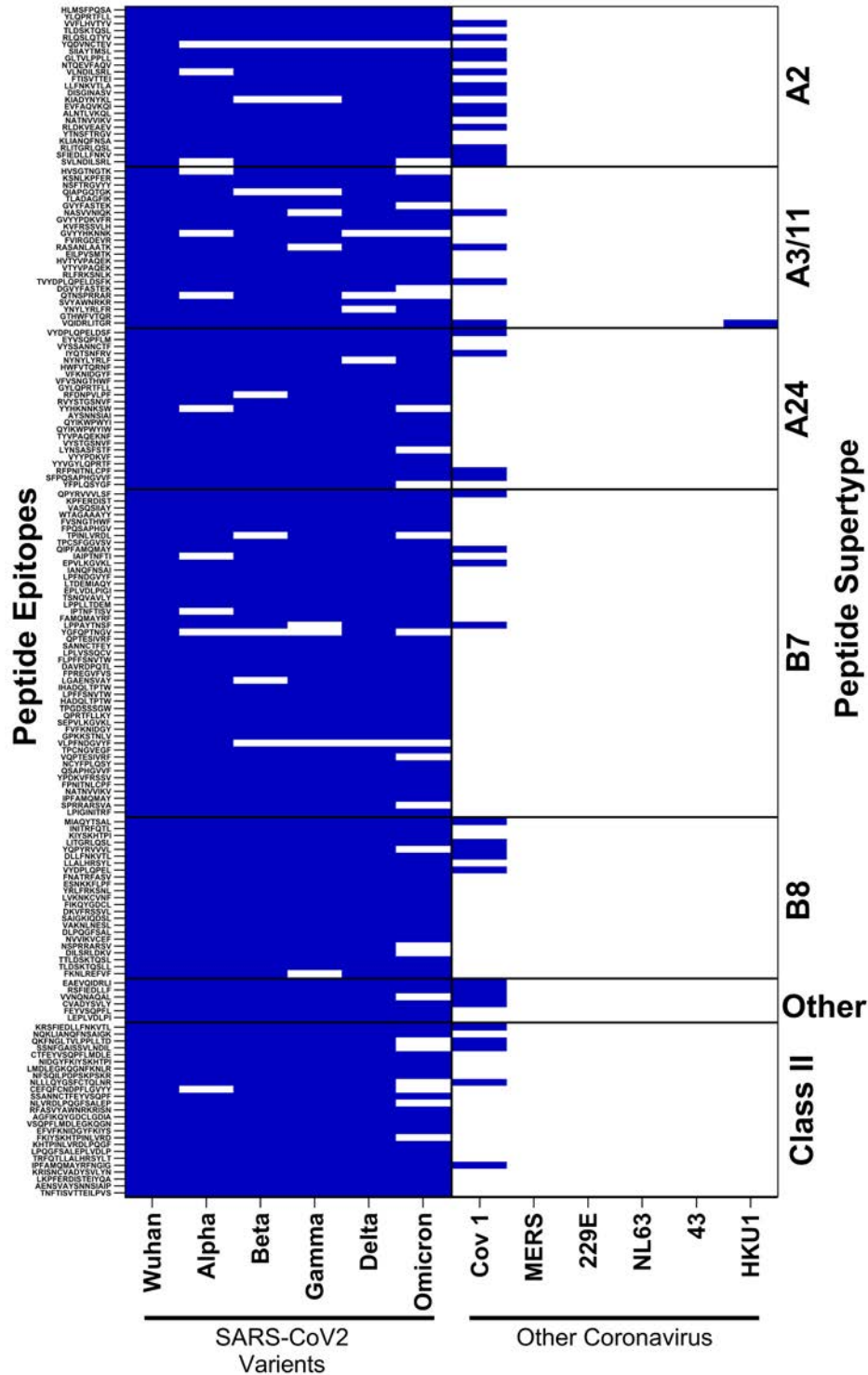
Supplementary Figure S6.3. Homology of peptide epitopes to clinically relevant circulating SARS-CoV2 variants and other endemic coronaviruses. A heatmap visualisation of peptide homology to coronavirus spike-protein amino acid sequences where blue is 100% homology and white is at least one synonymous mutation. Heatmap is organised with SARS-CoV2 S-protein peptide epitopes (y-axis; left) sorted into HLA-A2, -A3/11, -A24, -B7, -B8, other, and Class II supertype classifications (y-axis; right).

Supplementary tables

Supplementary Table S6.1. SARS-CoV2 S-protein T cell peptide epitopes. Shown are the order of the epitopes (Number: Nᵒ) amino acid 1-letter symbols (Sequence), the predicted Human Leukocyte Antigen (HLA) allele with the highest affinity for the sequence, the HLA-Supertype of the allele, the amino acid number along the S-protein sequence that the epitope beings (Start), the amino acid number along the S-protein sequence that the epitope ends (End), the IEDB predicted binding score (Binding Score), and the sum of the response as identified from Tarke *et al*, 2021 [125] (Sum of Response), which immune status this epitope was identified as immunoreactive in this study (Positive Immune Status). Peptides sequentially ordered by HLA supertype, Sum of Response, then Binding Score. N/I – Natural Infection.

No.	Sequence	Allele	HLA supertype	Start	End	Binding score	Sum of response	Positive immune status
1	HLMSFPQSA	A*02:01	A2	1048	1056	0.798	1011	Naïve
2	YLQPRTFLL	A*02:01	A2	269	277	0.971	404	Vaccinated
3	VVFLHVTYV	A*02:03	A2	1060	1068	0.804	365	N/I
4	TLDSKTQSL	A*02:01	A2	109	117	0.915	296	
5	RLQSLQTYV	A*02:01	A2	1000	1008	0.874	264	Naïve, & Vaccinated
6	YQDVNCTEV	A*02:06	A2	612	620	0.584	243	Vaccinated & N/I
7	SIIAYTMSL	A*02:06	A2	691	699	0.69	165	Vaccinated
8	GLTVLPPLL	A*02:01	A2	857	865	0.622	151	Naïve
9	NTQEVFAQV	A*68:02	A2	777	785	0.976		
10	VLNDILSRL	A*02:01	A2	976	984	0.938		Naïve & Vaccinated
11	FTISVTTEI	A*68:02	A2	718	726	0.924		
12	LLFNKVTLA	A*02:03	A2	821	829	0.89		
13	DISGINASV	A*68:02	A2	1168	1176	0.887		N/I
14	KIADYNYKL	A*02:06	A2	417	425	0.879		Naïve, & Vaccinated
15	EVFAQVKQI	A*68:02	A2	780	788	0.866		
16	ALNTLVKQL	A*02:03	A2	958	966	0.843		Naïve
17	NATNVVIKV	A*68:02	A2	122	130	0.833		

No.	Sequence	Allele	HLA supertype	Start	End	Binding score	Sum of response	Positive immune status
18	RLDKVEAEV	A*02:01	A2	983	991	0.825		
19	YTNSFTRGV	A*68:02	A2	28	36	0.824		
20	KLIANQFNSA	A*02:03	A2	920	929			
21	RLITGRLQSL	A*02:03	A2	995	1004			
22	SFIEDLLFNKV	A*02:06	A2	817	826			
23	SVLNDILSRL	A*02:03	A2	974	983			
24	HVSGTNGTK	A*68:01	A3/A11	69	78	0.792	972	
25	KSNLKPFER	A*11:01	A3/A11	458	466	0.415	701	
26	NSFTRGVYY	A*68:01	A3/A11	30	38	0.414	600	Naïve
27	QIAPGQTGK	A*11:01	A3/A11	409	417	0.738	518	
28	TLADAGFIK	A*03:01	A3/A11	827	835	0.556	398	
29	GVYFASTEK	A*68:01	A3/A11	89	97	0.497	340	N/I
30	NASVVNIQK	A*68:01	A3/A11	1173	1181	0.876	326	
31	GVYYPDKVFR	A*31:01	A3/A11	35	44	0.811	314	Naïve
32	KVFRSSVLH	A*03:01	A3/A11	41	49	0.86	272	
33	GVYYHKNNK	A*03:01	A3/A11	142	150	0.898	270	Naïve
34	FVIRGDEVR	A*68:01	A3/A11	400	408	0.658	269	
35	RASANLAATK	A*03:01	A3/A11	1019	1028	0.471	268	Vaccinated
36	EILPVSMTK	A*03:01	A3/A11	725	733	0.532	253	
37	HVTYVPAQEK	A*68:01	A3/A11	1064	1073	0.821	250	Vaccinated
38	VTYVPAQEK	A*03:01	A3/A11	1065	1073	0.932	235	
39	RLFRKSNLK	A*11:01	A3/A11	454	462	0.671	233	
40	TVYDPLQPELD SFK	A*03:01	A3/A11	1135	1149		225	
41	DGVYFASTEK	A*68:01	A3/A11	88	97	0.719	205	Naïve
42	QTNSPRRAR	A*31:01	A3/A11	677	685	0.879	200	N/I
43	SVYAWNRKR	A*31:01	A3/A11	349	357	0.92	190	Naïve, & Vaccinated

No.	Sequence	Allele	HLA supertype	Start	End	Binding score	Sum of response	Positive immune status
44	YNYLYRLFR	A*33:01	A3/A11	449	457	0.545	170	
45	GTHWFVTQR	A*03:01	A3/A11	1099	1107	0.486	164	
46	VQIDRLITGR	A*68:01	A3/A11	1000	1009			
47	VYDPLQPELDSF	A*23:01	A24	1137	1145	0.79	2244	
48	EYVSQPFLM	A*24:02	A24	169	177	0.686	815	Naïve
49	VYSSANNCTF	A*24:02	A24	159	168	0.895	719	Naïve, & Vaccinated
50	IYQTSNFRV	A*24:02	A24	312	320	0.518	710	Naïve
51	NYNYLYRLF	A*24:02	A24	448	456	0.883	606	
52	HWFVTQRNF	A*24:02	A24	1101	1109	0.656	551	Vaccinated & N/I
53	VFKNIDGYF	A*24:02	A24	193	201	0.473	467	
54	VFVSNGTHWF	A*24:02	A24	1094	1102	0.755	465	N/I
55	GYLQPRTFLL	A*24:02	A24	268	277	0.549	378	
56	RFDNPVLPF	A*24:02	A24	78	86	0.606	365	N/I
57	RVYSTGSNVF	A*24:02	A24	634	643	0.516	349	Naïve & Vaccinated
58	YYHKNNKSW	A*23:01	A24	144	152	0.774	348	Naïve
59	AYSNNSIAI	A*24:02	A24	706	714	0.277	278	
60	QYIKWPWYI	A*24:02	A24	1208	1216	0.952	214	
61	QYIKWPWYIW	A*23:01	A24	1208	1217	0.943	193	
62	TYVPAQEKNF	A*24:02	A24	1066	1075	0.936		Naïve
63	VYSTGSNVF	A*24:02	A24	635	643	0.925		
64	LYNSASFSTF	A*24:02	A24	368	377	0.89		
65	VYYPDKVF	A*24:02	A24	34	43		167	Naïve
66	YYVGYLQPRTF	A*24:02	A24	264	275		1452	
67	RFPNITNLCPF	A*24:02	A24	327	338		539	
68	SFPQSAPHGVVF	A*24:02	A24	1050	1062		234	Vaccinated
69	YFPLQSYGF	A*29:02	A24	489	497			N/I

No.	Sequence	Allele	HLA supertype	Start	End	Binding score	Sum of response	Positive immune status
70	QPYRVVVLSF	B*07:02	B7	506	515	0.452	3589	
71	KPFERDIST	B*07:02	B7	462	470	0.329	2921	Naïve
72	VASQSIIAY	B*35:01	B7	687	695	0.979	1444	
73	WTAGAAAYY	B*35:01	B7	258	266	0.332	1401	
74	FVSNGTHWF	B*35:01	B7	1095	1103	0.373	436	
75	FPQSAPHGV	B*51:01	B7	1052	1060	0.853	413	
76	TPINLVRDL	B*07:02	B7	208	216	0.548	406	
77	TPCSFGGVSV	B*07:02	B7	588	597	0.319	405	
78	QIPFAMQMAY	B*35:01	B7	895	904	0.703	404	N/I
79	IAIPTNFTI	B*51:01	B7	712	720	0.88	355	
80	EPVLKGVKL	B*07:02	B7	1262	1270	0.553	313	
81	IANQFNSAI	B*51:01	B7	923	931	0.532	307	
82	LPFNDGVYF	B*35:01	B7	84	92	0.985	299	
83	LTDEMIAQY	B*35:01	B7	865	873	0.541	294	N/I
84	EPLVDLPIGI	B*51:01	B7	224	233	0.261	294	
85	TSNQVAVLY	B*35:01	B7	604	612	0.618	278	Vaccinated & N/I
86	LPPLLTDEM	B*35:01	B7	861	869	0.608	264	Vaccinated & N/I
87	IPTNFTISV	B*51:01	B7	714	722	0.943	254	Naïve, & Vaccinated
88	FAMQMAYRF	B*35:01	B7	898	906	0.688	236	
89	LPPAYTNSF	B*53:01	B7	24	32	0.622	232	
90	YGFQPTNGV	B*51:01	B7	495	503	0.306	208	
91	QPTESIVRF	B*51:01	B7	321	329	0.496	193	N/I
92	SANNCTFEY	B*35:01	B7	162	170	0.753	192	Vaccinated
93	LPLVSSQCV	B*51:01	B7	8	16	0.673	175	
94	FLPFFSNVTW	B*35:01	B7	55	64	0.4	163	

No.	Sequence	Allele	HLA supertype	Start	End	Binding score	Sum of response	Positive immune status
95	DAVRDPQTL	B*51:01	B7	574	582	0.639	157	N/I
96	FPREGVFVS	B*35:01	B7	1089	1097	0.31	156	
97	LGAENSVAY	B*35:01	B7	699	707	0.795	125	
98	IHADQLTPTW	B*53:01	B7	624	633	0.405	122	
99	LPFFSNVTW	B*53:01	B7	56	64	0.981		
100	HADQLTPTW	B*53:01	B7	625	633	0.966		
101	TPGDSSSGW	B*53:01	B7	250	258	0.834		
102	QPRTFLLKY	B*35:01	B7	271	279	0.738		Vaccinated & N/I
103	SEPVLKGVKL	B*07:02	B7	1261	1270	0.718		
104	FVFKNIDGY	B*35:01	B7	192	200	0.7		
105	GPKKSTNLV	B*07:02	B7	526	534	0.679		
106	VLPFNDGVYF	B*53:01	B7	83	92	0.633		
107	TPCNGVEGF	B*35:01	B7	478	486	0.622		
108	VQPTESIVRF	B*53:01	B7	320	329	0.613		Naïve & N/I
109	NCYFPLQSY	B*35:01	B7	487	495	0.606		
110	QSAPHGVVF	B*35:01	B7	1054	1062	0.606		
111	YPDKVFRSSV	B*07:02	B7	38	47	0.586		
112	FPNITNLCPF	B*35:01	B7	329	338	0.581		
113	LPFFSNVTWF	B*53:01	B8	56	65	0.56		
114	IPFAMQMAY	B*35:01	B7	896	904	0.994		N/I
115	SPRRARSVA	B*07:02	B7	680	688	0.919		
116	LPIGINITRF	B*35:01	B7	229	238	0.828		
117	MIAQYTSAL	B*08:01	B8	869	877	0.332	1025	
118	INITRFQTL	B*08:01	B8	233	241	0.741	402	
119	KIYSKHTPI	B*08:01	B8	202	210	0.325	298	N/I
120	LITGRLQSL	B*08:01	B8	996	1004	0.637		

No.	Sequence	Allele	HLA supertype	Start	End	Binding score	Sum of response	Positive immune status
121	YQPYRVVVL	B*08:01	B8	505	513	0.571		
122	DLLFNKVTL	B*08:01	B8	820	828	0.539		N/I
123	LLALHRSYL	B*08:01	B8	241	249	0.505		N/I
124	VYDPLQPEL	B*08:01	B8	1137	1145	0.479		
125	FNATRFASV	B*08:01	B8	342	350	0.444		
126	ESNKKFLPF	B*08:01	B8	554	562	0.438		
127	YRLFRKSNL	B*08:01	B8	453	461	0.376		
128	LVKNKCVNF	B*08:01	B8	533	541	0.34		
129	FIKQYGDCL	B*08:01	B8	833	841	0.324		
130	DKVFRSSVL	B*08:01	B8	40	48	0.306		
131	SAIGKIQDSL	B*08:01	B8	929	938	0.28		Vaccinated
132	VAKNLNESL	B*08:01	B8	1189	1197	0.271		
133	DLPQGFSAL	B*08:01	B8	215	223	0.267		Naïve
134	NVVIKVCEF	B*08:01	B8	125	133	0.214		
135	NSPRRARSV	B*08:01	B8	679	687	0.199		Vaccinated & N/I
136	DILSRLDKV	B*08:01	B8	979	987	0.194		Vaccinated
137	TTLDSKTQSL	B*08:01	B8	108	117	0.192		
138	TLDSKTQSLL	B*08:01	B8	109	118	0.179		
139	FKNLREFVF	B*08:01	B8	186	194	0.177		
140	EAEVQIDRLI	B*49:01	Other	987	997			
141	RSFIEDLLF	B*58:01	Other	754	763			
142	VVNQNAQAL	A*26:01	Other	950	959			Vaccinated
143	CVADYSVLY	A*26:01	Other	360	369			Naïve
144	FEYVSQPFL	B*40:01	Other	167	176			
145	LEPLVDLPI	B*40:01	Other	222	231			
146	KRSFIEDLLFNKVTL	DPB1*02:01	MHC II	753	768			

No.	Sequence	Allele	HLA supertype	Start	End	Binding score	Sum of response	Positive immune status
147	NQKLIANQFNSAIGK	DRB1*13:02	MHC II	918	933			Vaccinated
148	QKFNGLTVLPPLLTD	DRB1*01:01	MHC II	852	867			Naïve
149	SSNFGAISSVLNDIL	DRB1*01:01 DPA1*01:03	MHC II	966	981			Naïve & N/I
150	CTFEYVSQPFLMDLE	DQB1*02:01 DQB1*02:02 DQB1*05:02 DQB1*05:03 DRB1*07:01 DRB1*16:01	MHC II	165	180			
151	NIDGYFKIYSKHTPI	DRB1*07:01 DRB1*15:01 DRB1*16:01	MHC II	195	210			
152	LMDLEGKQGNFKNLR		MHC II	175	192			N/I
153	NFSQILPDPSKPSKR	DRB1*03:01	MHC II	800	815			
154	NLLLQYGSFCTQLNR	DQB1*05:03 DRB1*04:04 DRB1*15:01	MHC II	750	765			N/I
155	CEFQFCNDPFLGVYY	DQB1*05:02 DQB1*05:03	MHC II	130	145			N/I
156	SSANNCTFEYVSQPF		MHC II	160	175			Naïve
157	NLVRDLPQGFSALEP	DRB1*03:01	MHC II	210	225			
158	RFASVYAWNRKRISN	DRB1*07:01 DRB1*13:01 DRB1*14:01	MHC II	345	360			
159	AGFIKQYGDCLGDIA	DQB1*05:03	MHC II	830	845			
160	VSQPFLMDLEGKQGN	DRB1*03:01	MHC II	170	185			
161	EFVFKNIDGYFKIYS	DQB1*05:03 DRB1*14:01 DRB1*15:01	MHC II	190	205			

No.	Sequence	Allele	HLA supertype	Start	End	Binding score	Sum of response	Positive immune status
162	FKIYSKHTPINLVRD	DRB1*07:01 DRB1*13:01	MHC II	200	215			
163	KHTPINLVRDLPQGF	DRB1*03:01	MHC II	204	219			N/I
164	LPQGFSALEPLVDLP	DQB1*02:02 DQB1*03:03 DQB1*05:03	MHC II	215	230			Naïve & N/I
165	TRFQTLLALHRSYLT	DQB1*05:03 DRB1*12:01 DRB1*14:01	MHC II	235	250			
166	IPFAMQMAYRFNGIG	DQB1*04:02 DQB1*05:03 DRB1*12:01 DRB1*14:01 DRB1*15:01	MHC II	895	910			
167	KRISNCVADYSVLYN	DQB1*02:01 DQB1*02:02 DRB1*03:01	MHC II	355	370			
168	LKPFERDISTEIYQA		MHC II	460	475			
169	AENSVAYSNNSIAIP	DQB1*03:01 DRB1*15:01	MHC II	700	715			Naïve
170	TNFTISVTTEILPVS	DQB1*02:02 DQB1*06:03 DRB1*07:01 DRB1*14:01	MHC II	715	730			Naïve, & Vaccinated

Supplementary Table S6.2. Donor characteristics and number of PBMCs stimulated per T cell peptide epitope. The count of peripheral blood mononuclear cells (PBMCs) stimulated in each reaction was normalised across donor immune status of Naïve, Vaccinated or Naturally Infected, but varied between individual donors

Donor number	HLA type				PBMCs / Stimulation (x10^5)		
	HLA A		HLA B		Naïve	Vaccinated	Naturally infected
1	A*24:02	A*30:01	B*07:02	B*13:02	0.68	0.68	0.68
2	A*02:01	A*32:01	B*51:01	B*51:01	0.70	0.70	0.70
3	A*01:01	A*32:01	B*08:01	B*27:08	0.34	0.34	0.34
4	A*24:02	A*30:01	B*07:02	B*13:02	0.73	0.73	0.73
5	A*11:01	A*32:01	B*51:06	B*51:07	0.68	0.68	0.68
6	A*02:01	A*32:01	B*51:01	B*51:01	1.15	1.15	1.15
7	A*01:01	A*32:01	B*08:01	B*27:08	0.98	NA	NA
8	A*01:01	A*33:03	B*13:02	B*44:03	0.78	0.78	NA
9	A*01:01	A*30:04	B*08:01	B*27:05	0.97	0.97	NA
10	A*02:01	A*03:01	B*44:02	B*51:01	NA	1.02	1.02
11	A*01:01	A*11:01	B*27:05	B*35:03	NA	0.60	0.60

Supplementary Table S6.3. Immunoreactive peptide epitopes and previously reported immunogenicity. Epitope immunoreactivity is presented increased *Interferon gamma* (*IFN-γ*) expression following peptide epitope stimulation relative to media-only stimulation. Data are provided for naïve, vaccinated, and naturally infected groups. Cells display Fold Change (ΔΔCt) *IFN-γ* expression and the identification number of the reactive donor (Donor ID) when ΔΔCt > 2 (Shaded Grey). A selected citation from the literature is provided when the peptide epitope has been found to be immunoreactive following stimulation of human T cells in the specific group [Reference]. When no data is available, or epitope was not immunoreactive, no reference is provided [Nil]. The HLA-allele the epitope binds to with highest affinity, and the sum of epitope specific references on the Immune Epitope Database (IEDB) inclusive of negative assays are shown.

ID	Peptide	HLA allele (supertype)	ΔΔCt (Donor ID) [Reference][+]			IEDB references*	Summary of literature
			Naïve	Vaccinated	Naturally infected		
1	HLMSFPQSA	A*02:01 (A2)	2.93 (8) [Nil]	- - [Nil]	- - [125]	10	Immunoreactive in the naturally infected [125]. Exhibits high homology to the tumour-associated epitope LLWSFQTSA, which is immunoreactive in the healthy [618]. Pre-existing epitope-specific T cells were identified in the naïve [602].
2	YLQPRTFLL	A*02:01 (A2)	- - [619]	4.50 (8) [620]	- - [125]	61	Highly immunodominant epitope [621, 622] that is immunoreactive in the naïve [619] and elicits a robust response following vaccination [620], although not universally [597]. Can readily bind to several common HLA-C alleles [623].
3	VVFLHVTYV	A*02:03 (A2)	- - [624]	- - [125]	2.94 (2) [125]	27	Sub-dominant epitope elicits responses in the naturally infected [596, 625, 626], and following vaccination [580, 624]. Pre-existing epitope-specific T cells have been identified in the naïve [602].
5	RLQSLQTYV	A*02:01 (A2)	2.20 (1) [622]	3.24, 2.20 (3, 1) [627]	- - [125]	30	Immunodominant S-protein epitope [622]. Immunoreactive in the naïve, but relatively rarely [622]. Has been found to elicit a response following vaccination [620]. Immunogenicity has been linked to positive patient outcomes [628].

ID	Peptide	HLA allele (supertype)	ΔΔCt (Donor ID) [Reference][+]			IEDB references*	Summary of literature
			Naïve	Vaccinated	Naturally infected		
6	YQDVNCTEV	A*02:06 (A2)	- - [Nil]	2.86 (3) [Nil]	2.06 (3) [125]	7	Mutated in all commonly circulating SARS-CoV2 variants [629]. Pre-existing epitope-specific T cells have been identified in the naïve [602], however was not immunoreactive following vaccination [597].
7	SIIAYTMSL	A*02:06 (A2)	- - [619]	2.11 (1) [620]	- - [125]	28	Immunoreactive in the vaccinated and naturally infected [125, 620], also in the naïve [619]. Pre-existing epitope-specific T cells were identified in the naïve [602].
8	GLTVLPPLL	A*02:01 (A2)	2.14 (8) [Nil]	- - [Nil]	- [125]	6	Has been found to be immunoreactive in convalescent COVID-19 patients. [125]. No specific-clonal prevalence has been identified in T cells of the unexposed [602].
10	VLNDILSRL	A*02:01 (A2)	2.57 (8) [594]	2.78 (1) [580]	- - [568]	36	Sub-dominant epitope in the naturally infected [568]. In 2009, this epitope was identified as immunoreactive in SARS-CoV1 naïve donors [595] and is relatively highly conserved among other coronaviruses, including SARS-CoV2. When tested recently in the naïve, this epitope elicited a response [594] and a similar frequency of immunoreactive CD8^{+} T cells were found between naïve and convalescent donors [630]. In contrast, others have also found no immunoreactive in the naïve [596] and no specific T cell clonal prevalence in the unexposed [602]. This epitope is immunoreactive in various vaccination strategies [580], but not universally [597].
13	DISGINASV	A*68:02 (A2)	- - [Nil]	- - [Nil]	2.14 (3) [Nil]	0	Is within a CD4^{+} epitope LGDISGINASVVNIQ that has been found to be immunogenic within convalescent patients [631]. But no immunogenicity data is available in the literature as a standalone CD8^{+} epitope.

ID	Peptide	HLA allele (supertype)	ΔΔCt (Donor ID) [Reference][+]			IEDB references*	Summary of literature
			Naïve	Vaccinated	Naturally infected		
14	KIADYNYKL	A*02:06 (A2)	2.51 (1) [596]	2.11 (1) [632]	- - [633]	16	Despite non-perfect homology this epitope may provide cross-species reactivity to other endemic coronaviruses [634]. Found to be immunoreactive in young convalescent patients but not old convalescent patients [633]. Is immunoreactive in the naïve [596] and following vaccination [632], but not universally [597].
16	ALNTLVKQL	A*02:03 (A2)	2.33 (8) [595]	- [623]	- [628]	16	In 2009, this epitope was identified as immunoreactive in SARS-CoV1 naïve donors [595]. Sporadic responses identified it as subdominant following infection [622], while immunogenicity is linked to positive patient outcomes [628]. Can bind to HLA-C alleles to elicit potent immunoreactivity following vaccination [623].
26	NSFTRGVYY	A*68:01 (A3/11)	7.67 (8) [Nil]	- [Nil]	- [125]	4	Sporadic responses identified this subdominant epitope following infection [622]. No specific information is available regarding immunoreactivity in the naïve. Multiple studies found this epitope was not immunoreactive following vaccination [635, 636].
29	GVYFASTEK	A*68:01 (A3/11)	- [Nil]	- [620]	2.05 (3) [125]	11	Has been described as an immunodominant [125] and subdominant [637] epitope in convalescent patients [626]. Has been found to elicit a response following vaccination [620]. No data is available on immunoreactivity in the naïve.
31	GVYYPDKVFR	A*31:01 (A3/11)	5.42, 3.08 (2, 8) [Nil]	- [Nil]	- [125]	3	Immunoreactive in convalescent patients [125]. The epitope 'GVYYPDKVF' is immunoreactive in various vaccination strategies [580]. No data is available on full epitope immunoreactivity in the naïve or vaccinated.
33	GVYYHKNNK	A*03:01 (A3/11)	17.06 (2) [Nil]	- [632]	- [125]	8	Immunoreactive in convalescent patients [125], and following vaccination [632]. No specific information is available regarding immunoreactivity in the naïve.

ID	Peptide	HLA allele (supertype)	ΔΔCt (Donor ID) [Reference][+]			IEDB references*	Summary of literature
			Naïve	Vaccinated	Naturally infected		
35	RASANLAATK	A*03:01 (A3/11)	- - [Nil]	2.90 (1) [620]	- - [125]	4	Immunoreactive in convalescent patients [125] and following vaccination [620]. No specific information is available regarding immunoreactivity in the naïve.
37	HVTYVPAQEK	A*68:01 (A3/11)	- - [Nil]	2.80 (1) [Nil]	- - [125]	1	Immunoreactive in convalescent patients [125]. No data is available on immunoreactivity in the naïve or vaccinated.
41	DGVYFASTEK	A*68:01 (A3/11)	2.97 (8) [Nil]	- - [Nil]	- - [125]	1	Immunoreactive in convalescent patients [125]. No data is available on immunoreactivity in the naïve or vaccinated.
42	QTNSPRRAR	A*31:01 (A3/11)	- - [Nil]	- - [Nil]	2.68 (3) [125]	3	Immunoreactive in convalescent patients [125]. Was found to not be immunoreactive following adenovirus vector vaccination [624].
43	SVYAWNRKR	A*31:01 (A3/11)	4.62 (1) [Nil]	2.16 (1) [Nil]	- - [125]	7	Immunoreactive in convalescent patients [125]. Did not elicit a response following mRNA vaccination [620]. No data is available on immunoreactivity in the naïve.
48	EYVSQPFLM	A*24:02 (A24)	2.33 (8) [Nil]	- - [Nil]	- - [125]	7	Has been identified as immunoreactive in convalescent patients [125], in multiple studies [638]. Did not elicit a response following mRNA vaccination [639]. No studies have tested the immunoreactivity of this epitope in naïve patients

241

ID	Peptide	HLA allele (supertype)	ΔΔCt (Donor ID) [Reference][+]			IEDB references*	Summary of literature
			Naïve	Vaccinated	Naturally infected		
49	VYSSANNCTF	A*24:02 (A24)	3.29 (1) [Nil]	2.37 (1) [639]	- - [125]	7	Immunoreactive in convalescent patients [125], and elicited a response following mRNA vaccination [639]. Has been identified as an epitope with relatively high homology to other endemic coronaviruses [640].
50	IYQTSNFRV	A*24:02 (A24)	2.60 (1) [Nil]	- - [Nil]	- - [125]	6	Has been identified as immunoreactive in convalescent patients [125], in multiple studies [638]. Did not elicit a response following mRNA vaccination [639]. No data is available on immunoreactivity in the naïve.
52	HWFVTQRNF	A*24:02 (A24)	- - [Nil]	6.21 (11) [Nil]	3.49 (6) [125]	6	Has been identified as immunoreactive in convalescent patients [125], in multiple studies [638]. Did not elicit a response following mRNA vaccination [639]. No data is available on immunoreactivity in the naïve.
54	VFVSNGTHWF	A*24:02 (A24)	- - [Nil]	- - [639]	2.91 (3) [125]	3	Immunoreactive in convalescent patients [125], and following mRNA vaccination [639]. No data is available on immunoreactivity in the naïve. Contains the epitope 'FVSNGTHWF' which is immunoreactive following vaccination [580].
56	RFDNPVLPF	A*24:02 (A24)	- - [Nil]	- - [Nil]	2.17 (3) [125]	10	Has been identified as immunoreactive in convalescent patients [125], in multiple studies [626], but did not elicit a response following mRNA vaccination [639]. Has been identified an epitope with very low homology to other coronaviruses [640].
57	RVYSTGSNVF	A*24:02 (A24)	2.60 (1) [596]	2.51 (1) [639]	- - [125]	4	This epitope has been found to be immunoreactive in the naïve [596], following mRNA vaccination [639], and in convalescent patients [125].

ID	Peptide	HLA allele (supertype)	ΔΔCt (Donor ID) [Reference]+			IEDB references*	Summary of literature
			Naïve	Vaccinated	Naturally infected		
58	YYHKNNKSW	A*23:01 (A24)	3.01 (1) [Nil]	- - [Nil]	- - [125]	7	A high-order nullomer (*i.e.,* a rarely occurring natural epitope) that binds strongly to eight common HLA and facilitates rapid HLA-Peptide processing (*i.e.,* TAP transport and protease action) [641]. Found to have immunoreactivity in convalescent patients [125], while none was identified following vaccination [639]. No data is available on immunoreactivity in the naïve.
62	TYVPAQEKN F	A*24:02 (A24)	2.39 (3) [Nil]	- - [Nil]	- - [596]	4	No specific study demonstrating immunoreactivity in the naïve, but the peptide has been identified as having a relatively higher homology to other endemic coronaviruses [640], and induces responses in the convalescent [596]. All IEDB references report no immunogenicity following natural infection [642].
65	VYYPDKVF	A*24:02 (A24)	2.37 (1) [Nil]	- - [Nil]	- - [125]	1	Immunoreactive in convalescent patients [125]. No data is available on immunoreactivity in the naïve or the vaccinated.
68	SFPQSAPHGV VF	A*24:02 (A24)	- - [Nil]	4.29 (11) [Nil]	- - [125]	4	Immunoreactive in convalescent patients [125], No data is available on immunoreactivity in the naïve or the vaccinated. Contains the epitope 'QSAPHGVVF' which is immunoreactive in various vaccination strategies [580].
69	YFPLQSYGF	A*29:02 (A24)	- - [Nil]	- - [636]	4.13 (3) [643]	15	Relatively well characterised A24 epitope [593] that has been identified as an immunodominant epitope in convalescent [643] and vaccinated individuals [636].
71	KPFERDIST	B*07:02 (B7)	2.52 (1) [Nil]	- - [Nil]	- - [125]	0	Immunoreactive in convalescent patients [125]. No data is available on immunoreactivity in the naïve or the vaccinated.

ID	Peptide	HLA allele (supertype)	ΔΔCt (Donor ID) [Reference]+			IEDB references*	Summary of literature
			Naïve	Vaccinated	Naturally infected		
78	QIPFAMQMAY	B*35:01 (B7)	- - [Nil]	- - [Nil]	2.43 (1) [125]	1	Immunoreactive in convalescent patients [125]. No data is available on immunoreactivity in the naïve or the vaccinated.
83	LTDEMIAQY	B*35:01 (B7)	- - [596]	- - [620]	2.70 (1) [626]	20	Relatively well characterised epitope [593], which has been found to induce a response in convalescent patients [626], in multiple studies [125, 593]. Can elicit a response following mRNA vaccination [620], and in the naïve [596]. Although, no epitope specific T cells were identified in the unexposed [602].
85	TSNQVAVLY	B*35:01 (B7)	- - [Nil]	2.38 (3) [620]	2.45 (2) [125]	7	Has been identified as immunoreactive in convalescent patients [125], and following vaccination [620]. No data is available on immunoreactivity in the naïve; however, no epitope specific T cells were identified in the unexposed [602].
86	LPPLLTDEM	B*35:01 (B7)	- - [Nil]	2.44 (2) [580]	2.41 (1) [125]	8	Immunoreactive in convalescent patients [125], and the vaccinated [580], across various vaccination strategies [580]. No data is available on immunoreactivity in the naïve.
87	IPTNFTISV	B*51:01 (B7)	2.60 (1) [Nil]	2.51 (10) [Nil]	- - [125]	8	Immunoreactive in convalescent patients [125]. Despite carrying an alpha variant defining mutation it's still likely to elicit a response [644]. While pre-existing epitope-specific T cells were identified in the naïve [602], no response from naïve donors has been reported [644].
91	QPTESIVRF	B*51:01 (B7)	- - [Nil]	- - [645]	5.09 (1) [125]	7	Has been found to elicit a response following mRNA vaccination [620], in several studies [645], and is immunoreactive in convalescent patients [125].

ID	Peptide	HLA allele (supertype)	ΔΔCt (Donor ID) [Reference][+]			IEDB references*	Summary of literature
			Naïve	Vaccinated	Naturally infected		
92	SANNCTFEY	B*35:01 (B7)	- - [Nil]	8.829 (10) [636]	- - [125]	4	Immunoreactive in convalescent patients [125], and the vaccinated [636]. Has the capacity to bind to many HLA alleles [646]. No epitope specific T cells were identified in the unexposed [602].
95	DAVRDPQTL	B*51:01 (B7)	- - [Nil]	- - [Nil]	2.85 (1) [125]	2	Immunoreactivity was identified in convalescent patients [125].
102	QPRTFLLKY	B*35:01 (B7)	- - [Nil]	3.97 (5) [Nil]	3.22, 2.45 (1, 3) [Nil]	2	This epitope was not immunoreactive in convalescent patients [643], or in vaccinated mice [647].
108	VQPTESIVRF	B*53:01 (B7)	2.83 (1) [Nil]	- - [Nil]	2.15 (1) [648]	1	Identified as immunoreactive in convalescent patients following breakthrough infections [648]. No data is available on immunoreactivity in the naïve or in the vaccinated.
114	IPFAMQMAY	B*35:01 (B7)	- - [Nil]	- - [620]	2.01 (1) [125]	7	Has been found to be immunoreactive in the convalescent [125], in multiple studies [582, 648], and the vaccinated [620]. No data is available on immunoreactivity in the naïve.
119	KIYSKHTPI	B*08:01 (B8)	- - [Nil]	- - [Nil]	2.13 (3) [125]	3	Immunoreactive in convalescent patients [125]. No data is available on immunoreactivity in the naïve or the vaccinated.
122	DLLFNKVTL	B*08:01 (B8)	- - [Nil]	- - [Nil]	3.77 (1) [Nil]	1	This epitope was found to not be immunoreactive following natural infection in one study [643]. No data is available on immunoreactivity in the naïve or the vaccinated.

ID	Peptide	HLA allele (supertype)	ΔΔCt (Donor ID) [Reference][+]			IEDB references*	Summary of literature
			Naïve	Vaccinated	Naturally infected		
123	LLALHRSYL	B*08:01 (B8)	- - [Nil]	- - [649]	3.52 (1) [Nil]	3	Epitope was identified as immunogenic following immunisation with a trailed peptide vaccine that generated strong T cell responses [649]. Pre-existing epitope-specific T cells were identified in the naïve [602]. No immunoreactivity data is available in the naïve or the naturally infected.
131	SAIGKIQDSL	B*08:01 (B8)	- - [Nil]	3.70 (11) [Nil]	- - [Nil]	0	No immunoreactivity data is available and there are no results in IEDB
133	DLPQGFSAL	B*08:01 (B8)	2.80 (3) [Nil]	- - [Nil]	- - [Nil]	1	Peptide aligns with sequences in the human proteome [650]. Epitope was found to not be immunoreactive following inactivated virus vaccination [597]. No immunoreactivity data has been recorded on IEDB.
135	NSPRRARSV	B*08:01 (B8)	- - [Nil]	2.73 (1) [Nil]	2.41 (2) [Nil]	0	In the BriSΔ variant of SARS-CoV2 this sequence was replaced with a single isoleucine (I), which significantly reduced transmissibility by abrogating S1/S2 cleavage [651]. No immunoreactivity data has been recorded on IEDB.
136	DILSRLDKV	B*08:01 (B8)	- - [Nil]	2.71 (1) [Nil]	- - [Nil]	0	No immunoreactivity data is available and there are no results in IEDB.
142	VVNQNAQAL	A*26:01 (Other)	- - [Nil]	7.56 (11) [580]	- - [Nil]	2	Immunoreactive following various vaccination strategies [580]. No immunoreactivity data is available in the naïve or the naturally infected.

ID	Peptide	HLA allele (supertype)	ΔΔCt (Donor ID) [Reference][+]			IEDB references*	Summary of literature
			Naïve	Vaccinated	Naturally infected		
143	CVADYSVLY	A*26:01 (Other)	6.50 (9) [596]	3.51 (11) [636]	- - [125]	9	Immunoreactive in the naïve [596], following vaccination [636], and in convalescent COVID-19 patients [125].
145	LEPLVDLPI	B*40:01 (Other)	4.84 (4) [Nil]	- - [Nil]	- - [Nil]	1	T cell binding assays were positive in convalescent COVID-19 patients [652]. No data is available on epitope immunoreactivity.
147	NQKLIANQFN SAIGK	DRB1*13:0 2[#] (Class II)	- - [Nil]	7.56 (5) [Nil]	- - [Nil]	5	No assays assessing immunogenicity are reported. However, this CD4^{+} epitope is readily presented on several MHC Class II alleles [653] and contains immunogenic CD8^{+} epitopes, such as the C*03:04 epitope 'IANQFNSAI,' which was found to be immunoreactive in various vaccination strategies [580].
148	QKFNGLTVLP PLLTD	DRB1*01:0 1[#] (Class II)	3.00 (1) [Nil]	- - [Nil]	- - [Nil]	11	His epitope was found to be immunoreactive in HLA transgenic mice [654], however, no studies assessing human immunogenicity are reported. This peptide is readily presented on several MHC Class II alleles [653], and contains potentially immunoreactive epitopes such as A2 epitope 'NGLTVLPPL' [597].
149	SSNFGAISSV LNDIL	DRB1*01:0 1[#] (Class II)	- - [Nil]	- - [655]	3.51 (5) [655]	7	Identified as readily presented on several MHC Class II alleles [653]. Found to be immunoreactive in the vaccinated and subsequently convalescent [655]. This response was preserved when infected with omicron despite the mutation [655].
152	LMDLEGKQG NFKNLR	(Class II)	- - [Nil]	- - [580]	2.03 (4) [125]	8	Have been identified as immunoreactive epitopes in vaccinated [580] and convalescent patients [125].

ID	Peptide	HLA allele (supertype)	ΔΔCt (Donor ID) [Reference][+]			IEDB references*	Summary of literature
			Naïve	Vaccinated	Naturally infected		
154	NLLLQYGSFC TQLNR	DQB1*05:03[#] (Class II)	- - [Nil]	- - [580]	2.59 (3) [577]	18	Well characterized immunodominant Class II epitope, found to be immunoreactive following vaccination [580, 620] and infection [577, 656].
155	CEFQFCNDPF LGVYY	DQB1*05:02[#] (Class II)	- - [657]	- - [656]	2.00 (1) [656]	12	Well characterized sub-dominant Class II epitope, found to be immunoreactive following vaccination and infection [656], and in the naïve [657]. A2 epitope 'CNDPFLGVYY' was found to not be immunoreactive following inactivated virus vaccination [597]; and A2 epitope 'FCNDPFLGV' was found to be immunoreactive in various vaccination strategies [580].
156	SSANNCTFEY VSQPF	(Class II)	3.72 (1) [Nil]	- - [Nil]	- - [125]	17	Found to be immunoreactive following infection [125] in multiple studies [648, 656]. Was found not immunoreactive following vaccination [656]. Contains the A1 epitope 'SSANNCTFEY' shown to have immunoreactivity in the naïve [596].
163	KHTPINLVRD LPQGF	DRB1*03:01[#] (Class II)	- - [Nil]	- - [656]	5.08 (1) [620]	9	Found to be immunoreactive following vaccination [656] and infection [577, 620]. Was found not immunoreactive in the naïve [577].
164	LPQGFSALEP LVDLP	DQB1*02:02[#] (Class II)	2.17 (1) [Nil]	- - [656]	7.47 (1) [125]	9	Epitope shares pentapeptides with human proteins linked to oogenesis, placentation, and/or decidualization [658]. B7:02 epitope 'LPQGFSALEPL' and B8:01 epitope 'LPQGFSAL' have both been shown to have immunoreactivity in the naïve [596]. Immunoreactive following vaccination [656] and infection [125].
169	AENSVAYSN NSIAIP	DQB1*03:01[#] (Class II)	2.32 (7) [Nil]	- - [Nil]	- - [125]	15	Identified as immunoreactive following infection [125]. Found not to be immunoreactive following vaccination [656].

ID	Peptide	HLA allele (supertype)	ΔΔCt (Donor ID) [Reference][+]			IEDB references*	Summary of literature
			Naïve	Vaccinated	Naturally infected		
170	TNFTISVTTEI LPVS	DQB1*02:02 [#] (Class II)	2.82 (1) [Nil]	2.14 (9) [580]	- - [125]	10	Well characterised immunodominant Class II epitope immunoreactive following vaccination [656] and infection [125, 580]. Contains the A2 epitope 'FTISVTTEI' which was immunoreactive in various immunisation strategies [580].
	Positive Stimulations		30 / 1500	26 / 1674	29 / 1360		
	Positive Epitopes		29 / 170	25 / 170	28 / 170		

[+] Selected reference demonstrating immunoreactivity within a specific donor group. * Collected 2024.07.23 [#] High affinity for multiple class II alleles

Supplementary Table S6.4. Categorical analysis of donor specific SARS-CoV2 S-protein epitope immunoreactivity following vaccination and natural infection. The immunoreactivity from donors SARS-CoV-2 S-protein naïve (Naïve), following COVID-19 vaccination (Vaccinated), and following infection with SARS-CoV2 (Naturally Infected) following S-protein peptide epitope stimulation. Immunoreactivity was quantified with high-throughput RT-qPCR (HTS-RT-qPCR) determining IFN-γ expression fold-change ($\Delta\Delta Ct$). Tested were the relative number of reactive stimulations ($\Delta\Delta Ct > 2$; Positive) to non-reactive stimulations ($\Delta\Delta Ct < 2$; Negative) across classes of immune status.

Donor	Immune status	Positive	Negative	Total	*P* value *vs.* naive	*P* value *vs.* vaccination
1	Naive	15	155	170	-	-
	Vaccinated	11	159	170	0.5412	-
	Naturally infected	13	157	170	0.8440	0.8328
2	Naive	2	168	170	-	-
	Vaccinated	1	169	170	>0.9999	-
	Naturally infected	3	167	170	>0.9999	0.6228
3	Naive	2	168	170	-	-
	Vaccinated	3	167	170	>0.9999	-
	Naturally infected	10	160	170	0.0353	0.0861
4	Naive	1	169	170	-	-
	Vaccinated	0	170	170	>0.9999	-
	Naturally infected	1	169	170	>0.9999	>0.9999
5	Naive	0	170	170	-	-
	Vaccinated	2	168	170	0.4985	-
	Naturally infected	1	169	170	>0.9999	>0.9999
6	Naive	0	170	170	-	-
	Vaccinated	0	170	170	>0.9999	-
	Naturally infected	1	169	170	>0.9999	>0.9999
7	Naive	1	169	170	-	-
	Vaccinated	-	-	-	-	-

Donor	Immune status	Positive	Negative	Total	*P* value *vs.* naive	*P* value *vs.* vaccination
	Naturally infected	-	-	-	-	-
8	Naive	8	162	170	-	-
	Vaccinated	1	169	170	0.0366	-
	Naturally infected	-	-	-	-	-
9	Naive	1	169	170	-	-
	Vaccinated	1	169	170	>0.9999	-
	Naturally infected	-	-	-	-	-
10	Naive	-	-	-	-	-
	Vaccinated	2	168	170	-	-
	Naturally infected	0	170	170	-	0.4985
11	Naive	-	-	-	-	-
	Vaccinated	5	165	170	-	-
	Naturally infected	0	170	170	-	0.0607

Supplementary Table S6.5. Categorical analysis of HLA restriction grouped SARS-CoV2 S-protein epitope immunoreactivity following vaccination and natural infection. The combined (n=12) immunoreactivity from donors SARS-CoV2 S-protein naïve (Naïve), following COVID-19 vaccination (Vaccinated), and following infection with SARS-CoV2 (Naturally infected) following S-protein peptide epitope stimulation. Immunoreactivity was quantified with high-throughput RT-qPCR (HTS-RT-qPCR) determining IFN-γ expression fold-change ($\Delta\Delta Ct$). Tested were the relative number of reactive stimulations ($\Delta\Delta Ct > 2$; Positive) to non-reactive stimulations ($\Delta\Delta Ct < 2$; Negative) across classes of immune status, considering the predicted peptide HLA restriction (Peptide HLA).

Peptide HLA	Status	Positive	Negative	*P* value* *vs.* naive	*P* value* *vs.* post-vaccination
A2	Naive	6	201	-	-
	Vaccinated	7	224	>0.9999	-
	Naturally infected	3	182	0.5091	0.5226
A3/11	Naive	6	201	-	-
	Vaccinated	3	227	0.3185	-
	Naturally infected	2	182	0.2909	>0.9999
A24	Naive	7	200	-	-
	Vaccinated	4	226	0.3631	-
	Naturally infected	4	180	0.5510	>0.9999
B7	Naive	3	419	-	-
	Vaccinated	5	464	0.7284	-
	Naturally infected	10	365	0.0462	0.1139
B8	Naive	1	206	-	-
	Vaccinated	3	227	0.6254	-
	Naturally infected	4	180	0.1920	0.7048
Other	Naive	2	52	-	-
	Vaccinated	2	58	>0.9999	-
	Naturally infected	0	48	0.4968	0.5016

Peptide HLA	Status	Positive	Negative	*P* value* *vs.* naive	*P* value* *vs.* post-vaccination
Class II	Naive	5	220	-	-
	Vaccinated	2	248	0.2640	-
	Naturally infected	6	194	0.1469	0.7622
HLA - A	Naive	21	654		
	Vaccinated	16	735	0.2491	
	Naturally infected	9	592	0.0650	0.4240
HLA - B	Naive	4	625		
	Vaccinated	8	691	0.3936	
	Naturally infected	14	545	0.0149	0.0675
HLA A *vs.* B	Naïve *vs.* naïve			*P* = 0.0010	
	Vaccinated *vs.* vaccinated			*P* = 0.1545	
	Naturally infected *vs.* naturally infected			*P* = 0.2921	

Supplementary Table S6.6. Categorical analysis of homology of immunoreactive SARS-CoV2 S-protein peptide epitopes following vaccination and natural infection. The homology of immunoreactive epitopes ($\Delta\Delta Ct > 2$) were tested relative to the number of epitopes with complete homology (100% Homology) and those containing at least one variable amino acid, in at least one SARS-CoV2 variant (<100% Homology) across combined (n=12) donors of various immune statuses. Epitopes that were positive across multiple donors of the same immune status were counted once.

Immune status	Homology < 100%	100% = Homology	Total	Homology < 100% (%)	*P* value *vs.* naive	*P* value *vs.* vaccination	*P* value *vs.* naturally infected
Total peptides	38	132	170	22.3%	0.6336	0.3154	0.1449
Naïve	8	21	29	27.6%			
Vaccinated	8	17	25	32.0%	0.7718		
Naturally infected	10	17	27	37.0%	0.5695	0.7756	

Supplementary Table S6.7. Categorical analysis of immunoreactive epitope localization within SARS-CoV2 S-protein domains following vaccination and natural infection. The location of immunoreactive epitopes ($\Delta\Delta Ct > 2$) were tested relative to the number of epitopes inside and outside of domains across combined (n=12) donors of various immune statuses. Tested were Sub-Domain 1 (1-681 aa), and Sub-Domain 2 (686-1273 aa), and the, Receptor Binding Motif (438-508 aa), the RAAR Motif (682-685aa), the S1/S2 Cleavage Site (672-709 aa), the Fusion Peptide (788-806 aa), the Internal Fusion Peptide (816-833 aa), Heptad Repeat 1 (981-983 aa), Heptad Repeat 2 (1162-1203 aa), and peptide epitopes that were in do discreetly defined regions (No Region).

Domain	Immune status	Epitopes in domain	Epitopes outside domain	Total	In domain (%)	P value vs. naive	P value vs. vaccination
Sub Domain 1	Naïve	20	10	30	66.6%	-	
	Vaccinated	11	15	26	42.3%	0.1056	-
	Naturally infected	18	11	29	62.1%	0.1811	0.7892
Sub Domain 2	Naïve	10	20	30	33.3%	-	
	Vaccinated	15	11	26	57.7%	0.1056	-
	Naturally infected	11	18	29	37.9%	0.1811	0.7892
Receptor Binding Motif	Naïve	1	29	30	3.3%	-	
	Vaccinated	0	26	26	0.0%	>0.9999	-
	Naturally infected	1	28	29	3.4%	>0.9999	>0.9999
RAAR Motif	Naïve	0	30	30	0.0%	-	
	Vaccinated	0	26	26	0.0%	>0.9999	-
	Naturally infected	0	29	29	0.0%	>0.9999	>0.9999
S1/S2 Cleavage Site	Naïve	1	29	30	3.3%	-	
	Vaccinated	2	24	26	7.7%	0.5920	-
	Naturally infected	2	27	29	6.9%	0.6120	>0.9999

Domain	Immune status	Epitopes in domain	Epitopes outside domain	Total	In domain (%)	*P* value *vs.* naive	*P* value *vs.* vaccination
Fusion Peptide	Naïve	0	30	30	0.0%	-	
	Vaccinated	0	26	26	0.0%	>0.9999	-
	Naturally infected	0	29	29	0.0%	>0.9999	>0.9999
Internal Fusion Peptide	Naïve	0	30	30	0.0%	-	
	Vaccinated	0	26	26	0.0%	>0.9999	-
	Naturally infected	1	28	29	3.5%	0.4915	>0.9999
Heptad Repeat 1	Naïve	2	28	30	0.06%	-	
	Vaccinated	4	22	26	15.4%	0.4006	-
	Naturally infected	1	28	29	3.5%	>0.9999	0.1777
Heptad Repeat 2	Naïve	0	30	30	0.0%	-	
	Vaccinated	0	26	26	0.0%	>0.9999	-
	Naturally infected	1	28	29	3.5%	0.4915	>0.9999
No Region	Naïve	8	22	30	26.7%	-	
	Vaccinated	13	13	26	50.0%	0.0990	-
	Naturally infected	10	19	29	34.5%	0.5796	0.2832

Chapter 7: Discussion

7.1 General discussion

For many diseases, effective vaccines which can provide long-term protection still do not exist. *Plasmodium* spp., the parasites which cause the disease malaria, have proven to be particularly challenging to develop effective vaccines against. Conversely, while safe and effective vaccines against the SARS-CoV2 virus, the cause of the COVID-19 pandemic, were developed extremely rapidly, the long-term efficacy of those vaccines is challenged by very short-term efficacy necessitating repeated booster vaccinations. Understanding cellular immunity, specifically the T cell response to infection and vaccination, is expected to provide valuable insights to inform the development of effective vaccines which provide long-term sustained protection. However, developing a comprehensive understanding of cellular immunity is challenging especially when the number of potential T cell peptide epitopes within a pathogen is very high, such as for complex eukaryotes such as *Plasmodium*. Therefore, enhancing the efficiency, sensitivity, and throughput of epitope screening is crucial for advancing T cell research. Especially as clinically relevant samples, such as human PBMCs, are often limited. The work presented in this doctoral thesis sought to develop a more detailed understanding of T cell epitope immunogenicity and immunodominance, and to generate an immunodominance hierarchy of T cell epitopes. It builds on work previously conducted by the Doolan laboratory, to identify immunoreactive *P. falciparum* T cell epitopes, characterize the host immune response, and test T cell antigens for protection against *Plasmodium* sporozoite challenge.

Accordingly, the first study presented in this thesis (**Chapter 2**) focused on the optimization of a molecular-based technique to detect peptide epitope stimulatory responses from very low numbers of PBMCs [356]. That study optimised an RT-qPCR protocol to detect IFN-γ mRNA expression changes from human PBMCs and demonstrated a high correlation between IFN-γ mRNA and protein quantification. This protocol had single-cell analytical sensitivity and a diagnostic sensitivity which could detect an epitope response hierarchy from as few as 1×10^4 PBMCs. Therefore, this optimized protocol provided a robust alternative to protein-based assays when measuring changes in cytokine mRNA expression in low numbers of PBMCs in response to peptide epitope *in vitro* stimulation. However, widespread application of this protocol remained limited by relatively high costs and was not optimised for high-throughput screening. Therefore, in the second study presented in this thesis (**Chapter 3**), the above-mentioned protocol was optimised as a high-throughput screening (HTS) tool [511]. This study initially miniaturised and cost-optimised the assay for each stage, in a 96-well or 384-well

format. Using peptide epitope stimulation responses, we confirmed that the protocol had high throughput screening uniformity and meet signal variance testing standards. Furthermore, following HTS-optimisation, we demonstrated the assay retained its single-cell analytical sensitivity, and when measuring IFN-γ mRNA expression following stimulation, the assay had an accuracy of 90.8% relative to IFN-γ protein expression.

Future optimisation of the HTS-RTqPCR screening assay may include further cost optimisation, integration into robotic automation technologies, expansion into 1536-well formats, or inclusion of multiplex capacity to detect additional surrogate markers of immunity. The utility of this assay is broad. Alongside establishing of immunodominance hierarchies for various disease, this assay could track epitope immunoreactivity over time, profile personalised T-cell responses to pathogen or cancer antigens, study immune heterogeneity across populations and generally facilitate peptide-immunoreactivity studies where sample is limited, and cost is an important consideration. Nevertheless, this assay remains limited by a reliance on detecting *IFN-γ* mRNA expression, which does not perfectly correlate with IFN-γ protein production. Investigating the cause of variation between transcriptomic IFN-γ responses and IFN-γ protein production following antigenic stimulation may provide further insight into T cell biology.

The third study in this thesis (**Chapter 4**) was concerned with the optimisation of a murine model to evaluate host T cell responses and parasite challenge protection following immunisation with a recombinant adenovirus vaccine platform [659]. The DNA-adenovirus IV 'Prime-Target' immunization model was selected as adenovirus vaccinations have a cold chain deployment of 4°C and, therefore, are suitable for deployment in malaria endemic regions. Additionally, the 'Prime-Target' vaccination strategy had been found to induce the formation of a robust population of tissue resident memory T cells (T_{RM}). This study found that many host reference genes in common use in RT-qPCR assays were influenced by both parasite challenge and vaccination strategy. To address this variability, this study identified a set of stable reference genes suitable for relative quantification of host-liver parasite burden. Additionally, this study defined a threshold of 'partial-protection' and developed a strategy to simultaneously quantify matched host cytokine mRNA expression responses and parasite burden. Therefore, this optimized model will allow more precise definitions of partial-protection and provide an enhanced understanding of the host immune response in studies exploring antigen immunoreactivity using a recombinant adenovirus vaccine platform. Although researchers employing alternative murine models will be required to conduct specific

reference gene optimisation, this study highlight that immunisation and *Plasmodium* challenge can significantly influence endogenous host reference gene expression.

The fourth study of this thesis (**Chapter 5**) aimed to determine the immunodominance hierarchy of pre-erythrocytic *Plasmodium falciparum* antigens in Malian donors, using HTS-RT-qPCR to deconvolute immunoreactive peptides from antigen peptide pools. These antigen peptide pools had been identified previously as immunoreactive in PNG donors with malaria immunity. There were two classes of immunoreactive peptide pools assessed: i) 'cross-reactive' antigens which were immunoreactive in the malaria naïve; and ii) 'specific' antigens which were found to be immunoreactive in malaria exposed individuals. Despite attempts to optimize HTS-RT-qPCR for low precursor frequency epitope responses, only one immunoreactive peptide epitope within one cross-reactive antigen was identified as immunoreactive. The identification of immunoreactive 'Specific' antigen peptide pools in Malian PBMCs was hindered by low cell viability. By using IMPAACT protocols, enough viable Malian cells were obtained for testing. Although several Malian donors responded to stimulation, no significant difference from the media background could be found. This limited response was confirmed by ELIspot, and expansion of the study was not possible since additional samples required for in-depth comparison studies could not be obtained as a result of the COVID-19 pandemic.

The final study for this thesis therefore pivoted to investigate the immunoreactivity of peptide epitopes derived from the SARS-CoV2 Spike-protein (S-protein), in SARS-CoV2 naïve, vaccinated, and naturally infected individuals (**Chapter 6**). Immunodominant peptide epitopes were predicted *in silico* with the Immune Epitope DataBase (IEDB) and through searching the literature. Strong immunogenicity was detected in individuals who were S-protein naïve or following subsequent COVID vaccination or natural infection. Interestingly, the epitopes that were most immunoreactive following vaccination were generally not the most immunoreactive following infection. A more comprehensive study with donors matched across demographics, disease outcomes, HLA-type, and other conditions would be expected to significantly improve the impact of the collected data. Identifying an immunodominance hierarchy of T cell epitopes allows researchers to prioritise epitopes most likely to induce a long-term protective immune response, and therefore, develop more effective vaccines. Once a validated immunodominance hierarchy is established, the subsequent step is to characterise the host adaptive immune response. Once the adaptive immune response is characterised, prioritised immunoreactive

antigens could be tested in murine models for protectivity. Ultimately, this approach enables optimisation of vaccines to induce robust, long-term memory T cells

7.2 Technical pitfalls when collecting, cryopreserving, thawing, and stimulating human T-cells

7.2.1   Section introduction

Another explanation for the discrepancy between the limited immunogenicity observed in malaria-experienced Malian donors and the high immunogenicity previously reported in PNG donors may be difference in the quality of the tested PBMCs from the two populations. In the study reported in this thesis, the viability of PBMCs from Malian donors was found to be very low. Decreasing PBMC viability is generally assumed to be a stochastic process affecting all cell populations equally. However, it is plausible that T cells immunoreactive to specific *Plasmodium falciparum* peptide epitopes were overrepresented in the 'dead' fraction removed during the IMPAACT protocol's thawing process, while such immunoreactive T cells were viable in the previously tested PNG samples. Nevertheless, cell death alone cannot account for the variation observed when assessing the 'cross-reactive' peptide epitopes. Both this thesis and the previous studies reported high PBMC viability from locally recruited malaria-naïve donors. These samples were processed following standard laboratory standard operating protocols, which align with best practices. Therefore, this section of the thesis reviewed the literature to investigate the impact of potential technical variations during PBMC processing; specifically, during i) whole blood collection, ii) PBMC cryopreservation, iii) PBMC thawing, and iv) T cell stimulation, may have contributed to the variation in reported results.

The work presented in this chapter comprises a publication.

Browne, D. J., Miller, C. M., & Doolan, D. L. (2024). Technical pitfalls when collecting, cryopreserving, thawing, and stimulating human T-cells. Front Immunol, 15, 1382192. https://doi.org/10.3389/fimmu.2024.1382192

7.3 Published manuscript

Technical pitfalls when collecting, cryopreserving, thawing, and stimulating human T-cells

Running head: Pitfalls studying T cells

Daniel J. Browne[1], Catherine M. Miller[2#], Denise L. Doolan[3#*]

[1] Centre for Molecular Therapeutics, Australian Institute of Tropical Health and Medicine, James Cook University, Cairns, QLD 4878, Australia

[2] College of Medicine and Dentistry, James Cook University, Cairns, QLD 4878, Australia

[3] Institute for Molecular Bioscience, The University of Queensland, St Lucia, QLD 4067, Australia

7.3.1 Abstract

The collection, cryopreservation, thawing, and culture of peripheral blood mononuclear cells (PBMCs) can profoundly influence T cell viability and immunogenicity. Gold-standard PBMC processing protocols have been developed by the *Office of HIV/AIDS Network Coordination* (HANC); however, these protocols are not universally observed. Herein, we have explored the current literature assessing how technical variation during PBMC processing can influence cellular viability and T cell immunogenicity, noting inconsistent findings between many of these studies. Amid the mounting concerns over scientific replicability, there is growing acknowledgement that improved methodological rigour and transparent reporting is required to facilitate independent reproducibility. This review highlights that in human T cell studies, this entails adopting stringent standardised operating procedures (SOPs) for PBMC processing. We specifically propose the use of HANC's *Cross-Network PBMC Processing SOP*, when collecting and cryopreserving PBMCs, and the HANC member network *International Maternal Pediatric Adolescent AIDS Clinical Trials* (IMPAACT) *PBMC Thawing SOP* when thawing PBMCs. These stringent and detailed protocols include comprehensive reporting procedures to document unavoidable technical variations, such as delayed processing times. Additionally, we make further standardisation and reporting recommendations to minimise and document variability during this critical experimental period. This review provides a detailed overview of the challenges inherent to a procedure often considered routine, highlighting the importance of carefully considering each aspect of SOPs for PBMC collection, cryopreservation, thawing, and culture to ensure accurate interpretation and comparison between studies.

7.3.2 Introduction

T-lymphocytes (T cells) are integral components of adaptive immunity [660], and are essential for clearing infections [661], responding to vaccinations [580] or emergent tumorigenesis [662], and maintaining immune system homeostasis [663]. Given these broad and critical effector functions, T cells have been the focus of intensive research which predominantly aims to: i) characterise and compartmentalise T cell phenotypes [664, 665], and ii) understand and modulate T cell immunogenicity [666, 667]. T cells can be broadly characterised as either CD4$^+$ Helper T cells, or CD8$^+$ cytotoxic T cells [660]. CD4$^+$ T cells are crucial for regulating the immune response by releasing signalling molecules that activate, modulate, or direct other immune cells against a particular pathogen [580, 663]. Cytotoxic CD8$^+$ T cells are primarily responsible for killing dangerous self-cells, such as those infected with intracellular pathogens or cells undergoing tumorigenesis [580, 662]. Both CD4$^+$ and CD8$^+$ T cell immunogenicity is commonly studied through functional immunoassays that investigate the activation and behaviour of T cells in response to specific stimuli [356]. These experiments generally involve the *in vitro* stimulation of peripheral blood mononuclear cells (PBMCs) with antigenic peptide epitopes or cross-reactive mitogens. This mimics the *in vivo* activation of T cells, which initiates various responses including cytokine production [427], proliferation [668], or apoptosis [669]. Optimal assessment of T cell phenotypes and immunogenicity requires PBMCs that are viable, and which retain their natural *in vivo* immunogenic capabilities.

The *in vitro* loss of PBMC viability or *in vivo* T cell immunogenicity can critically impact immunological research and clinical trials [436, 670]. A notable example is the differential response of T cells when stimulated either *in vitro* or *in vivo* with the CD28 agonist antibody TGN1412 [671]. In 2006, a phase I clinical study triggered life threatening cytokine release syndrome in patients infused with TGN1412 [672]. Further studies revealed that T-cell activation by TGN1412 was dependent upon co-stimulatory signals [673], which were restored to *in vivo* conditions *in vitro* when PBMCs were pre-cultured (rested) in high densities [376, 436]. More broadly, persistent controversies in T cell research, such as inconsistencies between vaccine antigen testing and vaccine clinical trial immunogenicity [674-676], disagreements on immunodominant antigen or epitopes [677, 678], or other debated aspects of immunological responses [679], may be partly explainable by technical variation during PBMC processing.

PBMC processing involves collecting, storing, thawing, and culturing PBMCs from human donors [680]. This protocol typically involves: i) collecting peripheral blood using

venepuncture, ii) separating PBMCs from other blood components, iii) immediately experimenting on, or cryopreserving the cells, iv) thawing cryopreserved cells, and v) *in vitro* cell culture. Following the outbreak of the HIV/AIDS epidemic there was a heightened need for a globally coordinated T cell clinical trial network with a standardised PBMC processing protocol [681, 682]. In response, the *Office of HIV/AIDS Network Coordination* (HANC) established gold-standard PBMC processing standard operating procedures (SOPs), which were widely, but not universally adopted [683, 684]. The current SOPs include the HANC's *Cross-Network PBMC Processing SOP*, for collecting and cryopreserving PBMCs [685], and the HANC member network *International Maternal Pediatric Adolescent AIDS Clinical Trials* (IMPAACT) *PBMC Thawing SOP* when thawing PBMCs [686]. This review will demonstrate even relatively minor deviations from these SOPs can have profound consequences for PBMC viability and T cell immunogenicity, and indeed that many studies investigating the effect of technical variation during PBMC processing have reported contradictory results (**Supp Table S7.1**). The objective of this review is to briefly discuss the key research that has demonstrated technical variation during this process can profoundly influence cellular viability and immunogenicity (**Fig. 7.2**), highlight the challenges of comparing immunogenicity across samples exposed to variant protocols, and emphasize the need for stringent protocol standardization.
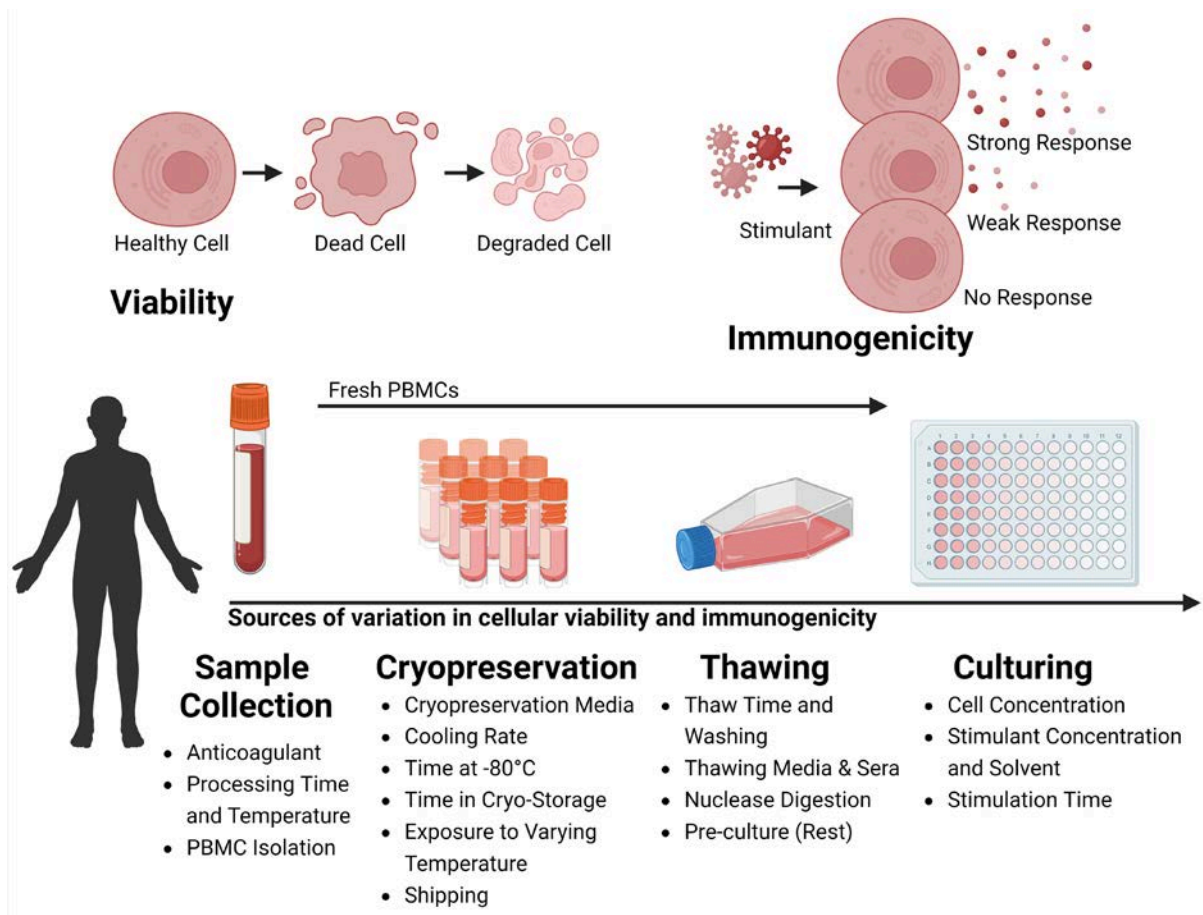
Figure 7.2. Variability factors in cellular viability and immunogenicity in sample processing. The process of collection, storage, thawing, and culturing cells collected from the peripheral blood of human donors can influence the viability and the immunogenicity of the sample. During **Sample Collection**, variability arises from the type of anticoagulant used, the time and temperature of processing, and the strategy for isolating Peripheral Blood Mononuclear Cells (PBMCs). During **Cryopreservation** variability is influenced by the choice of cryopreservation media, cooling rate, duration at -80°C before long-term storage, storage duration, temperature fluctuations during storage, and conditions during shipping. During **Thawing**, factors include thawing time, wash strategies, thawing media and sera, nuclease digestion, and whether cells are rested before experiments. During **Culturing**, the cell concentration, stimulant dose, and duration of stimulation affect outcomes. **Viability** is marked by a transition from healthy to dead cells, increasing cellular debris. **Immunogenicity**, is the ability of cells to react to stimulants like antigenic peptides or mitogens, is typically assessed through functional immunoassays measuring the immune response via the production of surrogate markers of immunity.

7.3.3 Sources of variation in cellular viability and immunogenicity

Sample collection

Choice of anticoagulant

When collecting peripheral blood for PBMC isolation, clinically convenient anticoagulant-lined vacuum-tubes are commonly used for venepuncture. Different anticoagulants, typically Ethylenediaminetetraacetic acid (EDTA), heparin, or citrate, serve specific purposes and have advantages and disadvantages relative to others (**Supp Table S7.2**) [687]. According to the HANC-SOP, it is mandatory to document the type of anticoagulant used for each sample [685]. Use of EDTA rather than heparin has been linked to diminished immunogenicity following PBMC stimulation [688]. Conversely, other studies have found no significant change of functionality between EDTA and sodium-heparin isolated PBMCs [689], nor between sodium-heparin and lithium-heparin collection [690]. Anticoagulant has been shown to not be associated with PBMC viability [689]; however, this study did note viability was statistically associated with anticoagulant when the cryopreservation of PBMCs was delayed. Taken together, these studies report a potential connection between anticoagulant and PBMC viability and functionality, and highlight the first potential technical pitfall when studying T cells: the absence of standardised or intentional anticoagulant selection.

Processing time and temperature

It is generally accepted the post-venepuncture processing time and temperature are critical parameters affecting cellular viability and T cell immunogenicity [689, 691]. However, PBMCs are routinely isolated from peripheral blood well beyond 24 hours after venepuncture, especially in clinical trials [680, 692]. The HANC-SOP recommends that processing time should not exceed 8 hours [685]. Processing delays of 24 hours or more have been associated with reduced cell viability [689], and ambient temperatures less than 22°C reduced PBMC viability and immunogenicity [693]. Nucleic acid recovery from whole blood was profoundly reduced following exposure to suboptimal processing times and temperatures [694]. However, these results are challenged by another study which found a 24-hour delay in blood sample processing did not affect the viability of PBMCs, nor the amount of mitogen-induced protein secretion [691]. Although conflicting studies exist, discrepancies in the timing and temperature conditions of PBMC processing clearly pose a significant challenge for T cell research. The HANC-SOP requires the collection, processing, and freezing date and time to be documented [685]. We propose the ambient temperature should also be reported.

PBMC isolation

PBMCs are typically isolated from peripheral blood using density-gradient centrifugation methods, such as Ficoll-Paque, or in clinically-convenient cell preparation tubes (CPTs), including SepMate™ and Vacutainer® CPTs [695]. The HANC-SOP requires the isolation method and processing technician to be documented [685]. Ficoll-processed PBMCs were found to have higher viability when compared to CPT-processed PBMCs [696]. Another study reported that differences in viability due to isolation method were detected in one laboratory but not another [697]. In contrast, others have reported no significant differences in cell viability and recovery when isolating PBMCs with either Ficoll-Paque or CPTs [689, 698]. Immunogenicity has also been associated with isolation method, as PBMCs isolated using Ficoll-Paque were found to secrete lower levels of the cytokine Interferon-gamma (IFN-γ) compared to those isolated with CPTs [695]. However, transcriptomic profiles were not found to be influenced by isolation method [698]. These results may be confounded by technician experience, which has been estimated to contribute to approximately 60% of the variability of cell recovery [695]. The findings of these studies suggest that standardising PBMC isolation procedures and technician training is likely to enhance the reproducibility and reliability of T cell research.

Cryopreservation

Fresh PBMCs

PBMCs are used in immunoassays either immediately (fresh) or following cryopreservation. Cryopreservation can profoundly influence the viability and immunogenicity of T cells. Indeed, the kinetics of cytokine expression, proliferation, cell viability, and immunophenotypes were demonstrated to differ between freshly isolated and matched cryopreserved PBMCs [699]. However, many studies have demonstrated minimal post-cryopreservation differences. A multi-site study across nine laboratories was able to recover similar PBMC numbers following cryopreservation without significant loss of viability [700], while others have demonstrated full functionality of cryopreserved T cells [701]. Nevertheless, results from these single studies have not significantly influenced typical PBMC cryopreservation protocols, and reporting the status of cells, whether fresh or cryopreserved, is generally expected.

Cryopreservation media

The first stage of cryopreservation is typically to suspend PBMCs in a cryoprotective agent, such as dimethylsulfoxide (DMSO) [702]. The HANC-SOP specifies PBMCs should be gently

resuspended to 10^7/mL in a 10% DMSO 90% Foetal Calf Serum (FCS) cryopreservation media cooled to 2 to 8°C with continuous swirling [685]. The concentration of DMSO has been found to be usually the most important factor determining cellular viability [703] and is generally 10% [704, 705]. However, one study has reported PBMC recovery was significantly improved when using 5% DMSO [706]. A cell concentration greater than 6×10^6 PBMC/mL has been associated with improved viability [707] and sera in the cryopreservation media has been found to improve viability [708] and immunogenicity [709]. Sera is typically either FCS or 'normal' human AB serum, and although human sera may be more physiologically relevant [710], one study reported the use of FCS improved human PBMC viability [709], while another reported no significant difference between the two [711]. Other studies have reported only a minimal cell viability [712] or immunogenicity [689, 712] improvement when supplementing cryopreservation media with sera, or noted heightened background immunoreactivity when supplementing with bovine serum albumin (BSA) [711]. Gradually resuspending PBMCs in cooled cryopreservation media, such as by a drip-wise method, may improve PBMC viability and immunogenicity by minimising toxic shock or cell membrane damage [702, 713]. However, the impact of cryoprotectant addition rate on PBMC viability has not been specifically contrasted, unlike in spermatozoa cryopreservation studies, which have yielded inconsistent findings [714, 715]. Cooling the cryopreservation media to 4°C has been associated with preserving T cell immunogenicity [716], although others have shown that cooling temperature did not show any significant effects [703]. Taken together, these studies demonstrate that cryopreservation media can significantly influence T cell viability and immunogenicity.

Cooling rate

Once cells are suspended in the cryopreservation media, they must be cooled to their storage temperature, generally aiming to reduce cell temperature by -1°C min^{-1}. Cryopreservation of highly concentrated PBMCS using an automated controlled-rate freezer is the gold-standard, having been found to enhance T cell activation [717]. However, typically, cryopreservation is achieved with two-stage cooling, where cells are cooled in ultra-low freezers (ULFs) to -80°C, then in vapor phase liquid nitrogen (LN$_2$) to below -150°C in commercial freezing containers, such as a Mr Frosty™. The HANC-SOP requires samples to be immediately frozen in commercial controlled rate freezing containers, first in ULF then LN$_2$ to reduce temperature by -1°C min^{-1} [685]. Strategies have been developed which avoid cell viability loss during rapid freezing, such as media ice seeding (nucleation) which allowed PBMCs to be cooled at -90°C

min^{-1} [718]. Another study found cooling rate did not influence viability, as long as thawing rates were high (113°C min^{-1} and 45°C min^{-1}) [719]. Others have reported no change in cell viability when cells were initially cooled in LN$_2$ [720]. Despite these reports from single studies, cooling rate is generally accepted to significantly influence T cell viability and immunogenicity. We propose that the freezing container brand should be recorded.

Time at -80°C

Cells may be left briefly in ULFs before long-term storage in LN$_2$. The HANC-SOP requires samples to be transferred to LN$_2$ within 72 hours of freezing [685]. Studies have demonstrated storage at -80°C can influence gene expression [721], and significantly reduce PBMC viability and immunogenicity [722]. Others have demonstrated a linear relationship between decreasing viability and time on dry ice (-70°C) over 12 weeks [723]. Another study found that viability had been lost with as little as 48 hours of storage at -80°C [709]. Conversely, others found PBMCs stored on dry ice for three weeks had no significant difference in viability or immunogenicity compared to those immediately cryo-stored [528], while others have reported storing PBMCs on dry ice for three weeks did not reduce the T cell immunogenicity [689]. Although some studies found relatively short-term storage at -80°C had a minimal influence on PBMC viability and immunogenicity, the consensus on its potential effect highlights the need to record and standardise the date and time of transfer to LN$_2$.

Time in cryo-storage

Cells stored in liquid nitrogen can remain viable and functional for very long periods of time and the HANC-SOP states cells may be stored in LN$_2$ indefinitely [685]. Several studies which directly investigated cryo-storage viability found no clinically significant variation in cellular viability over 15 months [528], or viability and hematopoietic stem cell populations over 60 months [724]. However, immunogenicity may be influenced by small but statistically significant variations in the populations of lymphocytes, which have been found to vary following 3-to-6-months of cryo-storage [725, 726]. Despite a limited number of studies which have demonstrated an impact of LN$_2$ storage duration on PBMC viability or immunogenicity, we nevertheless propose the length of time in cryo-storage should be reported.

Exposure to varying temperatures

During long-term cryo-storage, cells are often transiently exposed to briefly varying temperatures as other co-stored aliquots are added or removed from the facility. One study found reduced cell viability and immunogenicity when cyclically exposing cryo-stored PBMCs

briefly to room temperature [727]. However, another study found viability was not influenced when aliquots of PBMCs went through repeated rounds of temperature cycling [728], while another study investigating gene expression profiles found no significant change of PBMC gene expression following brief but repetitive temperature cycling [721]. The HANC-SOP states PBMCs are not to be transferred back to ULF storage [685]. Additional studies are required to precisely assess the impact of brief but potentially repetitive temperature fluctuations on the viability and immunogenicity of cryopreserved PBMCs.

Shipping

The gold-standard practise to ship cryo-stored PBMCs is with LN_2-dry shippers, however, dry ice is also used. The HANC-SOP requires PBMCs stored in LN_2 to be shipped in cold-shippers which maintain LN_2 temperatures [685]. Both viability and immunogenicity were influenced by cold-shipping strategy [723]. However, one study found that the shipping method influenced viability, but did not influence immunogenicity [689], while another found that viability was not influenced but lymphocyte populations (*i.e.,* the ratio of $CD4^+/CD8^+$ T cells) were affected [385]. It is unclear why one population of T cell would be more sensitive to shipping than another. Significant temperature changes during shipping certainly will impact PBMC viability and immunogenicity. However, similarly to the potential fluctuations which can occur during long-term cryo-storage, exposure to varying temperatures during shipping may be brief but recurrent, and more research is required on the effects of smaller or repeated fluctuations.

Thawing

Thaw time and washing

The IMPAACT-SOP calls for cells to be thawed rapidly at 37°C, then added to the thawing media in a drip-wise action [686]. When returning cryo-preserved cells to physiological conditions PBMC viability and immunogenicity has been improved with rapid thawing [719, 729], and therefore, rapid thawing is widely recognized as the preferred method to thaw cryo-preserved cells. However, this effect has been found to be minimal in a single study when the cells were cooled at the rate required by the HANC-SOP ($-1°C$ min^{-1}) [719]. Once cells are thawed, they are routinely immediately washed to minimise contact with the cryoprotectant. However, one study has controversially reported no change in cell viability following either immediate washing or leaving in the water bath for five minutes [730]. Cells and washing medium may be combined by swiftly diluting the cells into the thawing media or by adding in a drip-wise action. No difference in the absolute count of live PBMCs was reported when cells

were added rapidly [730]. While further studies may identify protocols with more refined thawing rates and washing steps, standardising the current SOP would likely improve the reproducibility and reliability of T cell research.

Thawing media and sera

The media used during the thawing process can include various salt-balanced and buffered solutions such as phosphate buffered saline (PBS) or culture media, typically RPMI 1640 medium (RPMI) supplemented with additives including FCS. Sera can vary significantly between batches [731], and the HANC group reserve lots of FCS for batched experiments [686]. Several studies investigating various combinations of washing medias have found PBMC viability was highest following washing with media including sera [709, 730], and noted improved cell viability [709, 730], and functionality [732], when thawing with media at a temperature of 37°C rather than 4°C. No significant difference in viability was observed when thawing cells in either 50mL or 15mL of thawing media [709]. Collectively, these studies indicate that both thawing media and sera significantly affect T cell viability and immunogenicity, underscoring the importance of standardizing these components to the greatest extent feasible. The IMPAACT-SOP requires the use of 10% approved lot FCS in RPMI [686], we furthermore recommend the media is warmed to 37°C. The optimal sera for human T cell assays are human sera, which although impractical, would ideally be autologously matched [680]. FCS is a popular alternative, especially in clinical trials due to its greater consistency, scalability, and cost efficiency.

Nuclease digestion

To prevent cell clumping due to nucleic material released from lysed cells, post-thawed and washed cells may be incubated with a nuclease. The use of a DNase endonuclease was reported to have little effect on cell morphology, function, or viability [733]. However, a flow cytometry-based study found changes in cell populations with varying forward and side scatter profiles following DNase treatment [734], but no detectable changes in cell viability, expression of standard lymphocyte surface markers, nor intracellular cytokine expression. Benzonase is another commonly used nuclease which allows efficient degradation of all types of DNA and RNA. The use of Benzonase® during PBMC processing has been reported to not influence T cell immunogenicity [735]. The IMPAACT-SOP includes the optional inclusion of Benzonase® during the first wash [686], as the enzyme's properties suggest that it could potentially influence PCR outcomes [736]. Further research will be required to provide clearer guidelines for the use of nuclease digestion; however, as no study has demonstrated

Benzonase® influences PCR outcomes when used during PBMC thawing, we therefore recommend the routine inclusion of Benzonase®.

Pre-culture (rest)

Post-thawing, cells can be experimented upon immediately or undergo preculture (or resting). The IMPAACT-SOP includes an optional rest in culture for 14-18 hours [686]. Overnight resting has been found to be optimal to increase the immunogenicity of PBMCs [737], while even 1 hour of pre-culture can replicate the surface marker expression of fresh cells [738]. However, others have reported preculture had no statistically significant influence on PBMC immunogenicity [739]. The concentration of cells during the rest period has also been found to influence cellular immunoreactivity. Short term pre-culture of PBMCs at high concentrations has been found to improve immunogenicity [376], and others reported the immunogenic response varied relative to PBMC preculture concentration [356]. Longer term incubation, upwards of 48 hours in extremely high densities (1×10^7 cells/mL), has been reported to greatly improve the immunogenicity of $CD8^+$ T cell responses [436], without influencing viability. The results from these combined studies demonstrate that pre-culture conditions, especially cellular density, can significantly influence T cell immunogenicity, and therefore, we propose that the rest period and cell density should be standardised and recorded.

Cell culture

Cell concentration

During functional immunoassays cell density is typically between $1\text{-}4\times10^6$ cells/mL to facilitate inter-cellular contact and antigen presentation, which is a concentration not expected to influence cell viability [356, 740]. The immunogenic response of PBMCs is profoundly influenced by the concentration of cells in the stimulation reaction, particularly when stimulating with weakly immunoreactive antigenic peptides [356]. More highly reactive stimulants are also influenced by cell concentration, with one study determining a PBMC concentration of 2.5×10^6 cells/mL was optimal to detect cytokine responses following mitogen stimulation [741]. There are, however, a relatively limited number of studies which have optimised stimulation cell concentrations. Such optimisation may be impractical, particularly when considering experiments involving antigenic T cell peptide epitopes which may involve thousands of stimulatory conditions. Nevertheless, standardising and reporting cell density during culture is generally expected.

Stimulant concentration and solvent

Stimulant concentration is a critical determinant of T-cell functionality. For example, increasing the concentration of antigen is recognised to generally increase the number of IFN-γ^+ PBMCs [436]. Titrated antigen experiments have identified ranges between 1 µg/ml [742] to 10 µg/ml [690] as optimal for MHC-class I peptide epitope-induced immunogenicity. However, a donor-specific effect on the optimal antigen stimulant concentration to induce immunoreactivity has been described [690]. While these studies cumulatively confirm that, as expected, stimulant concentration does influence T cell immunoreactivity, there are limited studies optimising stimulant concentrations. Identifying universally optimal stimulant concentrations is impractical, especially for T cell peptide epitope screening studies. Lyophilized peptide epitopes are typically resuspended in DMSO, which has several key advantages and disadvantages relative to other common solvents (**Supp Table S7.3**) [743]. Even relatively low concentrations of DMSO in cell culture have been found to induce changes to cellular phenotypes [744], with as little as 0.25% DMSO influencing immunogenicity [745], and marginal toxicity reported at 2-5% DMSO [745]. While reporting the stimulant concentration is common practise, we further recommend reporting the concentration and type of solvent in the stimulation.

Stimulation time

The length of time cells are incubated in the presence of the stimulant can influence the number and intensity of responsive cells. Six-hour long incubations are frequently reported [511, 746], however, longer incubations are also common [747]. Overnight incubations have been reported to increase antigen immunogenicity [748]. The optimal timepoint to measure mitogen stimulations has been reported to be between 72 and 96 hours [749]. Similarly, kinetic studies investigating whole-blood stimulations found 72 hours as optimal for mitogen stimulants [750]. While antigenic peptide stimulation time length has been found to not decrease cell viability, longer mitogen stimulations have been associated with increased numbers of non-viable cells [699]. Interestingly, a recent study over a 12 hour time course noted peak cytokine mRNA expression occurred between 3-6 hours post peptide epitope stimulation, and occurred in a peptide- and donor-specific fashion [511].

7.3.4 Discussion

Taken together these studies demonstrate that technical variation during PBMC collection, cryopreservation, thawing, and culture may profoundly impact cell viability and

immunogenicity. Notably, many of the conclusions of these studies are contradictory, suggesting the influence and interaction of underreported factors. Although several of the results discussed in this review are derived from single studies, these results from well-controlled, high-quality studies nevertheless underscore the importance of maintaining stringently consistent protocols and reporting guidelines when analysing human T cells. Therefore, we propose the use of the HANC's-SOP when collecting and cryopreserving PBMCs [685]; and the IMPAACT networks-SOP when thawing PBMCs [686]. Furthermore, we have made additional recommendations to standardise the protocol during PBMC collection, storage, thawing, and culture (**Table 7.1**).

The biological mechanisms underlying variations in cell viability and immunogenicity during PBMC processing are complex and incompletely understood. The various reagents used during processing may significantly influence T cells by impacting cellular integrity, agonistically or antagonistically influencing cellular activation, or changing media chemistry. For example, the anticoagulant EDTA can impair T cell activation by disrupting cellular calcium levels [751], while heparin may interfere with cell-to-cell interactions [752]. The more profound influences which have been found following delays in processing and fluctuations in temperature during storage can be attributed to induced metabolic stress which may have activated apoptosis pathways [753, 754]. Techniques like density-gradient centrifugation and cryopreservation introduce stress through physical forces [755], and if cryoprotectants are not completely removed after thawing, they may further alter cell functions [756]. This complexity highlights the critical need for strict standardisation and detailed documentation in T cell research to avoid the technical pitfalls when collecting, cryopreserving, thawing, and stimulating human T-cells.

The development of PBMC processing SOPs by HANC and its affiliated members such as IMPAACT were driven by an awareness that technical variation during this critical experiment window may reduce the reproducibility of experimental findings. There is a growing concern that the social, behavioural, and biomedical sciences are facing a 'reproducibility crisis' [757], as many influential published findings have failed reproducibility testing [758, 759]. Indeed, a relatively recent large meta-analysis proposed that, at best, around 50% of preclinical biomedical research was reproducible [760]. The cause of this low reproducibility is likely complex, ranging from poor statistical literacy [761] and noise discovery [762], to unconscious or conscious bias induced by a pressure to publish [763]. While a low rate of reproducibility is certainly not ideal, it has been argued that some irreproducibility is expected [764], even potentially beneficial [765], when cutting-edge science is investigating competing hypotheses.

Nevertheless, there is a growing appreciation that insufficient communication of experimental methods is a major contributing factor [400, 766-768]. We expect that strict adherence to HANC's and HANC affiliates SOPs during PBMC collection, cryopreservation, thawing, and culture will greatly improve the replicability of human T cell research.

Table 7.1. Standardised protocol for the collection, cryopreservation, thawing and culturing of human PBMCs for T cell studies

Major sources of technical variation	HANC and IMPAACT protocol instructions	Further recommendations
Collection		
Anticoagulation	The type of anticoagulant must be recorded*	
Processing time & temperature	The collection, processing, and freezing date and time must be recorded*	The ambient temperature should be recorded
Isolation method	The processing method and processing technician must be recorded*	
Cryopreservation		
Cryopreservation media	10% DMSO in FCS cryopreservation media cooled to 2 to 8°C must be used*	
Cooling rate	Immediately freeze in a ULF using a commercial controlled-rate freezing container*	Commercial product should be recorded
Time at -80°C	Transfer to LN_2 within 72 hours of freezing*	The date and time of transfer to LN_2 should be recorded
Time in cryo-storage	Frozen PBMC samples can be stored safely in vapor phase LN_2 indefinitely*	The date and time of transfer from LN_2 should be recorded
Exposure to varying temperatures	Do not transfer back to ULF*	
Shipping	All transfers must be maintained in LN_2 *	

Major sources of technical variation	HANC and IMPAACT protocol instructions	Further recommendations
Thawing		
Thaw time and washing	Thaw cells rapidly at 37°C, added in a drip-wise action †	
Thawing media & sera	Wash in RPMI 10% FCS thawing media †	Warm media to 37°C
Nuclease digestion	Optional inclusion of Benzonase® during the first wash †	Benzonase® use should be routine and reported
Preculture	Cells may be optionally rested in culture for 14-18 hours †	The rest period and cell density should be recorded
Culturing		
Cell concentration	Reporting cell density is generally expected.	
Stimulant concentration	Reporting stimulant concentration is generally expected	The solvent type and concentration should be reported
Stimulation time	Reporting the stimulation time is generally expected	

* The Office of HIV/AIDS Network Coordination (HANC)-SOP; † International Maternal Pediatric Adolescent AIDS Clinical Trials (IMPAACT)-SOP, LN2: vapour phase liquid nitrogen (-180°C), ULF: Ultra-low freezer (-80°C), SOP: standard operating procedure, DMSO: Dimethyl sulfoxide, FCS: Foetal Calf Serum

7.3.5 Supplementary material

Supplementary Table S7.1. Representative studies investigating PBMC collection, storage, thawing and culture

	Viability		Immunogenicity	
	Influenced	**Not influenced or minor**	**Influenced**	**Not influenced or minor**
Collection				
Anticoagulation	Not directly associated with viability [689]	Associated with viability when processing was delayed [689]	Use of EDTA linked to reduced immunogenicity [688]	No significant changed between EDTA or sodium-heparin [689]
				No significant changed between sodium-heparin and lithium-heparin [690]
Processing time	Processing delay greater than 24 hours reduced viability [689]	A 24-hour delay did not influence viability [691]	Temperature lower than 22°C reduced immunogenicity [693]	A 24-hour delay did not influence immunogenicity [691]
	Temperature lower than 22°C reduced viability [693]		RNA was significantly degraded after 24 hours [694]	
Isolation method	Ficoll-processed PBMCs had higher viability when compared to CPT-processed PBMCs [696]	No significant difference Ficoll-processed PBMCs when compared to CPT-processed PBMCs [689, 698]	Ficol plaque PBMCs secreted lower levels of IFN-γ when compared to CPT-processed PBMCs [695]	Transcriptomic profiles were not influenced by isolation method [698]
	Differences were found to be laboratory specific [697]			

	Viability		Immunogenicity	
	Influenced	**Not influenced or minor**	**Influenced**	**Not influenced or minor**
Storage				
Fresh PBMCs	Cell viability differed between freshly isolated and matched cryopreserved PBMCs [699]	A multi-site study across nine laboratories was able to recover similar PBMC numbers following cryopreservation without significant loss of viability [700]	The kinetics of cytokine expression, proliferation differed between freshly isolated and matched cryopreserved PBMCs [699]	Full functionality was demonstrated of cryopreserved T cells [701]
Cryopreservation media	The concentration of DMSO was found to be the most important factor determining cellular viability [703] PBMC recovery was significantly improved when using 5% DMSO [706] A cell concentration greater than 6×10^6 PBMC/mL has been associated with improved viability [707] Sera in the cryopreservation media has been found to improve viability [708] FCS improved human PBMC viability [709]	No significant difference between FCS and human sera [711] Only minimal improvement in cellular viability 2011 [712]	Sera in the cryopreservation media has been found to improve immunogenicity [709] Background immunoreactivity when supplementing with BSA [711] Cooling the cryopreservation media to 4°C has been associated with preserving T cell immunogenicity [716]	Only minimal improvement in immunogenicity [689] [712] Cooling the media had not significant effect [703]

	Viability		Immunogenicity	
	Influenced	**Not influenced or minor**	**Influenced**	**Not influenced or minor**
Cooling rate	The cooling rate did not influence viability, as long as thawing rates were high (113°C min^{-1} and 45°C min^{-1}) [719] PBMCs cooled at -90°C min^{-1} did not have viability loss [718]	No change in cell viability when cells were initially cooled in LN$_2$ [720]	Cryopreservation of highly concentrated PBMCS using an automated controlled-rate freezer enhanced T cell activation [717]	
Time at -80°C	Storage at -80°C can influence gene expression [721] Viability had been lost with as little as 48 hours of storage at -80°C [709] A linear relationship between decreasing viability and time on dry ice (-70°C) over 12 weeks [723] Storage at -80°C significantly reduced PBMC viability [722]	PBMCs stored on dry ice for three weeks had no significant difference in viability compared to those immediately cryo-stored [528]	Storage at -80°C significantly reduced PBMC immunogenicity [722]	PBMCs stored on dry ice for three weeks did not reduce T cell immunogenicity [689] PBMCs stored on dry ice for three weeks had no significant difference in immunogenicity compared to those immediately cryo-stored [528]
Time in cryo-storage		No clinically significant variation in cellular viability over 15 months [528] No clinically significant variation in cellular viability over 60 months [724]	Small but statistically significant variations in the populations of lymphocytes [725, 726]	No clinically significant variation in cellular immunogenicity over 60 months [724]

	Viability		Immunogenicity	
	Influenced	**Not influenced or minor**	**Influenced**	**Not influenced or minor**
Varying temperatures	Reduced cell viability when cyclically exposing cryo-stored PBMCs briefly to room temperature [727]	Viability was not influenced when aliquots of PBMCs went through repeated rounds of temperature cycling [728]	Reduced cell immunogenicity when cyclically exposing cryo-stored PBMCs briefly to room temperature [727]	No significant change of PBMC gene expression following brief but repetitive temperature cycling [721]
Shipping	Shipping method influenced viability [689] Viability was influenced by cold-shipping strategy [723]	Lymphocyte viability was not affected [385]	Lymphocyte populations were affected [385] Immunogenicity was influenced by cold-shipping strategy [723]	Shipping method did not influence immunogenicity [689]
Thawing				
Thaw time	PBMC viability has been improved with rapid thawing [719, 729]	No change in cell viability following either immediate washing or leaving in the water bath for five minutes [730]	PBMC immunogenicity has been improved with rapid thawing [729]	
Thawing media & sera	Viability was highest following washing with media including sera [709, 730]		Immunogenicity was highest when washing with media including sera [732]	

	Viability		Immunogenicity	
	Influenced	**Not influenced or minor**	**Influenced**	**Not influenced or minor**
Nuclease digestion		DNase endonuclease was reported to have little effect on cell viability [733] Found changes in cell populations with varying forward and side scatter profiles following DNase treatment [734]		DNase endonuclease was reported to have little effect on cell function [733] Benzonase during PBMC processing has been reported to not influence T cell immunogenicity [735]
Preculture			Overnight resting has been found to be optimal to increase the immunogenicity of PBMCs [737] 1 hour of pre-culture can replicate the surface marker expression of fresh cells [738] Short term pre-culture of PBMCs at high concentrations has been found to improve immunogenicity [376] Longer term incubation, upwards of 48 hours in extremely high densities (1×10^7 cells/mL), has been reported to greatly improve the immunogenicity of CD8+ T cell responses [436]	Preculture had no statistically significant influence on PBMC immunogenicity [739]

	Viability		Immunogenicity	
	Influenced	**Not influenced or minor**	**Influenced**	**Not influenced or minor**
Culturing				
Cell concentration		1-4×10^6 cells/mL is a concentration not expected to influence cell viability [356, 740].	The immunogenic response of PBMCs is profoundly influenced by the concentration of cells in the stimulation reaction, particularly when stimulating with weakly immunoreactive antigenic peptides [356]. PBMC concentration of 2.5×10^6 cells/mL was optimal to detect cytokine responses following mitogen stimulation [741].	
Antigen concentration		Marginal PBMC toxicity reported at 2-5% DMSO [745]	Increasing the concentration of antigen is recognised to generally increase the number of IFN-γ+ PBMCs [436] Titrated antigen experiments have identified ranges between 1 μg/mL [742] to 10 μg/mL [690] as optimal for MHC-class I peptide epitope-induced immunogenicity	

	Viability		Immunogenicity	
	Influenced	**Not influenced or minor**	**Influenced**	**Not influenced or minor**
			A donor-specific effect on the optimal antigen stimulant concentration to induce immunoreactivity has been described [690]	
			Relatively low concentrations of DMSO in cell culture have been found to induce changes to cellular phenotypes [744]	
			As little as 0.25% DMSO influences immunogenicity [745]	
Stimulation time		Antigenic peptide stimulation time length has been found to not decrease cell viability [699]	Overnight incubations have been reported to increase antigen immunogenicity [748]	
			The optimal timepoint to measure mitogen stimulations has been reported to be between 72 and 96 hours [749]	
			Kinetic studies investigating whole-blood stimulations found 72 hours as optimal for mitogen stimulants [750]	
			Peak cytokine mRNA expression	

	Viability		Immunogenicity	
	Influenced	**Not influenced or minor**	**Influenced**	**Not influenced or minor**
			occurred between 3-6 hours post peptide epitope stimulation, and occurred in a peptide- and donor-specific fashion [511].	

* Mitogen stimulation; † mRNA measured

Supplementary Table S7.2. Advantages and disadvantages of anticoagulants used during venepuncture to isolate PBMCs for immune phenotyping and functional immunoassays

Anticoagulant	Blood tube lid	Typical use	Advantage	Disadvantage
Routinely used anticoagulants				
K2 potassium salt of EDTA	Purple	Haematological examinations	• Preserves cell morphology	• Calcium chelation may inhibit cytokine production • Overuse may lead to cell shrinkage
Sodium or lithium heparin	Green	White blood cell analysis	• Minimal cell morphology alteration	• Tends to cause white blood cell clumping • May inhibit PCR
Less commonly used anticoagulants				
Sodium citrate	Blue	Coagulation and platelet function testing	• Reversable coagulation • Preserves the coagulation factors for study	• Changes blood chemistry (pH, ionic concentration) • Dilutes sample
Acid citrate dextrose	Yellow	Whole blood and erythrocyte survival, blood storage	• Maintains cell viability	• Changes blood chemistry (pH, ionic concentration) • Dilutes sample

EDTA: Ethylenediaminetetraacetic acid

Supplementary Table S7.3. Advantages and disadvantages of representative solvents available for resuspension of lyophilized peptides

Solvent	Advantage	Disadvantage
DMSO	• Solubility of both polar and non-polar peptides • Relatively low reactivity • Protects peptides from degradation that would otherwise occur in H_2O • Miscible with cell culture media	• Toxicity • Not biologically inert • Can penetrate skin and cell walls relatively rapidly • Not universally effective solubility
Ethanol	• Moderate polarity allows resuspension of a range of peptides • Lower toxicity than DMSO • Protects peptides from degradation that would otherwise occur in H_2O • Miscible with cell culture media	• Toxicity • May denature sensitive peptides • Solubility of non-polar peptides is low
H_2O	• Biocompatibility as water is non-toxic • More closely mimics physiological conditions • Effective solvent for polar hydrophilic peptides	• Is unsuitable as a solvent for non-polar hydrophobic peptides • Microbial contamination as microbes can survive in this solvent • Stability of some peptides may be low

DMSO: Dimethyl sulfoxide

7.4 Conclusion

This thesis sought to evaluate T cell dominance in malaria, but pivoted to assess COVID-19, following the outbreak of the COVID-19 pandemic. The data generated during this doctoral thesis have established that RT-qPCR can be effectively used to delineate a T cell epitope immunoreactivity hierarchy from very low numbers of PBMCs. Furthermore, this protocol can be optimized for HTS and to meet screening uniformity and signal variance testing standards. These studies and the optimised assay provide a valuable tool for T cell research by facilitating the immunoreactivity screening of large numbers of putative T cell epitopes. Rapid, accurate, and cost-effective determination of epitope immunoreactivity hierarchies would be expected to provide important insights into and inform T cell research, thereby improving future vaccine design. Additionally, this doctoral study optimized readout of T cell responses and protection in a murine model of *Plasmodium* challenge using a DNA-adenovirus IV 'Prime-Target' immunization. For the first time, it was demonstrated that host reference gene expression is influenced by both sporozoite challenge and vaccination. This study also identified optimal stable reference genes for accurate parasite burden quantification. Accurate quantification of host-immune response and parasite burden in the liver following *Plasmodium* sporozoite challenge is expected to greatly enhance pre-erythrocytic stage malaria-vaccine antigen testing.

When using the optimized HTS-RT-qPCR protocol, studies presented in this thesis found that although some individuals responded to stimulation with T cell peptide epitopes, the overall response in Malian PBMCs stimulated with liver-stage *P. falciparum* T cell epitopes was not significantly greater than background immunogenicity. This contrasts with data collected from PNG donors in 2009, which demonstrated that the antigen peptide pools selected for this study were significantly antigenic in all tested PNG donors. This may be a highly significant finding with dramatic consequences for malaria vaccine design. However, the COVID-19 pandemic, which occurred during this PhD study, made it impossible to collect more PNG and Mali samples for the side-by-side comparison required to draw further conclusions. Furthermore, this thesis found lower than expected immunogenicity among malaria-naïve donors when stimulated with 'cross-reactive' *P. falciparum* antigen peptide pools. A comprehensive review of the literature was undertaken to investigate factors that may influence T cell peptide immunogenicity and identified several relatively minor and underreported factors during PBMC processing that may contribute to the differences in observed immunogenicity.

Finally, following a pivot to study COVID-19, this thesis identified immunoreactive T cell epitopes within the SARS-CoV2 S-protein and tracked the kinetics of these epitopes across pre-vaccinated, post-vaccinated, and post-SARS-CoV2 infected individuals. These data demonstrated that the immunoreactive epitopes following vaccination were generally not boosted by natural infection. Additionally, a clustering of epitopes in two regions of the S-protein following vaccination was identified. These findings may inform future vaccine design, where future COVID-19 vaccines may specifically aim to boost the immunogenicity of these epitopes.

Taken together, the studies presented in this doctoral thesis report significant advances in the molecular identification of T cell dominance, tested in the context of both malaria and COVID-19.

References

1.	WHO. *Malaria Fact Sheet 2019*. 2019; Available from: https://www.who.int/news-room/fact-sheets/detail/malaria.
2.	Cox, F.E., *History of the discovery of the malaria parasites and their vectors.* Parasites & Vectors, 2010. **3**(1): p. 5-5.
3.	Crompton, P.D., et al., *Malaria immunity in man and mosquito: insights into unsolved mysteries of a deadly infectious disease.* Annual Review of Immunology, 2014. **32**: p. 157-87.
4.	Bloland, P.B. and H.A. Williams, in *Malaria Control during Mass Population Movements and Natural Disasters*. 2002: Washington (DC).
5.	Laveran, A., *A new parasite found in the blood of malarial patients. Parasitic origin of malarial attacks.* Bulletins et mémoires de la Société Médicale des Hôpitaux de Paris., 1880: p. 158-164.
6.	Ross, R., *Mosquitos and Malaria: The Infection of Birds by Mosquitos.* British Medical Journal, 1899. **1**(1990): p. 432-3.
7.	Maccallum, W.G., *On the flagellated form of the malarial parasite.* The Lancet, 1897. **150**(3872): p. 1240-1241.
8.	Shortt, H.E. and P.C.C. Garnham, *Pre-erythrocytic stage in mammalian malaria parasites.* Nature, 1948. **161**(4082): p. 126.
9.	Pauling, L., H.A. Itano, and et al., *Sickle cell anemia, a molecular disease.* Science, 1949. **109**(2835): p. 443.
10.	Neel, J.V., *The Inheritance of Sickle Cell Anemia.* Science, 1949. **110**(2846): p. 64-6.
11.	Cutbush, M., P.L. Mollison, and D.M. Parkin, *A New Human Blood Group.* Nature, 1950. **165**(4188): p. 188-189.
12.	Mak, T.W. and M.E. Saunders, *Chapter 27 - Transplantation*, in *The Immune Response*, T.W. Mak and M.E. Saunders, Editors. 2006, Academic Press: Burlington. p. 873-921.
13.	Howes, R.E., et al., *The global distribution of the Duffy blood group.* Nature Communications, 2011. **2**: p. 266.
14.	Guttmacher, A.E. and F.S. Collins, *Welcome to the genomic era.* The New England Journal of Medicine, 2003. **349**(10): p. 996-8.
15.	Ravenhall, M., et al., *Novel genetic polymorphisms associated with severe malaria and under selective pressure in North-eastern Tanzania.* PLOS Genetics, 2018. **14**(1): p. e1007172.
16.	Kountouris, P., et al., *IthaGenes: an interactive database for haemoglobin variations and epidemiology.* PLOS ONE, 2014. **9**(7): p. e103020.
17.	Arama, C., et al., *Epigenetics and Malaria Susceptibility/Protection: A Missing Piece of the Puzzle.* Frontiers in Immunology, 2018. **9**: p. 1733.
18.	Alonso, P.L., et al., *A Research Agenda for Malaria Eradication: Vector Control.* PLOS Medicine, 2011. **8**(1).
19.	Chin, T. and P.D. Welsby, *Malaria in the UK: past, present, and future.* Postgraduate Medical Journal, 2004. **80**(949): p. 663-666.
20.	WHO, *A framework for malaria elimination.* 2017.
21.	Shanks, G.D., *Historical Review: Problematic Malaria Prophylaxis with Quinine.* American Journal of Tropical Medicine and Hygiene, 2016. **95**(2): p. 269-72.
22.	Hay, S.I., et al., *The global distribution and population at risk of malaria: past, present, and future.* The Lancet Infectious Diseases, 2004. **4**(6): p. 327-336.

23. Caminade, C., et al., *Impact of climate change on global malaria distribution.* Proceedings of the National Academy of Sciences of the United States of America, 2014. **111**(9): p. 3286-91.

24. WHO, *World Malaria Report.* 2022.

25. Rosen, G., *A history of public health.* 2015: Jhu Press.

26. WHO, *The global eradication of smallpox: final report of the Global Commission for the Certification of Smallpox Eradication, Geneva, December 1979.* 1980: World Health Organization.

27. Care, A.G.D.o.H.a.A. *Childhood immunisation schedule.* 2024 15 April 2024 [cited 2024 08/05/2024]; Available from: https://www.health.gov.au/childhood-immunisation/immunisation-schedule.

28. Diseases, N.C.f.I.a.R. *Child and Adolescent Immunization Schedule by Age.* 2024 November 16, 2023 [cited 2024 08/05/2024]; Available from: https://www.cdc.gov/vaccines/schedules/hcp/imz/child-adolescent.html.

29. Datoo, M.S., et al., *Efficacy of a low-dose candidate malaria vaccine, R21 in adjuvant Matrix-M, with seasonal administration to children in Burkina Faso: a randomised controlled trial.* The Lancet, 2021. **397**(10287): p. 1809-1818.

30. Hassert, M., S. Arumugam, and J.T. Harty, *Memory CD8+ T cell-mediated protection against liver-stage malaria.* Immunological Reviews, 2023. **316**(1): p. 84-103.

31. WHO, *Malaria Vaccine Rainbow Tables*, in *World Malaria Report.* 2019, Geneva: World Health Organization.

32. Moorthy, V.S., R.D. Newman, and J.M. Okwo-Bele, *Malaria vaccine technology roadmap.* The Lancet, 2013. **382**(9906): p. 1700-1701.

33. Dondorp, A.M., et al., *Artemisinin resistance in Plasmodium falciparum malaria.* The New England Journal of Medicine, 2009. **361**(5): p. 455-67.

34. Doolan, D.L., *Malaria research in Australia: looking through the lens of the past towards the future.* International Journal for Parasitology, 2021. **51**(13-14): p. 1255-1263.

35. Leander, B.S., R.E. Clopton, and P.J. Keeling, *Phylogeny of gregarines (Apicomplexa) as inferred from small-subunit rDNA and beta-tubulin.* International Journal of Systematic and Evolutionary Microbiology, 2003. **53**(Pt 1): p. 345-54.

36. Falkowski, P.G., et al., *The evolution of modern eukaryotic phytoplankton.* Science, 2004. **305**(5682): p. 354-60.

37. Leander, B.S. and P.J. Keeling, *Early evolutionary history of dinoflagellates and apicomplexans (Alveolata) as inferred from hsp90 and actin phylogenies.* Journal of Phycology, 2004. **40**(2): p. 341-350.

38. Frenal, K., et al., *Gliding motility powers invasion and egress in Apicomplexa.* Nature Reviews Microbiology, 2017. **15**(11): p. 645-660.

39. Perkins, S.L., *Malaria's Many Mates: Past, Present, and Future of the Systematics of the Order Haemosporida.* Journal of Parasitology, 2014. **100**(1): p. 11-25.

40. Poinar, G. and S.R. Telford, *Paleohaemoproteus burmacis gen. n., sp n. (Haemospororida : Plasmodiidae) from an early cretaceous biting midge (Diptera : Ceratopogonidae).* Parasitology, 2005. **131**: p. 79-84.

41. Garnham, P.C.C., *Malaria Parasites and other Haemosporidia.* 1966: Blackwell Scientific Publications Ltd.

42. Wilson, M.E., A. Kantele, and T.S. Jokiranta, *Review of cases with the emerging fifth human malaria parasite, Plasmodium knowlesi.* Clinical Infectious Diseases, 2011. **52**(11): p. 1356-1362.

43. Sato, S., *Plasmodium-a brief introduction to the parasites causing human malaria and their basic biology.* Journal of Physiological Anthropology, 2021. **40**(1): p. 1.

44. Brasil, P., et al., *Outbreak of human malaria caused by Plasmodium simium in the Atlantic Forest in Rio de Janeiro: a molecular epidemiological investigation.* The Lancet Global Health, 2017. **5**(10): p. e1038-e1046.

45. Lalremruata, A., et al., *Natural infection of Plasmodium brasilianum in humans: Man and monkey share quartan malaria parasites in the Venezuelan Amazon.* eBioMedicine, 2015. **2**(9): p. 1186-92.

46. Nada Raja, T., et al., *Malaria parasites of long-tailed macaques in Sarawak, Malaysian Borneo: a novel species and demographic and evolutionary histories.* BMC Evolutionary Biology, 2018. **18**(1): p. 49.

47. Mackintosh, C.L., J.G. Beeson, and K. Marsh, *Clinical features and pathogenesis of severe malaria.* Trends in Parasitology, 2004. **20**(12): p. 597-603.

48. Liu, W.M., et al., *Origin of the human malaria parasite Plasmodium falciparum in gorillas.* Nature, 2010. **467**(7314): p. 420-+.

49. Cornejo, O.E. and A.A. Escalante, *The origin and age of Plasmodium vivax.* Trends in Parasitology, 2006. **22**(12): p. 558-63.

50. Brauer, G., *Origins of anatomically modern humans - Nitecki,MH, Nitecki,DV.* Homo, 1997. **48**(2): p. 199-200.

51. Bruce, M.C., et al., *Characterization and application of multiple genetic markers for Plasmodium malariae.* Parasitology, 2007. **134**(Pt 5): p. 637-50.

52. Rutledge, G.G., et al., *Plasmodium malariae and P. ovale genomes provide insights into malaria parasite evolution.* Nature, 2017. **542**(7639): p. 101-104.

53. Chen, I., et al., *"Asymptomatic" Malaria: A Chronic and Debilitating Infection That Should Be Treated.* PLOS Medicine, 2016. **13**(1): p. e1001942.

54. Protzer, U., M.K. Maini, and P.A. Knolle, *Living in the liver: hepatic infections.* Nature Reviews Immunology, 2012. **12**: p. 201.

55. Usynin, I., C. Klotz, and U. Frevert, *Malaria circumsporozoite protein inhibits the respiratory burst in Kupffer cells.* Cellular Microbiology, 2007. **9**(11): p. 2610-28.

56. Delves, M., et al., *The activities of current antimalarial drugs on the life cycle stages of Plasmodium: a comparative study with human and rodent parasites.* PLOS Medicine, 2012. **9**(2): p. e1001169.

57. Andrews, M., et al., *Bottoms up! Malaria parasite invasion the right way around.* Trends in Parasitology, 2023. **39**(12): p. 1004-1013.

58. Tilley, L., M.W. Dixon, and K. Kirk, *The Plasmodium falciparum-infected red blood cell.* The International Journal of Biochemistry & Cell Biology, 2011. **43**(6): p. 839-842.

59. Paul, A.S., E.S. Egan, and M.T. Duraisingh, *Host-parasite interactions that guide red blood cell invasion by malaria parasites.* Current Opinion in Hematology, 2015. **22**(3): p. 220-6.

60. Beeson, J.G., et al., *Merozoite surface proteins in red blood cell invasion, immunity and vaccines against malaria.* FEMS Microbiology Reviews, 2016. **40**(3): p. 343-72.

61. Bartoloni, A. and L. Zammarchi, *Clinical aspects of uncomplicated and severe malaria.* Mediterranean Journal of Hematology and Infectious Diseases, 2012. **4**(1): p. e2012026-e2012026.

62. Baker, D.A., *Malaria gametocytogenesis.* Molecular and Biochemical Parasitology, 2010. **172**(2): p. 57-65.

63. Bennink, S., M.J. Kiesow, and G. Pradel, *The development of malaria parasites in the mosquito midgut.* Cellular Microbiology 2016. **18**(7): p. 905-918.

64. Aly, A.S., A.M. Vaughan, and S.H. Kappe, *Malaria parasite development in the mosquito and infection of the mammalian host.* Annual Review of Immunology, 2009. **63**: p. 195-221.

65. Cowman, A.F. and B.S. Crabb, *Invasion of red blood cells by malaria parasites.* Cell, 2006. **124**(4): p. 755-766.

66. Nguyen, Q.P., et al., *Origins of CD4+ circulating and tissue-resident memory T-cells.* Immunology, 2019. **157**(1): p. 3-12.

67. Kurup, S.P., N.S. Butler, and J.T. Harty, *T cell-mediated immunity to malaria.* Nature Reviews Immunology, 2019. **19**(7): p. 457-471.

68. Doolan, D.L. and S.L. Hoffman, *DNA-based vaccines against malaria: status and promise of the Multi-Stage Malaria DNA Vaccine Operation.* International Journal for Parasitology, 2001. **31**(8): p. 753-62.

69. Hoffman, S.L. and D.L. Doolan, *Malaria vaccines-targeting infected hepatocytes.* Nature Medicine, 2000. **6**(11): p. 1218-9.

70. Kengne-Ouafo, J.A., et al., *Immune Responses to the Sexual Stages of Plasmodium falciparum Parasites.* Frontiers in Immunology, 2019. **10**: p. 136.

71. Ménard, R., et al., *Circumsporozoite protein is required for development of malaria sporozoites in mosquitoes.* Nature, 1997. **385**(6614): p. 336-40.

72. Wright, G.J. and J.C. Rayner, *Plasmodium falciparum Erythrocyte Invasion: Combining Function with Immune Evasion.* PLOS Pathogens, 2014. **10**(3): p. e1003943.

73. Scherf, A., et al., *Antigenic variation in malaria: in situ switching, relaxed and mutually exclusive transcription of var genes during intra-erythrocytic development in Plasmodium falciparum.* EMBO Journal, 1998. **17**(18): p. 5418-26.

74. D'Ombrain, M.C., et al., *Plasmodium falciparum erythrocyte membrane protein-1 specifically suppresses early production of host interferon-gamma.* Cell Host & Microbe, 2007. **2**(2): p. 130-8.

75. Oyedeji, S.I., et al., *Genetic diversity and complexity of Plasmodium falciparum infections in the microenvironment among siblings of the same household in North-Central Nigeria.* Malaria Journal, 2020. **19**(1): p. 338.

76. Doolan, D.L., C. Dobano, and J.K. Baird, *Acquired immunity to malaria.* Clinical Microbiology Reviews, 2009. **22**(1): p. 13-36, Table of Contents.

77. Vanderberg, J.P., *Reflections on early malaria vaccine studies, the first successful human malaria vaccination, and beyond.* Vaccine, 2009. **27**(1): p. 2-9.

78. Freund, J., H.E. Sommer, and A.W. Walter, *Immunization Against Malaria: Vaccination of Ducks with Killed Parasites Incorporated with Adjuvants.* Science, 1945. **102**(2643): p. 200-202.

79. Vincke I, H., *Un nouveau plasmodium d'un rangeur du Congo (Plasmodium berghei n. sp.).* Annals Societe Belgique Medicine Tropicale, 1948. **28**: p. 97.

80. Stanisic, D.I. and M.F. Good, *Malaria Vaccines: Progress to Date.* BioDrugs, 2023.

81. Nussenzweig, R.S., et al., *Protective immunity produced by the injection of x-irradiated sporozoites of plasmodium berghei.* Nature, 1967. **216**(5111): p. 160-2.

82. Clyde, D.F., *Immunization of man against falciparum and vivax malaria by use of attenuated sporozoites.* American Journal of Tropical Medicine and Hygiene, 1975. **24**(3): p. 397-401.

83. McCarthy, V.C. and D.F. Clyde, *Plasmodium vivax: correlation of circumsporozoite precipitation (CSP) reaction with sporozoite-induced protective immunity in man.* Experimental Parasitology, 1977. **41**(1): p. 167-71.

84. Kumar, K.A., et al., *The circumsporozoite protein is an immunodominant protective antigen in irradiated sporozoites.* Nature, 2006. **444**(7121): p. 937-940.

85. Cohen, S., et al., *Acquired immunity and vaccination in malaria.* American Journal of Tropical Medicine and Hygiene, 1977. **26**(6 Pt 2): p. 223-32.

86. Carter, R. and D.H. Chen, *Malaria transmission blocked by immunisation with gametes of the malaria parasite.* Nature, 1976. **263**(5572): p. 57-60.

87. Nussenzweig, R., *Use of radiation-attenuated sporozoites in the immunoprophylaxis of malaria.* International Journal of Nuclear Medicine and Biology, 1980. **7**(2): p. 89-96.

88. Hoffman, S.L., et al., *Protection of Humans against Malaria by Immunization with Radiation-Attenuated Plasmodium falciparum Sporozoites.* The Journal of Infectious Diseases, 2002. **185**(8): p. 1155-1164.

89. Clyde, D.F., et al., *Immunization of man against sporozite-induced falciparum malaria.* The American Journal of the Medical Sciences, 1973. **266**(3): p. 169-77.

90. Zavala, F., et al., *Circumsporozoite proteins of malaria parasites contain a single immunodominant region with two or more identical epitopes.* Journal of Experimental Medicine, 1983. **157**(6): p. 1947-57.

91. Nardin, E.H. and R.S. Nussenzweig, *Stage-specific antigens on the surface membrane of sporozoites of malaria parasites.* Nature, 1978. **274**(5666): p. 55-57.

92. Enea, V., et al., *DNA Cloning of Plasmodium falciparum Circumsporozoite Gene: Amino Acid Sequence of Repetitive Epitope.* Science, 1984. **225**(4662): p. 628-630.

93. Vanderberg, J.P. and U. Frevert, *Intravital microscopy demonstrating antibody-mediated immobilisation of Plasmodium berghei sporozoites injected into skin by mosquitoes.* International Journal for Parasitology, 2004. **34**(9): p. 991-6.

94. Doolan, D.L., *Plasmodium immunomics.* International Journal for Parasitology, 2011. **41**(1): p. 3-20.

95. Afolabi, M.O., et al., *Safety and Immunogenicity of ChAd63 and MVA ME-TRAP in West African Children and Infants.* Molecular Therapy, 2016. **24**(8): p. 1470-1477.

96. Ewer, K.J., et al., *Protective CD8+ T-cell immunity to human malaria induced by chimpanzee adenovirus-MVA immunisation.* Nature Communications, 2013. **4**: p. 2836.

97. Chatterjee, D. and I.A. Cockburn, *The challenges of a circumsporozoite protein-based malaria vaccine.* Expert Review of Vaccines, 2021. **20**(2): p. 113-125.

98. Tarun, A.S., et al., *A combined transcriptome and proteome survey of malaria parasite liver stages.* Proceedings of the National Academy of Sciences of the United States of America, 2008. **105**(1): p. 305-10.

99. Schofield, L., *The circumsporozoite protein of Plasmodium: a mechanism of immune evasion by the malaria parasite?* Bull World Health Organ, 1990. **68 Suppl**(Suppl): p. 66-73.

100. Doolan, D.L., S.H. Apte, and C. Proietti, *Genome-based vaccine design: the promise for malaria and other infectious diseases.* International Journal for Parasitology, 2014. **44**(12): p. 901-913.

101. Bennett, B.L. and P. Sinnis, *What can we learn from an unnatural immune response?* Trends in Parasitology, 2010. **26**(7): p. 319-21.

102. Proietti, C. and D.L. Doolan, *The case for a rational genome-based vaccine against malaria.* Frontiers in Microbiology, 2014. **5**: p. 741.

103. Tiono, A.B., et al., *First field efficacy trial of the ChAd63 MVA ME-TRAP vectored malaria vaccine candidate in 5-17 months old infants and children.* PLOS ONE, 2018. **13**(12): p. e0208328.

104. Olsen, T.M., et al., *Prime-and-Trap Malaria Vaccination To Generate Protective CD8(+) Liver-Resident Memory T Cells.* Journal of Immunology, 2018. **201**(7): p. 1984-1993.

105. Thomson-Luque, R., et al., *Plasmodium falciparum merozoite surface protein 1 as asexual blood stage malaria vaccine candidate.* Expert Review of Vaccines, 2024. **23**(1): p. 160-173.

106.   Minassian, A.M., et al., *Reduced blood-stage malaria growth and immune correlates in humans following RH5 vaccination.* Med, 2021. **2**(6): p. 701-719.e19.

107.   Rts, S.C.T.P., *Efficacy and safety of RTS,S/AS01 malaria vaccine with or without a booster dose in infants and children in Africa: final results of a phase 3, individually randomised, controlled trial.* The Lancet, 2015. **386**(9988): p. 31-45.

108.   Laurens, M.B., *RTS,S/AS01 vaccine (Mosquirix™): an overview.* Human Vaccines & Immunotherapeutics, 2020. **16**(3): p. 480-489.

109.   WHO. *WHO recommends R21/Matrix-M vaccine for malaria prevention in updated advice on immunization.* 2023 [cited 2024 26/04/2024].

110.   Datoo, M.S., et al., *Safety and efficacy of malaria vaccine candidate R21/Matrix-M in African children: a multicentre, double-blind, randomised, phase 3 trial.* The Lancet, 2024. **403**(10426): p. 533-544.

111.   Almeida, M.E.M., et al., *Circumsporozoite Surface Protein-based malaria vaccines: a review.* Revista do Instituto de Medicina Tropical de São Paulo, 2021. **63**: p. e11.

112.   Davies, D.H., et al., *Large screen approaches to identify novel malaria vaccine candidates.* Vaccine, 2015. **33**(52): p. 7496-7505.

113.   Hoffman, S.L., et al., *Development of a metabolically active, non-replicating sporozoite vaccine to prevent Plasmodium falciparum malaria.* Human Vaccines, 2010. **6**(1): p. 97-106.

114.   Mwakingwe-Omari, A., et al., *Two chemoattenuated PfSPZ malaria vaccines induce sterile hepatic immunity.* Nature, 2021. **595**(7866): p. 289-294.

115.   Murphy, S.C., et al., *PfSPZ-CVac efficacy against malaria increases from 0% to 75% when administered in the absence of erythrocyte stage parasitemia: A randomized, placebo-controlled trial with controlled human malaria infection.* PLOS Pathogens, 2021. **17**(5): p. e1009594-e1009594.

116.   Oneko, M., et al., *Safety, immunogenicity and efficacy of PfSPZ Vaccine against malaria in infants in western Kenya: a double-blind, randomized, placebo-controlled phase 2 trial.* Nature Medicine, 2021. **27**(9): p. 1636-1645.

117.   Jongo, S.A., et al., *Immunogenicity and Protective Efficacy of Radiation-Attenuated and Chemo-Attenuated PfSPZ Vaccines in Equatoguinean Adults.* American Journal of Tropical Medicine and Hygiene, 2021. **104**(1): p. 283-293.

118.   Jongo, S.A., et al., *Safety, Immunogenicity, and Protective Efficacy against Controlled Human Malaria Infection of Plasmodium falciparum Sporozoite Vaccine in Tanzanian Adults.* American Journal of Tropical Medicine and Hygiene, 2018. **99**(2): p. 338-349.

119.   Ripley Ballou, W., *Obstacles to the development of a safe and effective attenuated pre-erythrocytic stage malaria vaccine.* Microbes and Infection, 2007. **9**(6): p. 761-766.

120.   Sharma, A., et al., *Severe acute respiratory syndrome coronavirus-2 (SARS-CoV-2): a global pandemic and treatment strategies.* International Journal of Antimicrobial Agents, 2020. **56**(2): p. 106054.

121.   Yanow, S.K. and M.F. Good, *Nonessential Research in the New Normal: The Impact of COVID-19.* American Journal of Tropical Medicine and Hygiene, 2020. **102**(6): p. 1164-1165.

122.   Krammer, F., *SARS-CoV-2 vaccines in development.* Nature, 2020. **586**(7830): p. 516-527.

123.   Mathieu, E., et al., *A global database of COVID-19 vaccinations.* Nature Human Behaviour, 2021. **5**(7): p. 947-953.

124.   Yarlagadda, H., et al., *COVID-19 Vaccine Challenges in Developing and Developed Countries.* Cureus, 2022. **14**(4): p. e23951.

125. Tarke, A., et al., *Comprehensive analysis of T cell immunodominance and immunoprevalence of SARS-CoV-2 epitopes in COVID-19 cases.* Cell Reports Medicine, 2021. **2**(2).

126. Kojima, N. and J.D. Klausner, *Protective immunity after recovery from SARS-CoV-2 infection.* The Lancet Infectious Diseases, 2022. **22**(1): p. 12-14.

127. Doolan, D.L. and S.L. Hoffman, *Multi-gene vaccination against malaria: A multistage, multi-immune response approach.* Parasitology Today, 1997. **13**(5): p. 171-8.

128. Good, M.F. and D.L. Doolan, *Malaria vaccine design: immunological considerations.* Immunity, 2010. **33**(4): p. 555-66.

129. Halfmann, P.J., et al., *Multivalent S2-based vaccines provide broad protection against SARS-CoV-2 variants of concern and pangolin coronaviruses.* eBioMedicine, 2022. **86**.

130. Joyce, M.G., et al., *SARS-CoV-2 ferritin nanoparticle vaccines elicit broad SARS coronavirus immunogenicity.* Cell Reports, 2021. **37**(12): p. 110143.

131. Peter, J.H., et al., *COVID-19 vaccines and the pandemic: lessons learnt for other neglected diseases and future threats.* BMJ Global Health, 2023. **8**(6): p. e011883.

132. Bonam, S.R., et al., *Plasmodium falciparum Malaria Vaccines and Vaccine Adjuvants.* Vaccines (Basel), 2021. **9**(10).

133. Knoll, M.D. and C. Wonodi, *Oxford-AstraZeneca COVID-19 vaccine efficacy.* The Lancet, 2021. **397**(10269): p. 72-74.

134. Greinacher, A., et al., *Thrombotic Thrombocytopenia after ChAdOx1 nCov-19 Vaccination.* New England Journal of Medicine, 2021. **384**(22): p. 2092-2101.

135. Deming, M.E. and K.E. Lyke, *A 'mix and match' approach to SARS-CoV-2 vaccination.* Nature Medicine, 2021. **27**(9): p. 1510-1511.

136. Barros-Martins, J., et al., *Immune responses against SARS-CoV-2 variants after heterologous and homologous ChAdOx1 nCoV-19/BNT162b2 vaccination.* Nature Medicine, 2021. **27**(9): p. 1525-1529.

137. Schmidt, T., et al., *Immunogenicity and reactogenicity of heterologous ChAdOx1 nCoV-19/mRNA vaccination.* Nature Medicine, 2021. **27**(9): p. 1530-1535.

138. Lu, S., *Heterologous prime–boost vaccination.* Current Opinion in Immunology, 2009. **21**(3): p. 346-351.

139. Hill, A.V., et al., *Prime-boost vectored malaria vaccines: progress and prospects.* Human Vaccines, 2010. **6**(1): p. 78-83.

140. Hoffman, S.L. and D.L. Doolan, *Can malaria DNA vaccines on their own be as immunogenic and protective as prime-boost approaches to immunization?* Developmental Biology (Basel), 2000. **104**: p. 121-32.

141. Moore, A.C. and A.V. Hill, *Progress in DNA-based heterologous prime-boost immunization strategies for malaria.* Immunological Reviews, 2004. **199**: p. 126-43.

142. Chuang, I., et al., *DNA Prime/Adenovirus Boost Malaria Vaccine Encoding P. falciparum CSP and AMA1 Induces Sterile Protection Associated with Cell-Mediated Immunity.* PLOS ONE, 2013. **8**(2): p. e55571.

143. Garg, I., et al., *Mix-and-Match COVID-19 Vaccinations (Heterologous Boost): A Review.* Infectious Disease Reports, 2022. **14**(4): p. 537-546.

144. Siddiqui, A., et al., *Revival of the heterologous prime-boost technique in COVID-19: An outlook from the history of outbreaks.* Health Science Reports, 2022. **5**(2): p. e531.

145. Faden, H., et al., *Long-term immunity to poliovirus in children immunized with live attenuated and enhanced-potency inactivated trivalent poliovirus vaccines.* The Journal of Infectious Diseases, 1993. **168**(2): p. 452-4.

146. Thompson, M.G., et al., *Prevention and Attenuation of Covid-19 with the BNT162b2 and mRNA-1273 Vaccines.* New England Journal of Medicine, 2021. **385**(4): p. 320-329.

147. Hogan, A.B., P. Winskill, and A.C. Ghani, *Estimated impact of RTS,S/AS01 malaria vaccine allocation strategies in sub-Saharan Africa: A modelling study.* PLOS Medicine, 2020. **17**(11): p. e1003377.

148. Datoo, M.S., et al., *Efficacy and immunogenicity of R21/Matrix-M vaccine against clinical malaria after 2 years' follow-up in children in Burkina Faso: a phase 1/2b randomised controlled trial.* The Lancet Infectious Diseases, 2022. **22**(12): p. 1728-1736.

149. Rotival, M. and L. Quintana-Murci, *Environmental variation and genetic diversity contribute to population differences in immune responses to SARS-CoV-2 and COVID-19 risk.* Genes & Immunity, 2023.

150. Bobrovitz, N., et al., *Protective effectiveness of previous SARS-CoV-2 infection and hybrid immunity against the omicron variant and severe disease: a systematic review and meta-regression.* The Lancet Infectious Diseases, 2023. **23**(5): p. 556-567.

151. Camponovo, F., et al., *Proteome-wide analysis of a malaria vaccine study reveals personalized humoral immune profiles in Tanzanian adults.* eLife, 2020. **9**.

152. Nunes-Cabaço, H., D. Moita, and M. Prudêncio, *Five decades of clinical assessment of whole-sporozoite malaria vaccines.* Frontiers in Immunology, 2022. **13**: p. 977472.

153. Jung, S., et al., *Leveraging systems biology for predicting modulators of inflammation in patients with COVID-19.* Science Advances, 2021. **7**(6): p. eabe5735.

154. Djordjevic, M., et al., *Chapter Nine - A systems biology approach to COVID-19 progression in population*, in *Advances in Protein Chemistry and Structural Biology*, R. Donev and T. Karabencheva-Christova, Editors. 2021, Academic Press. p. 291-314.

155. Jaiswal, S., et al., *Systems Biology Approaches for Therapeutics Development Against COVID-19.* Frontiers in Cellular and Infection Microbiology, 2020. **10**: p. 560240.

156. Bullock, J.L., A.; Pham, K.H.;Lam, C.S.N; Luengo-Orzo, M., *Mapping the Landscape of Artificial Intelligence Applications against COVID-19.* Journal of Aritificial Intelligence Research, 2020. **69**.

157. Alimadadi, A., et al., *Artificial intelligence and machine learning to fight COVID-19.* Physiological Genomics, 2020. **52**(4): p. 200-202.

158. Hinton, G., *Deep Learning - A Technology With the Potential to Transform Health Care.* Journal of the American Medical Association, 2018. **320**(11): p. 1101-1102.

159. Gulshan, V., et al., *Development and Validation of a Deep Learning Algorithm for Detection of Diabetic Retinopathy in Retinal Fundus Photographs.* Journal of the American Medical Association, 2016. **316**(22): p. 2402-2410.

160. Ye, Q.-H., et al., *Predicting hepatitis B virus–positive metastatic hepatocellular carcinomas using gene expression profiling and supervised machine learning.* Nature Medicine, 2003. **9**(4): p. 416-423.

161. Lee, E.K., et al., *Machine Learning for Predicting Vaccine Immunogenicity.* Interfaces, 2016. **46**(5): p. 368-390.

162. Doolan, D.L., et al., *Identification of Plasmodium falciparum antigens by antigenic analysis of genomic and proteomic data.* Proceedings of the National Academy of Sciences of the United States of America, 2003. **100**(17): p. 9952-9957.

163. Loiseau, C., M.M. Cooper, and D.L. Doolan, *Deciphering host immunity to malaria using systems immunology.* Immunological Reviews, 2020. **293**(1): p. 115-143.

164. Burel, J.G., S.H. Apte, and D.L. Doolan, *Systems Approaches towards Molecular Profiling of Human Immunity.* Trends in Immunology, 2016. **37**(1): p. 53-67.

165. Maucourant, C., et al., *Natural killer cell immunotypes related to COVID-19 disease severity.* Science Immunology, 2020. **5**(50).

166. Ryan, F.J., et al., *A systems immunology study comparing innate and adaptive immune responses in adults to COVID-19 mRNA and adenovirus vectored vaccines.* Cell Reports Medicine, 2023. **4**(3): p. 100971.

167. Stephenson, E., et al., *Single-cell multi-omics analysis of the immune response in COVID-19.* Nature Medicine, 2021. **27**(5): p. 904-916.

168. Tran, T.M. and P.D. Crompton, *Decoding the complexities of human malaria through systems immunology.* Immunological Reviews, 2020. **293**(1): p. 144-162.

169. Burel, J.G., et al., *Dichotomous miR expression and immune responses following primary blood-stage malaria.* JCI Insight, 2017. **2**(15).

170. Nuwarda, R.F., et al., *Vaccine Hesitancy: Contemporary Issues and Historical Background.* Vaccines (Basel), 2022. **10**(10).

171. Vosoughi, S., D. Roy, and S. Aral, *The spread of true and false news online.* Science, 2018. **359**(6380): p. 1146-1151.

172. Sulemane, N., et al., *Vaccines hesitancy in Africa: how COVID-19 pandemic may affect malaria vaccination campaigns.* Journal of Preventive Medicine and Hygiene, 2022. **63**(1): p. E1-e3.

173. Webb Hooper, M., A.M. Nápoles, and E.J. Pérez-Stable, *No Populations Left Behind: Vaccine Hesitancy and Equitable Diffusion of Effective COVID-19 Vaccines.* Journal of General Internal Medicine, 2021. **36**(7): p. 2130-2133.

174. Hanney, S.R., et al., *From COVID-19 research to vaccine application: why might it take 17 months not 17 years and what are the wider lessons?* Health Research Policy and Systems, 2020. **18**(1): p. 61.

175. Hodgson, J., *The pandemic pipeline.* Nature Biotechnology, 2020. **38**(5): p. 523-532.

176. WHO, *A world in disorder: Global Preparedness Monitoring Board annual report 2020.* 2020, WHO: Geneva.

177. Lalani, H.S., et al., *US public investment in development of mRNA covid-19 vaccines: retrospective cohort study.* BMJ, 2023. **380**: p. e073747.

178. WHO. *Statement on the fifteenth meeting of the IHR (2005) Emergency Committee on the COVID-19 pandemic.* 2023 [cited 2024 26/04/2024]; Available from: https://www.who.int/news/item/05-05-2023-statement-on-the-fifteenth-meeting-of-the-international-health-regulations-(2005)-emergency-committee-regarding-the-coronavirus-disease-(covid-19)-pandemic.

179. Kaushansky, A., et al., *Of men in mice: the success and promise of humanized mouse models for human malaria parasite infections.* Cellular Microbiology, 2014. **16**(5): p. 602-11.

180. White, N.J., *Severe malaria.* Malaria Journal, 2022. **21**(1): p. 284.

181. WHO, *World Malaria Report.* 2023.

182. Andrade, M.V., et al., *The economic burden of malaria: a systematic review.* Malaria Journal, 2022. **21**(1): p. 283.

183. CDC. *Malaria.* 2020 [cited 2021; Available from: https://www.cdc.gov/dpdx/malaria/index.html.

184. Miller, L.H., et al., *The pathogenic basis of malaria.* Nature, 2002. **415**(6872): p. 673-9.

185. Ejigiri, I. and P. Sinnis, *Plasmodium sporozoite-host interactions from the dermis to the hepatocyte.* Current Opinion in Microbiology, 2009. **12**(4): p. 401-7.

186. Sinnis, P. and A. Coppi, *A long and winding road: the Plasmodium sporozoite's journey in the mammalian host.* Parasitology International, 2007. **56**(3): p. 171-178.

187. Yamauchi, L.M., et al., *Plasmodium sporozoites trickle out of the injection site.* Cellular Microbiology, 2007. **9**(5): p. 1215-22.

188.   Goswami, D., N.K. Minkah, and S.H.I. Kappe, *Malaria parasite liver stages.* Journal of Hepatology, 2022. **76**(3): p. 735-737.

189.   Prudêncio, M., A. Rodriguez, and M.M. Mota, *The silent path to thousands of merozoites: the Plasmodium liver stage.* Nature Reviews Microbiology, 2006. **4**(11): p. 849-856.

190.   Moore, J.M. and J.C. Morales Aparicio, *Enhancing Pathogen Resistance: The Gut Microbiota and Malaria*, in *Comprehensive Gut Microbiota*, M. Glibetic, Editor. 2022, Elsevier: Oxford. p. 143-167.

191.   Ménard, R., et al., *Looking under the skin: the first steps in malarial infection and immunity.* Nature Reviews Microbiology, 2013. **11**(10): p. 701-712.

192.   Garg, S., et al., *Visualization and quantification of Plasmodium falciparum intraerythrocytic merozoites.* Systems and Synthetic Biology, 2015. **9**(Suppl 1): p. 23-6.

193.   Zaki, S.A. and P. Shanbag, *Atypical manifestations of malaria.* Research and Reports in Tropical Medicine, 2011. **2**: p. 9-22.

194.   White, N.J., et al., *Lethal Malaria: Marchiafava and Bignami Were Right.* The Journal of Infectious Diseases, 2013. **208**(2): p. 192-198.

195.   Mzilahowa, T., P.J. McCall, and I.M. Hastings, *"Sexual" population structure and genetics of the malaria agent P. falciparum.* PLOS ONE, 2007. **2**(7): p. e613.

196.   Siciliano, G. and P. Alano, *Enlightening the malaria parasite life cycle: bioluminescent Plasmodium in fundamental and applied research.* Frontiers in Microbiology, 2015. **6**(391).

197.   Wipasa, J., et al., *Immunity to asexual blood stage malaria and vaccine approaches.* Immunology and Cell Biology, 2002. **80**(5): p. 401-14.

198.   McCarthy, J.S. and M.F. Good, *Whole parasite blood stage malaria vaccines: a convergence of evidence.* Human Vaccines, 2010. **6**(1): p. 114-23.

199.   Khoury, D.S., et al., *Within-host modeling of blood-stage malaria.* Immunological Reviews, 2018. **285**(1): p. 168-193.

200.   Draper, S.J., et al., *Malaria Vaccines: Recent Advances and New Horizons.* Cell Host & Microbe, 2018. **24**(1): p. 43-56.

201.   Cohen, S., G.I. Mc, and S. Carrington, *Gamma-globulin and acquired immunity to human malaria.* Nature, 1961. **192**: p. 733-7.

202.   Bonilla, F.A. and H.C. Oettgen, *Adaptive immunity.* Journal of Allergy and Clinical Immunology, 2010. **125**(2 Suppl 2): p. S33-40.

203.   Silk, S.E., et al., *Blood-stage malaria vaccine candidate RH5.1/Matrix-M in healthy Tanzanian adults and children; an open-label, non-randomised, first-in-human, single-centre, phase 1b trial.* The Lancet Infectious Diseases, 2024.

204.   Duffy, P.E., et al., *Pre-erythrocytic malaria vaccines: identifying the targets.* Expert Review of Vaccines, 2012. **11**(10): p. 1261-80.

205.   Aitken, E.H., S. Mahanty, and S.J. Rogerson, *Antibody effector functions in malaria and other parasitic diseases: a few needles and many haystacks.* Immunology & Cell Biology, 2020. **98**(4): p. 264-275.

206.   Doolan, D.L. and N. Martinez-Alier, *Immune response to pre-erythrocytic stages of malaria parasites.* Current Molecular Medicine, 2006. **6**(2): p. 169-85.

207.   Dups, J.N., M. Pepper, and I.A. Cockburn, *Antibody and B cell responses to Plasmodium sporozoites.* Frontiers in Microbiology, 2014. **5**(625).

208.   Schneider, B.S., et al., *Anopheles stephensi saliva enhances progression of cerebral malaria in a murine model.* Vector-Borne and Zoonotic Diseases, 2011. **11**(4): p. 423-32.

209. Guilbride, D.L., P. Gawlinski, and P.D. Guilbride, *Why functional pre-erythrocytic and bloodstage malaria vaccines fail: a meta-analysis of fully protective immunizations and novel immunological model.* PLOS ONE, 2010. **5**(5): p. e10685.

210. Chakravarty, S., et al., *CD8+ T lymphocytes protective against malaria liver stages are primed in skin-draining lymph nodes.* Nature Medicine, 2007. **13**(9): p. 1035-41.

211. Sinnis, P. and F. Zavala, *The skin: where malaria infection and the host immune response begin.* Seminars in Immunopathology, 2012. **34**(6): p. 787-92.

212. Flores-Garcia, Y., et al., *Antibody-Mediated Protection against Plasmodium Sporozoites Begins at the Dermal Inoculation Site.* mBio, 2018. **9**(6): p. e02194-18.

213. Sack, B.K., et al., *Model for in vivo assessment of humoral protection against malaria sporozoite challenge by passive transfer of monoclonal antibodies and immune serum.* Infection and Immunity, 2014. **82**(2): p. 808-17.

214. Aliprandini, E., et al., *Cytotoxic anti-circumsporozoite antibodies target malaria sporozoites in the host skin.* Nature Microbiology, 2018. **3**(11): p. 1224-1233.

215. Cockburn, I.A. and R.A. Seder, *Malaria prevention: from immunological concepts to effective vaccines and protective antibodies.* Nature Immunology, 2018. **19**(11): p. 1199-1211.

216. Narum, D.L., et al., *Immunization with parasite-derived apical membrane antigen 1 or passive immunization with a specific monoclonal antibody protects BALB/c mice against lethal Plasmodium yoelii yoelii YM blood-stage infection.* Infection and Immunity, 2000. **68**(5): p. 2899-906.

217. Chatterjee, S., et al., *Immunity to Plasmodium berghei exoerythrocytic forms derived from irradiated sporozoites.* Parasitology Research, 1996. **82**(4): p. 297-303.

218. Yoshida, N., et al., *Hybridoma produces protective antibodies directed against the sporozoite stage of malaria parasite.* Science, 1980. **207**(4426): p. 71-3.

219. Danforth, H.D., et al., *Sporozoites of mammalian malaria: attachment to, interiorization and fate within macrophages.* Journal of Protozoology, 1980. **27**(2): p. 193-202.

220. Seguin, M.C., W.R. Ballou, and C.A. Nacy, *Interactions of Plasmodium berghei sporozoites and murine Kupffer cells in vitro.* Journal of Immunology, 1989. **143**(5): p. 1716-22.

221. Vanderberg, J.P., S. Chew, and M.J. Stewart, *Plasmodium sporozoite interactions with macrophages in vitro: a videomicroscopic analysis.* Journal of Protozoology, 1990. **37**(6): p. 528-36.

222. Bleriot, C. and F. Ginhoux, *Understanding the Heterogeneity of Resident Liver Macrophages.* Frontiers in Immunology, 2019. **10**: p. 2694.

223. Chua, C.L.L., et al., *Factors influencing phagocytosis of malaria parasites: the story so far.* Malaria Journal, 2021. **20**(1): p. 319.

224. Behet, M.C., et al., *The Complement System Contributes to Functional Antibody-Mediated Responses Induced by Immunization with Plasmodium falciparum Malaria Sporozoites.* Infection and Immunity, 2018. **86**(7): p. e00920-17.

225. Kurtovic, L., et al., *Human antibodies activate complement against Plasmodium falciparum sporozoites, and are associated with protection against malaria in children.* BMC Medicine, 2018. **16**(1): p. 61.

226. Zenklusen, I., et al., *Immunization of Malaria-Preexposed Volunteers With PfSPZ Vaccine Elicits Long-Lived IgM Invasion-Inhibitory and Complement-Fixing Antibodies.* The Journal of infectious diseases, 2018. **217**(10): p. 1569-1578.

227. Khodadadi, L., et al., *The Maintenance of Memory Plasma Cells.* Frontiers in Immunology, 2019. **10**.

228. Silveira, E.L.V., M.R. Dominguez, and I.S. Soares, *To B or Not to B: Understanding B Cell Responses in the Development of Malaria Infection.* Frontiers in Immunology, 2018. **9**: p. 2961-2961.

229. Stebegg, M., et al., *Regulation of the Germinal Center Response.* Frontiers in Immunology, 2018. **9**.

230. Klein, U. and R. Dalla-Favera, *Germinal centres: role in B-cell physiology and malignancy.* Nature Reviews Immunology, 2008. **8**(1): p. 22-33.

231. Nutt, S.L., et al., *The generation of antibody-secreting plasma cells.* Nature Reviews Immunology, 2015. **15**(3): p. 160-171.

232. Pérez-Mazliah, D., et al., *B-cell memory in malaria: Myths and realities.* Immunological Reviews, 2020. **293**(1): p. 57-69.

233. Supargiyono, S., et al., *Seasonal changes in the antibody responses against Plasmodium falciparum merozoite surface antigens in areas of differing malaria endemicity in Indonesia.* Malaria Journal, 2013. **12**(1): p. 444.

234. Moncunill, G., et al., *High antibody responses against Plasmodium falciparum in immigrants after extended periods of interrupted exposure to malaria.* PLOS ONE, 2013. **8**(8): p. e73624-e73624.

235. Medina Costa, R., et al., *Prevalence and Level of Antibodies Anti-Plasmodium spp. in Travellers with Clinical History of Imported Malaria.* Journal of Parasitology Research, 2013. **2013**: p. 247273.

236. Ndungu, F.M., et al., *Long-lived Plasmodium falciparum specific memory B cells in naturally exposed Swedish travelers.* European journal of immunology, 2013. **43**(11): p. 2919-2929.

237. Dolo, A., et al., *Epidemiology of malaria in a village of Sudanese savannah in Mali (Bancoumana). Anti-TRAP and anti-CS humoral immunity response].* Bulletin de la Société de Pathologie Exotique, 2003. **96**(4): p. 287-90.

238. Kinyanjui, S.M., et al., *IgG antibody responses to Plasmodium falciparum merozoite antigens in Kenyan children have a short half-life.* Malaria Journal, 2007. **6**(1): p. 82.

239. Rogers, K.J., R. Vijay, and N.S. Butler, *Anti-malarial humoral immunity: the long and short of it.* Microbes and Infection, 2021. **23**(4): p. 104807.

240. Aye, R., et al., *Malaria exposure drives both cognate and bystander human B cells to adopt an atypical phenotype.* European Journal of Immunology, 2020. **50**(8): p. 1187-1194.

241. Ubillos, I., et al., *Chronic Exposure to Malaria Is Associated with Inhibitory and Activation Markers on Atypical Memory B Cells and Marginal Zone-Like B Cells.* Frontiers in Immunology, 2017. **8**.

242. Portugal, S., et al., *Malaria-associated atypical memory B cells exhibit markedly reduced B cell receptor signaling and effector function.* eLife, 2015. **4**: p. e07218.

243. Sullivan, R.T., et al., *FCRL5 Delineates Functionally Impaired Memory B Cells Associated with Plasmodium falciparum Exposure.* PLOS Pathogens, 2015. **11**(5): p. e1004894.

244. Sutton, H.J., et al., *Atypical B cells are part of an alternative lineage of B cells that participates in responses to vaccination and infection in humans.* Cell Reports, 2021. **34**(6): p. 108684.

245. Inoue, T. and T. Kurosaki, *Memory B cells.* Nature Reviews Immunology, 2024. **24**(1): p. 5-17.

246. Ambegaonkar, A.A., et al., *Atypical B cells in chronic infectious diseases and systemic autoimmunity: puzzles with many missing pieces.* Current Opinion in Immunology, 2022. **77**: p. 102227.

247. Rivera-Correa, J., et al., *Atypical memory B-cells and autoantibodies correlate with anemia during Plasmodium vivax complicated infections.* PLOS Neglected Tropical Diseases, 2020. **14**(7): p. e0008466.

248. Holz, L.E., D. Fernandez-Ruiz, and W.R. Heath, *Protective immunity to liver-stage malaria.* Clinical & Translational Immunology, 2016. **5**(10): p. e105.

249. Baer, K., et al., *Kupffer cells are obligatory for Plasmodium yoelii sporozoite infection of the liver.* Cellular Microbiology, 2007. **9**(2): p. 397-412.

250. Ivashkiv, L.B. and L.T. Donlin, *Regulation of type I interferon responses.* Nature Reviews Immunology, 2014. **14**(1): p. 36-49.

251. Mota, M.M., J.C. Hafalla, and A. Rodriguez, *Migration through host cells activates Plasmodium sporozoites for infection.* Nature Medicine, 2002. **8**(11): p. 1318-22.

252. Tavares, J., et al., *Role of host cell traversal by the malaria sporozoite during liver infection.* Journal of Experimental Medicine, 2013. **210**(5): p. 905-15.

253. Mota, M.M., et al., *Migration of Plasmodium sporozoites through cells before infection.* Science, 2001. **291**(5501): p. 141-4.

254. Tweedell, R.E., et al., *Kupffer Cells Survive Plasmodium berghei Sporozoite Exposure and Respond with a Rapid Cytokine Release.* Pathogens, 2018. **7**(4).

255. Warren, A., et al., *T lymphocytes interact with hepatocytes through fenestrations in murine liver sinusoidal endothelial cells.* Hepatology, 2006. **44**(5): p. 1182-1190.

256. McCuskey, R.S. and F.D. Reilly, *Hepatic microvasculature: dynamic structure and its regulation.* Seminars in Liver Disease, 1993. **13**(1): p. 1-12.

257. Horst, A.K., et al., *Modulation of liver tolerance by conventional and nonconventional antigen-presenting cells and regulatory immune cells.* Cellular & Molecular Immunology, 2016. **13**(3): p. 277-92.

258. Bertolino, P., et al., *Antigen-specific primary activation of CD8+ T cells within the liver.* Journal of Immunology, 2001. **166**(9): p. 5430-8.

259. Crouse, J., et al., *NK cells regulating T cell responses: mechanisms and outcome.* Trends in Immunology, 2015. **36**(1): p. 49-58.

260. Hart, G.T., et al., *Adaptive NK cells in people exposed to Plasmodium falciparum correlate with protection from malaria.* Journal of Experimental Medicine, 2019. **216**(6): p. 1280-1290.

261. von Andrian, U.H., *NK cell memory: discovery of a mystery.* Nature Immunology, 2021. **22**(6): p. 669-671.

262. O'Leary, J.G., et al., *T cell- and B cell-independent adaptive immunity mediated by natural killer cells.* Nature Communications, 2006. **7**(5): p. 507-16.

263. Reeves, R.K., et al., *Antigen-specific NK cell memory in rhesus macaques.* Nature immunology, 2015. **16**(9): p. 927-932.

264. Zamora, A.E., et al., *Models to Study NK Cell Biology and Possible Clinical Application.* Current Protocols in Immunology, 2015. **110**: p. 14.37.1-14.37.14.

265. Keppel, M.P., L. Yang, and M.A. Cooper, *Murine NK cell intrinsic cytokine-induced memory-like responses are maintained following homeostatic proliferation.* Journal of Immunology, 2013. **190**(9): p. 4754-62.

266. Sun, J.C., J.N. Beilke, and L.L. Lanier, *Adaptive immune features of natural killer cells.* Nature, 2009. **457**(7229): p. 557-561.

267. Cerwenka, A. and L.L. Lanier, *Natural killer cell memory in infection, inflammation and cancer.* Nature Reviews Immunology, 2016. **16**(2): p. 112-23.

268. Marcus, A. and D.H. Raulet, *Evidence for natural killer cell memory.* Current Biology, 2013. **23**(17): p. R817-20.

269. O'Sullivan, T.E. and J.C. Sun, *Generation of Natural Killer Cell Memory during Viral Infection.* Journal of Innate Immunity, 2015. **7**(6): p. 557-62.

270. Peng, H. and Z. Tian, *Natural Killer Cell Memory: Progress and Implications*. Frontiers in Immunology, 2017. **8**: p. 1143-1143.

271. Doolan, D.L. and S.L. Hoffman, *IL-12 and NK cells are required for antigen-specific adaptive immunity against malaria initiated by CD8+ T cells in the Plasmodium yoelii model*. Journal of Immunology, 1999. **163**(2): p. 884-92.

272. Doolan, D.L. and S.L. Hoffman, *The complexity of protective immunity against liver-stage malaria*. Journal of Immunology, 2000. **165**(3): p. 1453-62.

273. Burrack, K.S., G.T. Hart, and S.E. Hamilton, *Contributions of natural killer cells to the immune response against Plasmodium*. Malaria Journal, 2019. **18**(1): p. 321.

274. Subleski, J., et al., *Chapter Nineteen - NK and NKT cells: The innate–adaptive interface including humoral responses*, in *Natural Killer Cells*, M.T. Lotze and A.W. Thomson, Editors. 2010, Academic Press: San Diego. p. 255-277.

275. Rossjohn, J., et al., *Recognition of CD1d-restricted antigens by natural killer T cells*. Nature Reviews Immunology, 2012. **12**(12): p. 845-57.

276. Miller, Jessica L., et al., *Interferon-Mediated Innate Immune Responses against Malaria Parasite Liver Stages*. Cell Reports, 2014. **7**(2): p. 436-447.

277. Hansen, D.S., et al., *CD1d-restricted NKT cells contribute to malarial splenomegaly and enhance parasite-specific antibody responses*. European Journal of Immunology, 2003. **33**(9): p. 2588-98.

278. Gonzalez-Aseguinolaza, G., et al., *Natural killer T cell ligand alpha-galactosylceramide enhances protective immunity induced by malaria vaccines*. Journal of Experimental Medicine, 2002. **195**(5): p. 617-24.

279. Ho, M., et al., *Polyclonal Expansion of Peripheral Gamma-Delta T-Cells in Human Plasmodium-Falciparum Malaria*. Infection and Immunity, 1994. **62**(3): p. 855-862.

280. Roussilhon, C., et al., *Human Tcr-Gamma-Delta(+) Lymphocyte-Response on Primary Exposure to Plasmodium-Falciparum*. Clinical and Experimental Immunology, 1994. **95**(1): p. 91-97.

281. Ishizuka, A.S., et al., *Protection against malaria at 1 year and immune correlates following PfSPZ vaccination*. Nature Medicine, 2016. **22**(6): p. 614-23.

282. Zaidi, I., et al., *gammadelta T Cells Are Required for the Induction of Sterile Immunity during Irradiated Sporozoite Vaccinations*. Journal of Immunology, 2017. **199**(11): p. 3781-3788.

283. Jagannathan, P., et al., *Loss and dysfunction of Vδ2⁺ γδ T cells are associated with clinical tolerance to malaria*. Science Translational Medicine, 2014. **6**(251): p. 251ra117.

284. Jagannathan, P., et al., *Vδ2+ T cell response to malaria correlates with protection from infection but is attenuated with repeated exposure*. Scientific Reports, 2017. **7**(1): p. 11487.

285. Stanisic, D.I., et al., *γδ T cells and CD14+ Monocytes Are Predominant Cellular Sources of Cytokines and Chemokines Associated With Severe Malaria*. The Journal of Infectious Diseases, 2014. **210**(2): p. 295-305.

286. Pamplona, A. and B. Silva-Santos, *γδ T cells in malaria: a double-edged sword*. The FEBS Journal, 2021. **288**(4): p. 1118-1129.

287. Dusseaux, M., et al., *Human MAIT cells are xenobiotic-resistant, tissue-targeted, CD161hi IL-17–secreting T cells*. Blood, 2011. **117**(4): p. 1250-1259.

288. Ng, S.S. and C.R. Engwerda, *Innate Lymphocytes and Malaria - Players or Spectators?* Trends in Parasitology, 2019. **35**(2): p. 154-162.

289. Schmaler, M., et al., *Human unconventional T cells in Plasmodium falciparum infection*. Seminars in Immunopathology, 2020. **42**(3): p. 265-277.

290. Dantzler, K.W. and P. Jagannathan, *gamma delta T Cells in Antimalarial Immunity: New Insights Into Their Diverse Functions in Protection and Tolerance.* Frontiers in Immunology, 2018. **9**.

291. Germain, R.N., *The Cellular Determinants of Adaptive Immunity.* The New England Journal of Medicine, 2019. **381**(11): p. 1083-1085.

292. Gasteiger, G., et al., *Cellular Innate Immunity: An Old Game with New Players.* Journal of Innate Immunity, 2017. **9**(2): p. 111-125.

293. Clem, A.S., *Fundamentals of vaccine immunology.* Journal of Global Infectious Diseases, 2011. **3**(1): p. 73-8.

294. Kalia, V. and S. Sarkar, *Regulation of Effector and Memory CD8 T Cell Differentiation by IL-2-A Balancing Act.* Frontiers in Immunology, 2018. **9**: p. 2987.

295. Rodrigues, M.M., et al., *CD8+ cytolytic T cell clones derived against the Plasmodium yoelii circumsporozoite protein protect against malaria.* International Immunology, 1991. **3**(6): p. 579-585.

296. Mellouk, S., et al., *IFN-gamma inhibits development of Plasmodium berghei exoerythrocytic stages in hepatocytes by an L-arginine-dependent effector mechanism.* Journal of Immunology, 1991. **146**(11): p. 3971-6.

297. Schofield, L., et al., *Gamma interferon, CD8+ T cells and antibodies required for immunity to malaria sporozoites.* Nature, 1987. **330**(6149): p. 664-6.

298. Ferreira, A., et al., *Inhibition of development of exoerythrocytic forms of malaria parasites by gamma-interferon.* Science, 1986. **232**(4752): p. 881-4.

299. Tsuji, M., et al., *Development of antimalaria immunity in mice lacking IFN-gamma receptor.* Journal of Immunology, 1995. **154**(10): p. 5338-44.

300. Hoffman, S.L., et al., *Protection of humans against malaria by immunization with radiation-attenuated Plasmodium falciparum sporozoites.* The Journal of Infectious Diseases, 2002. **185**(8): p. 1155-64.

301. Van Braeckel-Budimir, N. and J.T. Harty, *CD8 T-cell-mediated protection against liver-stage malaria: lessons from a mouse model.* Frontiers in Microbiology, 2014. **5**: p. 272.

302. Fernandez-Ruiz, D., et al., *Liver-Resident Memory CD8+ T Cells Form a Front-Line Defense against Malaria Liver-Stage Infection.* Immunity, 2016. **45**(4): p. 889-902.

303. Obeid, M., et al., *Skin-draining lymph node priming is sufficient to induce sterile immunity against pre-erythrocytic malaria.* EMBO Molecular Medicine, 2013. **5**(2): p. 250-63.

304. Schmidt, N.W., et al., *Memory CD8 T cell responses exceeding a large but definable threshold provide long-term immunity to malaria.* Proceedings of the National Academy of Sciences of the United States of America, 2008. **105**(37): p. 14017-14022.

305. Schmidt, N.W., N.S. Butler, and J.T. Harty, *Plasmodium–host interactions directly influence the threshold of memory CD8 T cells required for protective immunity.* The Journal of Immunology, 2011. **186**(10): p. 5873-5884.

306. Riley, E.M. and V.A. Stewart, *Immune mechanisms in malaria: new insights in vaccine development.* Nature Medicine, 2013. **19**(2): p. 168-78.

307. Romagnani, S., *Th1/Th2 cells.* Inflammatory Bowel Diseases, 1999. **5**(4): p. 285-94.

308. Montes de Oca, M., et al., *The Impact of Established Immunoregulatory Networks on Vaccine Efficacy and the Development of Immunity to Malaria.* Journal of Immunology, 2016. **197**(12): p. 4518-4526.

309. Hartigan-O'Connor, D.J., et al., *Th17 cells and regulatory T cells in elite control over HIV and SIV.* Current Opinion in HIV and AIDS, 2011. **6**(3): p. 221-7.

310. Troye-Blomberg, M., et al., *Production of IL 2 and IFN-gamma by T cells from malaria patients in response to Plasmodium falciparum or erythrocyte antigens in vitro.* Journal of Immunology, 1985. **135**(5): p. 3498-504.

311. Shear, H.L., et al., *Role of IFN-gamma in lethal and nonlethal malaria in susceptible and resistant murine hosts.* Journal of Immunology, 1989. **143**(6): p. 2038-44.

312. Castro, F., et al., *Interferon-Gamma at the Crossroads of Tumor Immune Surveillance or Evasion.* Frontiers in Immunology, 2018. **9**: p. 847.

313. Spolski, R., P. Li, and W.J. Leonard, *Biology and regulation of IL-2: from molecular mechanisms to human therapy.* Nature Reviews Immunology, 2018. **18**(10): p. 648-659.

314. Hansen, D.S. and L. Schofield, *Natural regulatory T cells in malaria: host or parasite allies?* PLOS Pathogens, 2010. **6**(4): p. e1000771.

315. Muruganandah, V., et al., *A Systematic Review: The Role of Resident Memory T Cells in Infectious Diseases and Their Relevance for Vaccine Development.* Frontiers in Immunology, 2018. **9**: p. 1574.

316. Larbi, A. and T. Fulop, *From "truly naive" to "exhausted senescent" T cells: when markers predict functionality.* Cytometry A, 2014. **85**(1): p. 25-35.

317. Wherry, E.J., *T cell exhaustion.* Nature Communications, 2011. **12**(6): p. 492-9.

318. Willinger, T., et al., *Molecular signatures distinguish human central memory from effector memory CD8 T cell subsets.* Journal of Immunology, 2005. **175**(9): p. 5895-903.

319. Pawelec, G., *Is There a Positive Side to T Cell Exhaustion?* Frontiers in Immunology, 2019. **10**: p. 111.

320. Schenkel, J.M. and D. Masopust, *Tissue-resident memory T cells.* Immunity, 2014. **41**(6): p. 886-97.

321. Samji, T. and K.M. Khanna, *Understanding memory CD8+ T cells.* Immunology Letters, 2017. **185**: p. 32-39.

322. Schenkel, J.M., et al., *Sensing and alarm function of resident memory CD8+ T cells.* Nature Communications, 2013. **14**(5): p. 509-13.

323. Sano, G., et al., *Swift development of protective effector functions in naive CD8+ T cells against malaria liver stages.* Journal of Experimental Medicine, 2001. **194**(2): p. 173-80.

324. Gola, A., et al., *Prime and target immunization protects against liver-stage malaria in mice.* Science Translational Medicine, 2018. **10**(460).

325. McNamara, H.A., et al., *Up-regulation of LFA-1 allows liver-resident memory T cells to patrol and remain in the hepatic sinusoids.* Science Immunology, 2017. **2**(9): p. eaaj1996.

326. Thomas, S.Y., et al., *PLZF induces an intravascular surveillance program mediated by long-lived LFA-1-ICAM-1 interactions.* Journal of Experimental Medicine, 2011. **208**(6): p. 1179-88.

327. Moss, P., *The T cell immune response against SARS-CoV-2.* Nature Immunology, 2022. **23**(2): p. 186-193.

328. Scarpa, R., et al., *Impact of Hypogammaglobulinemia on the Course of COVID-19 in a Non-Intensive Care Setting: A Single-Center Retrospective Cohort Study.* Frontiers in Immunology, 2022. **13**: p. 842643.

329. Yewdell, J.W., *Confronting complexity: real-world immunodominance in antiviral CD8+ T cell responses.* Immunity, 2006. **25**(4): p. 533-43.

330. Chen, W., et al., *Dissecting the multifactorial causes of immunodominance in class I-restricted T cell responses to viruses.* Immunity, 2000. **12**(1): p. 83-93.

331. Yewdell, J.W. and J.R. Bennink, *Immunodominance in major histocompatibility complex class I-restricted T lymphocyte responses.* Annual Review of Immunology, 1999. **17**: p. 51-88.

332. van der Most, R.G., et al., *Analysis of cytotoxic T cell responses to dominant and subdominant epitopes during acute and chronic lymphocytic choriomeningitis virus infection.* Journal of Immunology, 1996. **157**(12): p. 5543-54.

333. Wieczorek, M., et al., *Major Histocompatibility Complex (MHC) Class I and MHC Class II Proteins: Conformational Plasticity in Antigen Presentation.* Frontiers in Immunology, 2017. **8**: p. 292.

334. Akram, A. and R.D. Inman, *Immunodominance: a pivotal principle in host response to viral infections.* Clinical Immunology, 2012. **143**(2): p. 99-115.

335. Vatti, A., et al., *Original antigenic sin: A comprehensive review.* Journal of Autoimmunity, 2017. **83**: p. 12-21.

336. Princiotta, M.F., et al., *Quantitating protein synthesis, degradation, and endogenous antigen processing.* Immunity, 2003. **18**(3): p. 343-54.

337. Welsh, R.M. and L.K. Selin, *No one is naive: the significance of heterologous T-cell immunity.* Nature Reviews Immunology, 2002. **2**(6): p. 417-26.

338. Singh, R.A., J.R. Rodgers, and M.A. Barry, *The role of T cell antagonism and original antigenic sin in genetic immunization.* Journal of Immunology, 2002. **169**(12): p. 6779-86.

339. La Gruta, N.L., et al., *Understanding the drivers of MHC restriction of T cell receptors.* Nature Reviews Immunology, 2018. **18**(7): p. 467-478.

340. Bogue, M. and D.B. Roth, *Mechanism of V(D)J recombination.* Current Opinion in Immunology, 1996. **8**(2): p. 175-80.

341. Sercarz, E.E., et al., *Dominance and crypticity of T cell antigenic determinants.* Annual Review of Immunology, 1993. **11**: p. 729-66.

342. Pires de Sousa, K., *Characterization of cross-reactive immune responses in the context of a complex host-pathogen system*, in *School of Medicine*. 2018, The University of Queensland. p. 294.

343. Gardner, M.J., et al., *Genome sequence of the human malaria parasite Plasmodium falciparum.* Nature, 2002. **419**(6906): p. 498-511.

344. Su, X.Z., et al., *Plasmodium Genomics and Genetics: New Insights into Malaria Pathogenesis, Drug Resistance, Epidemiology, and Evolution.* Clinical Microbiology Reviews, 2019. **32**(4).

345. Sidney, J., et al., *HLA class I supertypes: a revised and updated classification.* BMC Immunology, 2008. **9**: p. 1.

346. Wang, M. and M.H. Claesson, *Classification of human leukocyte antigen (HLA) supertypes.* Methods in Molecular Biology, 2014. **1184**: p. 309-17.

347. Greenbaum, J., et al., *Functional classification of class II human leukocyte antigen (HLA) molecules reveals seven different supertypes and a surprising degree of repertoire sharing across supertypes.* Immunogenetics, 2011. **63**(6): p. 325-35.

348. Sette, A., et al., *Optimizing vaccine design for cellular processing, MHC binding and TCR recognition.* Tissue Antigens, 2002. **59**(6): p. 443-51.

349. Vita, R., et al., *The Immune Epitope Database (IEDB): 2018 update.* Nucleic Acids Res, 2019. **47**(D1): p. D339-d343.

350. De Rosa, S.C., et al., *Vaccination in humans generates broad T cell cytokine responses.* Journal of Immunology, 2004. **173**(9): p. 5372-80.

351. Gill, D.K., et al., *Equivalence of ELISpot Assays Demonstrated between Major HIV Network Laboratories.* PLOS ONE, 2010. **5**(12): p. e14330.

352. Cossarizza, A., et al., *Guidelines for the use of flow cytometry and cell sorting in immunological studies (second edition).* European Journal of Immunology, 2019. **49**(10): p. 1457-1973.

353. Boulet, S., et al., *A dual color ELISPOT method for the simultaneous detection of IL-2 and IFN-gamma HIV-specific immune responses.* Journal of Immunological Methods, 2007. **320**(1-2): p. 18-29.

354. Karlsson, A.C., et al., *Comparison of the ELISPOT and cytokine flow cytometry assays for the enumeration of antigen-specific T cells.* Journal of Immunological Methods, 2003. **283**(1-2): p. 141-53.

355. Prokopec, S.D., et al., *Systematic evaluation of medium-throughput mRNA abundance platforms.* RNA, 2013. **19**(1): p. 51-62.

356. Browne, D.J., et al., *An analytically and diagnostically sensitive RNA extraction and RT-qPCR protocol for peripheral blood mononuclear cells.* Frontiers in Immunology, 2020. **11**: p. 402.

357. Chan, K., et al., *Rapid, Affordable and Portable Medium-Throughput Molecular Device for Zika Virus.* Scientific Reports, 2016. **6**: p. 38223.

358. Monleau, M., et al., *Comparison of different extraction techniques to profile microRNAs from human sera and peripheral blood mononuclear cells.* BMC Genomics, 2014. **15**: p. 395.

359. Eikmans, M., et al., *Blood cell mRNAs and microRNAs: optimized protocols for extraction and preservation.* Blood, 2013. **121**(11): p. e81-9.

360. de Weerdt, I., et al., *Improving CLL Vgamma9Vdelta2-T-cell fitness for cellular therapy by ex vivo activation and ibrutinib.* Blood, 2018. **132**(21): p. 2260-2272.

361. Yeomans, A., et al., *Engagement of the B-cell receptor of chronic lymphocytic leukemia cells drives global and MYC-specific mRNA translation.* Blood, 2016. **127**(4): p. 449-57.

362. Eikmans, M., D.L. Roelen, and F.H. Claas, *Molecular monitoring for rejection and graft outcome in kidney transplantation.* Expert Opinion on Medical Diagnostics, 2008. **2**(12): p. 1365-79.

363. Ebert, B.L. and T.R. Golub, *Genomic approaches to hematologic malignancies.* Blood, 2004. **104**(4): p. 923-32.

364. Carrera Silva, E.A., et al., *CD207+ CD1a+ cells circulate in pediatric patients with active Langerhans cell histiocytosis.* Blood, 2017. **130**(17): p. 1898-1902.

365. Yang, J., et al., *TRAIL mediates and sustains constitutive NF-kappaB activation in LGL leukemia.* Blood, 2018. **131**(25): p. 2803-2815.

366. van 't Veer, L.J., et al., *Gene expression profiling predicts clinical outcome of breast cancer.* Nature, 2002. **415**(6871): p. 530-6.

367. Burczynski, M.E., et al., *Transcriptional profiles in peripheral blood mononuclear cells prognostic of clinical outcomes in patients with advanced renal cell carcinoma.* Clinical Cancer Research, 2005. **11**(3): p. 1181-9.

368. Ries, J., et al., *Prognostic significance of altered miRNA expression in whole blood of OSCC patients.* Oncology Reports, 2017. **37**(6): p. 3467-3474.

369. Qu, X., et al., *Long Noncoding RNAs and mRNA Regulation in Peripheral Blood Mononuclear Cells of Patients with Chronic Obstructive Pulmonary Disease.* Mediators of Inflammation, 2018. **2018**: p. 7501851.

370. Chen, H., et al., *Enhanced Expression of NLRP3 Inflammasome-Related Inflammation in Diabetic Retinopathy.* Investigative Ophthalmology & Visual Science, 2018. **59**(2): p. 978-985.

371. Contreras, X., et al., *Nuclear RNA surveillance complexes silence HIV-1 transcription.* PLOS Pathogens, 2018. **14**(3): p. e1006950.

372. Laird, G.M., et al., *Measuring the Frequency of Latent HIV-1 in Resting CD4+ T Cells Using a Limiting Dilution Coculture Assay.* Methods in Molecular Biology, 2016. **1354**: p. 239-53.

373. Ming, M., et al., *An in vitro functional assay to measure the biological activity of TB vaccine candidate H4-IC31.* Vaccine, 2019. **37**(22): p. 2960-2966.

374. Higbee, R.G., et al., *An immunologic model for rapid vaccine assessment - a clinical trial in a test tube.* Alternatives to Laboratory Animals, 2009. **37 Suppl 1**: p. 19-27.

375. Saah, A.J. and D.R. Hoover, *"Sensitivity" and "specificity" reconsidered: the meaning of these terms in analytical and diagnostic settings.* Annals of Internal Medicine, 1997. **126**(1): p. 91-4.

376. Romer, P.S., et al., *Preculture of PBMCs at high cell density increases sensitivity of T-cell responses, revealing cytokine release by CD28 superagonist TGN1412.* Blood, 2011. **118**(26): p. 6772-82.

377. Kutscher, S., et al., *Overnight resting of PBMC changes functional signatures of antigen specific T- cell responses: impact for immune monitoring within clinical trials.* PLOS ONE, 2013. **8**(10): p. e76215.

378. Lamoreaux, L., M. Roederer, and R. Koup, *Intracellular cytokine optimization and standard operating procedure.* Nature Protocols, 2006. **1**(3): p. 1507-16.

379. Kingsmore, S.F., *Multiplexed protein measurement: technologies and applications of protein and antibody arrays.* Nature Reviews Drug Discovery, 2006. **5**(4): p. 310-20.

380. Barabas, S., et al., *An optimized IFN-gamma ELISpot assay for the sensitive and standardized monitoring of CMV protein-reactive effector cells of cell-mediated immunity.* BMC Immunology, 2017. **18**(1): p. 14.

381. Sharma, S., et al., *A Sensitive Method for Detecting Peptide-specific CD4+ T Cell Responses in Peripheral Blood from Patients with Myasthenia Gravis.* Frontiers in Immunology, 2017. **8**: p. 1370.

382. Lin, Y., et al., *Optimization and validation of a robust human T-cell culture method for monitoring phenotypic and polyfunctional antigen-specific CD4 and CD8 T-cell responses.* Cytotherapy, 2009. **11**(7): p. 912-22.

383. Ashoor, I., et al., *Standardization and Cross Validation of Alloreactive IFNγ ELISPOT Assays Within the Clinical Trials in Organ Transplantation Consortium.* American Journal of Transplantation, 2013. **13**(7): p. 1871-1879.

384. Walsh, P.N., et al., *Optimization and qualification of a memory B-cell ELISpot for the detection of vaccine-induced memory responses in HIV vaccine trials.* Journal of Immunological Methods, 2013. **394**(1-2): p. 84-93.

385. Posevitz-Fejfar, A., et al., *Effects of blood transportation on human peripheral mononuclear cell yield, phenotype and function: implications for immune cell biobanking.* PLOS ONE, 2014. **9**(12): p. e115920.

386. Keller, C.C., et al., *Elevated nitric oxide production in children with malarial anemia: hemozoin-induced nitric oxide synthase type 2 transcripts and nitric oxide in blood mononuclear cells.* Infection and Immunity, 2004. **72**(8): p. 4868-73.

387. Azizi, A., *Protective Efficacy of Candidate Vaccines Prior to Human Clinical Trials.* Journal of Pharmaceutical Sciences, 2018. **107**(12): p. 2992-2994.

388. Tourdot, S. and T.P. Hickling, *Nonclinical immunogenicity risk assessment of therapeutic proteins.* Bioanalysis, 2019.

389. Cioni, M., et al., *Characterization of Immunodominant BK Polyomavirus 9mer Epitope T Cell Responses.* American Journal of Transplantation, 2016. **16**(4): p. 1193-206.

390. Masilamani, M., M. Pascal, and H.A. Sampson, *T-Cell Proliferation Assay: Determination of Immunodominant T-Cell Epitopes of Food Allergens.* Methods in Molecular Biology, 2017. **1592**: p. 189-198.

391. Zhang, J., et al., *Identification of Immunodominant Th2-Cell Epitopes in Chinese Patients with Bullous Pemphigoid.* Journal of Investigative Dermatology, 2018. **138**(9): p. 1917-1924.

392. Pescarmona, R., et al., *Comparison of RT-qPCR and Nanostring in the measurement of blood interferon response for the diagnosis of type I interferonopathies.* Cytokine, 2019. **113**: p. 446-452.

393. Bustin, S.A., *Quantification of mRNA using real-time reverse transcription PCR (RT-PCR): trends and problems.* Journal of Molecular Endocrinology, 2002. **29**(1): p. 23-39.

394. Bhatia, P., et al., *Comparison of glyceraldehyde-3-phosphate dehydrogenase and 28S-ribosomal RNA gene expression as RNA loading controls for northern blot analysis of cell lines of varying malignant potential.* Analytical Biochemistry, 1994. **216**(1): p. 223-6.

395. Lowe, R., et al., *Transcriptomics technologies.* PLOS Computational Biology, 2017. **13**(5): p. e1005457.

396. Chin, E.L., C. da Silva, and M. Hegde, *Assessment of clinical analytical sensitivity and specificity of next-generation sequencing for detection of simple and complex mutations.* BMC Genetics, 2013. **14**: p. 6.

397. Taylor, S.C., G. Laperriere, and H. Germain, *Droplet Digital PCR versus qPCR for gene expression analysis with low abundant targets: from variable nonsense to publication quality data.* Scientific Reports, 2017. **7**(1): p. 2409.

398. Nfonsam, L., et al., *Leveraging the power of new molecular technologies in the clinical setting requires unprecedented awareness of limitations and drawbacks: experience of one diagnostic laboratory.* Journal of Medical Genetics, 2019. **56**(6): p. 408-412.

399. Escobar-Escamilla, N., et al., *Utility of high-throughput DNA sequencing in the study of the human papillomaviruses.* Virus Genes, 2018. **54**(1): p. 17-24.

400. Bustin, S.A., et al., *The MIQE guidelines: minimum information for publication of quantitative real-time PCR experiments.* Clinical Chemistry, 2009. **55**(4): p. 611-22.

401. Bas, A., et al., *Utility of the housekeeping genes 18S rRNA, beta-actin and glyceraldehyde-3-phosphate-dehydrogenase for normalization in real-time quantitative reverse transcriptase-polymerase chain reaction analysis of gene expression in human T lymphocytes.* Scandinavian Journal of Immunology, 2004. **59**(6): p. 566-73.

402. Ledderose, C., et al., *Selection of reliable reference genes for quantitative real-time PCR in human T cells and neutrophils.* BMC Research Notes, 2011. **4**: p. 427.

403. Nolan, T., R.E. Hands, and S.A. Bustin, *Quantification of mRNA using real-time RT-PCR.* Nature Protocols, 2006. **1**(3): p. 1559-82.

404. Ruijter, J.M., et al., *Amplification efficiency: linking baseline and bias in the analysis of quantitative PCR data.* Nucleic Acids Res, 2009. **37**(6): p. e45.

405. Stahlberg, A. and M. Kubista, *The workflow of single-cell expression profiling using quantitative real-time PCR.* Expert Review of Molecular Diagnostics, 2014. **14**(3): p. 323-31.

406. Pattinson, D.J., et al., *Chimeric Murine Polyomavirus Virus-Like Particles Induce Plasmodium Antigen-Specific CD8(+) T Cell and Antibody Responses.* Frontiers in Cellular and Infection Microbiology, 2019. **9**.

407. Wang, R., et al., *Induction of CD4+ T cell-dependent CD8+ type 1 responses in humans by a malaria DNA vaccine.* Proceedings of the National Academy of Sciences of the United States of America, 2001. **98**(19): p. 10817-22.

408. Luchting, B., et al., *Disrupted TH17/Treg balance in patients with chronic low back pain.* PLOS ONE, 2014. **9**(8): p. e104883.

409. Trinite, B., et al., *Suppression of Foxo1 activity and down-modulation of CD62L (L-selectin) in HIV-1 infected resting CD4 T cells.* PLOS ONE, 2014. **9**(10): p. e110719.

410. Spandidos, A., et al., *PrimerBank: a resource of human and mouse PCR primer pairs for gene expression detection and quantification.* Nucleic Acids Res, 2010. **38**(Database issue): p. D792-9.

411. Al-Soud, W.A. and P. Radstrom, *Purification and characterization of PCR-inhibitory components in blood cells.* Journal of Clinical Microbiology, 2001. **39**(2): p. 485-93.

412. Schrader, C., et al., *PCR inhibitors - occurrence, properties and removal.* Journal of Applied Microbiology, 2012. **113**(5): p. 1014-26.

413. Kermekchiev, M.B., et al., *Mutants of Taq DNA polymerase resistant to PCR inhibitors allow DNA amplification from whole blood and crude soil samples.* Nucleic Acids Res, 2009. **37**(5): p. e40.

414. Liang, F., et al., *Development of a Multiplexed Microsphere PCR for Culture-Free Detection and Gram-Typing of Bacteria in Human Blood Samples.* ACS Infectious Diseases, 2018. **4**(5): p. 837-844.

415. Gutierrez-Loli, R., et al., *Development of a Novel Protocol Based on Blood Clot to Improve the Sensitivity of qPCR Detection of Toxoplasma gondii in Peripheral Blood Specimens.* American Journal of Tropical Medicine and Hygiene, 2019. **100**(1): p. 83-89.

416. Archin, N.M., et al., *HIV-1 expression within resting CD4+ T cells after multiple doses of vorinostat.* The Journal of Infectious Diseases, 2014. **210**(5): p. 728-35.

417. Oliver-Ferrando, S., et al., *Comparison of cytokine profiles in peripheral blood mononuclear cells between piglets born from Porcine circovirus 2 vaccinated and non-vaccinated sows.* Veterinary Microbiology, 2018. **214**: p. 148-153.

418. Williams, W.V., H. Rosenbaum, and D.B. Weiner, *Effect of RNA concentration on cDNA synthesis for DNA amplification.* PCR Methods and Applications, 1992. **2**(1): p. 86-8.

419. Bustin, S. and T. Nolan, *Talking the talk, but not walking the walk: RT-qPCR as a paradigm for the lack of reproducibility in molecular research.* European Journal of Clinical Investigation, 2017. **47**(10): p. 756-774.

420. Liu, Y., A. Beyer, and R. Aebersold, *On the Dependency of Cellular Protein Levels on mRNA Abundance.* Cell, 2016. **165**(3): p. 535-50.

421. Brennan, K., et al., *Type 1 IFN Induction by Cytosolic Nucleic Acid Is Intact in Neonatal Mononuclear Cells, Contrasting Starkly with Neonatal Hyporesponsiveness to TLR Ligation Due to Independence from Endosome-Mediated IRF3 Activation.* Journal of Immunology, 2018. **201**(4): p. 1131-1143.

422. Misra, R.S., et al., *Flow-based sorting of neonatal lymphocyte populations for transcriptomics analysis.* Journal of Immunological Methods, 2016. **437**: p. 13-20.

423. Sellin Jeffries, M.K., et al., *A comparison of commercially-available automated and manual extraction kits for the isolation of total RNA from small tissue samples.* BMC Biotechnology, 2014. **14**: p. 94.

424. Richards, J., E.R. Unger, and M.S. Rajeevan, *Simultaneous extraction of mRNA and microRNA from whole blood stabilized in tempus tubes.* BMC Research Notes, 2019. **12**(1): p. 39.

425. Kaufmann, S.H.E., *Immunology's coming of age.* Frontiers in Immunology, 2019. **10**: p. 684.

426. Fahey, J.L., *Cytokines, plasma immune activation markers, and clinically relevant surrogate markers in human immunodeficiency virus infection.* Clinical and Diagnostic Laboratory Immunology, 1998. **5**(5): p. 597-603.

427. Boaz, M.J., et al., *Concordant proficiency in measurement of T-cell immunity in human immunodeficiency virus vaccine clinical trials by peripheral blood mononuclear cell and enzyme-linked immunospot assays in laboratories from three continents.* Clinical and Vaccine Immunology, 2009. **16**(2): p. 147-55.

428. Zhang, H. and G. Zhu, *Quantitative RT-PCR assay for high-throughput screening (HTS) of drugs against the growth of Cryptosporidium parvum in vitro.* Frontiers in Microbiology, 2015. **6**: p. 991.

429. Koussounadis, A., et al., *Relationship between differentially expressed mRNA and mRNA-protein correlations in a xenograft model system.* Scientific Reports, 2015. **5**: p. 10775.

430. Shebl, F.M., et al., *Comparison of mRNA and protein measures of cytokines following vaccination with human papillomavirus-16 L1 virus-like particles.* Cancer Epidemiology, Biomarkers & Prevention, 2010. **19**(4): p. 978-81.

431. Bittker, J.A., *High-Throughput RT-PCR for small-molecule screening assays.* Current Protocols in Chemical Biology, 2012. **4**(1): p. 49-63.

432. Zhang, J.H., T.D. Chung, and K.R. Oldenburg, *A Simple Statistical Parameter for Use in Evaluation and Validation of High Throughput Screening Assays.* Journal of Biomolecular Screening, 1999. **4**(2): p. 67-73.

433. Coussens, N.P., et al., *Assay Guidance Manual: Quantitative Biology and Pharmacology in Preclinical Drug Discovery.* Clinical and Translational Science, 2018. **11**(5): p. 461-470.

434. Friedman, N., L. Cai, and X.S. Xie, *Linking stochastic dynamics to population distribution: an analytical framework of gene expression.* Physical Review Letters, 2006. **97**(16): p. 168302.

435. Moodie, Z., et al., *Response definition criteria for ELISPOT assays revisited.* Cancer Immunology, Immunotherapy, 2010. **59**(10): p. 1489-501.

436. Wegner, J., et al., *High-density preculture of PBMCs restores defective sensitivity of circulating CD8 T cells to virus- and tumor-derived antigens.* Blood, 2015. **126**(2): p. 185-94.

437. Kierstead, L.S., et al., *Enhanced rates and magnitude of immune responses detected against an HIV vaccine: effect of using an optimized process for isolating PBMC.* AIDS Research and Human Retroviruses, 2007. **23**(1): p. 86-92.

438. Best, A., et al., *Issues concerning the large scale cryopreservation of peripheral blood mononuclear cells (PBMC) for immunotherapy trials.* Cryobiology, 2007. **54**(3): p. 294-297.

439. Higdon, L.E., et al., *Virtual global transplant laboratory standard operating procedures for blood collection, PBMC isolation, and storage.* Transplant Direct, 2016. **2**(9): p. e101.

440. Aziz, N., et al., *Value of a Quality Assessment Program in Optimizing Cryopreservation of Peripheral Blood Mononuclear Cells in a Multicenter Study.* Clinical and Vaccine Immunology, 2013. **20**(4): p. 590-595.

441. Ortega-Pinazo, J., et al., *Quality assessment on the long-term cryopreservation and nucleic acids extraction processes implemented in the andalusian public biobank.* Cell Tissue Bank, 2019. **20**(2): p. 255-265.

442. Schmittgen, T.D., E.J. Lee, and J. Jiang, *High-throughput real-time PCR.* Methods in Molecular Biology, 2008. **429**: p. 89-98.

443. Pfefferle, S., et al., *Evaluation of a quantitative RT-PCR assay for the detection of the emerging coronavirus SARS-CoV-2 using a high throughput system.* Eurosurveillance, 2020. **25**(9): p. 18-22.

444. Wallis, J., D.P. Shenton, and R.C. Carlisle, *Novel approaches for the design, delivery and administration of vaccine technologies.* Clinical and Experimental Immunology, 2019. **196**(2): p. 189-204.

445. Ntege, E.H., et al., *Blood-stage malaria vaccines: post-genome strategies for the identification of novel vaccine candidates.* Expert Review of Vaccines, 2017. **16**(8): p. 769-779.

446. Davis, G.F., et al., *Comparison of high throughput screening technologies for luminescence cell-based reporter screens.* Journal of Biomolecular Screening, 2002. **7**(1): p. 67-77.

447. Beer, D.G., et al., *Gene-expression profiles predict survival of patients with lung adenocarcinoma.* Nature Medicine, 2002. **8**(8): p. 816-24.

448. Bittner, M., et al., *Molecular classification of cutaneous malignant melanoma by gene expression profiling.* Nature, 2000. **406**(6795): p. 536-40.

449. Sorlie, T., et al., *Repeated observation of breast tumor subtypes in independent gene expression data sets.* Proceedings of the National Academy of Sciences of the United States of America, 2003. **100**(14): p. 8418-23.

450. Burska, A., M. Boissinot, and F. Ponchel, *Cytokines as biomarkers in rheumatoid arthritis.* Mediators of Inflammation, 2014. **2014**: p. 545493.

451. Huang, Q., et al., *A non-radioactive method for small RNA detection by northern blotting.* Rice, 2014. **7**(1): p. 26.

452. Moorman, A.F., et al., *Sensitive nonradioactive detection of mRNA in tissue sections: novel application of the whole-mount in situ hybridization protocol.* Journal of Histochemistry & Cytochemistry, 2001. **49**(1): p. 1-8.

453. Zhao, S., et al., *Comparison of RNA-Seq and microarray in transcriptome profiling of activated T cells.* PLOS ONE, 2014. **9**(1): p. e78644.

454. Lih, C.J., et al., *Analytical validation of the next-generation sequencing assay for a nationwide signal-finding clinical trial: molecular analysis for therapy choice clinical trial.* Journal of Molecular Diagnostics, 2017. **19**(2): p. 313-327.

455. Quan, P.L., M. Sauzade, and E. Brouzes, *dPCR: A technology review.* Sensors (Basel), 2018. **18**(4).

456. Miranda, J.P., et al., *Analytical and clinical validation for RT-qPCR detection of SARS-CoV-2 without RNA extraction.* Frontiers in Medicine (Lausanne), 2020. **7**: p. 567572.

457. Sedegah, M., et al., *Sterile immunity to malaria after DNA prime/adenovirus boost immunization is associated with effector memory CD8+T cells targeting AMA1 class I epitopes.* PLOS ONE, 2014. **9**(9): p. e106241.

458. Sheikh, Q.M., et al., *Towards the knowledge-based design of universal influenza epitope ensemble vaccines.* Bioinformatics, 2016. **32**(21): p. 3233-3239.

459. Gao, X.M., F.Y. Liew, and J.P. Tite, *Identification and characterization of T helper epitopes in the nucleoprotein of influenza A virus.* Journal of Immunology, 1989. **143**(9): p. 3007-14.

460. Choo, J.A., et al., *The immunodominant influenza A virus M158-66 cytotoxic T lymphocyte epitope exhibits degenerate class I major histocompatibility complex restriction in humans.* Journal of Virology, 2014. **88**(18): p. 10613-23.

461. Gotch, F., et al., *Cytotoxic T lymphocytes recognize a fragment of influenza virus matrix protein in association with HLA-A2.* Nature, 1987. **326**(6116): p. 881-2.

462. Chen, Y., et al., *Interplay of cellular and humoral immune responses against BK virus in kidney transplant recipients with polyomavirus nephropathy.* Journal of Virology, 2006. **80**(7): p. 3495-505.

463. Ambalathingal, G.R., et al., *Proteome-wide analysis of T-cell response to BK polyomavirus in healthy virus carriers and kidney transplant recipients reveals a*

unique transcriptional and functional profile. Clinical & Translational Immunology, 2020. **9**(1): p. e01102.

464. Giest, S., et al., *Cytomegalovirus-specific CD8+ T cells targeting different peptide/HLA combinations demonstrate varying T-cell receptor diversity.* Immunology, 2012. **135**(1): p. 27-39.

465. Khan, N., et al., *Persistent viral infection in humans can drive high frequency low-affinity T-cell expansions.* Immunology, 2010. **131**(4): p. 537-48.

466. Prod'homme, V., et al., *Modulation of HLA-A*0201-restricted T cell responses by natural polymorphism in the IE1(315-324) epitope of human cytomegalovirus.* Journal of Immunology, 2003. **170**(4): p. 2030-6.

467. Quinzo, M.J., et al., *Computational assembly of a human Cytomegalovirus vaccine upon experimental epitope legacy.* BMC Bioinformatics, 2019. **20**(Suppl 6): p. 476.

468. Kuzushima, K., et al., *Efficient identification of HLA-A*2402-restricted cytomegalovirus-specific CD8+ T-cell epitopes by a computer algorithm and an enzyme-linked immunospot assay.* Blood, 2001. **98**(6): p. 1872-81.

469. Huth, A., et al., *Antigen-Specific TCR Signatures of Cytomegalovirus Infection.* Journal of Immunology, 2019. **202**(3): p. 979-990.

470. Tey, S.K., F. Goodrum, and R. Khanna, *CD8+ T-cell recognition of human cytomegalovirus latency-associated determinant pUL138.* Journal of General Virology, 2010. **91**(Pt 8): p. 2040-2048.

471. Lautscham, G., et al., *Identification of a TAP-independent, immunoproteasome-dependent CD8+ T-cell epitope in Epstein-Barr virus latent membrane protein 2.* Journal of Virology, 2003. **77**(4): p. 2757-61.

472. Bharadwaj, M., et al., *Contrasting Epstein-Barr virus-specific cytotoxic T cell responses to HLA A2-restricted epitopes in humans and HLA transgenic mice: implications for vaccine design.* Vaccine, 2001. **19**(27): p. 3769-77.

473. Lin, X., et al., *Chimerically fused antigen rich of overlapped epitopes from latent membrane protein 2 (LMP2) of Epstein-Barr virus as a potential vaccine and diagnostic agent.* Cellular & Molecular Immunology, 2016. **13**(4): p. 492-501.

474. Khanna, R., et al., *Identification of cytotoxic T cell epitopes within Epstein-Barr virus (EBV) oncogene latent membrane protein 1 (LMP1): evidence for HLA A2 supertype-restricted immune recognition of EBV-infected cells by LMP1-specific cytotoxic T lymphocytes.* European Journal of Immunology, 1998. **28**(2): p. 451-8.

475. Straathof, K.C., et al., *Characterization of latent membrane protein 2 specificity in CTL lines from patients with EBV-positive nasopharyngeal carcinoma and lymphoma.* Journal of Immunology, 2005. **175**(6): p. 4137-47.

476. Khanna, R., et al., *Molecular characterization of antigen-processing function in nasopharyngeal carcinoma (NPC): evidence for efficient presentation of Epstein-Barr virus cytotoxic T-cell epitopes by NPC cells.* Cancer Research, 1998. **58**(2): p. 310-4.

477. Hill, A., et al., *Characterization of two Epstein-Barr virus epitopes restricted by HLA-B7.* European Journal of Immunology, 1995. **25**(1): p. 18-24.

478. Falco, D.A., et al., *Identification of Epstein-Barr virus-specific CD8+ T lymphocytes in the circulation of pediatric transplant recipients.* Transplantation, 2002. **74**(4): p. 501-10.

479. Witney, A.A., et al., *Determining liver stage parasite burden by real time quantitative PCR as a method for evaluating pre-erythrocytic malaria vaccine efficacy.* Molecular and Biochemical Parasitology, 2001. **118**(2): p. 233-45.

480. Pichugin, A. and U. Krzych, *Detection of Plasmodium berghei and Plasmodium yoelii Liver-Stage Parasite Burden by Quantitative Real-Time PCR.* Methods in Molecular Biology, 2015. **1325**: p. 81-9.

481. Schussek, S., et al., *Highly sensitive quantitative real-time PCR for the detection of Plasmodium liver-stage parasite burden following low-dose sporozoite challenge.* PLOS ONE, 2013. **8**(10): p. e77811.

482. Sack, B.K., et al., *Humoral protection against mosquito bite-transmitted Plasmodium falciparum infection in humanized mice.* NPJ Vaccines, 2017. **2**: p. 27.

483. Foquet, L., et al., *Plasmodium falciparum Liver Stage Infection and Transition to Stable Blood Stage Infection in Liver-Humanized and Blood-Humanized FRGN KO Mice Enables Testing of Blood Stage Inhibitory Antibodies (Reticulocyte-Binding Protein Homolog 5) In Vivo.* Frontiers in Immunology, 2018. **9**: p. 524.

484. Mueller, A.K., et al., *Plasmodium liver stage developmental arrest by depletion of a protein at the parasite-host interface.* Proceedings of the National Academy of Sciences of the United States of America, 2005. **102**(8): p. 3022-7.

485. Kumar, H., et al., *Protective efficacy and safety of liver stage attenuated malaria parasites.* Scientific Reports, 2016. **6**: p. 26824.

486. Tsuji, M. and F. Zavala, *T cells as mediators of protective immunity against liver stages of Plasmodium.* Trends in Parasitology, 2003. **19**(2): p. 88-93.

487. Mo, A.X. and G. McGugan, *Understanding the Liver-Stage Biology of Malaria Parasites: Insights to Enable and Accelerate the Development of a Highly Efficacious Vaccine.* American Journal of Tropical Medicine and Hygiene, 2018. **99**(4): p. 827-832.

488. Kefi, M., et al., *New rapid one-step PCR diagnostic assay for Plasmodium falciparum infective mosquitoes.* Scientific Reports, 2018. **8**(1): p. 1462.

489. Murphy, S.C., et al., *Real-time quantitative reverse transcription PCR for monitoring of blood-stage Plasmodium falciparum infections in malaria human challenge trials.* American Journal of Tropical Medicine and Hygiene, 2012. **86**(3): p. 383-94.

490. Azikiwe, C.C., et al., *A comparative laboratory diagnosis of malaria: microscopy versus rapid diagnostic test kits.* Asian Pacific Journal of Tropical Biomedicine, 2012. **2**(4): p. 307-10.

491. Apte, S.H., et al., *High-throughput multi-parameter flow-cytometric analysis from micro-quantities of Plasmodium-infected blood.* International Journal for Parasitology, 2011. **41**(12): p. 1285-94.

492. Andrews, L., et al., *Quantitative real-time polymerase chain reaction for malaria diagnosis and its use in malaria vaccine clinical trials.* American Journal of Tropical Medicine and Hygiene, 2005. **73**(1): p. 191-198.

493. Kozera, B. and M. Rapacz, *Reference genes in real-time PCR.* Journal of Applied Genetics, 2013. **54**(4): p. 391-406.

494. Livak, K.J. and T.D. Schmittgen, *Analysis of relative gene expression data using real-time quantitative PCR and the 2(-Delta Delta C(T)) Method.* Methods, 2001. **25**(4): p. 402-8.

495. Mosley, Y.C. and H. HogenEsch, *Selection of a suitable reference gene for quantitative gene expression in mouse lymph nodes after vaccination.* BMC Research Notes, 2017. **10**(1): p. 689.

496. Siddiqui, A.J., et al., *Assessment of real-time method to detect liver parasite burden under different experimental conditions in mice infected with Plasmodium yoelii sporozoites.* Microbial Pathogenesis, 2015. **89**: p. 35-42.

497. Bruna-Romero, O., et al., *Detection of malaria liver-stages in mice infected through the bite of a single Anopheles mosquito using a highly sensitive real-time PCR.* International Journal for Parasitology, 2001. **31**(13): p. 1499-502.

498. Siddiqui, A.J., J. Bhardwaj, and S.K. Puri, *mRNA expression of cytokines and its impact on outcomes after infection with lethal and nonlethal Plasmodium vinckei parasites.* Parasitology Research, 2012. **110**(4): p. 1517-24.

499. Al-Quraishy, S., et al., *Gene expression of the liver of vaccination-protected mice in response to early patent infections of Plasmodium chabaudi blood-stage malaria.* Malaria Journal, 2018. **17**(1): p. 215.

500. Raja, A.I., et al., *Chemically Attenuated Blood-Stage Plasmodium yoelii Parasites Induce Long-Lived and Strain-Transcending Protection.* Infection and Immunity, 2016. **84**(8): p. 2274-2288.

501. Troye-Blomberg, M., et al., *Production of IL 2 and IFN-gamma by T cells from malaria patients in response to Plasmodium falciparum or erythrocyte antigens in vitro.* J Immunol, 1985. **135**(5): p. 3498-504.

502. Shear, H.L., et al., *Role of IFN-gamma in lethal and nonlethal malaria in susceptible and resistant murine hosts.* J Immunol, 1989. **143**(6): p. 2038-44.

503. Hoffman, S.L. and D.L. Doolan, *Malaria vaccines-targeting infected hepatocytes.* Nat Med, 2000. **6**(11): p. 1218-9.

504. Hu, X., et al., *Genome-wide liver transcriptomic profiling of a malaria mouse model reveals disturbed immune and metabolic responses.* Parasit Vectors, 2023. **16**(1): p. 40.

505. Miller, J.L., et al., *Interferon-mediated innate immune responses against malaria parasite liver stages.* Cell Rep, 2014. **7**(2): p. 436-447.

506. Toro-Moreno, M., et al., *RNA-Seq Analysis Illuminates the Early Stages of Plasmodium Liver Infection.* mBio, 2020. **11**(1).

507. Lefebvre, M.N., et al., *Expeditious recruitment of circulating memory CD8 T cells to the liver facilitates control of malaria.* Cell Rep, 2021. **37**(5): p. 109956.

508. Liehl, P., et al., *Innate immunity induced by Plasmodium liver infection inhibits malaria reinfections.* Infect Immun, 2015. **83**(3): p. 1172-80.

509. Siddiqui, A.J., et al., *Immune responses in liver and spleen against Plasmodium yoelii pre-erythrocytic stages in Swiss mice model.* J Adv Res, 2020. **24**: p. 29-41.

510. Duffy, A.M., et al., *Purification of adenovirus and adeno-associated virus: comparison of novel membrane-based technology to conventional techniques.* Gene Therapy, 2005. **12 Suppl 1**: p. S62-72.

511. Browne, D.J., et al., *A high-throughput screening RT-qPCR assay for quantifying surrogate markers of immunity from PBMCs.* Frontiers in Immunology, 2022. **13**: p. 962220.

512. Browne, D.J., et al., *Multiplex Microsphere PCR (mmPCR) Allows Simultaneous Gram Typing, Detection of Fungal DNA, and Antibiotic Resistance Genes.* Laboratory Medicine, 2022. **53**(5): p. 459-464.

513. Keniry, A., et al., *The H19 lincRNA is a developmental reservoir of miR-675 that suppresses growth and Igf1r.* Nature Cell Biology, 2012. **14**(7): p. 659-65.

514. Bruna-Romero, O., et al., *Complete, long-lasting protection against malaria of mice primed and boosted with two distinct viral vectors expressing the same plasmodial antigen.* Proceedings of the National Academy of Sciences of the United States of America, 2001. **98**(20): p. 11491-6.

515. Xie, F., et al., *miRDeepFinder: a miRNA analysis tool for deep sequencing of plant small RNAs.* Plant Molecular Biology, 2012.

516. Vandesompele, J., et al., *Accurate normalization of real-time quantitative RT-PCR data by geometric averaging of multiple internal control genes.* Genome Biol, 2002. **3**(7): p. RESEARCH0034.

517. Nygard, A.B., et al., *Selection of reference genes for gene expression studies in pig tissues using SYBR green qPCR.* BMC Molecular Biology, 2007. **8**: p. 67.

518. Zamani, A., et al., *Validation of reference genes for gene expression analysis following experimental traumatic brain injury in a pediatric mouse model.* Brain Research Bulletin, 2020. **156**: p. 43-49.

519. Rego, E.C.S., et al., *Stable reference genes for RT-qPCR analysis of gene expression in the Musa acuminata-Pseudocercospora musae interaction.* Scientific Reports, 2019. **9**(1): p. 14592.

520. Glare, E.M., et al., *beta-Actin and GAPDH housekeeping gene expression in asthmatic airways is variable and not suitable for normalising mRNA levels.* Thorax, 2002. **57**(9): p. 765-70.

521. Vaughan, A.M. and S.H.I. Kappe, *Malaria Parasite Liver Infection and Exoerythrocytic Biology.* Cold Spring Harbor Perspectives in Medicine, 2017. **7**(6).

522. McCall, M.N., et al., *On non-detects in qPCR data.* Bioinformatics, 2014. **30**(16): p. 2310-6.

523. Pfaffl, M.W., *A new mathematical model for relative quantification in real-time RT-PCR.* Nucleic Acids Res, 2001. **29**(9): p. e45.

524. WHO, *World Malaria Report.* 2021.

525. Good, M.F. and D.I. Stanisic, *Whole parasite vaccines for the asexual blood stages of Plasmodium.* Immunological Reviews, 2020. **293**(1): p. 270-282.

526. Gomes, P.S., et al., *Immune Escape Strategies of Malaria Parasites.* Frontiers in Microbiology, 2016. **7**: p. 1617.

527. McCall, C., *Disrupted care in Papua New Guinea: the harms of COVID-19.* The Lancet, 2022. **399**(10321): p. 226-227.

528. Weinberg, A., et al., *Optimization and limitations of use of cryopreserved peripheral blood mononuclear cells for functional and phenotypic T-cell characterization.* Clinical and Vaccine Immunology, 2009. **16**(8): p. 1176-86.

529. Currier, J.R., et al., *A panel of MHC class I restricted viral peptides for use as a quality control for vaccine trial ELISPOT assays.* J Immunol Methods, 2002. **260**(1-2): p. 157-72.

530. Browne, D.J., C.M. Miller, and D.L. Doolan, *Technical pitfalls when collecting, cryopreserving, thawing, and stimulating human T-cells.* Frontiers in Immunology, 2024. **15**: p. 1382192.

531. Evavold, B.D., et al., *Specific T cell recognition of minimally homologous peptides: evidence for multiple endogenous ligands.* Immunity, 1995. **2**(6): p. 655-63.

532. Montaner, S., et al., *The Role of Extracellular Vesicles in Modulating the Host Immune Response during Parasitic Infections.* Frontiers in Immunology, 2014. **5**.

533. Carlton, J.M., et al., *Comparative genomics of the neglected human malaria parasite Plasmodium vivax.* Nature, 2008. **455**(7214): p. 757-763.

534. Scherf, A., J.J. Lopez-Rubio, and L. Riviere, *Antigenic Variation in Plasmodium falciparum.* Annual Review of Microbiology, 2008. **62**(1): p. 445-470.

535. Calle, C.L., B. Mordmüller, and A. Singh, *Immunosuppression in Malaria: Do Plasmodium falciparum Parasites Hijack the Host?* Pathogens, 2021. **10**(10).

536. Soria-Guerra, R.E., et al., *An overview of bioinformatics tools for epitope prediction: Implications on vaccine development.* Journal of Biomedical Informatics, 2015. **53**: p. 405-414.

537. Matis, L.A., *The molecular basis of T-cell specificity.* Annual Review of Immunology, 1990. **8**: p. 65-82.

538. Blum, J.S., P.A. Wearsch, and P. Cresswell, *Pathways of antigen processing.* Annual Review of Immunology, 2013. **31**: p. 443-73.

539. Pollard, A.J. and E.M. Bijker, *A guide to vaccinology: from basic principles to new developments.* Nature Reviews Immunology, 2021. **21**(2): p. 83-100.

540. Lu, G., et al., *Novel vaccine design based on genomics data analysis: A review.* Scandinavian Journal of Immunology, 2021. **93**(3): p. e12986.

541. Takala, S.L. and C.V. Plowe, *Genetic diversity and malaria vaccine design, testing and efficacy: preventing and overcoming 'vaccine resistant malaria'.* Parasite Immunology, 2009. **31**(9): p. 560-573.

542. Song, I., et al., *Broad TCR repertoire and diverse structural solutions for recognition of an immunodominant CD8+ T cell epitope.* Nature Structural & Molecular Biology, 2017. **24**(4): p. 395-406.

543. Zhou, P., et al., *A pneumonia outbreak associated with a new coronavirus of probable bat origin.* Nature, 2020. **579**(7798): p. 270-273.

544. Arbel, R., et al., *Effectiveness of a bivalent mRNA vaccine booster dose to prevent severe COVID-19 outcomes: a retrospective cohort study.* The Lancet Infectious Diseases, 2023. **23**(8): p. 914-921.

545. León, T.M., *COVID-19 cases and hospitalizations by COVID-19 vaccination status and previous COVID-19 diagnosis—California and New York, May–November 2021.* Morbidity and Mortality Weekly Report, 2022. **71**.

546. Tenforde, M.W., *Effectiveness of mRNA vaccination in preventing COVID-19–associated invasive mechanical ventilation and death—United States, March 2021–January 2022.* Morbidity and Mortality Weekly Report, 2022. **71**.

547. Olson, S.M., *Effectiveness of Pfizer-BioNTech mRNA vaccination against COVID-19 hospitalization among persons aged 12–18 years—United States, June–September 2021.* Morbidity and Mortality Weekly Report, 2021. **70**.

548. Ferdinands, J.M., *Waning 2-dose and 3-dose effectiveness of mRNA vaccines against COVID-19–associated emergency department and urgent care encounters and hospitalizations among adults during periods of Delta and Omicron variant predominance—VISION Network, 10 states, August 2021–January 2022.* Morbidity and Mortality Weekly Report, 2022. **71**.

549. Fabiani, M., et al., *Effectiveness of mRNA vaccines and waning of protection against SARS-CoV-2 infection and severe covid-19 during predominant circulation of the delta variant in Italy: retrospective cohort study.* BMJ, 2022. **376**: p. e069052.

550. Tartof, S.Y., et al., *Effectiveness of BNT162b2 BA.4/5 bivalent mRNA vaccine against a range of COVID-19 outcomes in a large health system in the USA: a test-negative case-control study.* The Lancet Respiratory Medicine, 2023. **11**(12): p. 1089-1100.

551. Pooley, N., et al., *Durability of Vaccine-Induced and Natural Immunity Against COVID-19: A Narrative Review.* Infectious Diseases and Therapy, 2023. **12**(2): p. 367-387.

552. Shenai, M.B., R. Rahme, and H. Noorchashm, *Equivalency of Protection From Natural Immunity in COVID-19 Recovered Versus Fully Vaccinated Persons: A Systematic Review and Pooled Analysis.* Cureus, 2021. **13**(10): p. e19102.

553. Gazit, S., et al., *Comparing SARS-CoV-2 natural immunity to vaccine-induced immunity: reinfections versus breakthrough infections.* medRxiv, 2021.

554. Xu, K., et al., *Immunogenicity, efficacy and safety of COVID-19 vaccines: an update of data published by 31 December 2021.* International Immunology, 2022. **34**(12): p. 595-607.

555. Rose, R., et al., *Humoral immune response after different SARS-CoV-2 vaccination regimens.* BMC Medicine, 2022. **20**(1): p. 31.

556. Barros-Martins, J., et al., *Humoral and cellular immune response against SARS-CoV-2 variants following heterologous and homologous ChAdOx1 nCoV-19/BNT162b2 vaccination.* medRxiv, 2021: p. 2021.06.01.21258172.

557. Yang, H., Y. Xie, and C. Li, *Understanding the mechanisms for COVID-19 vaccine's protection against infection and severe disease.* Expert Review of Vaccines, 2023. **22**(1): p. 186-192.

558. Grifoni, A., et al., *SARS-CoV-2 human T cell epitopes: Adaptive immune response against COVID-19.* Cell Host & Microbe, 2021. **29**(7): p. 1076-1092.

559. Sadarangani, M., A. Marchant, and T.R. Kollmann, *Immunological mechanisms of vaccine-induced protection against COVID-19 in humans.* Nature Reviews Immunology, 2021. **21**(8): p. 475-484.

560. Collins, D.R., G.D. Gaiha, and B.D. Walker, *CD8+ T cells in HIV control, cure and prevention.* Nature Reviews Immunology, 2020. **20**(8): p. 471-482.

561. Luckheeram, R.V., et al., *CD4+ T cells: differentiation and functions.* Clinical and Developmental Immunology, 2012. **2012**: p. 925135.

562. Le Bert, N., et al., *SARS-CoV-2-specific T cell immunity in cases of COVID-19 and SARS, and uninfected controls.* Nature, 2020. **584**(7821): p. 457-462.

563. Liontos, A., et al., *Correlation of Lymphocyte Subpopulations, Clinical Features and Inflammatory Markers during Severe COVID-19 Onset.* Pathogens, 2023. **12**(3).

564. Mueller, A.L., M.S. McNamara, and D.A. Sinclair, *Why does COVID-19 disproportionately affect older people?* Aging, 2020. **12**(10): p. 9959-9981.

565. Lerner, A., C. Benzvi, and A. Vojdani, *HLA-DQ2/8 and COVID-19 in Celiac Disease: Boon or Bane.* Microorganisms, 2023. **11**(12): p. 2977.

566. Astbury, S., et al., *HLA-DR polymorphism in SARS-CoV-2 infection and susceptibility to symptomatic COVID-19.* Immunology, 2022. **166**(1): p. 68-77.

567. Warren, R.L. and I. Birol, *HLA alleles measured from COVID-19 patient transcriptomes reveal associations with disease prognosis in a New York cohort.* PeerJ, 2021. **9**: p. e12368.

568. Habel, J.R., et al., *Suboptimal SARS-CoV-2-specific CD8+ T cell response associated with the prominent HLA-A*02:01 phenotype.* Proceedings of the National Academy of Sciences of the United States of America, 2020. **117**(39): p. 24384-24391.

569. Frelinger, J.A., *Immunodominance: the choice of the immune system.* 2006: John Wiley & Sons.

570. and, J.W.Y. and J.R. Bennink, *Immunodominance in major histocompatibility complex class 1 restricted T lymphocyte responses* Annual Review of Immunology, 1999. **17**(1): p. 51-88.

571. Dendrou, C.A., et al., *HLA variation and disease.* Nature Reviews Immunology, 2018. **18**(5): p. 325-339.

572. Almehdi, A.M., et al., *SARS-CoV-2 spike protein: pathogenesis, vaccines, and potential therapies.* Infection, 2021. **49**(5): p. 855-876.

573. Schetelig, J., et al., *Individual HLA-A, -B, -C, and -DRB1 Genotypes Are No Major Factors Which Determine COVID-19 Severity.* Frontiers in Immunology, 2021. **12**: p. 698193.

574. Folegatti, P.M., et al., *Safety and immunogenicity of the ChAdOx1 nCoV-19 vaccine against SARS-CoV-2: a preliminary report of a phase 1/2, single-blind, randomised controlled trial.* The Lancet, 2020. **396**(10249): p. 467-478.

575. Jackson, L.A., et al., *An mRNA vaccine against SARS-CoV-2—preliminary report.* New England journal of medicine, 2020. **383**(20): p. 1920-1931.

576. Sahin, U., et al., *Concurrent human antibody and TH1 type T-cell responses elicited by a COVID-19 RNA vaccine.* medRxiv, 2020: p. 2020.07.17.20140533.

577. Peng, Y., et al., *Broad and strong memory CD4(+) and CD8(+) T cells induced by SARS-CoV-2 in UK convalescent individuals following COVID-19.* Nature Communications, 2020. **21**(11): p. 1336-1345.

578. Grifoni, A., et al., *Targets of T Cell Responses to SARS-CoV-2 Coronavirus in Humans with COVID-19 Disease and Unexposed Individuals.* Cell, 2020. **181**(7): p. 1489-1501 e15.

579. Ferretti, A.P., et al., *Unbiased Screens Show CD8+ T Cells of COVID-19 Patients Recognize Shared Epitopes in SARS-CoV-2 that Largely Reside outside the Spike Protein.* Immunity, 2020. **53**(5): p. 1095-1107.e3.

580. Tarke, A., et al., *SARS-CoV-2 vaccination induces immunological T cell memory able to cross-recognize variants from Alpha to Omicron.* Cell, 2022. **185**(5): p. 847-859.e11.

581. Naranbhai, V., et al., *T cell reactivity to the SARS-CoV-2 Omicron variant is preserved in most but not all individuals.* Cell, 2022. **185**(6): p. 1041-1051.e6.

582. Lineburg, K.E., et al., *Breakthrough SARS-COV-2 infection induces broad anti-viral T cell immunity.* iScience, 2023. **26**(12): p. 108474.

583. Kundu, R., et al., *Cross-reactive memory T cells associate with protection against SARS-CoV-2 infection in COVID-19 contacts.* Nature Communications, 2022. **13**(1): p. 80.

584. Wang, G., et al., *Seasonal coronaviruses and SARS-CoV-2: effects of preexisting immunity during the COVID-19 pandemic.* Journal of Zhejiang University. Science B, 2022. **23**(6): p. 451-460.

585. Young, H.A. and D.L. Hodge, *Interferon-γ*, in *Encyclopedia of Hormones*, H.L. Henry and A.W. Norman, Editors. 2003, Academic Press: New York. p. 391-397.

586. Reynisson, B., et al., *NetMHCpan-4.1 and NetMHCIIpan-4.0: improved predictions of MHC antigen presentation by concurrent motif deconvolution and integration of MS MHC eluted ligand data.* Nucleic Acids Research, 2020. **48**(W1): p. W449-W454.

587. Zhang, Z., et al., *Humoral and cellular immune memory to four COVID-19 vaccines.* Cell, 2022. **185**(14): p. 2434-2451.e17.

588. Sette, A., J. Sidney, and S. Crotty, *T Cell Responses to SARS-CoV-2.* Annual Review of Immunology, 2023. **41**: p. 343-373.

589. Trauet, J., et al., *Studying antigen-specific T cells through a streamlined, whole blood-based extracellular approach.* Cytometry A, 2024. **105**(4): p. 288-296.

590. Hodcroft, E.B., *CoVariants: SARS-CoV-2 mutations and variants of interest.* 2021.

591. Edgar, R.C., *MUSCLE: multiple sequence alignment with high accuracy and high throughput.* Nucleic Acids Res, 2004. **32**(5): p. 1792-7.

592. Currier, J.R., et al., *A panel of MHC class I restricted viral peptides for use as a quality control for vaccine trial ELISPOT assays.* Journal of Immunological Methods, 2002. **260**(1-2): p. 157-72.

593. Jin, X., X. Liu, and C. Shen, *A systemic review of T-cell epitopes defined from the proteome of SARS-CoV-2.* Virus Research, 2023. **324**: p. 199024.

594. Prakash, S., et al., *Genome-Wide B Cell, CD4+, and CD8+ T Cell Epitopes That Are Highly Conserved between Human and Animal Coronaviruses, Identified from SARS-CoV-2 as Targets for Preemptive Pan-Coronavirus Vaccines.* Journal of Immunology, 2021. **206**(11): p. 2566-2582.

595. Lv, Y., et al., *Identification of a novel conserved HLA-A*0201-restricted epitope from the spike protein of SARS-CoV.* BMC Immunology, 2009. **10**(1): p. 61.

596. Saini, S.K., et al., *SARS-CoV-2 genome-wide T cell epitope mapping reveals immunodominance and substantial CD8(+) T cell activation in COVID-19 patients.* Science Immunology, 2021. **6**(58).

597. Xiao, C., et al., *Insufficient epitope-specific T cell clones are responsible for impaired cellular immunity to inactivated SARS-CoV-2 vaccine in older adults.* Nature Aging, 2023. **3**(4): p. 418-435.

598. Martin, M.P. and M. Carrington, *Immunogenetics of HIV disease.* Immunological Reviews, 2013. **254**(1): p. 245-264.

599. Singh, R., et al., *A comparative review of HLA associations with hepatitis B and C viral infections across global populations.* World Journal of Gastroenterology, 2007. **13**(12): p. 1770-87.

600. Peng, Y., et al., *An immunodominant NP105–113-B*07:02 cytotoxic T cell response controls viral replication and is associated with less severe COVID-19 disease.* Nature Immunology, 2022. **23**(1): p. 50-61.

601. Augusto, D.G., et al., *A common allele of HLA is associated with asymptomatic SARS-CoV-2 infection.* Nature, 2023. **620**(7972): p. 128-136.

602. Francis, J.M., et al., *Allelic variation in class I HLA determines CD8+ T cell repertoire shape and cross-reactive memory responses to SARS-CoV-2.* Science Immunology, 2022. **7**(67): p. eabk3070.

603. Ng, M.H., et al., *Association of human-leukocyte-antigen class I (B*0703) and class II (DRB1*0301) genotypes with susceptibility and resistance to the development of severe acute respiratory syndrome.* The Journal of Infectious Diseases, 2004. **190**(3): p. 515-8.

604. Sanchez-Mazas, A., *HLA studies in the context of coronavirus outbreaks.* Swiss Medical Weekly, 2020. **150**(1516): p. w20248-w20248.

605. Kanduc, D., *From Anti-Severe Acute Respiratory Syndrome Coronavirus 2 Immune Response to Cancer Onset via Molecular Mimicry and Cross-Reactivity.* Global Medical Genetics, 2021. **8**(4): p. 176-182.

606. Sette, A. and S. Crotty, *Pre-existing immunity to SARS-CoV-2: the knowns and unknowns.* Nature Reviews Immunology, 2020. **20**(8): p. 457-458.

607. Tarke, A., et al., *Negligible impact of SARS-CoV-2 variants on CD4+ and CD8+ T cell reactivity in COVID-19 exposed donors and vaccinees.* bioRxiv, 2021.

608. Rodda, L.B., et al., *Imprinted SARS-CoV-2-specific memory lymphocytes define hybrid immunity.* Cell, 2022. **185**(9): p. 1588-1601.e14.

609. Swanson, P.A., et al., *T-cell mediated immunity after AZD1222 vaccination: A polyfunctional spike-specific Th1 response with a diverse TCR repertoire.* medRxiv, 2021.

610. Cox, R.J. and K.A. Brokstad, *Not just antibodies: B cells and T cells mediate immunity to COVID-19.* Nature Reviews Immunology, 2020. **20**(10): p. 581-582.

611. Yewdell, J.W., *MHC Class I Immunopeptidome: Past, Present, and Future.* Molecular & Cellular Proteomics, 2022. **21**(7): p. 100230.

612. Sette, A., et al., *The relationship between class I binding affinity and immunogenicity of potential cytotoxic T cell epitopes.* The Journal of Immunology, 1994. **153**(12): p. 5586-5592.

613. Bihl, F., et al., *Impact of HLA-B alleles, epitope binding affinity, functional avidity, and viral coinfection on the immunodominance of virus-specific CTL responses.* Journal of Immunology, 2006. **176**(7): p. 4094-101.

614. Yang, X., et al., *DeepNetBim: deep learning model for predicting HLA-epitope interactions based on network analysis by harnessing binding and immunogenicity information.* BMC Bioinformatics, 2021. **22**(1): p. 231.

615. Roemer, C., et al., *SARS-CoV-2 evolution in the Omicron era.* Nature Microbiology, 2023.

616. Cao, Y., et al., *Imprinted SARS-CoV-2 humoral immunity induces convergent Omicron RBD evolution.* Nature, 2023. **614**(7948): p. 521-529.

617. Merhi, G., et al., *SARS-CoV-2 genomic epidemiology: data and sequencing infrastructure.* Future Microbiology, 2022. **17**: p. 1001-1007.

618. Ragone, C., et al., *Molecular mimicry of SARS-COV-2 antigens as a possible natural anti-cancer preventive immunization.* Frontiers in Immunology, 2024. **15**: p. 1398002.

619. Quiros-Fernandez, I., et al., *Immunogenic T cell epitopes of SARS-CoV-2 are recognized by circulating memory and naïve CD8 T cells of unexposed individuals.* eBioMedicine, 2021. **72**.

620. Lang-Meli, J., et al., *SARS-CoV-2-specific T-cell epitope repertoire in convalescent and mRNA-vaccinated individuals.* Nature Microbiology, 2022. **7**(5): p. 675-679.

621. Szeto, C., et al., *Molecular Basis of a Dominant SARS-CoV-2 Spike-Derived Epitope Presented by HLA-A*02:01 Recognised by a Public TCR.* Cells, 2021. **10**(10).

622. Shomuradova, A.S., et al., *SARS-CoV-2 Epitopes Are Recognized by a Public and Diverse Repertoire of Human T Cell Receptors.* Immunity, 2020. **53**(6): p. 1245-1257.e5.

623. Wang, Y., et al., *Ad5-nCoV Vaccination Could Induce HLA-E Restricted CD8+ T Cell Responses Specific for Epitopes on Severe Acute Respiratory Syndrome Coronavirus 2 Spike Protein.* Viruses, 2023. **16**(1).

624. Titov, A., et al., *Immunogenic epitope panel for accurate detection of non-cross-reactive T cell response to SARS-CoV-2.* JCI Insight, 2022. **7**(9).

625. Qiu, C., et al., *CD8+ T-Cell Epitope Variations Suggest a Potential Antigen HLA-A2 Binding Deficiency for Spike Protein of SARS-CoV-2.* Frontiers in Immunology, 2021. **12**: p. 764949.

626. Kared, H., et al., *SARS-CoV-2-specific CD8+ T cell responses in convalescent COVID-19 individuals.* Journal of Clinical Investigation, 2021. **131**(5).

627. Sheetikov, S.A., et al., *Clonal structure and the specificity of vaccine-induced T cell response to SARS-CoV-2 Spike protein.* Frontiers in Immunology, 2024. **15**.

628. Coulon, P.G., et al., *High frequencies of alpha common cold coronavirus/SARS-CoV-2 cross-reactive functional CD4+ and CD8+ memory T cells are associated with protection from symptomatic and fatal SARS-CoV-2 infections in unvaccinated COVID-19 patients.* Frontiers in Immunology, 2024. **15**: p. 1343716.

629. Hamelin, D.J., et al., *The mutational landscape of SARS-CoV-2 variants diversifies T cell targets in an HLA-supertype-dependent manner.* Cell Systems, 2022. **13**(2): p. 143-157.e3.

630. Maino, A., et al., *Development of a New Off-the-Shelf Plasmacytoid Dendritic Cell–Based Approach for the Expansion and Characterization of SARS-CoV-2–Specific T Cells.* The Journal of Immunology, 2024. **212**(5): p. 825-833.

631. Mateus, J., et al., *Selective and cross-reactive SARS-CoV-2 T cell epitopes in unexposed humans.* Science, 2020. **370**(6512): p. 89-94.

632. Zhang, H., et al., *Profiling CD8+ T cell epitopes of COVID-19 convalescents reveals reduced cellular immune responses to SARS-CoV-2 variants.* Cell Reports, 2021. **36**(11): p. 109708.

633. Proietto, D., et al., *Ageing Curtails the Diversity and Functionality of Nascent CD8+ T Cell Responses against SARS-CoV-2.* Vaccines (Basel), 2023. **11**(1).

634. Antonio, E.C., et al., *Viral immunogenic footprints conferring T cell cross-protection to SARS-CoV-2 and its variants.* Frontiers in Immunology, 2022. **13**: p. 931372.

635. Lie-Andersen, O., et al., *Impact of peptide:HLA complex stability for the identification of SARS-CoV-2-specific CD8+T cells.* Frontiers in Immunology, 2023. **14**: p. 1151659.

636. Swaminathan, S., et al., *Ablation of CD8(+) T cell recognition of an immunodominant epitope in SARS-CoV-2 Omicron variants BA.1, BA.2 and BA.3.* Nature Communications, 2022. **13**(1): p. 6387.

637. Redd, A.D., et al., *Minimal cross-over between mutations associated with Omicron variant of SARS-CoV-2 and CD8+ T cell epitopes identified in COVID-19 convalescent individuals.* bioRxiv, 2021.

638. Hu, C., et al., *Identification of cross-reactive CD8+ T cell receptors with high functional avidity to a SARS-CoV-2 immunodominant epitope and its natural mutant variants.* Genes & Diseases, 2022. **9**(1): p. 216-229.

639. Kuse, N., et al., *Long-term memory CD8+ T cells specific for SARS-CoV-2 in individuals who received the BNT162b2 mRNA vaccine.* Nature Communications, 2022. **13**(1): p. 5251.

640. Pushpakumara, P.D., et al., *Identification of Novel Candidate CD8+ T Cell Epitopes of the SARS-CoV2 with Homology to Other Seasonal Coronaviruses.* Viruses, 2021. **13**(6).

641. Santoni, D. and D. Vergni, *In the search of potential epitopes for Wuhan seafood market pneumonia virus using high order nullomers.* Journal of Immunological Methods, 2020. **481-482**: p. 112787.

642. Shimizu, K., et al., *Identification of TCR repertoires in functionally competent cytotoxic T cells cross-reactive to SARS-CoV-2.* Communications Biology, 2021. **4**(1): p. 1365.

643. Gfeller, D., et al., *Improved predictions of antigen presentation and TCR recognition with MixMHCpred2.2 and PRIME2.0 reveal potent SARS-CoV-2 CD8(+) T-cell epitopes.* Cell Systems, 2023. **14**(1): p. 72-83 e5.

644. Gangaev, A., et al., *Identification and characterization of a SARS-CoV-2 specific CD8+ T cell response with immunodominant features.* Nature Communications, 2021. **12**(1): p. 2593.

645. Oberhardt, V., et al., *Rapid and stable mobilization of CD8+ T cells by SARS-CoV-2 mRNA vaccine.* Nature, 2021. **597**(7875): p. 268-273.

646. Gustiananda, M., et al., *Immunoinformatics Identification of the Conserved and Cross-Reactive T-Cell Epitopes of SARS-CoV-2 with Human Common Cold Coronaviruses, SARS-CoV, MERS-CoV and Live Attenuated Vaccines Presented by HLA Alleles of Indonesian Population.* Viruses, 2022. **14**(11).

647. Wang, Y., et al., *Effects of SARS-CoV-2 Omicron BA.1 Spike Mutations on T-Cell Epitopes in Mice.* Viruses, 2023. **15**(3).

648. Tarke, A., et al., *SARS-CoV-2 breakthrough infections enhance T cell response magnitude, breadth, and epitope repertoire.* Cell Reports Medicine, 2024. **5**(6): p. 101583.

649. Heitmann, J.S., et al., *A COVID-19 peptide vaccine for the induction of SARS-CoV-2 T cell immunity.* Nature, 2022. **601**(7894): p. 617-622.

650. Felipe Cuspoca, A., P. Isaac Estrada, and A. Velez-van-Meerbeke, *Molecular Mimicry of SARS-CoV-2 Spike Protein in the Nervous System: A Bioinformatics Approach.* Computational and Structural Biotechnology Journal, 2022. **20**: p. 6041-6054.

651. Bamford, C.G.G., et al., *Comparison of SARS-CoV-2 Evolution in Paediatric Primary Airway Epithelial Cell Cultures Compared with Vero-Derived Cell Lines.* Viruses, 2022. **14**(2).

652. Snyder, T.M., et al., *Magnitude and Dynamics of the T-Cell Response to SARS-CoV-2 Infection at Both Individual and Population Levels.* medRxiv, 2020.

653. Obermair, F.J., et al., *High-resolution profiling of MHC II peptide presentation capacity reveals SARS-CoV-2 CD4 T cell targets and mechanisms of immune escape.* Science Advances, 2022. **8**(17): p. eabl5394.

654. Dos Santos Alves, R.P., et al., *Human coronavirus OC43-elicited CD4+ T cells protect against SARS-CoV-2 in HLA transgenic mice.* Nature Communications, 2024. **15**(1): p. 787.

655. Emmelot, M.E., et al., *Omicron BA.1 Mutations in SARS-CoV-2 Spike Lead to Reduced T-Cell Response in Vaccinated and Convalescent Individuals.* Viruses, 2022. **14**(7).

656. Karsten, H., et al., *High-resolution analysis of individual spike peptide-specific CD4(+) T-cell responses in vaccine recipients and COVID-19 patients.* Clinical & Translational Immunology, 2022. **11**(8): p. e1410.

657. Zhang, Y., et al., *Three Specific Potential Epitopes That Could Be Recognized by T Cells of Convalescent COVID-19 Patients Were Identified From Spike Protein.* Frontiers in Immunology, 2022. **13**: p. 752622.

658. Dotan, A., et al., *Molecular mimicry between SARS-CoV-2 and the female reproductive system.* American Journal of Reproductive Immunology, 2021. **86**(6): p. e13494.

659. Browne, D.J., et al., *Evaluating the stability of host-reference gene expression and simultaneously quantifying parasite burden and host immune responses in murine malaria.* Scientific Reports, 2023. **13**(1): p. 21071.

660. Boehm, T. and J.B. Swann, *Origin and evolution of adaptive immunity.* Annual Review of Animal Biosciences, 2014. **2**(1): p. 259-283.

661. Appay, V., et al., *Dynamics of T cell responses in HIV infection.* The Journal of Immunology, 2002. **168**(7): p. 3660-3666.

662. Raskov, H., et al., *Cytotoxic CD8+ T cells in cancer and cancer immunotherapy.* British Journal of Cancer, 2021. **124**(2): p. 359-367.

663. Beissert, S., A. Schwarz, and T. Schwarz, *Regulatory T cells.* Journal of Investigative Dermatology, 2006. **126**(1): p. 15-24.

664. Crotty, S., *A brief history of T cell help to B cells.* Nature Reviews Immunology, 2015. **15**(3): p. 185-189.

665. Masopust, D., et al., *A brief history of CD8 T cells.* European Journal of Immunology, 2007. **37**(S1): p. S103-S110.

666. Sterner, R.C. and R.M. Sterner, *CAR-T cell therapy: current limitations and potential strategies.* Blood Cancer Journal, 2021. **11**(4): p. 69.

667. Li, K., et al., *T-cell-associated cellular immunotherapy for lung cancer.* Journal of Cancer Research and Clinical Oncology, 2015. **141**: p. 1249-1258.

668. Crough, T., et al., *Ex vivo functional analysis, expansion and adoptive transfer of cytomegalovirus-specific T-cells in patients with glioblastoma multiforme.* Immunology & Cell Biology, 2012. **90**(9): p. 872-880.

669. Vella, A.T., et al., *Cytokine-induced survival of activated T cells in vitro and in vivo.* Proceedings of the National Academy of Sciences of the United States of America, 1998. **95**(7): p. 3810-3815.

670. Yi, P.C., et al., *Impact of delayed PBMC processing on functional and genomic assays.* Journal of Immunological Methods, 2023. **519**: p. 113514.

671. Tabares, P., et al., *Human regulatory T cells are selectively activated by low-dose application of the CD28 superagonist TGN1412/TAB08.* European Journal of Immunology, 2014. **44**(4): p. 1225-36.

672. Suntharalingam, G., et al., *Cytokine storm in a phase 1 trial of the anti-CD28 monoclonal antibody TGN1412.* The New England Journal of Medicine, 2006. **355**(10): p. 1018-28.

673. Dennehy, K.M., et al., *Mitogenic CD28 signals require the exchange factor Vav1 to enhance TCR signaling at the SLP-76-Vav-Itk signalosome.* Journal of Immunology, 2007. **178**(3): p. 1363-71.

674. Mwangoka, G., et al., *Experience and challenges from clinical trials with malaria vaccines in Africa.* Malaria Journal, 2013. **12**: p. 86.

675. Burchill, M.A., et al., *T cell vaccinology: exploring the known unknowns.* Vaccine, 2013. **31**(2): p. 297-305.

676.   Flemming, A., *Why have T cell-inducing vaccines for HIV failed so far?* Nature Reviews Immunology, 2024. **24**(2): p. 89-89.

677.   Hamed, S.M., et al., *State of the art in epitope mapping and opportunities in COVID-19.* Future Science Open Access, 2023. **16**(3-06): p. Fso832.

678.   Li Pira, G., et al., *High throughput T epitope mapping and vaccine development.* Journal of Biomedical Biotechnology, 2010. **2010**: p. 325720.

679.   Pang, Z., et al., *Neoantigen-targeted TCR-engineered T cell immunotherapy: current advances and challenges.* Biomarker Research, 2023. **11**(1): p. 104.

680.   Mallone, R., et al., *Isolation and preservation of peripheral blood mononuclear cells for analysis of islet antigen-reactive T cell responses: position statement of the T-Cell Workshop Committee of the Immunology of Diabetes Society.* Clinical and Experimental Immunology, 2010. **163**(1): p. 33-49.

681.   Xiao, D., et al., *Quantitation of intracellular triphosphate metabolites of antiretroviral agents in peripheral blood mononuclear cells (PBMCs) and corresponding cell count determinations: review of current methods and challenges.* Expert Opinion on Drug Metabolism & Toxicology, 2018. **14**(8): p. 781-802.

682.   Spicer, N., et al., *National and subnational HIV/AIDS coordination: are global health initiatives closing the gap between intent and practice?* Global Health, 2010. **6**: p. 3.

683.   Sarzotti-Kelsoe, M., et al., *The Center for HIV/AIDS Vaccine Immunology (CHAVI) multi-site quality assurance program for cryopreserved human peripheral blood mononuclear cells.* Journal of Immunological Methods, 2014. **409**: p. 21-30.

684.   Ducar, C., et al., *Benefits of a comprehensive quality program for cryopreserved PBMC covering 28 clinical trials sites utilizing an integrated, analytical web-based portal.* Journal of Immunological Methods, 2014. **409**: p. 9-20.

685.   Coordination., H.A.N. *Procedures for the Isolation and Cryopreservation of PBMC.* [Standard Operating Procedure (SOP)] 2023 [cited 2023 22nd December 2023]; Available from: https://www.hanc.info/resources/sops-guidelines-resources/laboratory/cross-network-pbmc-processing-sop.html.

686.   Coordination., H.A.N. *Peripheral Blood Mononuclear Cell (PBMC) Thawing Standard Operating Procedure* [Standard Operating Procedure (SOP)] 2023 [cited 2023 22nd December 2023]; Available from: https://www.hanc.info/content/dam/hanc/documents/laboratory/actg-impaact-laboratory-manual/PBMC-Thawing.pdf.

687.   Bayot, M.L. and P. Tadi, *Laboratory Tube Collection*, in *StatPearls*. 2024: Treasure Island (FL).

688.   Kumar, P. and V. Satchidanandam, *Ethyleneglycol-bis-(beta-aminoethylether)tetraacetate as a blood anticoagulant: preservation of antigen-presenting cell function and antigen-specific proliferative response of peripheral blood mononuclear cells from stored blood.* Clinical and Diagnostic Laboratory Immunology, 2000. **7**(4): p. 578-83.

689.   Bull, M., et al., *Defining blood processing parameters for optimal detection of cryopreserved antigen-specific responses for HIV vaccine trials.* Journal of Immunological Methods, 2007. **322**(1-2): p. 57-69.

690.   Hoffmeister, B., et al., *Detection of antigen-specific T cells by cytokine flow cytometry: the use of whole blood may underestimate frequencies.* European Journal of immunology, 2003. **33**(12): p. 3484-3492.

691.   Navas, A., et al., *Phenotypic and functional stability of leukocytes from human peripheral blood samples: considerations for the design of immunological studies.* BMC Immunology, 2019. **20**(1): p. 5.

692. Langat, R.K., et al., *Performance of International AIDS Vaccine Initiative African clinical research laboratories in standardised ELISpot and peripheral blood mononuclear cell processing in support of HIV vaccine clinical trials.* African Journal of Laboratory Medicine, 2021. **10**(1): p. 1056.

693. Olson, W.C., et al., *Shipping blood to a central laboratory in multicenter clinical trials: effect of ambient temperature on specimen temperature, and effects of temperature on mononuclear cell yield, viability and immunologic function.* Journal of Translational Medicine, 2011. **9**(1): p. 26.

694. Sarathkumara, Y.D., et al., *The Effect of Tropical Temperatures on the Quality of RNA Extracted from Stabilized Whole-Blood Samples.* International Journal of Molecular Sciences, 2022. **23**(18).

695. Hendrika W. Grievink, T.L., Cornelis Kluft, Matthijs Moerland, and Karen E. Malone., *Comparison of Three Isolation Techniques for Human Peripheral Blood Mononuclear Cells: Cell Recovery and Viability, Population Composition, and Cell Functionality.* Biopreservation and Biobanking, 2016. **14**(5): p. 410-415.

696. Ruitenberg, J.J., et al., *VACUTAINER® CPT™ and Ficoll density gradient separation perform equivalently in maintaining the quality and function of PBMC from HIV seropositive blood samples.* BMC Immunology, 2006. **7**(1): p. 11.

697. Nilsson, C., et al., *Optimal Blood Mononuclear Cell Isolation Procedures for Gamma Interferon Enzyme-Linked Immunospot Testing of Healthy Swedish and Tanzanian Subjects.* Clinical and Vaccine Immunology, 2008. **15**(4): p. 585-589.

698. Chen, H., et al., *Functional comparison of PBMCs isolated by Cell Preparation Tubes (CPT) vs. Lymphoprep Tubes.* BMC Immunology, 2020. **21**(1): p. 15.

699. Jeurink, P.V., et al., *T cell responses in fresh and cryopreserved peripheral blood mononuclear cells: Kinetics of cell viability, cellular subsets, proliferation, and cytokine production.* Cryobiology, 2008. **57**(2): p. 91-103.

700. Reimann, K.A., et al., *Preservation of Lymphocyte Immunophenotype and Proliferative Responses in Cryopreserved Peripheral Blood Mononuclear Cells from Human Immunodeficiency Virus Type 1-Infected Donors: Implications for Multicenter Clinical Trials.* Clinical Diagnostic Laboratory Immunology, 2000. **7**(3): p. 352-359.

701. Kreher, C.R., et al., *CD4+ and CD8+ cells in cryopreserved human PBMC maintain full functionality in cytokine ELISPOT assays.* Journal of Immunological Methods, 2003. **278**(1): p. 79-93.

702. Raju, R., et al., *The need for novel cryoprotectants and cryopreservation protocols: Insights into the importance of biophysical investigation and cell permeability.* Biochimica et Biophysica Acta (BBA) - General Subjects, 2021. **1865**(1): p. 129749.

703. Nazarpour, R., et al., *Optimization of Human Peripheral Blood Mononuclear Cells (PBMCs) Cryopreservation.* International Journal of Molecular and Cellular Medicine, 2012. **1**(2): p. 88-93.

704. MAKINO, M. and M. BABA, *A Cryopreservation Method of Human Peripheral Blood Mononuclear Cells for Efficient Production of Dendritic Cells.* Scandinavian Journal of Immunology, 1997. **45**(6): p. 618-622.

705. Barcelo, H., et al., *A Practical Cryopreservation and Staining Protocol for Immunophenotyping in Population Studies.* Current Protocols in Cytometry, 2018. **84**(1): p. e35.

706. Kaiser, D., et al., *Freezing Medium Containing 5% DMSO Enhances the Cell Viability and Recovery Rate After Cryopreservation of Regulatory T Cell Products ex vivo and in vivo.* Frontiers in Cell and Developmental Biology, 2021. **9**.

707.   Hope, C.M., et al., *Optimization of Blood Handling and Peripheral Blood Mononuclear Cell Cryopreservation of Low Cell Number Samples.* International Journal of Molecular Sciences, 2021. **22**(17).

708.   Bogoslovsky, T., et al., *Cryopreservation and Enumeration of Human Endothelial Progenitor and Endothelial Cells for Clinical Trials.* Journal of Blood Disorders & Transfusions, 2013. **4**(5).

709.   Disis, M.L., et al., *Maximizing the retention of antigen specific lymphocyte function after cryopreservation.* Journal of Immunological Methods, 2006. **308**(1): p. 13-18.

710.   Alipour, R., et al., *Autologous plasma versus fetal calf serum as a supplement for the culture of neutrophils.* BMC Research Notes, 2020. **13**(1): p. 39.

711.   Filbert, H., et al., *Serum-free freezing media support high cell quality and excellent ELISPOT assay performance across a wide variety of different assay protocols.* Cancer Immunology, Immunotherapy, 2013. **62**(4): p. 615-627.

712.   Anja Germann, J.C.S., Beatrice Kemp-Kamke, Heiko Zimmermann, and Hagen von Briesen, *Standardized Serum-Free Cryomedia Maintain Peripheral Blood Mononuclear Cell Viability, Recovery, and Antigen-Specific T-Cell Response Compared to Fetal Calf Serum-Based Medium.* Biopreservation and Biobanking, 2011. **9**(3): p. 229-236.

713.   Kopeika, J., A. Thornhill, and Y. Khalaf, *The effect of cryopreservation on the genome of gametes and embryos: principles of cryobiology and critical appraisal of the evidence.* Human Reproduction Update, 2015. **21**(2): p. 209-27.

714.   Behnamifar, A., et al., *Research Note: Evaluation of two methods for adding cryoprotectant to semen and effects of bovine serum albumin on quality characteristics of cryopreserved rooster spermatozoa.* Poultry Science, 2021. **100**(6): p. 101093.

715.   Fabozzi, G., et al., *Evaluation of the Efficiency of Two Different Freezing Media and Two Different Protocols to Preserve Human Spermatozoa from Cryoinjury.* International Journal of Reproductive Medicine, 2016. **2016**: p. 6059757.

716.   Tree, T.I.M., B.O. Roep, and M. Peakman, *Enhancing the Sensitivity of Assays to Detect T Cell Reactivity: The Effect of Cell Separation and Cryopreservation Media.* Annals of the New York Academy of Sciences, 2004. **1037**(1): p. 26-32.

717.   Buhl, T., et al., *Controlled-rate freezer cryopreservation of highly concentrated peripheral blood mononuclear cells results in higher cell yields and superior autologous T-cell stimulation for dendritic cell-based immunotherapy.* Cancer Immunology, Immunotherapy, 2012. **61**(11): p. 2021-2031.

718.   Huang, Z., et al., *Cryopreservation of human T lymphocytes under fast cooling with controlled ice nucleation in cryoprotective solutions of low toxicity.* Cryobiology, 2021. **103**: p. 92-100.

719.   Baboo, J., et al., *The Impact of Varying Cooling and Thawing Rates on the Quality of Cryopreserved Human Peripheral Blood T Cells.* Scientific Reports, 2019. **9**(1): p. 3417.

720.   Mrowiec, Z.R., et al., *Comparison of Controlled vs Non-Controlled Rate Freezing of Umbilical Cord Blood Units.* Blood, 2004. **104**(11): p. 5011-5011.

721.   Yang, J., et al., *The effects of storage temperature on PBMC gene expression.* BMC Immunology, 2016. **17**(1): p. 6.

722.   Valeri, C.R. and L.E. Pivacek, *Effects of the temperature, the duration of frozen storage, and the freezing container on in vitro measurements in human peripheral blood mononuclear cells.* Transfusion, 1996. **36**(4): p. 303-8.

723.   Weinberg, A., et al., *Optimization of storage and shipment of cryopreserved peripheral blood mononuclear cells from HIV-infected and uninfected individuals for ELISPOT assays.* Journal of Immunological Methods, 2010. **363**(1): p. 42-50.

724. McCullough, J., et al., *Long-term storage of peripheral blood stem cells frozen and stored with a conventional liquid nitrogen technique compared with cells frozen and stored in a mechanical freezer.* Transfusion, 2010. **50**(4): p. 808-819.

725. Tollerud, D.J., et al., *Cryopreservation and long-term liquid nitrogen storage of peripheral blood mononuclear cells for flow cytometry analysis: effects on cell subset proportions and fluorescence intensity.* Journal of Clinical Laboratory Analysis, 1991. **5**(4): p. 255-61.

726. Li, B., et al., *Comprehensive evaluation of the effects of long-term cryopreservation on peripheral blood mononuclear cells using flow cytometry.* BMC Immunology, 2022. **23**(1): p. 30.

727. Germann, A., et al., *Temperature fluctuations during deep temperature cryopreservation reduce PBMC recovery, viability and T-cell function.* Cryobiology, 2013. **67**(2): p. 193-200.

728. Cosentino, L.M., et al., *Preliminary Report: Evaluation of Storage Conditions and Cryococktails during Peripheral Blood Mononuclear Cell Cryopreservation.* Cell Preservation Technology, 2007. **5**(4): p. 189-204.

729. Xu, Y., et al., *Effect of Warming Process on the Survival of Cryopreserved Human Peripheral Blood Mononuclear Cells.* Biopreservation and Biobanking, 2021. **19**(4): p. 318-323.

730. Hønge, B.L., et al., *Optimizing recovery of frozen human peripheral blood mononuclear cells for flow cytometry.* PLOS ONE, 2017. **12**(11): p. e0187440.

731. Yao, T. and Y. Asayama, *Animal-cell culture media: History, characteristics, and current issues.* Reproductive Medicine and Biology, 2017. **16**(2): p. 99-117.

732. Ramachandran, H., et al., *Optimal thawing of cryopreserved peripheral blood mononuclear cells for use in high-throughput human immune monitoring studies.* Cells, 2012. **1**(3): p. 313-24.

733. Darzynkiewicz, Z., X. Li, and J. Gong, *Chapter 2 Assays of Cell Viability: Discrimination of Cells Dying by Apoptosis*, in *Methods in Cell Biology*, Z. Darzynkiewicz, J. Paul Robinson, and H.A. Crissman, Editors. 1994, Academic Press. p. 15-38.

734. García-Piñeres, A.J., et al., *DNAse treatment following thawing of Cryopreserved PBMC is a procedure suitable for lymphocyte functional studies.* Journal of Immunological Methods, 2006. **313**(1): p. 209-213.

735. Smith, J.G., et al., *Development and Validation of a Gamma Interferon ELISPOT Assay for Quantitation of Cellular Immune Responses to Varicella-Zoster Virus.* Clinical Diagnostic Laboratory Immunology, 2001. **8**(5): p. 871-879.

736. Liao, Q., et al., *Investigation of Enzymatic Behavior of Benzonase/Alkaline Phosphatase in the Digestion of Oligonucleotides and DNA by ESI-LC/MS.* Analytical Chemistry, 2007. **79**(5): p. 1907-1917.

737. Santos, R., et al., *Improvement of IFNg ELISPOT Performance Following Overnight Resting of Frozen PBMC Samples Confirmed Through Rigorous Statistical Analysis.* Cells, 2015. **4**(1): p. 1-18.

738. Lemieux, J., et al., *A global look into human T cell subsets before and after cryopreservation using multiparametric flow cytometry and two-dimensional visualization analysis.* Journal of Immunological Methods, 2016. **434**: p. 73-82.

739. Kuerten, S., et al., *Resting of Cryopreserved PBMC Does Not Generally Benefit the Performance of Antigen-Specific T Cell ELISPOT Assays.* Cells, 2012. **1**(3): p. 409-27.

740. Lozano-Ojalvo, D., R. Lopez-Fandino, and I. Lopez-Exposito, *PBMC-Derived T Cells*, in *The Impact of Food Bioactives on Health: in vitro and ex vivo models*, K. Verhoeckx, et al., Editors. 2015: Cham (CH). p. 169-80.

741. Sävendahl, L. and L.E. Underwood, *Decreased Interleukin-2 Production from Cultured Peripheral Blood Mononuclear Cells in Human Acute Starvation*.* The Journal of Clinical Endocrinology & Metabolism, 1997. **82**(4): p. 1177-1180.

742. Kern, F., et al., *Cytomegalovirus (CMV) phosphoprotein 65 makes a large contribution to shaping the T cell repertoire in CMV-exposed individuals.* The Journal of Infectious Diseases, 2002. **185**(12): p. 1709-16.

743. Houghten, R.A. and C.H. Li, *Reduction of sulfoxides in peptides and proteins.* Analytical Biochemistry, 1979. **98**(1): p. 36-46.

744. Tunçer, S., et al., *Low dose dimethyl sulfoxide driven gross molecular changes have the potential to interfere with various cellular processes.* Scientific Reports, 2018. **8**(1): p. 14828.

745. Elisia, I., et al., *DMSO Represses Inflammatory Cytokine Production from Human Blood Cells and Reduces Autoimmune Arthritis.* PLOS ONE, 2016. **11**(3): p. e0152538.

746. Kaveh, D.A., A.O. Whelan, and P.J. Hogarth, *The duration of antigen-stimulation significantly alters the diversity of multifunctional CD4 T cells measured by intracellular cytokine staining.* PLOS ONE, 2012. **7**(6): p. e38926.

747. Portmann, K., et al., *Single-cell deep phenotyping of cytokine release unmasks stimulation-specific biological signatures and distinct secretion dynamics.* Cell Reports Methods, 2023. **3**(7): p. 100502.

748. Bourguignon, P., et al., *Processing of blood samples influences PBMC viability and outcome of cell-mediated immune responses in antiretroviral therapy-naïve HIV-1-infected patients.* Journal of Immunological Methods, 2014. **414**: p. 1-10.

749. Listvanova, S., et al., *Optimal kinetics for quantification of antigen-induced cytokines in human peripheral blood mononuclear cells by real-time PCR and by ELISA.* Journal of Immunological Methods, 2003. **281**(1): p. 27-35.

750. Godoy-Ramirez, K., et al., *Optimum culture conditions for specific and nonspecific activation of whole blood and PBMC for intracellular cytokine assessment by flow cytometry.* Journal of Immunological Methods, 2004. **292**(1): p. 1-15.

751. Mellau, L.S. and R.J. Jørgensen, *Does EDTA-infusion affect calcium homeostatis leading to increased resistance to challenge?* Acta Veterinaria Scandinavica Supplement, 2003. **97**: p. 29-34.

752. Xu, X. and Y. Dai, *Heparin: an intervenor in cell communication.* Journal of Cellular and Molecular Medicine, 2010. **14**(1-2): p. 175-80.

753. Gu, Z.T., et al., *Heat stress induces apoptosis through transcription-independent p53-mediated mitochondrial pathways in human umbilical vein endothelial cell.* Scientific Reports, 2014. **4**: p. 4469.

754. Hikim, A.P.S., et al., *Key Apoptotic Pathways for Heat-Induced Programmed Germ Cell Death in the Testis.* Endocrinology, 2003. **144**(7): p. 3167-3175.

755. Whaley, D., et al., *Cryopreservation: An Overview of Principles and Cell-Specific Considerations.* Cell Transplant, 2021. **30**: p. 963689721999617.

756. Ekpo, M.D., et al., *Incorporating Cryopreservation Evaluations Into the Design of Cell-Based Drug Delivery Systems: An Opinion Paper.* Frontiers in Immunology, 2022. **13**: p. 967731.

757. Romero, F., *Philosophy of science and the replicability crisis.* Philosophy Compass, 2019. **14**(11): p. e12633.

758. Errington, T.M., et al., *Challenges for assessing replicability in preclinical cancer biology.* eLife, 2021. **10**: p. e67995.

759. Open Science, C., *Estimating the reproducibility of psychological science.* Science, 2015. **349**(6251): p. aac4716.

760. Freedman, L.P., I.M. Cockburn, and T.S. Simcoe, *The Economics of Reproducibility in Preclinical Research.* PLOS Biology, 2015. **13**(6): p. e1002165.

761. Ioannidis, J.P., *Microarrays and molecular research: noise discovery?* The Lancet, 2005. **365**(9458): p. 454-455.

762. Branch, M.N., *The "Reproducibility Crisis:" Might the Methods Used Frequently in Behavior-Analysis Research Help?* Perspectives on Behavioral Science, 2019. **42**(1): p. 77-89.

763. Fanelli, D., *Do Pressures to Publish Increase Scientists' Bias? An Empirical Support from US States Data.* PLOS ONE, 2010. **5**(4): p. e10271.

764. Ioannidis, J.P.A., *Why Most Published Research Findings Are False.* PLOS Medicine, 2005. **2**(8): p. e124.

765. Hunter, P., *The reproducibility "crisis": Reaction to replication crisis should not stifle innovation.* EMBO Reports, 2017. **18**(9): p. 1493-1496.

766. Scudamore, C.L., et al., *Recommendations for minimum information for publication of experimental pathology data: MINPEPA guidelines.* The Journal of Pathology, 2016. **238**(2): p. 359-367.

767. Brazma, A., et al., *Minimum information about a microarray experiment (MIAME)—toward standards for microarray data.* Nature Genetics, 2001. **29**(4): p. 365-371.

768. Deutsch, E.W., et al., *Minimum information specification for in situ hybridization and immunohistochemistry experiments (MISFISHIE).* Nature Biotechnology, 2008. **26**(3): p. 305-312.